Migration processes of ^{137}Cs in the drinking water reservoir Lago Maggiore: Measurements and Modeling

DISSERTATION

Zur Erlangung des akademischen Grades

Doctor rerum naturalium

(Dr. rer. nat.)

vorgelegt:

der Fakultät Mathematik und Naturwissenschaften

der Technischen Universität Dresden

von

Viktoryia Putyrskaya

geboren am 05.06.1980 in Vileika, Belarus

Gutachter: Prof. Dr. habil. Gert Bernhard
               Prof. Dr. Eckehard Klemt

Eingereicht am: 19.05.2010
Tag der Verteidigung: 22.10.2010

ABSTRACT

Artificial ^{137}Cs has been introduced into the environment for more than half a century. Its first appearance in central European lake sediments corresponds to the nuclear weapons testing in the 1960s. The largest contamination of European lakes and rivers occurred as a consequence of the fallout after the Chernobyl accident in spring 1986. In this work the migration behaviour of artificial ^{137}Cs in Lago Maggiore and other pre-alpine lakes as a consequence of these fallouts was studied.

Lago Maggiore is one of the largest drinking water reservoirs in the south of the Alps. After the Chernobyl accident roughly 20 kBq·m^{-2} of ^{137}Cs were deposited onto the lake surface. From 2003 to 2005 bottom sediment cores and water samples were collected at 7 different locations of Lago Maggiore. Data on the ^{137}Cs distribution in tributaries, lake water, suspended matter, bottom sediments, and the ^{137}Cs association to different geochemical fractions are presented in this work.

To model the run-off of ^{137}Cs from the watershed into the lake a compartment model was used. For modeling the input of ^{137}Cs into and the vertical distribution within the sediment a diffusion–convection type model was developed. This model takes into account the uptake of activity by sedimentation, fixation and redissolution, retarded diffusion, the influence of competing ions on the retarded diffusion within the sediments, and compaction of sediments. The results of the parameter optimization – mainly the sedimentation rate and the ^{137}Cs distribution coefficient K_d, which determines the uptake of activity into the sediment – are discussed and compared with those of other European lakes characterized by similar ^{137}Cs deposition levels but different limnological properties.

To estimate the bioavailability of ^{137}Cs, its activity concentrations in fish samples from Lago Maggiore were measured. Combining the existing data with our measurements, ^{137}Cs fish–water concentration ratios were calculated and compared with those for other lakes which were affected by similar ^{137}Cs contamination.

ZUSAMMENFASSUNG

Das künstliche Radionuklid ^{137}Cs wurde seit über einem halben Jahrhundert in die Natur eingebracht. Sein erstes Erscheinen in Sedimenten der zentraleuropäischen Seen korrespondiert mit den Nuklearwaffentests in den 60er-Jahren des 20. Jahrhunderts. Die stärkste Kontaminierung der europäischen Seen und Flüsse entstand als Folge des radioaktiven Niederschlags nach dem Unfall in Tschernobyl im Frühjahr 1986. In dieser Arbeit wurde das Migrationsverhalten des künstlichen ^{137}Cs im Lago Maggiore und anderen Seen im Alpenvorland als Folge dieses Niederschlags untersucht.

Der Lago Maggiore zählt zu den größten Trinkwasserreservoiren südlich der Alpen. Nach dem Unfall in Tschernobyl gingen ungefähr 20 kBq·m^{-2} des ^{137}Cs auf die Oberfläche des Sees nieder. Im Zeitraum von 2003 bis 2005 wurden Sedimentkerne und Wasserproben an sieben unterschiedlichen Stellen des Lago Maggiore entnommen. Diese Arbeit beschäftigt sich mit Daten über die Verteilung des ^{137}Cs in den Zuflüssen, dem Wasser des Sees, in Schwebstoffen und Bodensedimenten und mit der Assoziierung von ^{137}Cs mit verschiedenen geochemischen Fraktionen.

Um den Abfluss des ^{137}Cs aus dem Wassereinzugsgebiet in den Fluss zu modellieren, wurde ein Compartmentmodell verwendet. Zur Modellierung der Aufnahmemenge von ^{137}Cs im Sediment und der vertikalen Verteilung innerhalb dessen wurde ein Diffusions-Konvektions-Modell entwickelt. Dieses Modell berücksichtigt die Aufnahme von Aktivität durch Sedimentation, Fixierung und Rücklösung, retardierte Diffusion, die Verdichtung des Sediments sowie den Einfluss konkurrierender Ionen auf die retardierte Diffusion innerhalb des Sediments. Die Ergebnisse der Parameteroptimierung – im Wesentlichen die Sedimentationsrate und der ^{137}Cs-Verteilungskoeffizient K_d, welcher die Aufnahme der Aktivität in das Sediment determiniert – werden erörtert und mit denen anderer europäischer Seen, die eine ähnliche ^{137}Cs-Deposition, aber unterschiedliche limnologische Eigenschaften aufweisen, verglichen.

Zur Beurteilung der Bioverfügbarkeit von ^{137}Cs wurde die ^{137}Cs-Aktivitätskonzentrationen von Fischproben aus dem Lago Maggiore gemessen. Aus bereits existierenden Daten und unseren Messergebnissen wurden ^{137}Cs Fisch-Wasser Konzentrations-Verhältnisse errechnet und mit denen für andere Seen, die von ähnlichen ^{137}Cs-Kontaminationen betroffen sind, verglichen.

TABLE OF CONTENT

LIST OF SYMBOLS

This list contains the most important symbols, notations, and abbreviations used. The dimension is indicated in square brackets [ ].

α – experimentally measured portion of exchangeable radioactivity [1];

$\alpha_{Cs}, \beta_{Cs}, \gamma_{Cs}$ – empirically determined constants of AQUASCOPE model [m^{-1}];

$A(x)$ – activity concentration of unsupported ^{210}Pb at a depth x [$Bq \cdot g^{-1}$];

$A_0(t)$ – initial activity concentration of unsupported ^{210}Pb in the sediment [$Bq \cdot g^{-1}$];

$A_r(x)$ – total residual activity concentration of unsupported ^{210}Pb in the sediment below the depth x [$Bq \cdot cm^{-2}$];

C_E – exchangeable part of radioactivity in the sediment [$Bq \cdot m^{-2} \cdot cm^{-1}$];

C_f – ^{137}Cs activity concentration in fish [$Bq\ kg^{-1}$];

C_F – fixed part of radioactivity in the sediment [$Bq \cdot m^{-2} \cdot cm^{-1}$];

CIC – constant initial concentration;

C_L – ^{137}Cs activity concentration in the lake water [$Bq \cdot m^{-3}$];

$C_L(0)$ – initial mean ^{137}Cs activity concentration in the lake water [$Bq \cdot m^{-3}$];

C_R – ^{137}Cs activity concentration in the runoff water, C_R [$Bq \cdot m^{-3}$];

CR (CF) – concentration ratio (concentration factor) of ^{137}Cs in fish [$l\ kg^{-1}$];

CRS – constant rate of supply;

d – mean depth of the lake [m];

D – diffusion coefficient of Cs^+ ions [$cm^2 \cdot a^{-1}$];

D_C – average deposition to the catchment area [$Bq \cdot m^{-2}$];

D_E – retarded constant of $^{137}Cs^+$ diffusion [$cm^2 \cdot a^{-1}$];

D_{phys} – combined bio- and physical turbation acting only in the top layers of the sediment [$cm^2 \cdot a^{-1}$];

D_L – average deposition to the lake surface [$Bq \cdot m^{-2}$];

$D_{T°C}, D_{25°C}$ – diffusion coefficients of Cs^+ ions at temperature T [°C] and 25 °C, respectively [$cm^2 \cdot a^{-1}$];

ε – porosity of the sediment [1];

E – emission probability [%];

f – first order fixation rate [a^{-1}];

F – diffusion flux, in [$Bq \cdot cm^{-2} \cdot a^{-1}$];

F_{phys} – diffusion flux which describes physical turbation [$Bq \cdot cm^{-2} \cdot a^{-1}$];

θ – volumetric water content [1];

k_1, k_2, k_3 – empirically determined constants of AQUASCOPE model [a^{-1}];

k_b – backward rate constant describing the excretion of radioactivity from fish [a^{-1}];

K_d – distribution coefficient which relates the concentration of adsorbed ^{137}Cs activity to its activity in the liquid phase [$1 \cdot kg^{-1}$];

K_d^{ex} – exchangeable distribution coefficient [$1 \cdot kg^{-1}$];

$K_{d\_dif}^{ex}$ – distribution coefficient which controls the diffusion within the sediment [$1 \cdot kg^{-1}$];

K_d^{tot} – total distribution coefficient [$1 \cdot kg^{-1}$];

k_f – rate constant describing the transfer of ^{137}Cs from water to fish [$l \cdot kg^{-1} \cdot a^{-1}$];

λ – radioactive decay constant of a radionuclide [a^{-1}];

MDA – minimum detectable activity which is defined as the smallest amount of activity that can be quantified;

$M_{T°C}$, **$M_{25°C}$** – viscosities of water at temperature T [°C] and 25 °C, respectively, [cp];

r – first order redissolution rate [a^{-1}];

R – retardation factor, a dimensionless parameter characterizing the retarding effect of adsorption on solute transport [1];

ρ_0 – density of the top layer of the sediment [$g \cdot cm^{-3}$];

ρ_b – experimentally measured bulk density of the dry sediment [$g \cdot cm^{-3}$];

ρ_p – mean particle density [$g \cdot cm^{-3}$];

R_s – sedimentation rate [$g \cdot cm^{-2} \cdot a^{-1}$];

t – time [a];

$\boldsymbol{\tau}$ ($\tau < 1$) – tortuosity factor which describes the decrease of D_E due to tortuous flow along the pores of the sediment; it is a measure of the path length of a pore over a given length of a sediment [1];

$\boldsymbol{\tau_s}$ – time constant of ^{137}Cs transfer to the sediments [a];

$\boldsymbol{\tau_w}$ – water residence time of the lake [a];

$\boldsymbol{T_{1/2}}$ – half-life of a radionuclide [a];

$\boldsymbol{v_S}$ – sedimentation speed [cm·a^{-1}];

$\boldsymbol{x}$ – depth of the sediment profile [cm].

GLOSSARY

Allochthonous – originating from outside (used to characterize materials transported from the catchment area to a lake).

Amorphous silicates – structure material of diatomic algae.

Benthos **–** organisms living on, or in, the bottom material of lakes and streams.

Catchment area (=watershed=drainage basin) **–** area that contains water that drains into a stream or river or lake.

Cryptodepression **–** the part of a lake basin that is below sea level.

Drainage basin– see *Catchment area.*

Epilimnion – the upper, well-mixed, freely circulating surface water of a nearly isothermal region of a stratified lake.

Eutrophic lake **–** very productive lake rich in plant nutrients.

Eutrophication – a gradual increase in the productivity of a lake ecosystem due to enrichment with plant nutrients, leading to changes in the biological community as well as physical and chemical changes.

Fulvic acid – a yellow to yellow-brown *humic substance* that is soluble in water under all pH conditions.

Humic acid – a dark-coloured *humic substance* that is insoluble in acid.

Humic substances – are major components of the natural *organic matter* formed in soils and sediments by the decay of dead plants, microbes and animals.

Hypolimnion – dark, cold, bottom waters of a lake that are thermally separated from the warmer surface waters when a lake is stratified.

Insubric line – a major tectonic line which marks the northern and western boundary of the Southern Alps.

Isobath **–** a subsurface contour line connecting points of equal temperature.

Limnology **–** the study of freshwater ecosystems**.**

Lithology **–** the study of rocks.

Mesotrophic lake – lake which is characterized by moderate concentrations of nutrients, algae, and water transparency. A mesotrophic lake is not as rich in nutrients as a eutrophic lake, but richer in nutrients than an oligotrophic lake.

Monomictic – a term used to describe lakes which undergo one period of complete mixing during the year separated by one period of thermal stratification. Monomictic lakes are also relatively deep and do not freeze over completely in winter.

Oligotrophic lake – relatively unproductive lake which is characterized by low concentrations of nutrients and algae resulting in good water transparency.

Organic matter –material containnig carbon, a basic component of all living matter.

Relief – change in elevation of a land surface between two points.

Residence time – the average time required to completely renew a lake's water volume.

Runoff – natural drainage of water away from an area

Secchi depth – measure of transparency of water obtained by lowering a 20-25 cm black and white disk into water until it is no longer visible.

Sediment – solid material including both soil particles and organic matter which is suspended in the water and gradually deposited in the bottom of a lake.

Stratification – the arrangement of water into distinct layers which differ by temperature and density (occurs in the ocean and deep lakes especially).

Thalweg – a line drawn to join the lowest points along the entire length of a streambed or valley.

Turbidity flow (turbidite) – the flow which takes place mostly in deep lakes, it is responsible for the redistribution of large amounts of sediment from the steep slopes of the lake basin.

Turnover – a complete mixing of the lake due to spring warming and autumn cooling of surface water which increases density, and gradually makes temperature and density uniform from top to bottom. This allows wind and wave action to mix the entire lake. Mixing allows bottom waters to contact the atmosphere, raising the water's oxygen content.

Watershed – see *Catchment area.*

INTRODUCTION

According to its location in the relief and system of runoff, lakes serve as accumulators of substances which circulate within the drainage basin and as a result get into lake water itself. The subsequent "fate" of the chemical elements including radionuclides which are forthcoming into the lake, can be determined by complex physical, chemical and biological processes leading to the considerable redistribution between different components of aqueous ecosystem (Ostapenya et al., 1999). There are no destruction mechanisms of technogenic radionuclides in the environment. Therefore, the studies of radionuclides distribution in the bottom sediments allow us not only to specify the dating of certain events but they also promote the development and implementation of complex investigations of the lake as a whole. In addition, extended studies of lake sedimentation processes in the conditions of radioactive contamination allow to observe and to follow the regularities of radionuclides migration in the catchment areas and within the distinct lacustrine basins.

The largest contamination of most European lakes and rivers with radiocaesium – ^{137}Cs (half-life 30.07 years) and ^{134}Cs (half-life 2.07 years) – occurred as a consequence of the fallout after the accident at the Nuclear power plant in Chernobyl (Ukraine) in spring 1986. Before the Chernobyl accident, the deposition of ^{137}Cs on the territory of Europe was mainly due to global fallout from the atmospheric testing of nuclear weapons in 1960s.

There are two forms of ^{137}Cs – sorbed and dissolved –present in water of tributaries and lakes. ^{137}Cs sorbed onto solid particles (suspended matter) can settle down to the bottom of the lake being removed by this way from the water column. Such processes as sedimentation and diffusion result in transport of ^{137}Cs within the sediment as well as exchange between the sediment and the overlaying water.

Artificial radionuclides, in particular ^{137}Cs and ^{210}Pb (half-life 22.3 years, introduced into the lake with a constant rate from the atmosphere), disappear from the environment only by radioactive decay with known half-lives. Thus, knowledge on the distribution of these radionuclides in the lake allows to date certain events and to explore the main processes in the lake.

A large number of studies on the behaviour of radionuclides in European lakes have been carried out during past decades (Davidson et al., 1993; Dominik and Span, 1992; Ilus and Saxén, 2005; Kaminski et al., 1998; Konoplev et al., 2002; Monte et al., 2005; Rezzoug et al., 2006; Robbins et al., 1992; Santschi et al., 1990; Schertz et al., 2006; Spezzano et al., 1993; Zibold et al., 2002). These studies showed that in lakes with different limnological character ^{137}Cs behaves differently and depends on many physical, geochemical and biological factors. However, taking these characteristics in mind, a common theoretical description valid for ^{137}Cs in many European lakes could be achieved (Håkanson, 2004; Monte et al., 2003; Smith and Beresford, 2005).

Modeling of migration processes in the lake can give the possibility not only to estimate the general characteristics and peculiarities of sediment accumulation, but also to reveal typical and irregular parameters such as compaction of sediments, sedimentation rates, and distribution coefficients. These parameters and others can be useful to establish the correlation between different components, to determine the prevalent processes, and to make prognosis for the future of the investigated ecosystem.

As an *object* of our investigations an Italian lake (Lago Maggiore) was chosen. It is one of the largest drinking water reservoirs in the south of the Alps. After the Chernobyl accident in 1986 roughly 20 kBq·m^{-2} of ^{137}Cs (Czarnecki et. al, 1986) were deposited onto the lake surface, about the same amount as onto the neighboring Lago di Lugano (24 kBq·m^{-2} according to Santschi et al., 1990). Lago Maggiore is the most thoroughly investigated lake in Italy in terms of the number of key biogeochemical parameters measured and the duration of their monitoring. However, nearly no research studies with respect to radionuclide distribution in this lake were performed so far. Only some data about radionuclide activity concentrations in surface lake water are available (Cazzaniga et al., 1996–1998; Cazzaniga et al., 1997; D'Alberti, 2001–2002; D'Alberti, 2003; D'Alberti and Osimani, 1995; Dominici, 1989–1990; Dominici and Risposi, 1990–1993; Osimani et al., 1994; Radioactivity Environmental Monitoring (REM) Database, 2005).

The *aims* of this work are the investigation and modeling of migration processes of ^{137}Cs in the water and bottom sediments of Lago Maggiore. According to these aims the following tasks have been performed during the research:

- in order to determine the distribution coefficient K_d which is an important parameter describing sorption process in the lake, ^{137}Cs activity concentrations in the water column of Lago Maggiore and its main tributaries (Toce, Ticino and Verzasca) as well as in the suspended matter were measured; additionally, other water parameters such as pH, K^+ and NH_4^+ concentrations, temperature and oxygen content were evaluated;

- to get the information about vertical distributions of ^{137}Cs and ^{210}Pb in the sediment gamma-spectrometric analysis of sediment samples was performed;

- to identify turbidites in Lago Maggiore sediments, the photos of sediment cores together with the information on the bulk density and radionuclides concentration in the sediments were used;

- to study the association of ^{137}Cs to the different geochemical fractions (exchangeable ions, organic matter, amorphous silicates, clay minerals, etc.) a set of sequential extractions was performed;

- to describe migration processes of ^{137}Cs and it's distribution in the sediment of Lago Maggiore, a model based on sedimentation-diffusion equations was developed;

- additional features such as compaction of sediments, deposition of turbidites, influence of competing ions on the retarded diffusion within the sediments were introduced. The model can cover the time period from the nuclear weapon testing to the present.

- to solve the system of differential equations a finite element method (FEM) was used;

- to introduce an independent time scale and to determine the age of sediment layers, two different versions of the ^{210}Pb method were used: Constant input concentration (CIC) and Constant rate of supply (CRS);

- finally, to estimate the bioavailability of ^{137}Cs, fish samples from Lago Maggiore were measured. Subsequently, combing the existing data with our measurements, ^{137}Cs concentration ratios were calculated.

This study is divided into six chapters. Chapter 1 gives an overview on the main chemical properties of radiocaesium and the sources of its appearance in European lakes. Chapter 2 contains the literature review of the present radioecological situation and different characteristics of Lago Maggiore. In Chapter 3 the description of the experimental work, of the equipment and procedure followed to accomplish the task are given. Chapter 4 gives the description of obtained results concerning the measurements and monitoring of the studied object. In Chapter 5 the mathematical modeling is discussed in details; main results of modeling are shown and compared to those for other European lakes. Finally, in Chapter 6, the results of radiocaesium activity concentration in fish in Lago Maggiore are discussed; fish–water concentration ratios of ^{137}Cs are calculated and compared with those for other lakes which were affected by similar contamination with radiocaesium. The last part of the thesis summarizes the obtained results and gives general conclusions.

1. RADIOCAESIUM IN THE ENVIRONMENT

1.1 Sources of radiocaesium in the environment

Radiocaesium – ^{137}Cs (half-life 30.07 years) and ^{134}Cs (half-life 2.07 years) – does not occur naturally on earth, it is exclusively anthropogenic in origin through nuclear fission. ^{137}Cs has a special significance due to its long half-live and due to the fact that it behaves in the environment like the important element potassium.

Global fallout

The first appearance of ^{137}Cs in central European lake sediments corresponds to the beginning of the nuclear weapons testing with maxima in 1959 and 1963 (Magnini et al., 1990). Radioactive materials were released, basically in vapor form, to an altitude of up to 12000 m and due to air flows spread in the atmosphere. When condensed, these materials led to radioactive contamination of vast territories in the Northern Hemisphere (UNSCEAR, 2000).

As a result of the atmospheric atomic bomb testing in the 1950's and 1960's the radioactive isotope ^{137}Cs is even today present in the environment worldwide.

Chernobyl fallout

The largest contamination of most European lakes and rivers with radiocaesium occurred as a consequence of the fallout after the accident at the Nuclear power plant in Chernobyl (Ukraine) in April 1986. Although a wide spectrum of radionuclides was released to the environment and deposited over Europe during this accident, for the long term radioactive contamination ^{137}Cs has the largest significance and radioecological impact. About half of the released radioactivity settled out within 60 km of the accident site (IAEA, 1991), while the remainder was spread unevenly over all of Europe (Fig. 1.1).
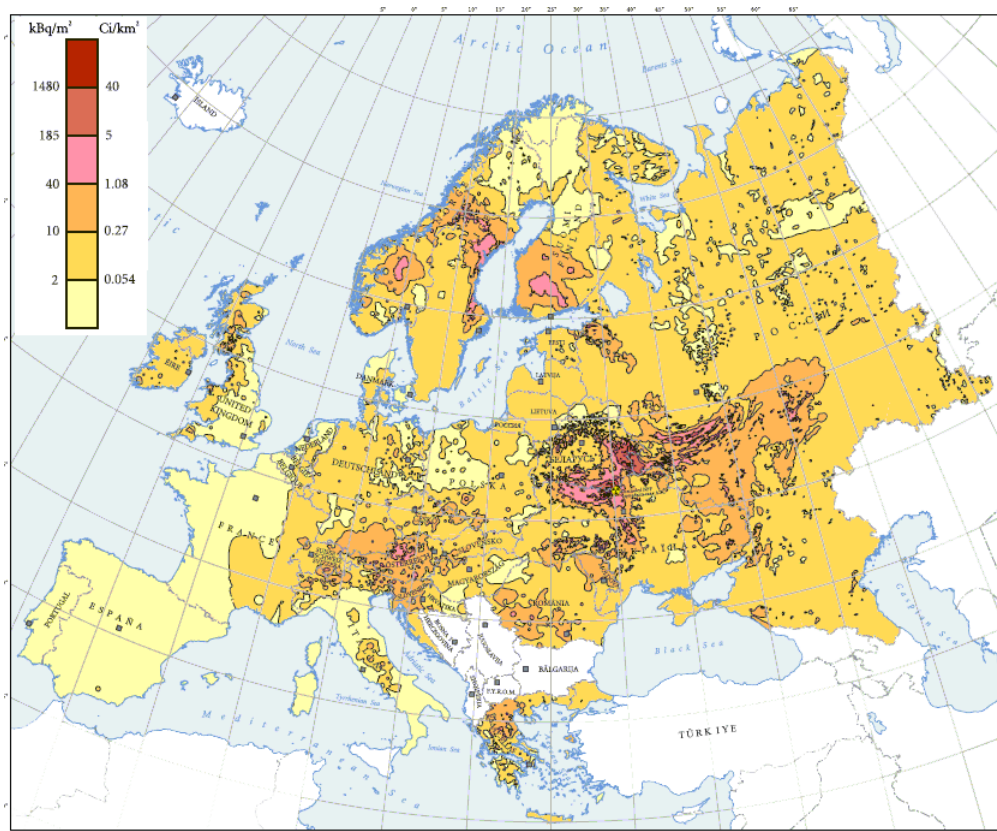
Fig. 1.1. Map of ^{137}Cs distribution after the Chernobyl fallout (from Atlas of caesium deposition on Europe after the Chernobyl accident, 1998).

During the first period after the Chernobyl accident radionuclides were deposited both on soil and water surfaces. Later on, a redistribution of radionuclides took place where such processes as runoff from the catchment area, transport of radionuclides into the sediments and their migration within the sediments, play the most important role (Hilton, 2001; Warner and Harrison, 1993).

1.2 Chemical properties of radiocaesium

Being deposited once on the soil or sediment surface, radiocaesium is very fast and very strong sorbed onto soil particles (Konoplev et al., 2002; Owens et al., 1996). This behaviour can be explained by its chemical properties. Caesium is soluble, existing in dissolved form as the monovalent cation Cs^+. It belongs to the alkali metals and it is the least inert and, therefore, the most reactive element in this group. Its chemical reactions are similar to those of potassium (Davis, 1963).

Sediments are a complex mixture of organic and inorganic components in which there are a variety of physical sites available for radiocaesium association. The most commonly analyzed geochemical fractions are: exchangeable, bound to carbonates, reducible, oxidizable and residual (Tessier *et al.*, 1979; Blanco *et al.*, 2004). One experimental approach commonly used to identify the speciation of a given radionuclide in a specific sample is the use of selective sequential extraction procedures. The most widely used technique for radionuclides extraction is the Tessier's method (Tessier et al., 1979). In this work a modified Tessier's method (Robbins *et al.*, 1992) was applied (see chapter 3.5.2). It is based on the assumption that in sediments radiocaesium can be associated with such geochemical fractions as exchangeable ions; organic matter; oxides and hydroxides of iron and manganese which are formed in the lake as coatings of particles; carbonates; and amorphous silicates which are the remnants of diatomic algae and occur in the waters of the world. The remaining residue mainly consists of clay minerals, feldspars, and quartz. Knowledge of where ^{137}Cs resides within sediments can help to predict its impact because some sites hold it more tenaciously than others. If ^{137}Cs is loosely bound to sediment, it is generally more biologically mobile. In Kaminski *et al.* (1998) it is shown that the mobility of ^{137}Cs in fresh water lakes depends on the limnological characteristics of the lakes, sometimes even of the different basins of one lake.

1.2.1 Binding of radiocaesium on clay minerals

Numerous studies showed that the behaviour of the artificial caesium isotopes in the aquatic environment is controlled by sorption on solid particles and depends on the clay

mineral composition of sediments. Clay minerals (< 2 μm) are primarily crystalline aluminum or magnesium silicates with stacked-layer structures. Each unit layer is in turn a sandwich of silica and gibbsite or brucite sheets (Stumm, 1981).

There are many different types of clay minerals, but the major part of them can be grouped into four main categories: montmorillonites, illites, kaolinites, and the vermiculites (Stevenson, 1994). As natural inorganic exchangers, montmorillonites, illites and vermiculites belong to the 2:1 clay family and their basic structural unit is composed of two tetrahedrally coordinated sheets of silicon ions surrounding a sandwiched octahedrally coordinated sheets of aluminum ions; they are also called three-layer clays. Kaolinites belong to the 1:1 clay family and have two-layer crystals (silicon-oxygen tetrahedral layer joined to alumina octahedral layer). Because of their structure characteristics, 1:1 clay minerals have excellent sorption properties and possess available sorption sites within its interlayer space (Wu *et al.*, 2009).

The potential for specific sorption and fixation of cations is typical for vermiculite, montmorillonite and other clay minerals with a 2:1 crystal lattice. Regarding Cs sorption, the group of illites is of special importance. Illites contain (in weight %) about 50–56 % SiO_2, 18-31 % Al_2O_3, and Fe_2O_3 (2 –5 %), TiO_2 (0–0.8 %), CaO (0–2 %), MgO (1–4 %), K_2O (4–7 %) and Na_2O (0–1 %) (Schachtschabel et al., 1989). They have a strong potential for selective sorption of Cs from aqueous solution and for almost irreversible incorporation at specific interlayer sites of their crystalline structure (Alexakhin and Krouglov, 2001; Comans at al., 1991; Cremers *et al.*, 1988). This is one of the reasons for the strong fixation of Cs in the sediment of many lakes (Kaminski et al., 1998).

Sediment clay content is important because Cs sorption is largely a surface area phenomenon: the greater the proportion of fine-grained clay particles, the more surface area there is for Cs to be sorbed to. However, there are several different binding sites in soils which have different selectivity and energies of sorption (Cremers *et al.*, 1988).

A simplified model of an illic clay mineral particle is shown in Fig. 1.2.
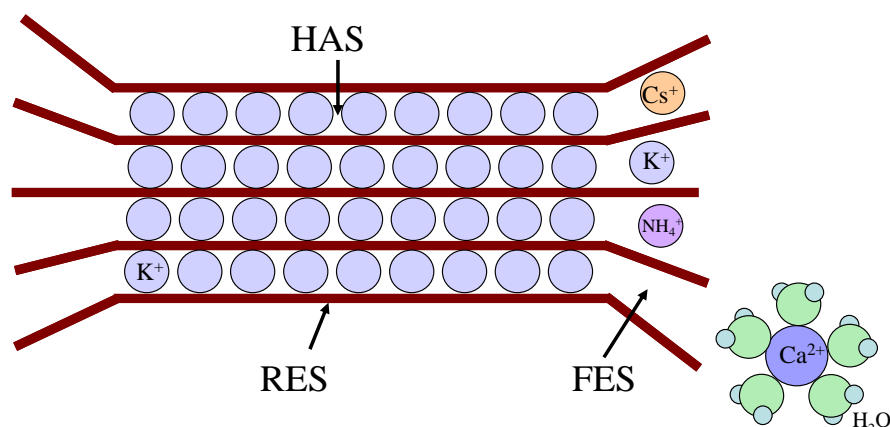
Fig. 1.2. A model of an illic clay mineral particle.

In Fig. 1.2 the brown lines represent the silicate layers and the light blue balls depict the potassium cations. The Regular Exchange Sites (RES) are located on the external planar surfaces of crystal lattice of the clay particle and are characterized by low selectivity. The highly selective sorption sites are located on the internal surfaces of crystal lattice of a clay particle. They are characterized by the presence of wedge-shaped zone with partially expanded edges and are called Frayed Edge Sites (FES). High-Affinity Sites (HAS) are located in the interlayer space of a clay mineral particle.

Cations such as Cs^+, K^+, and NH_4^+ have low hydration energy, therefore, they can easily loose their hydration sheath and enter the frayed edge sites. Only these cations are competitive for exchange on these sites, because divalent cations such as Ca^{2+} and Mg^{2+}, which are surrounded by a large and stable hydration shell, cannot enter the FES zone. Even for cations with low hydration energies, the sorption of Cs^+ by the FES is favorable (Kaminski et al., 1998). The sorption selectivity of monovalent ions declines in the following order: $Cs^+ > Rb^+ > NH_4^+ > K^+ > H^+ > Na^+$.

Caesium ions can be desorbed from frayed edge sites by ion exchange described by the following reaction (Cremers *et al.*, 1988):

$$FES\text{-}M^+ + Cs^+ <=> FES\text{-}Cs^+ + M^+,$$
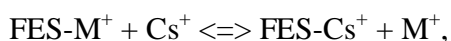
where the major metal (M^+) competing for ion-exchange sites is generally K^+ in soils (Cremers *et al.*, 1988) and NH_4^+ in anoxic sediments (Comans *et al.*, 1991). However, in

natural environment the influence of NH_4^+ is more important because the affinity to the selective sorption sites of NH_4^+ cations is about 5 times higher than the affinity of K^+ (De Preter, 1990; Wauters *et al.*, 1996).

The process of Cs exchanging with the competing ions is considered to be responsible for the redissolution from sediments in some lakes, especially NH_4^+ (Kaminski *et al.*, 1998).

1.2.2 Binding of radiocaesium on humic substances

Clay minerals under natural conditions are associated with varying amounts of organic matter. Humic substances are major components of the natural organic matter in lake sediments. They are complex and heterogeneous mixtures of polydispersed materials formed by biochemical and chemical reactions during the decay and transformation of plant and microbial remains. Humic substances are very important components that affect physical and chemical properties of the aquatic systems, e.g. pH and alkalinity, as well as bioavailability of chemical elements (Hessen and Tranvik, 1998). They act as soil stabilizers, sorbents for toxic metal ions and radionuclides; when leached into surface water, they bind and transport metal ions (Celebi *et al.*, 2009).

In soils and sediments humic substances usually can be divided into three main fractions distinguished by their solubility and adsorption properties: humic acids (soluble in alkali but insoluble in acid), fulvic acids (soluble in both alkali and acid) and humin (insoluble under the full range of pH). Structurally the three fractions are similar, they appear to differ in molecular weight and functional group content (Stumm and Morgan, 1981). The elemental composition of humic substances is approximately 50 % of carbon, 4–5 % hydrogen, 35–40 % oxygen, 1–2 % nitrogen, < 1% sulfur plus phosphorus (Tipping, 2002).

Despite a very high exchange capacity of humic substances, organic fraction of soils and sediments has a low capacity to fix Cs and similar cations (Alexakhin and Krouglov, 2001). Even though the negatively charged groups of humic substances sorb Cs ions via the ion-exchange mechanism, this sorption is much weaker as compared to the sorption of Cs by clay minerals. Caesium adsorption on clay minerals is strongly specific, whereas adsorption on humic substances is non-specific (Cremers *et al.*, 1988). Therefore, even if

organic matter is responsible for a large proportion of soil exchange capacity, radiocaesium will be preferentially adsorbed on clay minerals and its association with organic matter will be relatively unimportant (Alexakhin and Krouglov, 2001).

One of the main reasons for slow fixation of Cs in organic soils is their high content of humic substances. On the one hand, being adsorbed on the surface of clay particles, molecules of humic substances hinder sorption of Cs ions on the FES and their diffusion into the interlayer positions. On the other hand, being adsorbed on the edges of the mineral crystal lattices or in the edge-expanded zones, humic molecules stabilize the layers in an expanded state and this prevents interlayer collapse. If interlayer collapse does not occur, Cs ions adsorbed in the FES are strongly retained on the internal surfaces of layered minerals but are not immobilized.

Several investigations were done to study the effect of humic substances on the fixing capacity of clay minerals (Maguire et al., 1992; Staunton, S. and Rouband, M., 1997). It was shown that the addition of humic substances to the reference clays decreased their affinity for radiocaesium, and no differences were revealed between the actions of humic and fulvic acids. The presence of humic substances in soil and sediments could potentially inhibit Cs sorption onto clay minerals by blocking ion-exchange sites, or, alternatively, the functional groups of the organic matter could themselves participate in ion-exchange processes.

2. CHARACTERISTICS OF LAGO MAGGIORE

2.1 Origin and morphology

Lago Maggiore, also called Lago Verbano, with a surface area of 212.5 km^2 is the second largest pre-alpine lake after Lake Garda. It is located in the southern rim of the Alps. The maximum length of the lake along its thalweg (a line drawn to join the lowest points along the entire length of a streambed or valley) is 66 km, the maximum breadth is 12 km, with a perimeter of 170 km. Lago Maggiore lies at a latitude of 45°57' North, at a longitude of 8°33' West (Greenwich) and at an altitude of 193.5 m above sea level (Bonomi *et al.*, 1970). The most important morphometric characteristics of Lago Maggiore are presented in Table 2.1.

Table 2.1. Main morphometric and hydrological characteristics of Lago Maggiore.

Catchment area (km^2)	6 599
Mean altitude of catchment (m a.s.l.)	1 283
Lake area (km^2)	212.5
Percentage of glacial areas (%)	1.06
Ice cover in catchment area (km^2)	7.3
Lake length (km)	54
Length along the thalweg (km)	66
Mean width (km)	4
Maximum breadth (km)	12
Shoreline length (km)	170
Lake volume (km^3)	37.7
Maximum depth (m)	370
Mean depth (m)	177.4
Depth of cryptodepression (m)	177

The most interesting feature of all the basins of the sub-alpine lakes is the effect of glacial divergence. Thus, Lago Maggiore was formed over a period of about 100 000 years through excavation by two Würmian glaciers which moved down from the Alps and along the valleys of the rivers Ticino and Toce (de Bernardi *et al.*, 1984). The erosive power of these glaciers (approximately 1200-1500 m thick, moving at a speed of

5-10 m per day) is well shown by the depth of the lake (mean value 177.4 m; maximum value 370 m, corresponding to a cryptodepression – the deepest point of the lake bottom below sea level – of 177 m). However, the Toce glacier, the smaller of the two, was less effective in scouring out its own valley which consequently overhangs the valley of the Ticino by about 160 m (Barbanti *et al.*, 1963).

The lake is approximately 15 000 years old and it is a typical, very elongate piedmont lake. In Table 2.2 data about the areas corresponding to, and volumes between, successive isobaths are presented, which shows a U-shaped transverse profile.

Table 2.2. Areas corresponding to, and volumes between, successive isobaths of Lago Maggiore (Bonomi *et al.*, 1970).

Isobath	Area in km^2	Volume in km^3
+ 193	212.5115	3.653
+ 175	193.5276	4.633
+ 150	177.2445	4.262
+ 125	163.9275	3.888
+ 100	147.2500	3.406
+ 75	125.5525	2.974
+ 50	112.5000	2.666
+ 25	100.8800	2.409
0	91.8925	2.210
- 25	85.0050	2.015
- 50	76.2510	1.761
- 75	64.7650	1.419
- 100	49.1350	1.297
- 125	35.1550	0.821
- 150	30.5400	0.276
- 175	1 8850	0.0019
- 177		
Total volume, km^3		37.692

The southern end of Lago Maggiore is dammed by chains of moraines which account for bottom irregularities not present elsewhere in the lake bed. Small islands in the lake are remnants of a few rocky hills which were not planed away by the glaciers (de Bernardi *et al.*, 1984). The abundant amount of clastic or detrital materials is carried into the lake by the main tributaries which have modified the original shoreline (de Bernardi *et al.*, 1984).

2.2 Hydrological and geological features of the drainage basin

The drainage basin of Lago Maggiore covers 6 599 km^2. As much as 50 % of this area lies above 1283 m above sea level, and 1.1 % of it is composed of glaciers. The drainage basin belongs to Italy (3229 km^2) and to Switzerland (3370 km^2) in equal shares, while 80 % of the lake belongs to Italy and 20 % to Switzerland.

The basin of the lake is divided into sub-basins which consist of several lakes and reservoirs, nine of them having an area exceeding 0.5 km^2. There are 32 reservoirs and lakes with the total capacity more than half a million cubic meters formed by damming a valley, and five (Lago Ghirla, Lago d'Orta, Lago di Varese, Lago Comabbio and Lago Monate) have to be considered as natural lakes. The largest of these lakes – Lake Lugano and Lago di Varese – are eutrophic. Lago d'Orta has been studied for several decades due to severe industrial pollution by copper and ammonia (de Bernardi *et al.*, 1984).

Lago Maggiore is divided into two parts by the so-called 'Insubric line" which is the most important tectonic line crossing the southwestern part of the Alpine system and marks the northern and western boundary of the Southern Alps. This is the result of the collision between the African and the Eurasian plates which formed the Alps. Thus, eastern and western shores of the lake, south of the Insubric line, differ from one another in relation to their lithological features. The catchment area of Lago Maggiore is represented by a mosaic of eruptive rocks, in particular mostly granites, gneiss, phyllads and calcareous rocks which are the main component of the central part of the catchment area, where the eastern part of the lake and Lake Lugano are situated (Bonomi *et al.*, 1970). The lithological and geomorphological characterization of the catchment area is the background of the chemical characteristics of the waters reaching Lago Maggiore through the tributaries and surface washing of the watershed.

Originally, Lago Maggiore was an oligotrophic lake with a poor supply of nutrients and organic production but during the 1960s it was rapidly eutrophied which caused a shift to a mesotrophic state a decade later; Since the beginning of 1990s, it became oligotrophic again (Calderoni and Mosello, 1996; Prepas and Charette, 2003). See also Viel and Damiani (1985).

Major tributaries to Lago Maggiore are the rivers Ticino (drainage basin 1616.31 km^2), Toce (1550.84 km^2), Maggia (926.10 km^2), and Tresa (754.20 km^2) (see Fig. 2.1). They cover nearly 62 % of the whole drainage basin of the lake and bring to the lake waters coming from a basin reaching its greatest altitudes in the mountainous massifs of Monte Rosa and St. Gotthard (Bonomi *et al.*, 1970).
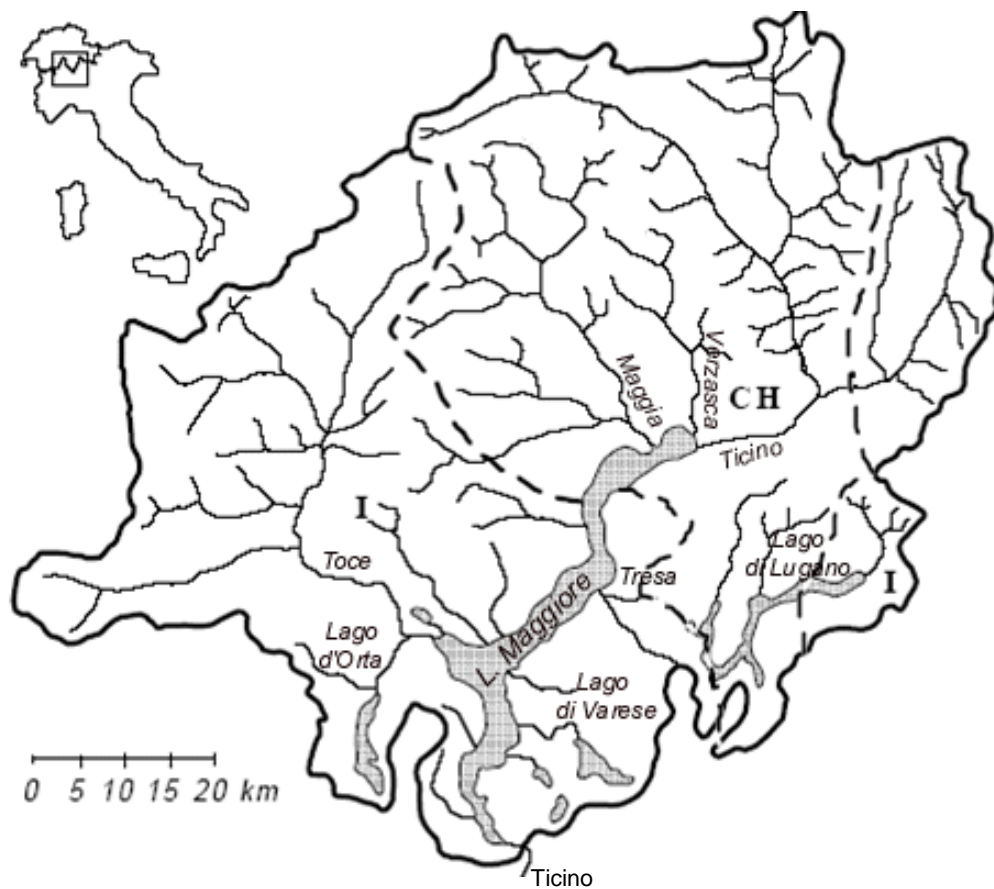
Fig. 2.1. Lago Maggiore and its watershed (Barbieri *et al.*, 1999).

The flows of the main tributaries entering Lago Maggiore are represented in Table 2.3, from which it appears that the mean annual water discharge of the Ticino river (for the period 1921-2000) is 71.1 m^3·s^{-1}, of Toce (1936-2000) 80.2 m^3·s^{-1}, of Verzasca (1990-2003) 10.8 m^3·s^{-1}, while the flow of the river Ticino at the outlet is (1921-1961) 317.8 m^3·s^{-1}.

Table 2.3. Surface area and mean annual water discharge of the main rivers from the watershed of Lago Maggiore (Commisione Internationale per la protezione delle Aque Italo-Svizzere, 2001; Bonomi et. al., 1970; Swiss FOWG).

River	Surface in km^2	Mean annual water discharge in m$^3 \cdot$s^{-1}
Verzasca	263.8	10.8
Tresa	754.2	28.3
Maggia	926.1	40.0
Toce	1550.8	80.2
Ticino	1616.2	71.1
Ticino outlet	6599.0	317.8

The maximum flows correspond to late spring – early summer which is the period of snow melting and of heavy rainfalls. This is connected to the fact that the mean altitude of the catchment area is rater high and that during the winter the bulk of precipitations is captured on the mountains in the form of snow or ice. Consequently, the possibility of a regular and uniform flow of waters into the lake is cut off (Bonomi *et al.*, 1970).

The outlet river Ticino is regulated by a dam which was built in 1942 at a distance of about 6 km from the outflow of the river from the lake. It is a dam with adjustable openings which can be operated horizontally allowing the control of the quantity of outflowing water.

2.3 Climatic and meteorological characteristics

Lago Maggiore belongs to the region which is characterized by high humidity and rather mild winters due to the presence of the lake itself and the Alps, which provide protection from northerly winds. The lowest temperatures are reached in January, with an average of 2.58°C (Barbanti, 1975). Maximum temperatures take place in July, with an average of 21.95°C. Prevailing winds are north-westerly.

From a recent analysis of the meteorological data collected by the Observatory of the Isituto Italiano di Idrobiologia at Pallanza during the period 1950 – 1966 it has been observed that the mean yearly value of precipitations is 1816 mm ranging between 1226 mm (1952) and 3352 mm (1960). At the same time the mean precipitation value for the Italian territory is only about 1000 mm which means that particularly heavy precipitations take place mostly in the catchment area of Lago Maggiore in Switzerland (Bonomi *et al.*, 1970).

Annual variations of the lake temperature are very limited due to the large volume of water. However, thermal conditions do change along the axis of the lake, with higher temperatures at the southern end (mean difference is about 2°C) (Tonolli, 1961). Maximum surface temperatures are reached during July-August.

Due to the location in the temperate zone, the large deep lakes in the pre-alpine areas to the south and north of the Alps are considered as warm monomictic lakes. That means that, in theory, a complete vertical mixing occurs only once a year, at the end of the limnological winter (Ambrosetti *et al.*, 2002). However, due to the great depth of the lake, as well as to the peculiar climatic conditions of the area a complete vertical homogenization of the waters of Lake Maggiore reaching the bottom before the new process of the thermal stratification begins at the surface, does not occur every year. That is why Lago Maggiore can be classified as a holo-oligomictic lake (Ambrosetti *et al.*, 2002). According to de Bernardi (1984), the layer usually involved in the winter overturn is 100 to 150 m deep, whereas a complete mixing occurs only every five to seven years. In studies of Ambrosetti and Barbanti, 1999, it is revealed that the 7-years cycles recorded up to 1970 were followed by period of 28 years (until 1999) during which the winter mixed layer only once (1981) reached a depth of 200 m, with only shallow depths (between 50 and 150 m) being reached

in the other years. The complete circulation of 1999 occurred as a result of a double mechanism with the motions down to a depth of 200 m, and the penetration of colder and more oxygenated waters of outside provenance into the layers below this level. The last complete turnover of Lago Maggiore was in winter 2004 – 2005 (Guilizzoni, personal communication).

If the mixing is complete, a mass of new water is formed with defined chemical and physical characteristics. This newly-formed water mass can retain its properties for several years or for a few months, the duration of its life depending on its initial state and on the kind of external forces that can bring about a change in its properties. This duration has been revealed for Lago Maggiore by an analysis of the heat content below 200 m depth. For example, after the complete vertical mixings of 1963 the water mass retained its properties for 4 years; and after the mixing of 1970, which was much less intense than the earlier one, this maintained only for 14 months (Ambrosetti and Barbanti, 1999).

The theoretical renewal time of the lake water which is calculated form the ratio between the volume of the lake and the outlet water discharge, for Lago Maggiore equals to 4 years. This time depends largely on the morphometric characteristics of the individual basins and of the lake watershed, as well as on the volume of precipitation over the whole area. However, Tonolli (Piontelli and Tonolli, 1964) after analyzing the thermal cycles reached the conclusion that the mean residence time of water in Lago Maggiore was around 14.5 years (Ambrosetti *et al.*, 2002). The same results are reported in the studies of Bonomi *et al.*, 1970.

2.4 Knowledge on the present radioecological situation

After the Chernobyl accident roughly 20 kBq·m^{-2} of ^{137}Cs were deposited onto the lake surface, about the same amount as onto the neighboring Lake Lugano. But in contrast to Lake Lugano or Lake Constance the fate of ^{137}Cs in Lago Maggiore was still practically non-investigated.

With the CNR – Institute of Ecosystem Study (ISE) on its shore, Lago Maggiore has the privilege of being the most thoroughly investigated lake in Italy in terms of the number of key biogeochemical parameters measured and the duration of their monitoring. However, nearly no research studies were performed in respect to radionuclide distribution in Lago Maggiore. Only some data about radionuclides activity in the lake water measured by the Joint research center in Ispra are available (D'Alberti, 2003; D'Alberti 2001–2002; Cazzaniga *et al.*, 1996–1998; Cazzaniga *et al.*, 1997; D'Alberti and Osmani, 1995; Osmani *et al.*, 1994; Dominici and Risposi, 1990–1993; Dominici, 1989 – 1980).

Therefore, in order to examine the ^{137}Cs balance in Lago Maggiore and, in particular, its migration behavior in the sediments by determination of the vertical distribution of ^{137}Cs and its association to the different geochemical fractions, water samples and sediment cores were taken in 2003 – 2005 from different positions and basins of the lake. Our measurements helped to get a more or less complete picture of the present radioecological situation of Lago Maggiore which is a rather complicated ecosystem.

An analysis of soil erosion in the alpine watersheds, of colloidal activity transport and colloid coagulation in river and lake water, as well as Cs activity associated with living objects was outside the scope of this work.

3. MATERIALS AND METHODS

3.1 Description of sampling positions

Bottom sediment cores from Lago Maggiore were collected at 7 locations (Fig. 3.1) in 2003–2005. At each location three cores of about 70 cm length were taken and stored at 4 ℃ in the refrigerator. One of these cores was used for the determination of radionuclide distribution (^{137}Cs, ^{134}Cs, ^{210}Pb, ^{241}Am), another for the ^{137}Cs sequential extractions (see chapter 3.5.2), and the third core was archived.
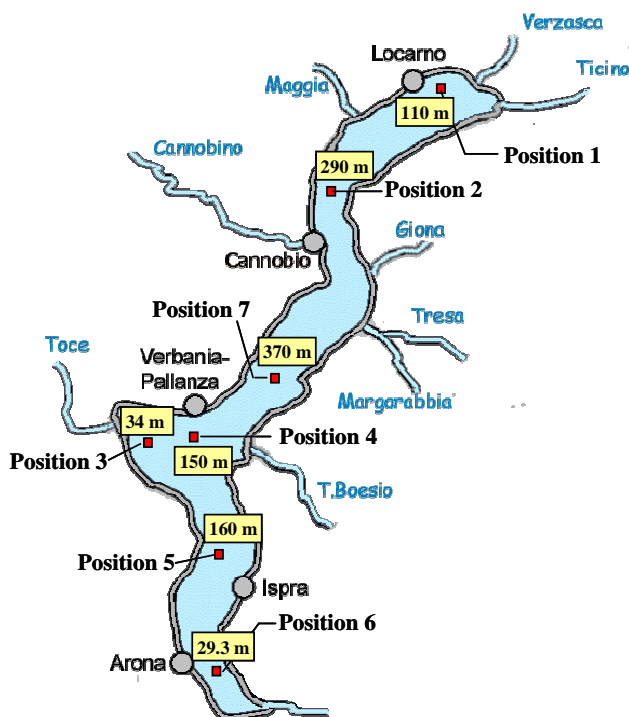
Fig. 3.1. Sampling position (1–7) and main tributaries (in blue) of Lago Maggiore.

Table 3.1 gives the detailed description of sampling sites including the information about geographical position, date of sampling, lake depth, core length and also about the measurements which were performed for the particular sediment core.

Table 3.1. Description of the sampling positions on Lago Maggiore.

Position / Core	Date of sampling	Coordinates	Lake depth in m	Core length in cm	Description of the position
Position 1 Core 1[1] Core 4[1] Core 6[2]	12.05.03	46° 10.03 N 8° 50.20 E	110 96 110	53 54 64	In front of the mouths of the rivers Verzasca and Ticino
Position 2* Core 1[1] Core 2[1] Core 3[2]	12.05.03	46° 05.18 N 8° 42.73 E	285 290 290	71 75 83	In the middle of the basin of Cannobio
Position 3 Core 1[2] Core 2[2] Core 3[1]	26.04.04	45° 54.37 N 8° 30.86 E	34 34 34	35 33 36	In front of the inflow of the river Toce, close to the city Baveno
Position 4 Core 2[1] Core 3[2]	26.04.04	45° 54.84 N 8° 33.02 E	150 146	93 89	Behind the small island Madre
Position 5* Core 2[2] Core 3[1]	26.04.04	45° 50.49 N 8° 35.15 E	160 160	80 65	In the middle of the southern basin of the lake
Position 6 Core 1[2] Core 3[1]	18.04.05	45° 44.55 N 8° 35.11 E	26.3 29.3	39 38	To the south of the city Arona, close to the outlet of the lake
Position 7* Core 1[1] Core 2[2]	18.04.05	45° 56.70 N 8° 37.76 E	370 370	88 74	Deepest position of the lake

[1] – measurement of radionuclides vertical distribution and modeling
[2] – extraction experiments and grain-size distribution
* – large volume water samples

Additionally, at three positions (2, 5 and 7) large volume water samples were collected from different depths including the maximum depth of 370 m.

In spring and autumn of 2004, and also in spring of 2005 surface water samples were taken from three tributaries (Ticino, Toce and Verzasca) of Lago Maggiore.

3.2 Lake water sampling

3.2.1 Sampling of water and suspended matter with the "Midiya" system

Large volume water samples were collected at positions 2, 5 and 7 from Lago Maggiore and its tributaries Ticino, Toce and Verzasca using the "Midiya" filtration system developed in SPA "Typhoon" (Makhonko, 1990) which enables to determine the content of ^{137}Cs both in water solution and in suspended material.

As shown in Fig. 3.3 the "Midiya" system consists of a vibrating submerged pump (315 W electric power), a filter block (with 10 parallel filter sets), a chamber for adsorber, and a flow meter. All these units are coupled by flexible pipes. A transformer regulates the speed of water pumping via the "Midiya" filter unit. The speed of water pumping is varying between 6 and 9 l·min^{-1}.

Fig. 3.3. Large volume water sampler "Midiya" with a pump (in front), a block for filters (in the middle), a chamber for adsorber (left); and a transformer (right).

In this system water samples of several hundred liters were filtered through 10 filter sets working in parallel with the total filtering area of 0.18 m². Each composite filter set consists of 2 paper filters (diameter of 150 mm) – a fast "black ribbon" paper filter (Schleicher & Schuell Company) with pore size of 7-12 µm on top and a slow "blue ribbon" paper filter with an initial pore size of 2 µm below.

In Fig. 3.4 the photo of the "Midiya" system preparation is shown.

Fig. 3.4. Installation of filter sets for large volume water sampling using the "Midiya" system.

Dissolved ^{137}Cs was fixed using an ANFEZH coarse-grained sorbent based on wood cellulose coated with potassium ferrohexacyanoferrate. This sorbent material is highly selective for cesium, and sorption is controlled by an ion exchange mechanism (Lehto et al., 1990). The capacity of the ANFEZH exceeds the concentration of radioisotopes found in natural waters by many orders of magnitude. An important attribute of this sorbent is that it has very low distribution coefficients for the major and minor salts (i.e., Na^+, K^+, Mg^{++}, Ca^{++}) commonly present in lake water. This means that large volumes of water can be processed to extract radioisotopes without loading the sorbent with unwanted salts.

In Semizhon (2005) the ^{137}Cs sorption efficiency (determined from the ratio of its activity measured in the sorbent to its activity in the solution being passed through the sorbent) of the ANFEZH material was tested. For the lake water it was determined as > 90 % which is rather high and is in agreement with the value asserted by the producers. This result is also comparable with the values reported in Bandong *et al.* (2001) which are (96.2 ± 0.8) % and (97.9 ± 1.4) % for river and sea water, respectively.

Steinmann et al. (1999) showed with [7]Be as an example that colloids play an important role in the scavenging of metal-ions from lake surface waters. With a "Midiya-system" the dissolved activity and the activity bound to colloids could not be separated. It has to be kept in mind that in this work the dissolved activity always includes the colloidal activity.

Description of handling, storage and measurement of sample

The quantity of the particulate material (suspended matter) can be estimated by the difference in mass of the filter before and after sampling. To get proper results, a special treatment of the filters and sorbent material is required.

Before the measurement each set of filters is dried separately at 60°C for 12 hours and afterwards kept in an exiccator for 1 day to reach an equilibrium in their weight. Ready filters are placed one by one into the sections of the filter column in the way that they are set out in parallel to the water flow. *After* sampling the composite filters, once delivered in the laboratory, are dried at 60°C for 24 hours and afterwards kept in the exiccator for 1 day. In fact, weighing of the filter before and after sampling (with regard to humidity absorption, accidental dust inclusion) brings the largest uncertainty in the calculation of the specific ^{137}Cs activity.

The preparation of the adsorber is provided immediately *before* sampling and consists in the saturation of the sorbent with water. Thus, in a 1 litre plastic beaker which is filled with a 200 g portion of dry adsorber (preliminary measured gamma-spectrometrically for ^{137}Cs-background), hot water (90–100 °C) is poured in small portions, while constantly mixing. Afterwards, the wet adsorber is put into the chamber. *After* sampling the wet adsorber is put back into the 1 litre plastic beaker.

Both filters and used adsorber are measured gamma-spectrometrically for ^{137}Cs using HPGe detectors as described in chapter 3.5.

3.2.2 Pore water sampling

The top 20 cm sediment layer of a sediment core was used for the pore water separation at each sampling position of the lake. The lake water left above the sample in the corer was carefully removed. Subsequently, the pore water was filtered (0.45 µm) and brought to the laboratory for the measurement of potassium and ammonium concentrations.

3.2.3 Temperature, pH, oxygen concentration measurements

For the determination of temperature, pH, dissolved oxygen content and concentration of main competing ions, water samples were taken from different depths of the lake using Niskin-bottles (Niskin, 1962) shown in Fig. 3.5.
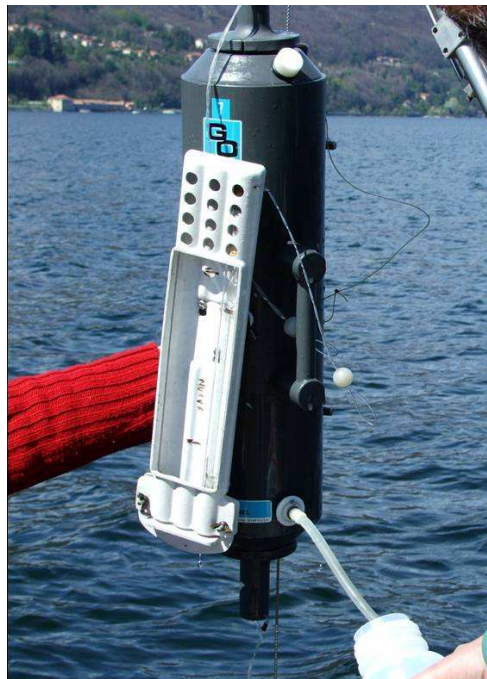
Fig. 3.5. Niskin-bottles used for water sampling from different depths of Lago Maggiore.

Such water parameters as temperature, pH and oxygen content were measured directly on the boat. For the *oxygen* concentration analysis a sensor (Mettler Toledo MO128) with automatic temperature balancing was used. During the measurement, the sample should be stirred with constant speed of about 20 cm·s^{-1}. Due to a low accuracy of the oxygen meter application, the oxygen concentration values appeared to be somewhat lower than they really were (see chapter 4.1).

The *pH* values were determined using a pH-sensor (Mettler Toledo MP120) with a silicaglass membrane. The automatic temperature balancing is controlled by integrated temperature sensors.

3.2.4 Distribution coefficient and competing ions

The partitioning of ^{137}Cs between solid and liquid phases in the lakes is often described by the distribution coefficient, K$_d$, which is an *equilibrium* parameter and can be given as a ratio of the concentration of adsorbed activity to the activity in the solution (pore water):

$$K_d = \frac{^{137}Cs \ (Bq\,/\,kg \ \text{in solid phase})}{^{137}Cs \ (Bq\,/\,l \ \text{in liquid phase})}. \tag{3.1}$$

The distribution coefficient varies depending on cationic composition of the water. Potassium and ammonium are the main competitive ions for Cs exchange, especially on frayed edge sites as described in chapter 1.

The measurements of the concentrations of K$^+$ and NH$_4^+$ in the lake and pore water were performed in the chemistry laboratory of the Hochschule Ravensburg-Weingarten, (Germany) and in the Spiez laboratory (Switzerland).

The concentration of NH$_4^+$ was measured in the laboratory using a spectrophotometric technique (Krom, 1980). Such analysis is based on the formation of a dyes which is produced in the reaction of NH$_4^+$ with hypochlorite and sodium salicylate at a pH=12.6

(in the presence of sodium nitroprussid as a catalyst). The extinction of light in the dye solution is a measure for the NH_4^+ concentration.

Potassium was determined using ICP-emission spectrometry (Spiez laboratory, Switzerland) and chromatography methods (Radioecological laboratory, Weingarten).

3.3 Sediment sampling

3.3.1 Sampling of sediments with a gravity corer

Bottom sediment cores from Lago Maggiore were collected at 7 locations (Fig. 3.6.A) in 2003–2005 using a gravity sampler (Meischner and Rumohr, 1974) with an inner diameter of 5.8 cm or 6.0 cm. The boat from CNR-Instituto per lo Studio degli Ecosystemi (Verbania Pallanza, Italy) was equipped with a revolving crane with a steel rope where the gravity corer was fixed (Fig. 3.6.B).
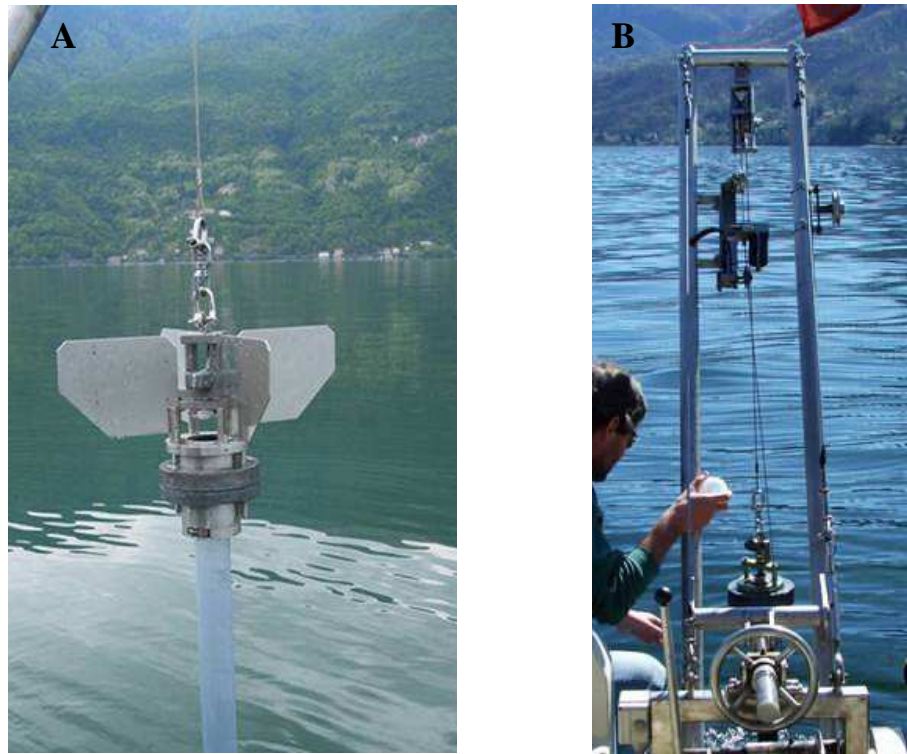
Fig. 3.6. A: Gravity sampler with a PVC-tube. **B:** Crane with a steel rope used for the bottom sediment sampling on Lago Maggiore.

The length of the rope and the lake depth are indicated, and when the corer is about 1–5 meters above the ground (depending on the sediment state), the crane is stopped and brought then on maximal speed so that the sediment gravity corer can bore itself into to the ground. While boring the valve on the upper part of the corer is opened so that the water can pass the PVC-tube without hindrance. After the sampler got into the sediment

the valve will be closed. The mechanism of closing the valve is performed by an extra weight which is transported down along the steel rope. Being closed, the valve prevents the sediment material of moving out of the PVC-tube while lifting. Directly after emerging the lower end of the tube is closed with a plastic tube cap. To keep the sediment core undisturbed it is fixed on the top with a soft foam material which absorbs the water and keeps the sediment material in position (Fig. 3.7).

Afterwards, both ends of the PVC-tube are secured additionally with adhesive tape.

Fig. 3.7. Closing the PVC-tube with the sampled sediment material using a soft foam material with absorbing properties.

3.3.2 Sediment samples preparation for gamma-spectrometry

In order to determine the vertical distribution of radionuclides in the sediment, first each sediment core was split longitudinally. For this purpose, an empty PVC-tube was cut lengthwise in advance. To keep both halves together some adhesive tape was used.

After careful pushing the sediment material out of the tube into one prepared half, it should be tightly closed with the second half. Using two thin metal sheets the sediment core is cut as it is shown in Fig. 3.8. Afterwards, the divided parts are photographed.

Fig. 3.8. Preparation of the sediment samples: lengthwise cut of the sediment core using metal sheets.

Fig. 3.9. Sediment slicing device.

Before slicing the sediment core, the longitudinally cut parts should be left for 1–2 days at open air to make the material drier which makes the further sample preparation easier. Later, using the sediment slicing device (Fig. 3.9), the sediment core was sliced in layers

31

of 1 cm thickness as shown in Fig .3.10. Each sample was placed in polyethylene boxes (50 ml), freeze dried, and homogenized by grinding in a mortar. Before analyses, the dry weight and accordingly the bulk density of the samples were determined.
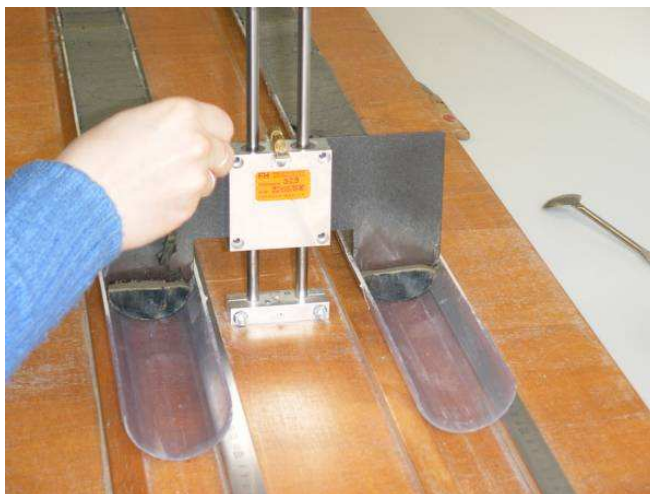
Fig. 3.10. Cutting the sediment core into 1 cm thickness layers using the sediment slicing device.

Afterwards, each milled sample was mixed with paraffin powder (1 part of sediment material and 10 parts of paraffin). After thorough mixing, each sample was pressed to a pellet (diameter of 105 mm) as can be seen in Fig. 3.11 (A–C).

Each pellet was wrapped and glued in aluminum foil (Fig. 3.12) in order to obtain equilibrium between ^{222}Rn and ^{214}Pb (see chapter 3.6) and to prevent the diffusion of gaseous ^{222}Rn out of the sample. Afterwards, pellets were stored for a period of more than five half-lives of ^{222}Rn (half-life 3.8 days) in order to obtain equilibrium between ^{222}Rn and ^{214}Pb.

The described method of sample preparation has several advantages: low amounts of sediments are distributed homogeneously into a known geometry, self absorption in the sample can be calculated as the main material is paraffin and due to the radioactive equilibrium there is a choice of radionuclides which can be detected gamma-spectrometrically (see next subchapter 3.4).
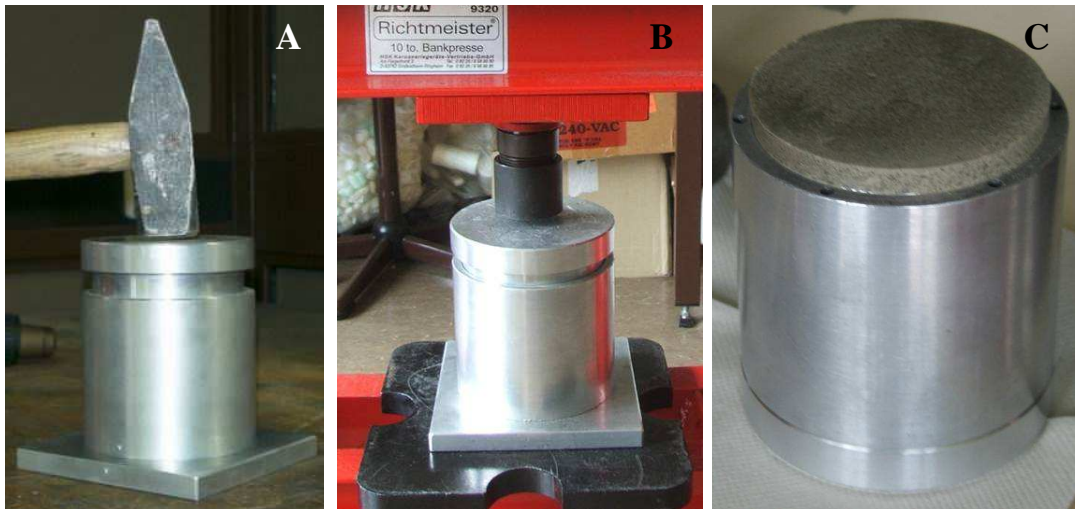
Fig. 3.11. Paraffin pellet preparation: pressing the sample (A, B), ready pallet (C).

Fig. 3.12. Photo of an opened paraffin pellet which was wrapped and glued into aluminium foil.

At each position only one core was studied for the vertical distribution of radionuclides. At positions 1 and 2, additional sediment cores were opened and dried and homogenized samples were measured γ-spectrometrically for ^{137}Cs in polyethylene boxes (50 ml) without further treatment.

3.4 Gamma-spectrometric analyses with BEGe detectors and LabSOCS

All water and sediment samples from Lago Maggiore were analyzed γ-spectrometrically with *B*road *E*nergy *Ge*rmanium (BEGe-5030) detectors of Canberra-Eurysis. The detectors have an active surface area of 50 cm^2 and a thickness of 30 mm. They are characterized by large detection efficiency over a wide range of energies (from 5 keV up to 2 MeV). This allows detecting radionuclides with low energies such as ^{210}Pb or [241]Am (see Table 3.2) as well as nuclides with high energies such as [40]K or [214]Bi at the same time.

Table 3.2. Radionuclides measured in the sediment samples of Lago Maggiore, their half-lives, energies and emission probabilities (yield).

Nuclide name	Half-live in a	Energy in keV	Yield in %
[7]Be	0.15	477.60	10.5
[134]Cs	2.07	569.32	15.4
		604.70	97.6
		795.85	97.6
[137]Cs	30.07	661.65	85.1
[210]Pb	22.3	46.52	4.05
[214]Bi	1.7	609.13	46.3
		1120.29	15.1
		1764.49	15.8
[214]Pb	2.2	77.11	10.7
		295.21	19.2
		351.92	37.2
[241]Am	432.86	59.54	36.3

The measuring times of water samples (adsorber and filters) varied between 48 and 72 hours (for some samples as much as 96 hours) depending on the ^{137}Cs activity concentration. Counting times for the surface layers of the sediment were shorter (≤ 24 hours) than those for the deeper layers.

The gamma spectrum analysis was done with the Genie 2000 Spectroscopy Software (Version 3.0).

A *M*inimum *D*etectable *A*ctivity (MDA) was always calculated for both the radionuclides which have not been found in the spectrum and those that have been found.

Calculation of single photon peak efficiency of the detector

The single photon peak efficiency of the detector is calculated with the *Lab*oratory *So*urce-less *C*alibration *S*oftware (LabSOCS). It takes into account the self-absorption of γ-rays in samples and beakers, and consequently produces accurate quantitative gamma analysis of samples mostly of any type and size.

The single photon efficiency for specified energies and geometries is calculated by Monte Carlo method. It is based on the simulation of the individual photon path (from its origin inside the source through the material and into the detector). The relative uncertainty of the calculated efficiency is in the order of 5 %.

The LabSOCS program requires a number of characteristics of both sample and beaker as input parameters. Thus, i.e. the geometric form of the beaker (cylinder, box, Marinelli beaker, etc.) has to be determined together with such parameters as the wall thickness of the container and density of the material which this container is made of. The presence of absorbers between the source and detector, multiple layers of sources or non-sources within a container, variable sample densities and distance from the sample to the detector active surface are also taken into account.

Thus, during the single photon peak efficiency calculation LabSOCS takes into account the self-absorption effect of gamma-rays both in sample and beaker, by combining the detector characterization with parameters of the sample and beaker where in the samples are measured.

Using this information the LabSOCS program generates an efficiency calibration file for the specified sample characteristics. This file is used in the analysis of the acquired spectra.

Efficiency calibration was verified with a mixed radionuclide standardized solution (QCYB12064, AEA Technology QSA GmbH).

3.5 Particle-size analysis and sequential extraction of ^{137}Cs

3.5.1 Grain-size distribution analysis

Grain size is the most fundamental property of sediment particles, affecting their entrainment, transport and deposition. Therefore, grain size analysis provides important information about the sediment provenance, transport history and depositional conditions (Blott and Pye, 2001).

There are various methods and techniques employed in grain size determination (by laser granulometry, dry and wet sieving, hydrometer method, pipette method, etc.), but the results obtained using different methods may not be directly comparable as they describe different aspects of particle size. However, all techniques involve the division of the sediment sample into a number of size fractions, enabling a grain size distribution to be constructed from the weight or volume percentage of sediment in each size fraction.

Fine soil (< 2 mm sieved sample) can be generally grouped into three different soil fractions such as sand, silt, and clay, but there are different standards for the classification of the soil by grain size group (Table 3.3).

Table 3.3. Classification of the soil by grain size group according to different standards.

	USDA (US Department of Agriculture)	ISSS (International Soil Society)	DIN 4022 (German Standard)
Sand, mm	0.05 – 2	0.02 – 2	0.063 – 2
Silt, mm	0.002 – 0.05	0.002 – 0.02	0.002 – 0.063
Clay, mm	< 0.002	< 0.002	< 0.002

In the present study the *hydrometer method* according to Gee and Bauder (Klute, 1992) was used. This method is based on a measurement of the soil solution density at different times. In a soil suspension, sedimentation of the different particles takes place with varying sinking speeds depending on their grain size. According to Stoke's law, larger particles sediment first. Hence, the density of the suspension is measured after first sand then silt have settled down below the immersion depth of the hydrometer. Sedimentation time of sand particles in a special 1 liter cylinder (see Klute, 1992) is between 40 s and

80 s (depending on temperature and density). Measurements with the hydrometer are carried out at these times. The percentage of sand in the sample is determined by interpolation between the two measuring points. Sedimentation time of silt particles is between 2.5 hours and 24 hours. Accordingly, measurements with the hydrometer are taken at these times as well, and the percentage of clay in the sample is determined by interpolation between these measured points. Finally, the percentage of silt results from the difference between sand plus clay and 100 %.

The described method was applied to wet sediments.

3.5.2 Sequential extraction of caesium

Sequential extraction experiments attempt to identify where ^{137}Cs is residing within sediments giving in that way an explanation for the mobility of the radionuclide. However, it is known that co-extraction from different phases and incomplete extraction in the single steps might occur (Förster, 1985). But, at least the dominant geochemical associations and differences between sediments from different positions in the lake can be determined. For modeling the vertical distribution (chapter 5) the results from sequential extractions are very informative, first of all for the determination of the fraction of exchangeable and fixed ^{137}Cs.

In 1979 Tessier *et al.* suggested an analytical procedure consisting of chemical extractions for the partitioning of particulate trace metals and radionuclides into five different fractions: the exchangeable fraction, the ones associated to carbonates, to oxides and hydroxides of iron and manganese, to organic matter and the residual fraction. The procedure has been applied to bottom sediments (Tessier *et al.*, 1979). Once the first four fractions have been removed, the residual solid should contain mainly minerals, which may hold radionuclides within their crystal structure.

In Robbins *et al.* (1992) a 5-step extraction procedure is described, in which dissolution of amorphous silicates as an additional step is applied. Caesium radionuclides are soluble, cationic species, which can be readily taken up from solution by biological organisms. As

the amorphous silicates are produced by dying diatoms (microalgae) they could incorporate radionuclides within their structure.

In this work extraction experiments were performed on wet samples using a modified five step extraction procedure according to Robbins *et al.* (1992). The procedure suggested by Robbins *et al.* (1992) was applied to sediments of Lake Constance and Lake Lugano (Kaminki *et al.*, 1998; Klemt *et al.*, 2000). In our research we reordered the step where ^{137}Cs is extracted with oxides and hydroxides of iron and manganese, and the step where ^{137}Cs is extracted with organic matter. The reason of such reordering was to prevent the decomposition of Fe- and Mn-oxides and hydroxides together with organic matter. The modified procedure was successfully used for the treatment of sediments from the river Yenisei (Spasova, 2003). The generalized sequential extraction method employed is given in Table 3.4.

Table 3.4. 5-step sequential extraction procedure.

	Chemical Reagent	**Treatment**	**Phases with target ions**
1.	CH_3COONH_4 (1 mol·l^{-1})	24 hours shaking	Exchangeable ions
2.	CH_3COONH_4 (1 mol·l^{-1}) + HNO_3 (1 mol·l^{-1}), pH $\geq$ 5	Shaking to equilibrium	Carbonates
3.	NH_2OH-HCl (0.2 mol·l^{-1}) in CH_3COOH (25 %)	3 hours shaking	Oxides and hydroxides of iron and manganese
4.	H_2O_2 (35 %) + HNO_3 (1 mol·l^{-1})	3 hours stirring at 75–80 ℃	Organic matter
5.	$NaOH$ (0.2 mol·l^{-1})	40 minutes stirring at 80 ℃	Amorphous silicates

The directly exchangeable ^{137}Cs is displaced by ammonium ions (Step 1), carbonates were dissolved by the addition of hydrochloric acid (Step 2), Fe- and Mn-oxides and hydroxides were extracted by the addition of hydroxylammonium chloride (NH_2OH-HCl) in acetic acid (Step 3), organic matter was decomposed by hydrogen peroxide (Step 4), and amorphous silicates were dissolved in sodium hydroxide (Step 5). The remaining residue mainly consists of clay minerals, feldspars, and quartz.

After each of the extraction steps, the treated sediment samples were centrifuged for 30 min, the supernatant liquid was decanted and then pressure filtered through a 0.45 µm cellulose acetate filter. All prepared extracts were put into plastic beakers (Fig. 3.13) for further gamma spectrometric analyses (see chapter 3.4).
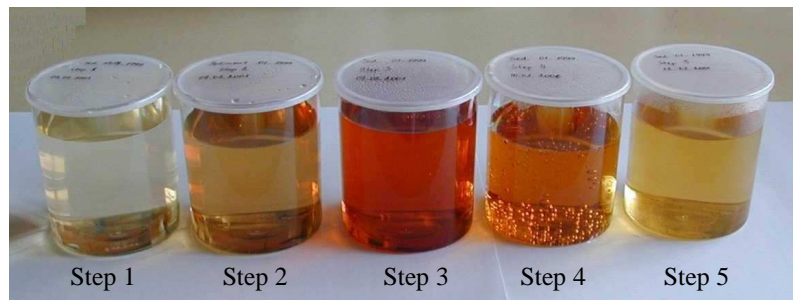
Fig. 3.13. Extracts obtained after the 5-step sequential extraction procedure.

The extraction degree was determined as a ratio between the ^{137}Cs activity concentration in the extract and its concentration in the sediment.

3.6 Determining the age of sediments using ^{210}Pb method

Lake sediments can be considered as the "diary" of a lake: Each year a new layer is deposited on top of the sediment. The particles that have settled on the bottom are covered by new sediment layers and are gradually buried in deeper and deeper sediment layers. The deposited particles form undisturbed lamina in a certain sequence on the bottom, creating in that way an archive recording the history of the lake.

The migration behavior of radionuclides can be analyzed by modeling the input into and the vertical distribution within the sediment. For this purpose a proper depth-age relation has to be established. Often the ^{210}Pb method is used to determine the age of sediment layers from the last 50 to 100 years (Robbins, 1978). By determination of the accumulation rate, the age of sediment from a particular depth in the sediment column can be estimated.

Following the decay of ^{226}Ra which is originally derived from ^{238}U ($T_{1/2}$ = 4.5·10^9 a) ^{210}Pb is produced. The ^{226}Ra chain can be presented as following:

^{226}Ra ($T_{1/2}$=1600 a) $\longrightarrow$ ^{222}Rn (3.8 d) $\longrightarrow$ ^{218}Po (3.1 m) $\longrightarrow$ ^{214}Pb (27 m) $\longrightarrow$ ^{214}Bi (20m) $\longrightarrow$ ^{214}Po (160 s) $\longrightarrow$ ^{210}Pb (22.3 a)
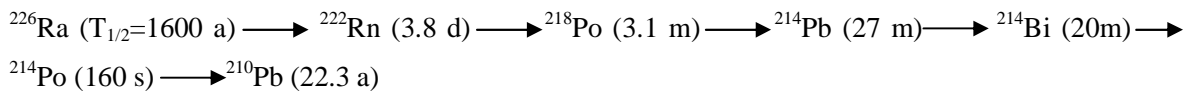
There are two different ways in which ^{210}Pb can be supplied to the sediments.

- ***Deposition from the atmosphere***

When radioactive ^{226}Ra decays (see Fig. 3.14), it produces the radioactive inert gas ^{222}Rn ($T_{1/2}$ = 3.8 d). From all over the world radon gas can emanate from the soils into the atmosphere. Radon concentration integrated over the year is rather constant and it depends mainly on the latitude. After several days residence time in the atmosphere, ^{222}Rn finally decays in the radioactive chain to ^{210}Pb ($T_{1/2}$ = 22.3 years). Minute quantities of ^{210}Pb fall constantly onto land and water surfaces. This material accompanies and mixes with sediments which settle down and accumulate at the bottom of the lake. Here it decays with a 22.3 years half-life and is used for dating. This is the *unsupported* (or 'excess') part of ^{210}Pb.
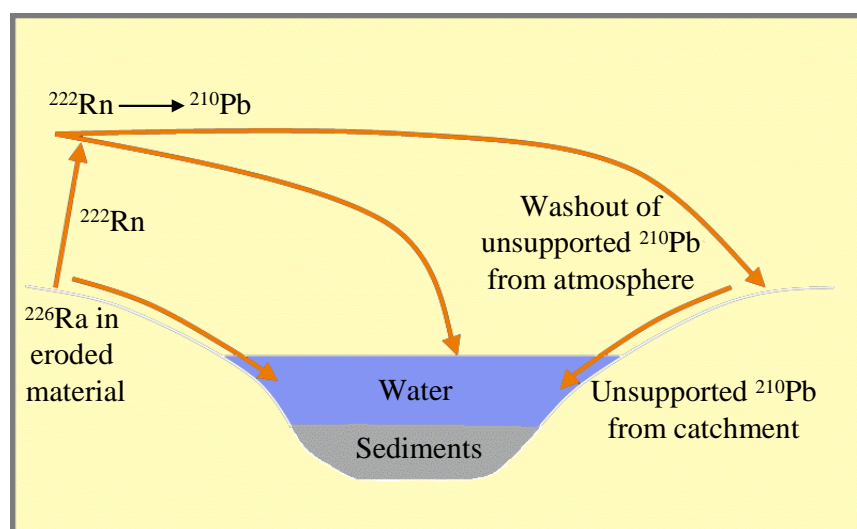
Fig. 3.14. Pathways in which ^{210}Pb can reach lake sediments (by Oldfield and Appleby, 1984).

- *Production within the sediment*

Another part, the *supported* [210]Pb, is produced within the sediment. Here, it is in radioactive equilibrium with [226]Ra that has been directly washed into the lake as part of eroded material. By this way ^{210}Pb is continuously produced and causes a background activity which must be subtracted from the total measured ^{210}Pb activity.

Hence, the unsupported ^{210}Pb activity concentration is obtained by subtraction of the supported [210]Pb (estimated from [226]Ra or its daughters, in particular, by [214]Pb) from the total measured ^{210}Pb at its gamma-line at 46.539 keV ($E = 4.25\%$).

If the sample is sealed so that [222]Rn cannot emanate from the sample (see chapter 3.3.2) in the decay chain [222]Rn, [218]Po, [214]Pb, [214]Bi, and [214]Po due to their short half-lives are in radioactive equilibrium. That means that the members of the radioactive chain have the same activity concentration in the sediment layers and each of these radionuclides can be chosen for the measurement of the supported ^{210}Pb activity concentration. The best candidate for γ-spectrometry is [214]Pb with its major gamma lines 295.2 keV (emission probability $E = 19.3\%$) and 351.9 keV ($E = 37.6\%$). It can be measured with high detection efficiency and the summation effect is low as compared to the other candidate [214]Bi.

In this study two modeling methods are used to estimate the sedimentation history from the unsupported ^{210}Pb: (1) the "constant rate of supply" (CRS) model; (2) the "constant initial concentration" (CIC) model.

3.6.1 CRS and CIC approaches

The **CRS** model assumes that the same amount of unsupported ^{210}Pb per time interval is deposited onto the sediments. So, this model does not require the rate of sediment accumulation to be constant over time. In the calculation of the sediment age at a certain depth, first described in 1978 by Appleby and Oldfield, the cumulative unsupported ^{210}Pb below that depth in a core has to be compared to the total unsupported ^{210}Pb in the core. A series of these age calculations can be used to develop a graph of age versus depth for the core.

$$t = \frac{1}{\lambda} \cdot \ln \frac{A_r(0)}{A_r(x)},$$ (3.2)

where $A_r(x)$ is the residual (cumulated) unsupported ^{210}Pb in the sediment below the depth x in Bq·cm^{-2}; λ is the radioactive decay constant for ^{210}Pb.

In the case of a constant sediment deposition rate CRS model becomes equivalent to **CIC** model which assumes that there is a constant initial concentration of ^{210}Pb from the atmosphere in the top layer of lake sediments. If the flux of ^{210}Pb to the sediment-water interface has remained constant over time and no post-depositional migration of ^{210}Pb has occurred, it is reasonable to suppose that each layer of the sediment will have the same initial unsupported ^{210}Pb activity.

Here the age of sediment layers can be calculated as:

$$t = \frac{1}{\lambda} \cdot \ln \frac{A(0)}{A(x)},$$ (3.3)

where $A(0)$ and $A(x)$ are the initial and present activity concentration of the unsupported ^{210}Pb in the layer at depth x.

The detailed calculations are given in Appendix E.

3.6.2 ^{137}Cs and ^{241}Am method

A complementary method of sediment dating is provided by the fallout nuclides ^{137}Cs and ^{241}Am with their known deposition pattern resulting from extensive testing of the nuclear weapons in the atmosphere in the late 1950s and early 1960s with maxima in 1959 and 1963. An additional more pronounced peak can be found in the upper part of the ^{137}Cs profile, caused by the accident in Chernobyl in 1986. There is no corresponding peak in the ^{241}Am profile, which in fact was not transported in measurable quantities from Chernobyl to Western Europe. The two ^{137}Cs maxima in the fallout related to the years 1963 and 1986 are usually well preserved in sediment profiles and they can be used as time markers.

This method of dating requires complete recovery of the top sediment layers. ^{7}Be with the half-life of 53 days is produced in the atmosphere by cosmic rays and it is expected to be present only in the uppermost sediment layers. The presence of ^{7}Be in the sediments thus ensures complete core recovery. If no mixing occurs, the upper layers in the sediment must be younger than the layers below.

While the ^{210}Pb dating method gives an average accumulation rate for the past 50–100 years, ^{137}Cs is only applicable for the period beginning from the 1960s.

4. MONITORING OF WATER AND SEDIMENTS IN LAGO MAGGIORE

4.1 Water measurements

To have a representative picture of the water body of Lago Maggiore, three deep positions from the center of the northern (position 2), southern (position 5) and middle basins (position 7) of the lake were chosen for water sampling (see chapter 3.2). In the water column at each position dissolved ^{137}Cs, pH, temperature, oxygen, K^+ and NH_4^+ concentrations were measured. The concentration of K^+ and NH_4^+ as main competitors to ^{137}Cs$^+$ ions on the selective sorption sites (e.g. frayed edge sites (FES), at clay mineral particles) were determined both in the lake water and in the pore water of the top 20 cm sediment layer.

To get the information about the inflow of ^{137}Cs to the lake via tributaries, its activity concentration was analyzed in water and transported suspended material of the rivers Ticino, Toce and Verzasca.

The distribution coefficients K_d which relate the ^{137}Cs activity concentration in suspended matter to the concentration in water and pore water are discussed in this chapter.

Additionally, a survey on measurements of ^{137}Cs in water of Lago Maggiore done by the Joint Research Centre (JRC) in Ispra, Italy, during the period from 1986 till 2002 is given. These data in combination with our measurements are compared to the predictions of a model for the runoff from the catchment area (Håkanson, 2004) which was applied to the conditions of Lago Maggiore watershed (Semizhon, 2005).

4.1.1 Concentration of dissolved and particulate ^{137}Cs in Lago Maggiore and its tributaries

The concentration of dissolved ^{137}Cs activity in water and the specific ^{137}Cs activity of suspended particles was determined both, in the lake and its tributaries, with the Midiya system described in chapter 3.2.1.

^{137}Cs in lake water

At position 2 (Fig. 4.1) the ^{137}Cs activity concentration in the lake water increases slightly with depth from 0.56 to 1.47 mBq·l^{-1} (Table 3.1). At other positions it stays rather constant (Fig. 4.2 and Fig. 4.3) and is less than 1 mBq·l^{-1} (Table 4.1).

Table 4.1. ^{137}Cs activity concentrations in water and suspended matter at positions 2, 5, and 7 of Lago Maggiore in 2003–2005.

Location	Date of sampling	Depth in m	Sampled volume in l	^{137}Cs act. conc. in water in mBq·l^{-1}	^{137}Cs act. conc. in susp. matter in Bq·kg^{-1}	Mass of susp. matter in g·(100 l)$^{-1}$
Pos 2	13.05.03	5	606	0.56 ± 0.05	18.7 ± 2.1	0.26
		50	564	0.58 ± 0.05	36.9 ± 16.0	0.03
		100	540	0.80 ± 0.05	180.2 ± 49.4	0.01
		196	402	1.00 ± 0.06	116.6 ± 33.7	0.02
	3.11.03	200	401	0.96 ± 0.08	114.5 ± 22.9	0.02
		275	403	1.47 ± 0.12	130.1 ± 22.2	0.03
Pos 5	27.04.04	5	423	0.58 ± 0.07	16.8 ± 3.1	0.01
		51	582	0.74 ± 0.06	205.4 ± 39.1	0.01
		110	600	0.84 ± 0.05	505.7 ± 63.5	0.01
		154	693	0.69 ± 0.05	217.1 ± 43.2	0.22
Pos 7	19.04.05	2	408	0.66 ± 0.07	-	-
		160	402	0.70 ± 0.07	-	-
		300	398	0.93 ± 0.08	-	-
		369	410	0.63 ± 0.06	-	-

^{137}Cs in river water

The ^{137}Cs activity concentration in tributaries is in the same order as in the lake as can be seen in Table 4.2. The highest value (1.4 mBq·l^{-1}) is observed in the river Verzasca

whereas the lowest concentration (0.2 mBq·l⁻¹) is found in the Toce. A minimum in ^{137}Cs activity concentration in the rivers is related to autumn season whereas a maximum is observed in spring. Such seasonal variations can be explained by the snow melting period, when the transport of caesium from land to water is rather large.

^{137}Cs in suspended matter

At positions 2 and 5 sampled in 2003 and 2004, the ^{137}Cs activity concentration of suspended matter varies from 17 Bq·kg⁻¹ up to 500 Bq·kg⁻¹ (Table 4.1). A similar situation is observed in tributaries of Lago Maggiore. Particularly, in the Ticino, a ^{137}Cs activity concentration of about 30 Bq·kg⁻¹ was measured in a high amount of trapped suspended material. In contrast, in the river Verzasca only 0.02 g of suspended material per 100 liters of water was trapped. Probably, this suspended material has finer grain size which explains the increase of the ^{137}Cs activity concentration there up to a factor of 10.

Table 4.2. ^{137}Cs activity concentrations in the water and suspended material from tributaries of Lago Maggiore in 2004–2005 (according to Semizhon, 2005).

Tributary	Date of sampling	Total volume in l	^{137}Cs act. conc. in water in mBq·l⁻¹	^{137}Cs act. conc. on suspended material in Bq·kg⁻¹	Mass of susp. material in g·(100 l)⁻¹
Ticino	26.03.04	410	0.50 ± 0.06	79.0 ± 5.0	0.25
	13.10.04	405	0.71 ± 0.07	33.1 ± 2.2	0.85
	16.04.05	217	1.18 ± 0.13	101.9 ± 6.7	0.45
Toce	24.03.04	406	0.83 ± 0.07	78.3 ± 3.2	0.73
	14.10.04	411	0.86 ± 0.07	128.9 ± 11.6	0.18
	17.10.05	137	0.20 ± 0.13	87.2 ± 5.4	1.17
Verzasca	14.10.04	401	1.14 ± 0.08	297.6 ± 74.1	0.02
	20.04.05	400	1.39 ± 0.10	70.0 ± 11.9	0.05

Sampling at position 7 was done in spring 2005 after the complete turnover of the lake in winter 2004–2005. There, it was not possible to collect enough suspended material on the paper filters for the determination of the mass and activity concentration of the suspended matter even by pumping of large volumes of water (about 400 liters).

4.1.2 Temperature, pH and dissolved oxygen concentration

At position 2 (Fig. 4.1) in the upper 30 m of the lake there is a warm water layer, the epilimnion, with a temperature of 11–12 $^{\circ}$C and 12–13 $^{\circ}$C in autumn and spring, respectively. In the layer below, the hypolimnion, the water temperature is about 8 $^{\circ}$C for both seasons and it decreases slightly with depth. The thickness of the epilimnion varies during the season due to the ambient air temperature, wind and internal wave activities. In our measurements the thickness of the epilimnion is about 20–30 m. At position 5 (Fig. 4.2) the temperature in the surface water is 10–11 $^{\circ}$C and it decreases down to 7 $^{\circ}$C in the hypolimnion. At position 7 lower temperatures of 7–9 $^{\circ}$C in the epilimnion were measured (Fig. 4.3).

The dissolved oxygen concentration is rather high throughout the water column at all positions (Fig. 4.1 to 4.3). Lago Maggiore is an oligotrophic lake, so there is only little organic matter or other material that could consume oxygen for decomposition or other oxidizing processes. The oxygen concentration varies between 6 mg·l^{-1} and 11 mg·l^{-1} with higher values in the epilimnion. These values are not very accurate and probably a bit too low due to the low accuracy of the application of the oxygen meter used for our in-situ measurements, but they clearly show that we have oxic conditions throughout the water column.

The pH value (about 7) stays rather constant through the entire water column. However, there is a tendency that the pH value slightly decreases with depth which is equal to an increase of the H^{+} concentration. This increase of [H^{+}] could possibly control the small increase of the ^{137}Cs^{+} concentration with depth (Albrecht, 1998).

4.1.3 Competing ions

At all positions the concentration of competing ions [K^{+}] and [NH$_4^{+}$] within the water column stays nearly constant (Fig. 4.1 to 4.3). The values of about 1.5 mg·l^{-1} for [K^{+}] and less than 0.03 mg·l^{-1} for [NH$_4^{+}$] are very small. With the transition from the lake water to the pore water at position 2 these values are substantially increased to 5.2 mg·l^{-1}

for K^+ and more than 9 mg·l^{-1} for NH_4^+. At the other two positions (5 and 7) the increase of potassium is not so pronounced, it is a factor of 2 higher in the pore water than in the lake water. But the concentration of NH_4^+ in the pore water is a factor of more than 50 larger than in the lake water and comparable to the K^+ concentration (Table 4.3).

Table 4.3. The concentrations of competing ions K^+ and NH_4^+ (in mg·l^{-1}) in lake water (several meters above the sediment) and pore water (top 20 cm sediment layer) from different positions of Lago Maggiore.

Competing ion		Pos 1	Pos 2	Pos 3	Pos 4	Pos 5	Pos 6	Pos 7
K^+ (mg·l^{-1})	lake water	–	1.4	–	–	2.0	–	1.6
	pore water	5.3	5.2	4.6	2.9	2.6	2.3	3.9
NH_4^+ (mg·l^{-1})	lake water	–	0.003	–	–	0.025	–	< 0.013
	pore water	8.6	9.6	1.6	1.1	1.2	1.4	1.6
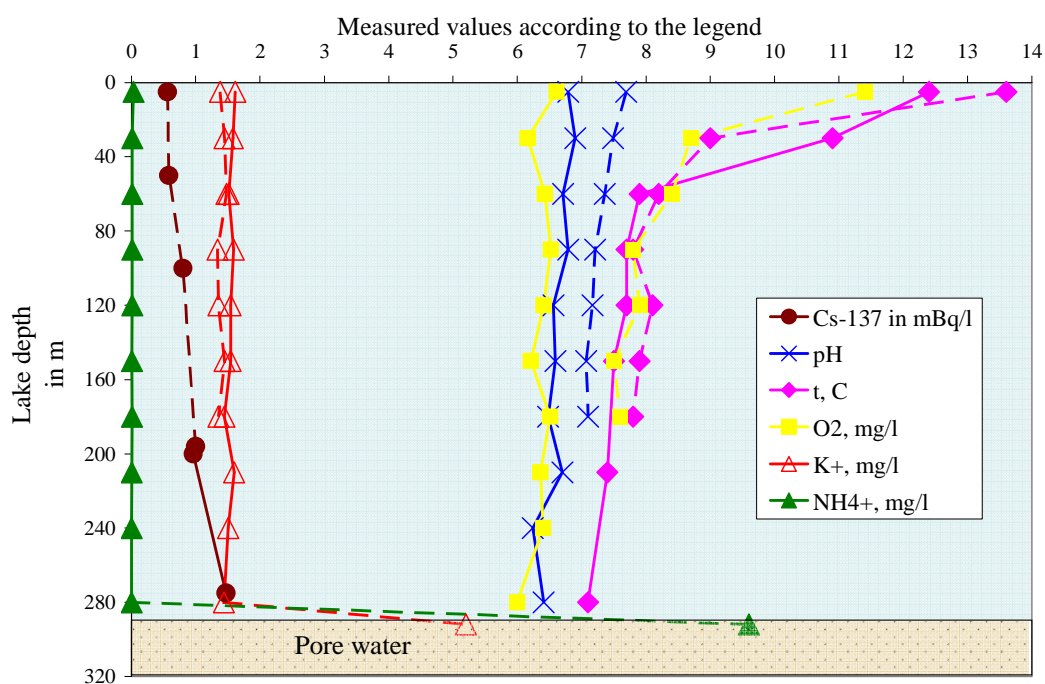
Fig. 4.1. Position 2. Vertical distributions of K^+ (green), ^{137}Cs (brown), NH_4^+ (red) and oxygen (yellow) concentrations, pH (blue) and temperature (pink) in the lake and pore water of Lago Maggiore. Dashed lines – water sampling on 13.05.2003; full lines – water sampling on 3.11.2003.
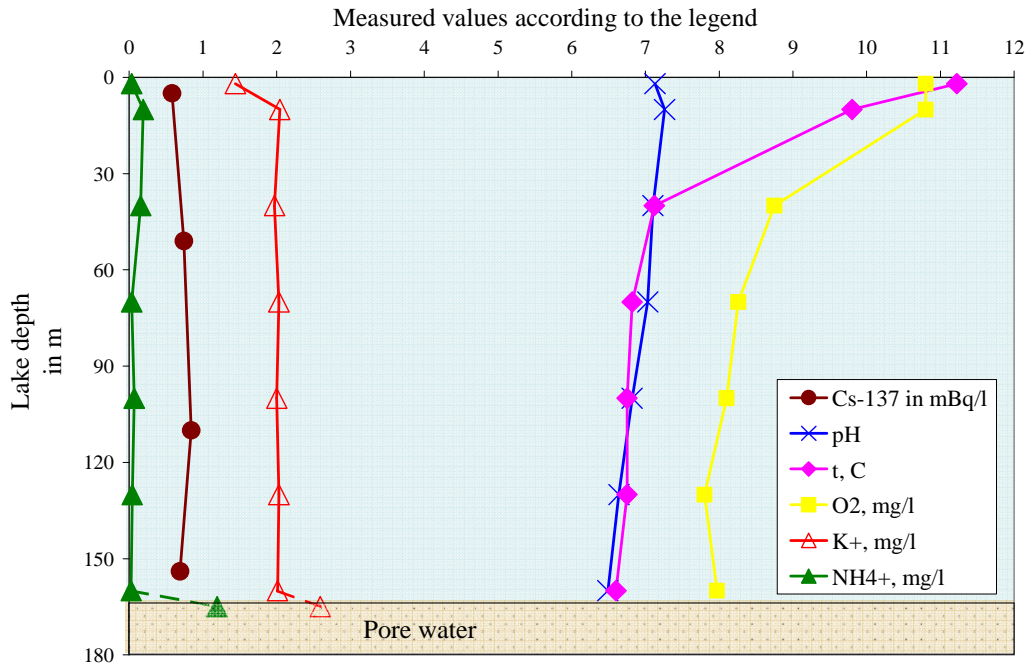
Fig. 4.2. Position 5. Vertical distributions of K^+ (green), ^{137}Cs (brown), NH_4^+ (red) and oxygen (yellow) concentrations, pH (blue) and temperature (pink) in the lake and pore water of Lago Maggiore. Date of water sampling is 27.04.2004.
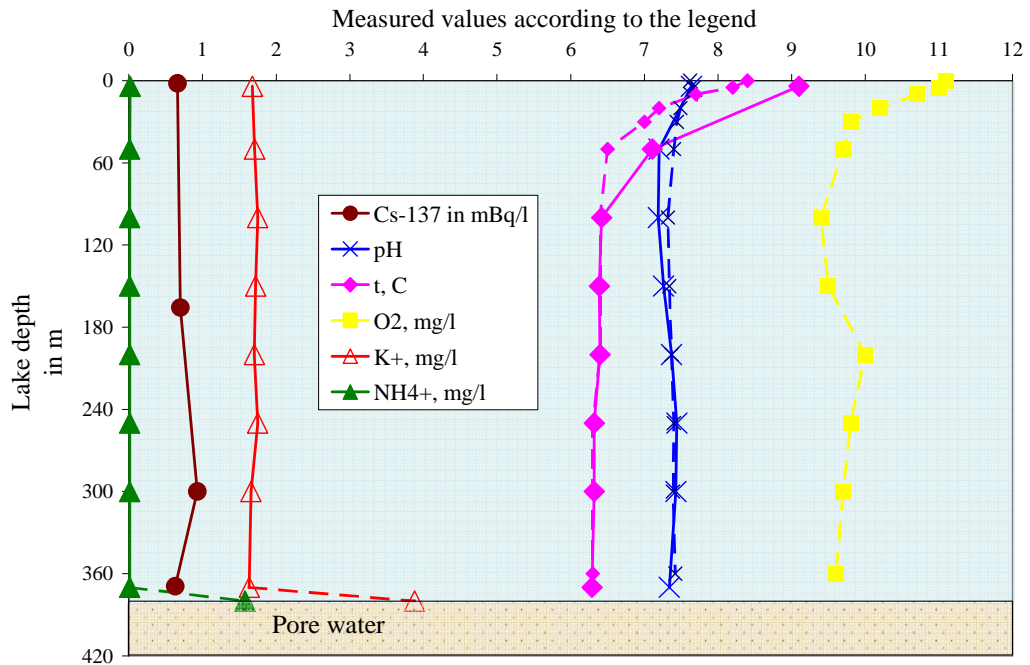
Fig. 4.3. Position 7. Vertical distributions of K^+ (green), ^{137}Cs (brown), NH_4^+ (red) and oxygen (yellow) concentrations, pH (blue) and temperature (pink) in the lake and pore water of Lago Maggiore. Dashed lines – water sampling on 11.04.2005 (P. Guilizzoni, personal communication), full lines – water sampling on 19.04.2005.

The main competing ion at all positions is potassium. A negligible NH_4^+ concentration is the result of the rather large oxygen concentration. However, the increased K^+ and NH_4^+ concentrations in the pore water have an influence on the ^{137}Cs migration by increasing the retarded diffusion in the sediment (see chapter 5).

4.1.4 Measured distribution coefficient K_d

Since the activity concentration of ^{137}Cs at positions 2 and 5 was determined both in water and in suspended matter (Table 4.1) the distribution coefficient K_d in the water column can be estimated (Table 4.4).

In the surface water (upper 5 m) the value of the distribution coefficient is about 30 000 l/kg for both positions while the weighted average over the rest of the water column at position 5 – (328 000 ± 110 000) $l \cdot kg^{-1}$ – is a factor 4 higher than at position 2 – (98 000 ± 12 000) $l \cdot kg^{-1}$. Low K_d values of the upper layer could be explained by a non-reached equilibrium between the ^{137}Cs activity concentration of settling particles and dissolved ^{137}Cs activity in the lake water.

Table 4.4. ^{137}Cs distribution coefficients (K_d) for suspended matter and top layer of the sediment of Lago Maggiore.

		Position 2		Position 5	
K_d ($l \cdot kg^{-1}$)	surface water (top 5 m)	33 000 ± 5 000		29 000 ± 6 000	
	water column	50 m	63 000 ± 28 000	51 m	278 000 ± 57 000
		100 m	226 000 ± 64 000	110 m	602 000 ± 84 000
		196 m	117 000 ± 35 000	154 m	315 000 ± 67 000
		200 m	119 000 ± 26 000		
		275 m	88 000 ± 17 000		
	top 1 cm layer of sediment / lake water	72 000 ± 7 000		136 000 ± 10 000	

Calculating a K_d as the ratio between the activity concentration in the top layer of the sediment and in the deep water results in (72 000 ± 7 000) $l \cdot kg^{-1}$ and (136 000 ±

10 000) $l \cdot kg^{-1}$ at positions 2 and 5, respectively. This is in a rough agreement with the distribution coefficients measured in the water column. As the concentration of both, K^+ and NH_4^+, is clearly larger within the sediment than in the water, lower K_d values are expected there as compared to those in the lake water. The direct measurements of the ^{137}Cs distribution coefficient K_d of about 10^5 $l \cdot kg^{-1}$ in the water column will later be compared to the distribution coefficient which is one of the free parameters of the model described in chapter 5.

Table 4.5 gives the calculated ^{137}Cs distribution coefficients for the tributaries of the lake.

Table 4.5. ^{137}Cs distribution coefficients (K_d) for suspended material in the tributaries of Lago Maggiore.

Tributary	Date of sampling	K_d ($l \cdot kg^{-1}$)
Ticino	26.03.04	$161\ 000 \pm 22\ 000$
	13.10.04	$46\ 300 \pm 5\ 500$
	16.04.05	$86\ 000 \pm 10\ 800$
Toce	24.03.04	$95\ 000 \pm 8\ 700$
	14.10.04	$150\ 000 \pm 18\ 000$
	17.10.05	$435\ 000 \pm 230\ 000$
Verzasca	14.10.04	$262\ 000 \pm 68\ 000$
	20.04.05	$50\ 500 \pm 9\ 300$

Rather strong variations are observed within each river which might be connected with the fluctuations in the water flow which influences the transported particle size fraction.

4.1.5 Other measurements of ^{137}Cs in water of Lago Maggiore and its tributaries

A compartment model of Håkanson (2004) which predicts the run-off of radiocaesium after the direct single-pulse deposition from the catchment area to the lake via tributaries was applied for the conditions of Lago Maggiore. This model comprises two compartments which describe the catchment area:

- Outflow areas or wetlands (upstream lakes, rivers, mires, bogs) with relatively fast turnover of substances and a horizontal transport of ^{137}Cs from land to surface water;

- Inflow areas or dry land dominated by much slower vertical transport processes (first through the soil horizons, then ground water transport, and finally tributary transport to the lake).

A detailed description of the application of the model to Lago Maggiore can be found in the work of Semizhon (2005).

There is a good agreement between empirical data and the model predictions of the ^{137}Cs activity concentration in the tributaries Ticino, Toce and Versasca.

Calibrating the model with the measured data the main parameters were defined for different tributaries and for the whole catchment:

- the initial inventory of ^{137}Cs in the catchment area;

- the percentage of outflow areas in the catchment;

- the soil permeability factor (SPF), which describes the processes of fixation and radiocaesium retention in soil by taking into account soil grain size characteristics;

- the seasonal moderator for the water flow in the tributaries, which creates a seasonal variability in the outflow rate and gives an increased transport of ^{137}Cs from land to the lake during peaks in water flow;

- the average precipitation.

A rather low average ^{137}Cs inventory in the catchment area of 3000 Bq·m^{-2} was determined. However, this value is in agreement with that which is required for other models describing the activity concentration in lake water and sediment (chapter 5.2.2). The fraction of outflow areas in the catchment equals to 5 % and according to Håkanson (2004) can be used for large cultivated catchment areas with a low percentage of wetlands. The default value for soil permeability factor SPF is 40 but it can vary greatly between 1 and 80 (Håkanson, 2000). The more permeable the soil is, the smaller the SPF-

value, the larger the fixation of ^{137}Cs which consequently leads to the fewer amounts of ^{137}Cs remained in soils. The mean annual precipitation is (1830 ± 100) mm per year.

Using these parameters a run-off model was applied also to the conditions of the whole Lago Maggiore watershed. Figure 4.4. shows a comparison between the measured ^{137}Cs activity concentration in the lake surface water (our data in combination with measurements performed by the Joint Research Center (JRC) in Ispra, D'Alberti, 2003; D'Alberti 2001–2002; Cazzaniga et al., 1996–1998; Cazzaniga et al., 1997; D'Alberti and Osmani, 1995; Osmani et al., 1994; Dominici and Risposi, 1990–1993; Dominici, 1989 – 1980) and the catchment area predictions for the run-off (Semizhon, 2005).

During the first year after the accident fallout the prominent difference between run-off model predictions and measured ^{137}Cs activity concentration in the surface water is observed. The higher radiocaesium activity concentration in the surface water during that period can be explained by the fact that the input of ^{137}Cs into the lake (in the epilimnion layer) was not only due to the water flow from the tributaries but also due to the direct ^{137}Cs deposition through the surface of the lake itself.
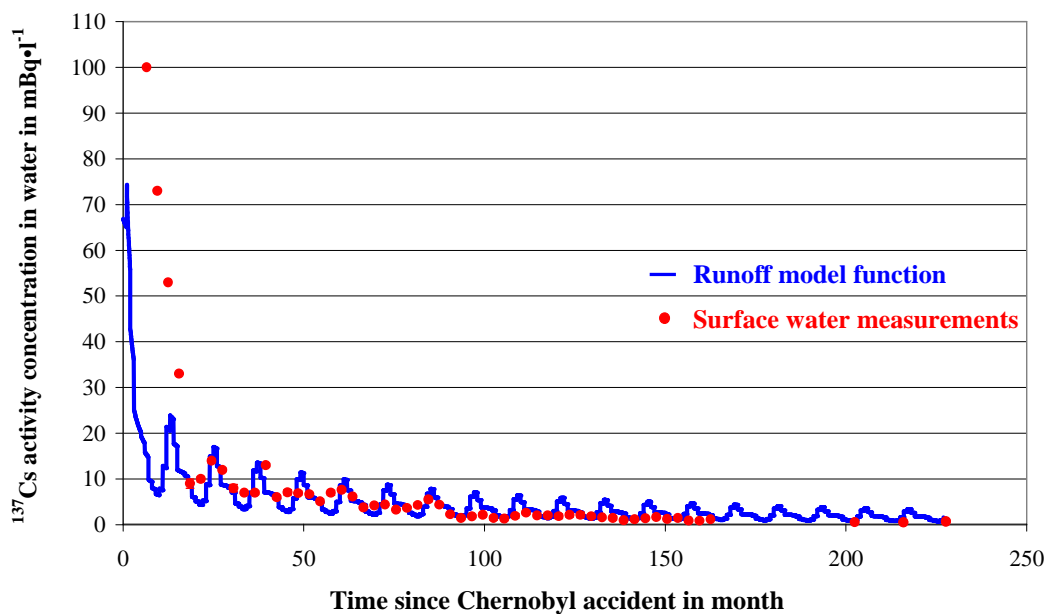
Fig. 4.4. Comparison between measured data (red points) of ^{137}Cs activity concentration in the surface water of Lago Maggiore and the run-off model predictions (blue line with seasonal variations).

54

A good agreement between measured ^{137}Cs activity concentration in the lake surface water and run-off model predictions is observed during the subsequent years. Here, distinct seasonal variations in the tributaries can be seen which are not so clearly observed in the whole lake (Fig. 4.4).

4.2 Vertical ^{137}Cs and ^{210}Pb distributions in the sediments

In the following chapter the measured vertical distributions of radionuclides and bulk density in sediment cores taken in spring 2003, 2004 and 2005 from 7 different positions of Lago Maggiore are discussed. The measured radionuclides are: ^{137}Cs, unsupported ^{210}Pb, ^{134}Cs and ^{241}Am. Whereas ^{137}Cs came into the sediment from the Chernobyl and after nuclear weapons testing fallouts, the unsupported ^{210}Pb (see chapter 3.6) is put into the sediment continuously after ^{222}Rn decay in the atmosphere. ^{134}Cs is related to the Chernobyl fallout in 1986, ^{241}Am to the peaks of the nuclear weapons testing fallouts in the 1960's. Additionally, in all sediment cores the activity concentration of ^{7}Be (which is a cosmogenic radionuclide with the half-life of 53.12 days) was measured for the top 0–0.5 cm or 0–1 cm layers.

The total inventories were determined by summing up the contribution of all sediment layers using the decay-corrected (1.05.1986) specific activity of ^{137}Cs and the corresponding specific weight of each layer. The measured vertical distribution of the bulk density is given in Appendix B.

A general classification of the sediment profiles from different positions will be performed.

4.2.1 Measured vertical distributions of activity concentration and bulk density of sediment cores from different positions

Position 1

Fig. 4.5 and Fig. 4.6 show the vertical distribution of ^{137}Cs in sediment cores taken at position 1 influenced by the rivers Ticino, Verzasca and Maggia. On the right side the photos and vertical distributions of the ^{137}Cs activity concentration within the sediment is shown. The consistence of the sediment material is rather hard so that the gravity corer could sample only 45 cm depth and the total ^{137}Cs inventory was not completely reached (inventory > 33 kBq·m^{-2}, decay-corrected to the 1.05.1986).

In the top layer ^{137}Cs has an activity of up to 100 Bq·kg^{-1}. Only one maximum with more than 600 Bq·kg^{-1} of ^{137}Cs is observed at the depth of 24–26 cm for core 1 (Fig. 4.5) and 17–18 cm for core 4 (Fig. 4.6). In the same layers traces of ^{134}Cs (not plotted) were found (2.1 Bq·kg^{-1}) whereas its activity concentration elsewhere was below the detection limit. At the depth of 45 cm the nuclear weapons testing fallout is probably not yet reached, while the ^{137}Cs activity concentration continues to increase with depth.

In both sediment cores the vertical distribution of ^{137}Cs is not a smooth function and substantial scattering of the ^{137}Cs activity concentration along to the profile can be seen. In Fig. 4.6 one can find light layers (photo) between 3 cm and 7 cm (2 sequential) or one between 32.5 cm and 36 cm which are characterized not only by constant ^{137}Cs activity concentration but also by different bulk density as compared to the neighboring layers. In Fig. 4.5 similar layers can be found between 4 cm and 8 cm (2 sequential) and one between 37 cm and 40 cm with constant ^{137}Cs and clearly different ^{210}Pb activity concentrations.

The bulk density practically does not vary with depth within both sediment cores. The activity concentration of unsupported ^{210}Pb decreases exponentially with depth (the dashed line in Fig. 4.5 for 'Unsupported' ^{210}Pb is an exponential fit to the measured data) from 150 Bq·kg^{-1} down to 50 Bq·kg^{-1}. No ^{7}Be was measured in the top 1 cm layer. Its activity concentration is less than MDA (< 29.5 Bq·kg^{-1}).

Position 2

The position 2 in the basin of Cannobio with 290 m lake depth is presented by two sediment cores. The vertical distributions of ^{137}Cs, and bulk density (cores 1 and 3) and unsupported ^{210}Pb (core 1) are shown in Fig. 4.7 and Fig. 4.8.

Two maxima of ^{137}Cs are recognizable which can be assigned to the fallouts after the Chernobyl accident and the atmospheric nuclear weapon testing fallouts in the 1960's. The ^{137}Cs activity concentration in the Chernobyl peak (6–8 cm for both cores) exceed the value of 1200 Bq·kg^{-1} as compared to that of the maxima after nuclear weapon testing peaks (39–43 cm) where its concentration with about 100 Bq·kg^{-1} is an order of magnitude less. Also ^{241}Am with the activity concentration of 3.5 Bq·kg^{-1}was detected in

the layer 38–39 cm. The total inventory of ^{137}Cs for both sediment cores is about 30 kBq·m^{-2} (decay-corrected to 1.05.1986).

Between 13 cm and 32 cm depth for both cores there is one layer with uniform colour. In Fig. 4.7 the activity concentrations of ^{137}Cs and unsupported ^{210}Pb as well as the bulk density within this layer are constant, and from that we can conclude that this layer corresponds only to one single event. A similar situation is observed in the sediment core 3 (Fig. 4.8).

Excluding the large layer between 13 cm and 32 cm from the common fit, the bulk density is linearly increasing with depth (Fig. 4.7 and 4.8). In the upper 1 cm layer ^{7}Be activity concentration was 29.1 Bq·kg^{-1} and 16.9 Bq·kg^{-1} for core 1 and core 3, respectively.

Position 3

The vertical distributions of ^{137}Cs, ^{210}Pb and bulk density of the sediment core taken at position 3 at depth of 46 m are shown in Fig. 4.9. One clear peak in the ^{137}Cs activity concentration (10–4 cm) is recognized which can be related to the Chernobyl fallout in 1986. This maximum is characterized by rather low specific activity of ^{137}Cs (450 Bq·kg^{-1}). The layer between 2 cm and 5 cm is characterized by very low ^{137}Cs and ^{210}Pb specific activities, and rather high bulk density. There is another layer between 18.5 cm and 20.5 cm (dark layer in the photo) which appears below the Chernobyl peak. Within this particular layer the bulk density has a sudden decrease while the unsupported ^{210}Pb activity concentration increases as compared with the neighboring layers. That is why it appears to be questionable whether this layer can be assigned to the Chernobyl or nuclear weapon testing fallout. ^{241}Am was not detected as its activity concentration is below MDA (3 Bq·kg^{-1}). This is not surprising as the ^{137}Cs activity concentration is only about 100 Bq·kg^{-1}. Below 30 cm the ^{137}Cs activity concentration decreases to zero, and from this we conclude that the layer 20–22 cm can be related to the nuclear weapons testing fallout. The total ^{137}Cs inventory of the sediment core is 20 kBq·m^{-2} (decay-corrected to 1.05.1986).

The bulk density stays nearly constant within the sediment profile. The light brown color of the top 0.5 cm indicates that no sediment was lost during sampling although no [7]Be was detected.

Position 4

Two distinct ^{137}Cs peaks in the sediment core taken at position 4 can clearly be seen in Fig. 4.10. One occurs at a depth of 7–9 cm with a maximum value of more than 900 Bq·kg^{-1}. Some traces of [134]Cs (up to 2 Bq·kg^{-1}) were measured in this layer, so it can be related to the Chernobyl fallout. Another peak with a broader shape is observed in the layer between 15 cm and 20 cm. This layer is due to the nuclear weapon testing fallouts which is proved by the presence of [241]Am (6.8 Bq·kg^{-1}). No ^{137}Cs was found at depths larger than 26 cm. In the top 3 cm (light layer in the photo) the bulk density is higher and ^{137}Cs activity concentration is constant. The specific activity in the top layer is not much larger than in the layers between the Chernobyl and nuclear weapons testing maxima. The total inventory is 15 kBq·m^{-2} (decay-corrected to 1.05.1986).

The bulk density is linearly increasing with depth. In the vertical distribution of unsupported ^{210}Pb some variations of activity concentration are observed in the upper 20 cm. Down to 45 cm it decreases exponentially. No [7]Be was measured in the top 0.5 cm; nonetheless, the upper layer is well recognized in the photo by a distinguished light brown colour.

Position 5

In the sediment core 3 of position 5 taken from 160 m depth, the ^{137}Cs maxima – 2500 Bq·kg^{-1} and 190 Bq·kg^{-1} – can be found in the layers between 10 – 11 cm and 23 – 24 cm for Chernobyl and nuclear weapon testing fallouts, respectively (Fig. 4.11). A very sharp maximum representing the input in 1986 is followed by a tail of enhanced specific activity of ^{137}Cs towards the sediment surface where it is in the same order as the maximum of the nuclear weapon testing peak. [241]Am was found only in one layer (24 cm) where its specific activity is 10 Bq·kg^{-1}. The total ^{137}Cs inventory is 19 kBq·m^{-2} (decay-corrected to 1.05.1986).

Although there is a clear distinction between different sediment layers (photo), there is no clear distribution of unsupported ^{210}Pb and bulk density in the upper 20 cm. Downwards from 20 cm to 45 cm a clear exponential decrease is observed in ^{210}Pb concentrations while the bulk density is increasing linearly.

The activity concentration of [7]Be in the layer 0–1 cm was less than MDA (20.1 Bq·kg^{-1}), nevertheless, in the photo of the sediment in Fig. 4.11 it can be seen that the top layer was not lost.

Position 6

The sediment core taken at position 6 (Fig. 4.12) at 29 m depth is characterized by a considerable broadening of both the nuclear weapon testing peak (10–16 cm) and the Chernobyl peak (2–7 cm). Very low specific ^{137}Cs activities (< 330 Bq·kg^{-1}) are apparent at that position. No [134]Cs was measured whereas at a depth of 11 cm [241]Am was detected with an activity concentration of about 7 Bq·kg^{-1} which is in the order of the MDA. The total ^{137}Cs inventory of 7 kBq·m^{-2} (decay-corrected to 1.05.1986) is very low.

The unsupported ^{210}Pb is decreasing with depth and can be well-described by an exponential function. The bulk density is increasing down the sediment profile. In the upper 0–1 cm layer the specific [7]Be activity was measured. Here, it is about 100 Bq·kg^{-1}.

Position 7

The vertical profiles from the deepest position 7 with 370 m lake depth are shown in Fig. 4.13. The activity maxima of the Chernobyl ^{137}Cs with about 1400 Bq·kg^{-1} (21 cm) and of the nuclear weapon testing ^{137}Cs with 160 Bq·kg^{-1} (35 cm) are well-separated. The Chernobyl peak is very sharp and it is broadened towards the sediment surface with some visible variations in the activity concentration of [137]Cs. At a depth of 36 cm the specific [241]Am activity is about 7 Bq·kg^{-1}. The total ^{137}Cs inventory at this position is about 33 kBq·m^{-2} (decay-corrected to 1.05.1986).

The vertical distribution of unsupported ^{210}Pb is varying substantially. Some layers (10–12 cm, 15.5 – 18.5 cm, and 53–66 cm) can be found with very low specific ^{210}Pb activity and high bulk density at the same time. [7]Be was measured in the top layer (0–1cm) and its activity is about 11 Bq·kg^{-1}.
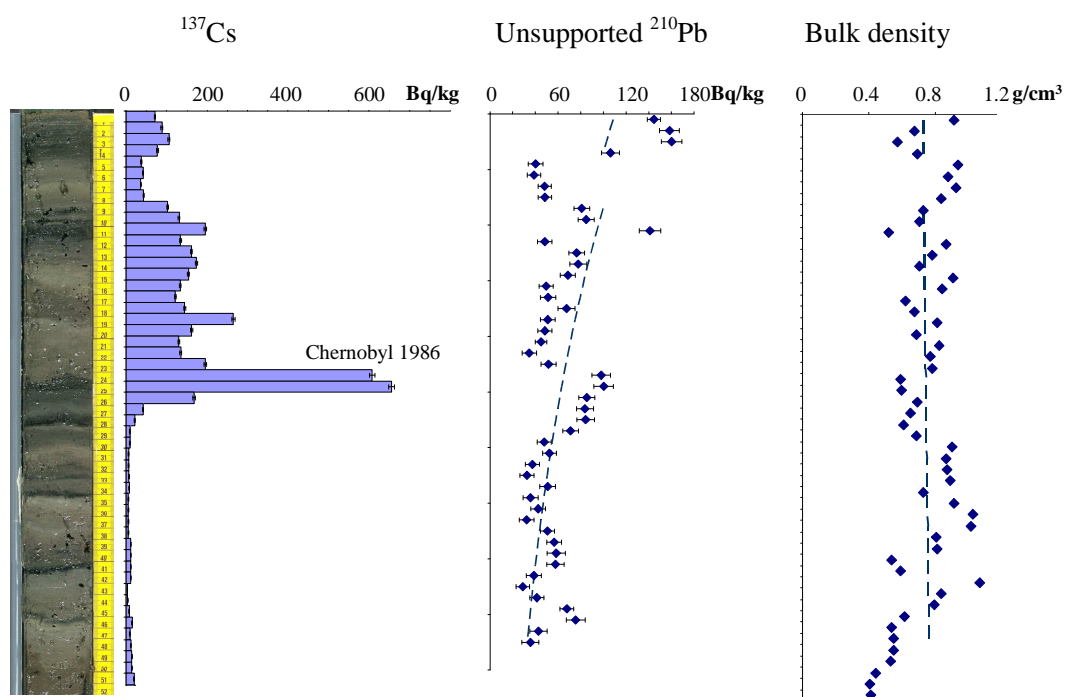
Fig. 4.5. Position 1, from left to right: Photo of the sediment core 1 (0-52 cm), the vertical distributions of [137]Cs (decay-corrected to the date of sampling 12.05.03), unsupported ^{210}Pb, and bulk density.
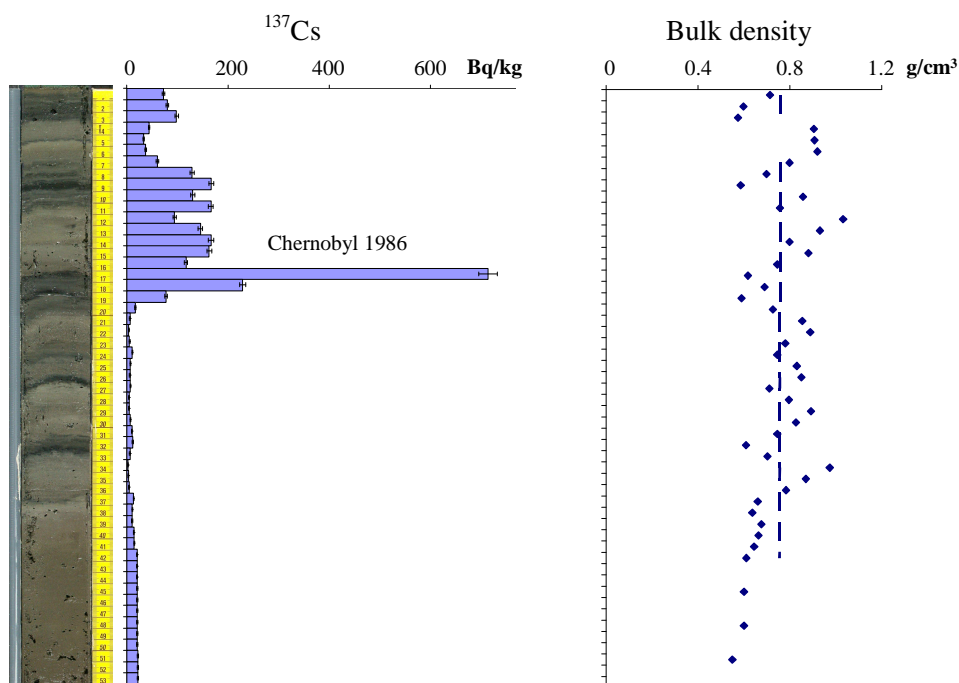
Fig. 4.6. Position 1, from left to right: Photo of the sediment core 4 (0-53 cm), the vertical distributions of [137]Cs (decay-corrected to the date of sampling 12.05.03), and bulk density.
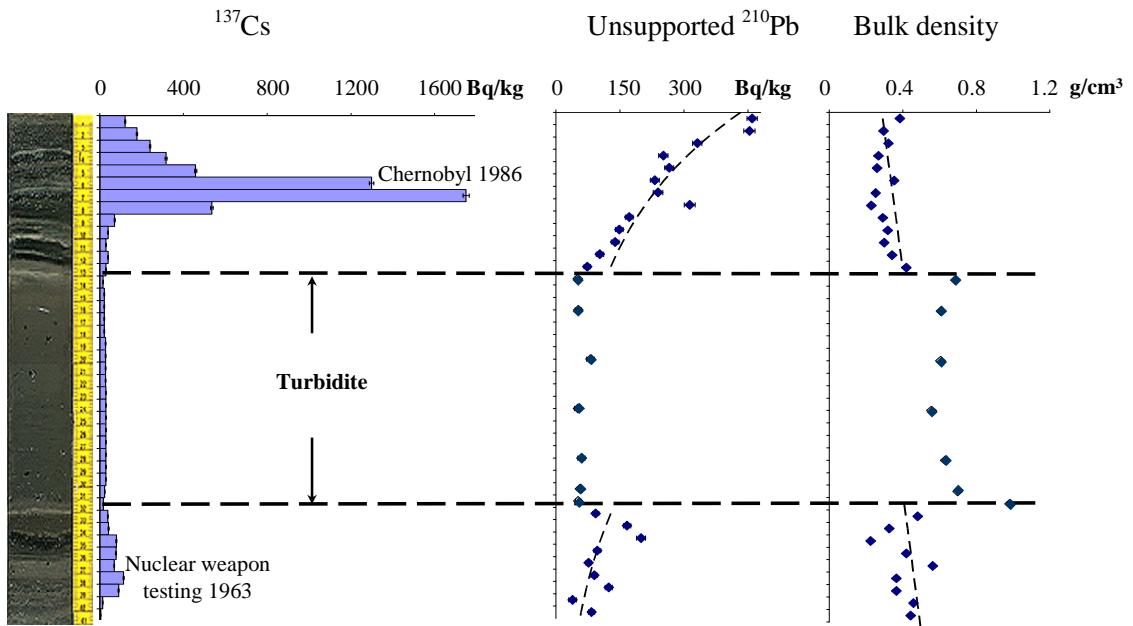
Fig. 4.7. Position 2, from left to right: Photo of the sediment core 1 (0-41 cm), the vertical distributions of ^{137}Cs (decay-corrected to the date of sampling 12.05.03), unsupported ^{210}Pb, and bulk density.
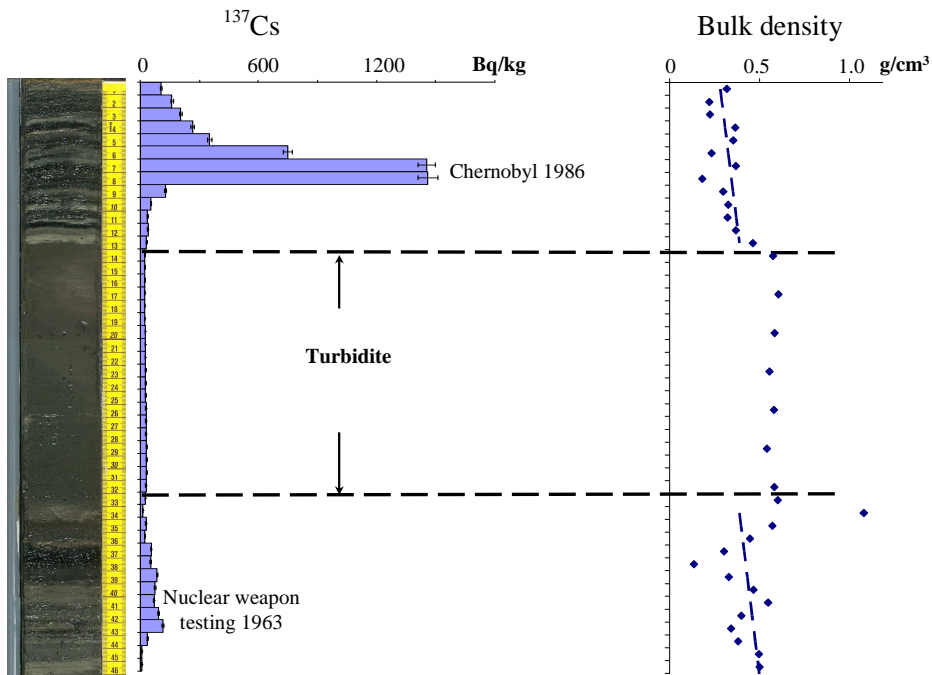
Fig. 4.8. Position 2, from left to right: Photo of the sediment core 3 (0-46 cm), the vertical distributions of ^{137}Cs (decay-corrected to the date of sampling 12.05.03), and bulk density.
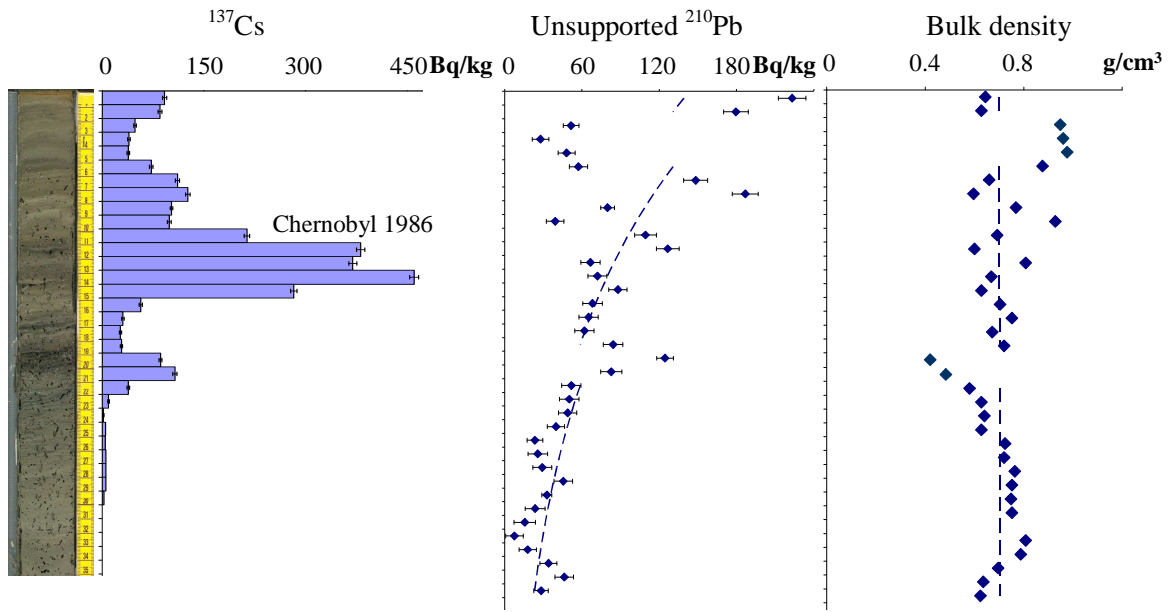
Fig. 4.9. Position 3, from left to right: Photo of the sediment core 3 (0-35 cm), the vertical distributions of ^{137}Cs (decay-corrected to the date of sampling 26.04.04), unsupported ^{210}Pb, and bulk density.
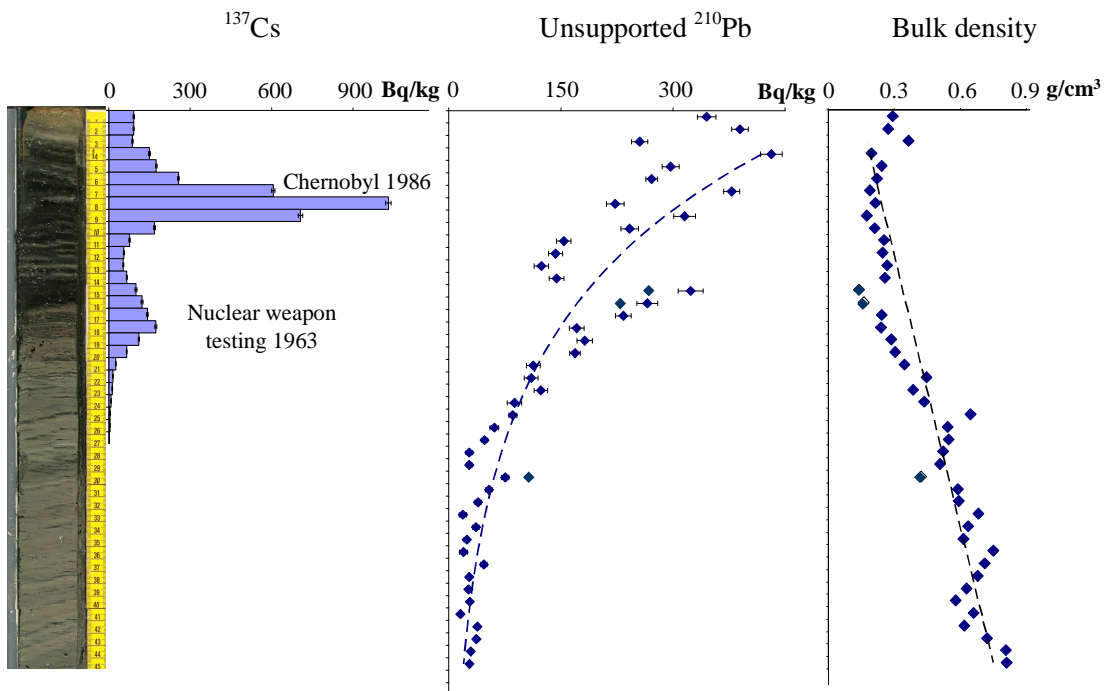
Fig. 4.10. Position 4, from left to right: Photo of the sediment core 2 (0-45 cm), the vertical distributions of ^{137}Cs (decay-corrected to the date of sampling 26.04.04), unsupported ^{210}Pb, and bulk density.
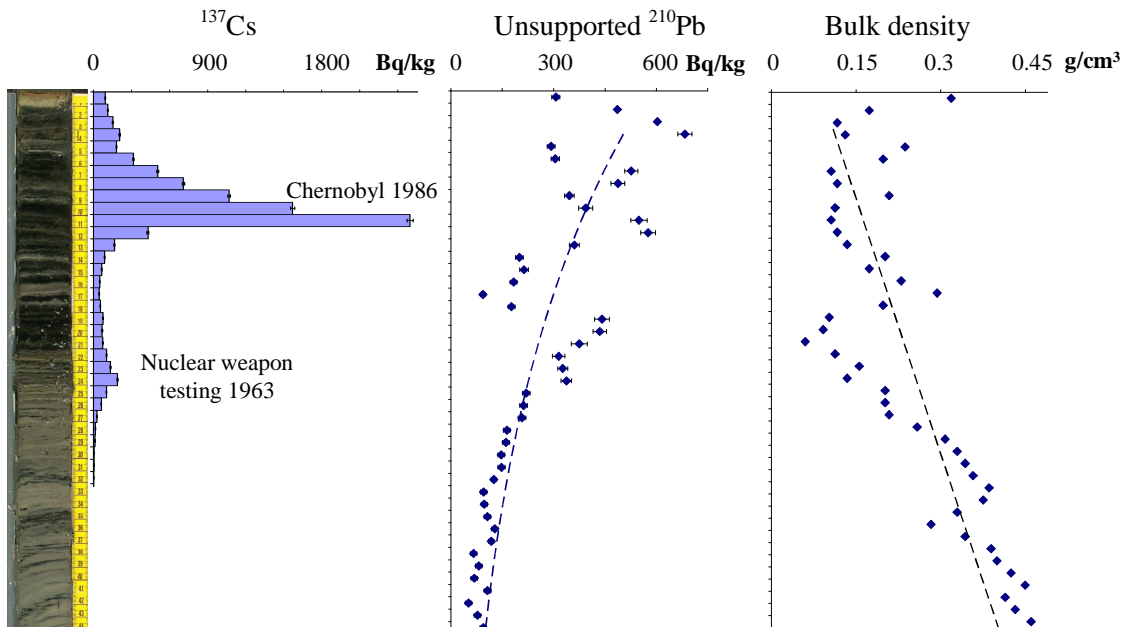
Fig. 4.11. Position 5, from left to right: Photo of the sediment core 3 (0-45 cm), the vertical distributions of ^{137}Cs (decay-corrected to the date of sampling 26.04.04), unsupported ^{210}Pb, and bulk density.
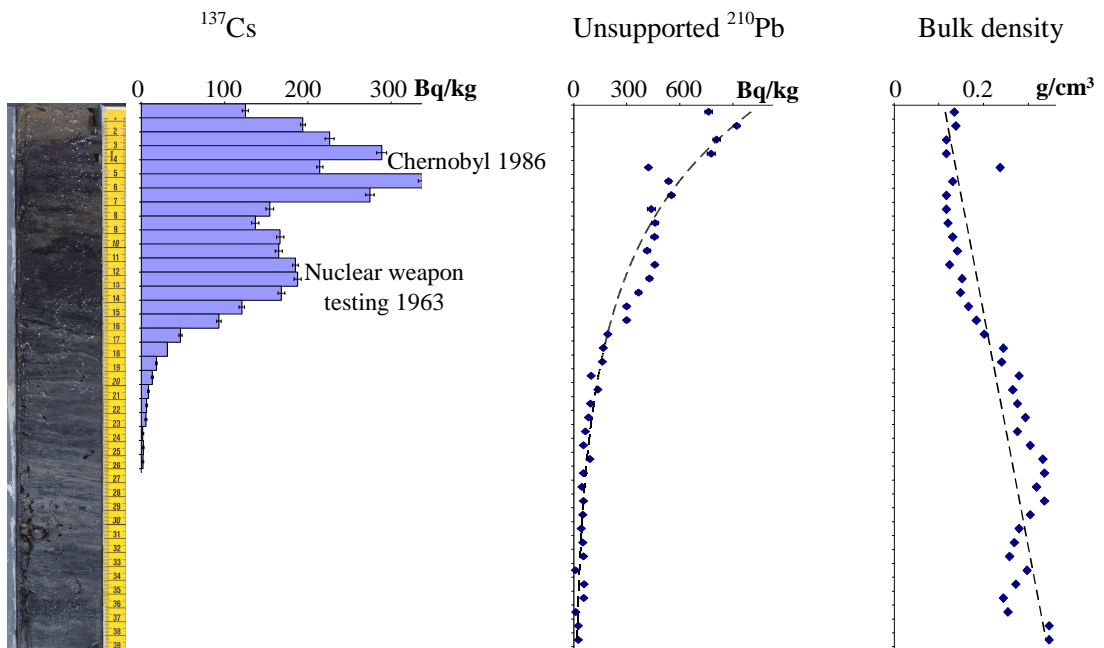
Fig. 4.12. Position 6, from left to right: Photo of the sediment core 3 (0-39 cm), the vertical distributions of ^{137}Cs (decay-corrected to the date of sampling 18.04.05), unsupported ^{210}Pb, and bulk density.
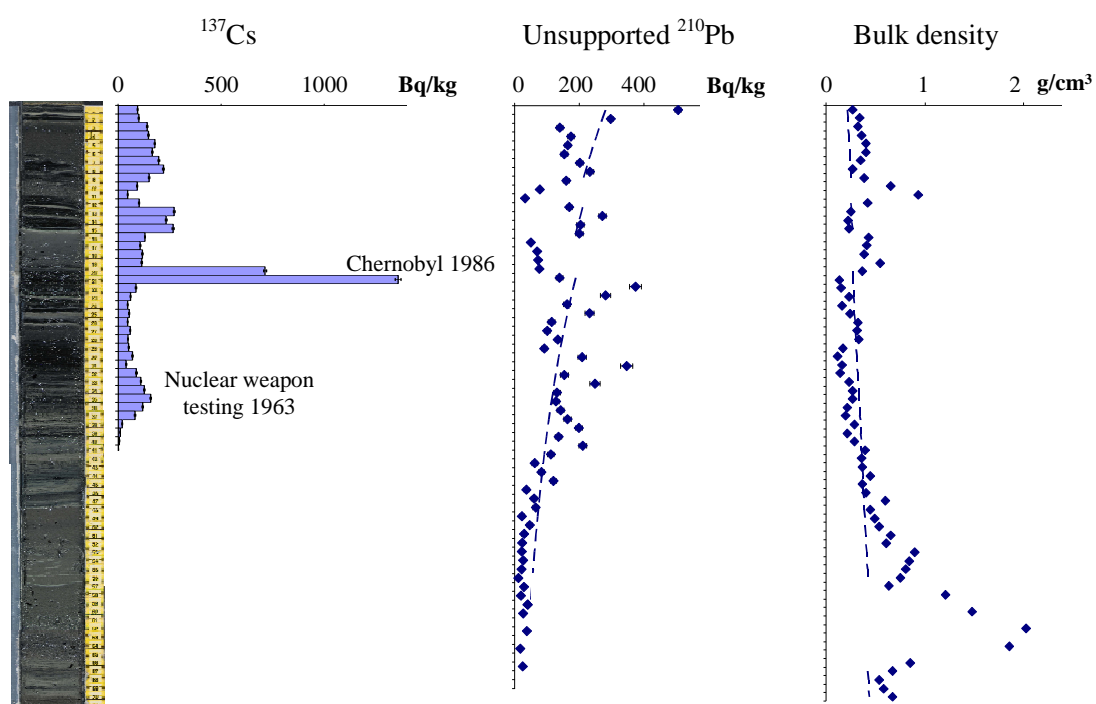
Fig. 4.13. Position 7, from left to right: Photo of the sediment core 1 (0-39 cm), the vertical distributions of ^{137}Cs (decay-corrected to the date of sampling 18.04.05), unsupported ^{210}Pb, and bulk density.

4.2.2 Introduction of turbidites

One peculiarity of deep lakes, and in particular of Lago Maggiore, is the presence of so called 'turbidite layers' in the sediment profiles. Turbidity flows can be described as "underwater avalanches" of sliding sediments from the steep slopes of lake basins which are responsible for the distribution of vast amounts of sediment into the deep lake (Fig. 4.14, A).
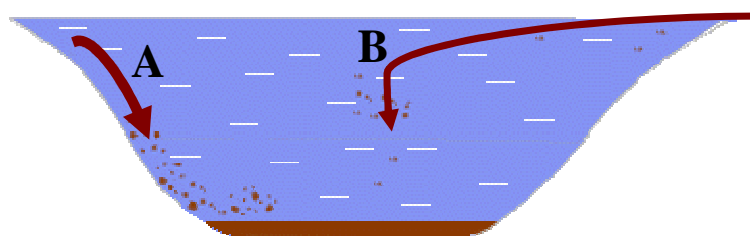
Fig. 4.14. Different ways of turbidite appearance in the deep lakes: **A** - due to steep slopes of the lake, **B** – with the incoming allochthonous material.

In Lago Maggiore the distinctive feature of the turbidite layers is that usually they have higher bulk density in comparison with the neighbouring layers and a rather constant activity concentration of ^{137}Cs and unsupported ^{210}Pb within this particular layer. Larger turbidites can be seen in photos of sediment profiles where the layers of the turbidites have a uniform colour. An example of such large turbidite layer is shown in Fig. 4.15.
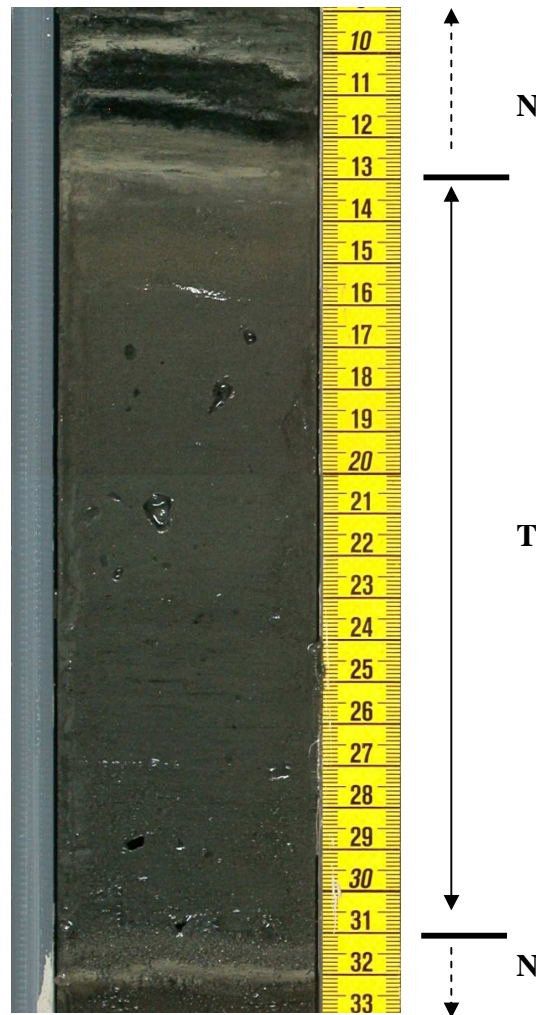
Fig. 4.15. A photos of alternating turbidite layer (T) and "normal" (N) sediments of the northern basin of Lago Maggiore.

An important fact is that in the deep basins of Lago Maggiore turbidity flows produce layers which are occasionally deposited on the surface at one instance without mixing the underlying layers. This is in contrast to turbidity flows, e.g. in the Black Sea

(Voitsekhovitch, personal communication), where the slope is not as steep and underlying layers are mixed heavily by the turbidity flow. In that case, the density within the turbidite layer increases with depth.

Another reason of the turbidity flow appearance might be a very heavy rain which often resides in the region of the Southern Alps and which supplies large quantities of allochthonous material into the lake via frequent river floods (Fig. 4.14, B). Such incidents may take place every year or sometimes several times in a year causing regions of 'mini-turbidites' in the vertical sediment profiles (Marchetto and Musazzi, 2001). The presence of such 'mini-turbidites' brings additional uncertainties in the model and makes it difficult to establish correctly the depth-age relation in the sediment profile.

4.2.3 Discussion on the vertical distributions

In most cores the lamination of the profile due to the seasonal variations in the sedimentation process or due to specific events can be well recognized. For example, in sediment cores from positions 2 (Fig. 4.7 and 4.8), 4 (Fig. 4.10), 5 (Fig. 4.11) and 7 (Fig. 4.13) in the upper 1–4 cm layer a distinct white layer is observed. According to Guilizzoni (2003) this layer corresponds to a large inundation in the year 2000.

In this chapter four factors which are used to classify the profiles of Lago Maggiore will be discussed:

- the shape and position of the Chernobyl peak;
- ^{137}Cs inventories in the sediment;
- bulk density;
- the appearance of turbidite layers.

Shape and position of the Chernobyl peak

According to the shape of the Chernobyl maximum, the profiles from the lake can be grouped into three different types.

The *first group* is characterized by a clear maximum which is observed in the upper 10 cm with relatively high specific activities. The peak is followed by a monotonously decreasing ^{137}Cs activity concentration towards the sediment surface. Cores of position 2 (Fig. 4.7 and 4.8) and position 5 (Fig. 4.11) can be designated to this group. They are located in the center of the northern and southern basins of Lago Maggiore, respectively, with water depths larger than 150 m. A similar situation is observed in the sediment profile of position 4 (Fig. 4.10). That position is located behind the small island Madre where there is no influence of inflowing or outflowing water.

The *second type* is introduced by a very sharp Chernobyl maximum occurred at a larger depth (below 17 cm). This group is depicted by the sediment profiles of positions 1 (Fig. 4.5, 4.6), 3 (Fig. 4.9) and 7 (Fig. 4.13). Profiles of that type are found in front of tributaries of the lake: Toce for position 3, Ticino and Verzasca for position 1. The exception is the deepest position 7 which is located in the middle of the central part of the lake. There, the larger depth of the Chernobyl peak and variations in the specific ^{137}Cs activities above it might be due to some allochthonous material which is transported not only by tributaries, but also with heavy rains. A low activity in the Chernobyl peak as compared with those from the first group is typical for these positions.

The *third type* is represented by a very broad Chernobyl peak which can be observed in the sediment profile of position 6 (Fig. 4.12). The core was taken at a water depth of less than 30 m close to the outlet of the lake. An enhanced diffusion of ^{137}Cs acting at that location can lead to such a broad structure (see chapter 5.1.3).

^{137}Cs inventories in the sediment

According to the total inventories of ^{137}Cs Lago Maggiore can be divided into three parts:

1. northern basin with values exceeding 30 kBq·m^{-2};
2. central part with the inventories varying between 15 and 20 kBq·m^{-2};
3. southern basin near the outflow area with 7 kBq·m^{-2}.

Here, a clear tendency of a decrease in total ^{137}Cs inventories from the northern basin to the southern part of the lake can be observed (Fig. 4.16, A).
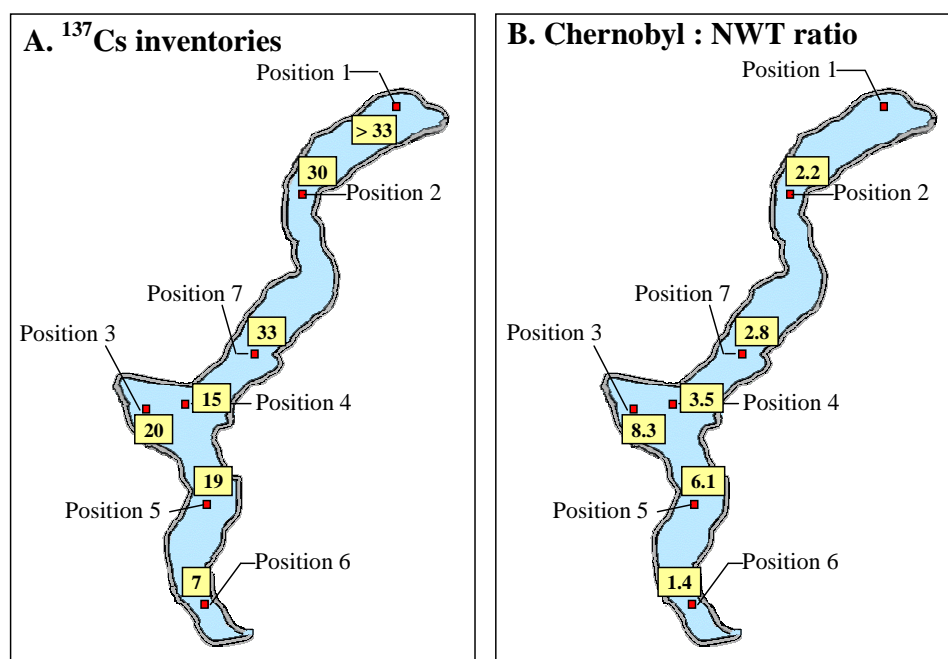
Fig. 4.16. A: Arial distribution of total ^{137}Cs inventories (kBq·m^{-2}) in the sediments of Lago Maggiore, decay-corrected to 1.05.1986. **B:** The ratios of Chernobyl to nuclear weapons testing ^{137}Cs inventories calculated at 1.05.1986.

Positions 1, 2 and 7 belong to the first group, whereas positions 3–5 describe the second group; the third part is presented by position 6.

Additionally, the ratios of Chernobyl to nuclear weapons testing ^{137}Cs inventories (both decay-corrected to 1.05.1986) were determined (Fig. 4.16, B). The ratio of Chernobyl to nuclear weapons testing ^{137}Cs is about 2 throughout the lake, except for positions 3, 4 and 5 which are influenced by the inflow of the river Toce and where the position of Chernobyl ^{137}Cs is increased by up to a factor of 4.

Bulk density

The bulk density of the sediment cores varies from 0.2 g·cm^{-3} up to more than 1 g·cm^{-3} at different positions in Lago Maggiore. However, two groups of profiles can be distinguished:

- with a relatively high and constant density,
- with a density linearly increasing with depth.

69

Thus, sediments taken at positions 2, 4 to 7 are characterized by linearly increasing bulk density. At the same time positions 1 and 3 are represented by harder material with constant density down the sediment profile.

Turbidite layer appearance

In all sediment profiles, except those taken at positions 2 and 6, many small turbidite layers appear due to the transport of allochthonous material after heavy rain falls.

Large variations in vertical distributions of ^{137}Cs and unsupported ^{210}Pb activity concentrations are typical for the layers above the Chernobyl peak at positions 1 and 7 which is probably due to appearance of 'mini-turbidite' layers that are rather difficult to identify and handle.

Positions 3 to5 are characterized by a turbidite deposition with a thickness of 2–3 cm in the upper sediment layer (Fig. 4.9 to 4.11). These positions belong to one basin and probably provide similar records of the sedimentation history.

A very large turbidite (a single layer with a sickness of about 20 cm) at position 2 (Fig. 4.7 and 4.8) was easily identified in the photo as well as from vertical distributions of ^{137}Cs, unsupported ^{210}Pb and bulk density. This layer is the result of turbidity flows which bring a large amount of material from the steep slopes of the lake basin.

The variations of the bulk density and unsupported ^{210}Pb specific activities, as observed in the layer 19–21 cm in profile of position 3 (Fig. 4.9), may be explained by changes in sedimentation conditions in the lake. In that case this layer is not assigned as a turbidite.

Turbidites have a problematic influence on the establishment of depth-age relation in the sediment profile (see chapter 4.4) and bring additional uncertainties to the parameters used for modeling the vertical distribution (see chapter 5.6).

4.3 Association of radiocaesium to different geo-chemical fractions

In the following subchapters the results of grain-size distribution analysis and of sequential extractions of ^{137}Cs from sediments of Lago Maggiore are described and summarized.

The knowledge of binding of ^{137}Cs to the different geo-chemical fractions of the sediment is important as the amount of exchangeable and fixed caesium will be used in the model of the vertical migration of ^{137}Cs within the sediment (chapter 5).

4.3.1 Grain-size distribution of sediments and organic matter content

In Fig. 4.17 the percentage of organic matter and the particle fractions sand (> 0.05 mm), silt (2–50 µm), and clay (< 2 µm) of the sediment profiles from the seven positions of Lago Maggiore is shown. The experiments are performed on wet sediments, whereas all values are related to the total mass of the dry samples including the organic matter content. The fraction of organic matter is of great interest especially due to rather large percentage of extractable ^{137}Cs associated with organic matter as will be shown in subchapter 4.3.2.

The results of grain-size distribution analysis are given in a table in Appendix C.

Silt content

The prevalent fraction mostly at all positions is silt. It varies between 50 % and 80 % in most of the sediments, except at position 2 where it is in the order of 20 % increasing with depth up to 40 %.

Sand fraction

The sediment of position 2 is characterized by a rather high percentage of sand (65 %) in the top layer. In the layers below down to 50 cm it is a factor of 2 less. The opposite situation is observed at position 4 where the sand fraction increases with depth from 1 % to 10 %. At other positions the percentage of sand is in the order of 10–20 %.

Clay minerals

A clay minerals fraction of more than 40 % is observed in the sediments at positions 4, 6, and 7. At position 2, with a minimum in the layer between 2–12.5 cm, it increases with depth up to 27 %. Other positions (1, 3 and 5) are characterized by a lower percentage of clay minerals which does not exceed 17 %.

Organic matter content

At most positions the percentage of organic matter is rather low (less than 3 %). It increases with depth at positions 1 and 4, whereas at positions 2 and 7 there is a tendency that it decreases (to 1 %) down the sediment profile. Position 5 is characterized by the highest content of organic matter of more than 7 %.

There is the common tendency that the clay content is inversely proportional to the sand content in all profiles.
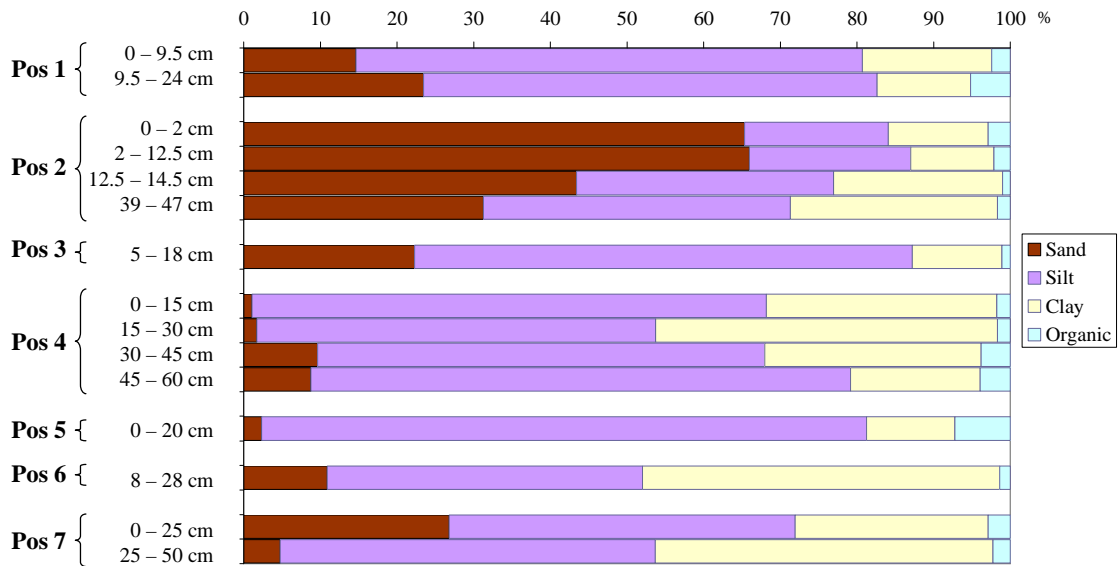
Fig. 4.17. Percentage of grain-size distribution and organic matter content of sediment profiles at different positions of Lago Maggiore.

4.3.2 Sequential extraction of ^{137}Cs in the sediment

Sequential extractions of the sediments give the association of ^{137}Cs to the different geo-chemical fractions within the sediment matrix. A set of 5-step sequential extraction experiments was performed with sediment material (mostly from the area of the Chernobyl maximum) from different positions of Lago Maggiore as described in chapter 3.5.2. The results of these experiments show that ^{137}Cs is very tightly bound to the sediment at almost all positions and generally only a few percent of ^{137}Cs could be extracted altogether. The results are given in Fig. 4.18 and in a table in Appendix D.

Position 1

At position 1 less than 10 % of the total ^{137}Cs could be extracted. Only 0.45 % of ^{137}Cs was associated with the exchangeable fraction. An even smaller percentage of ^{137}Cs was extracted with carbonates and oxides and hydroxides of manganese, respectively. Only the amount of ^{137}Cs associated to organic matter and to the amorphous silicates is in the order of several percents. More than 90 % is associated to the residue which mainly consists of clay minerals, feldspars and quartz.

Position 2

The measured percentage of exchangeable ^{137}Cs at position 2 is about 1 %. Less than a percent of radiocaesium was associated with carbonates, oxides and hydroxides of iron and manganese, and amorphous silicates, respectively. ^{137}Cs was extracted mainly from the organic matter even though the portion of organic phase was less than 3 % (see chapter above).

Position 3

The extraction experiments were performed on two different sediment cores from position 3. Both show a surprisingly low percentage of exchangeable ^{137}Cs of less than 0.3 %. The portion of about 1 % of ^{137}Cs could be extracted with the organic matter whereas the percentage of radiocaesium associated with oxides and hydroxides of iron

and manganese is negligible. Thus, about 98 % of radionuclide remains fixed to the sediments.

Performing the experiments on two sediment cores taken from one position but several meters apart, we tested the variability of our results. The measurements show that the differences between two cores of the same position in the lake are very small as compared to the differences between cores from different basins.

Position 4

The highest percentage of extracted ^{137}Cs (4.3 %) is found in the organic matter fraction which is followed by the fractions of exchangeable ions (1.6 %), carbonates (0.5 %) and oxides and hydroxides of iron and manganese (0.2 %). The 5th step of the extraction procedure could not be performed completely as with centrifuging it was not possible to separate the liquid phase from the solid. Thus, all the rest was put to the residue. This explains the question mark "?" in Fig. 4.17. Whether the white powder swimming on the liquid phase is amorphous silicates or poly-phosphates as suggested by Dr. Wessels from the Lake Research Institute at Langenargen, Germany, has still to be analyzed.

Position 5

Position 5 is characterized not only by the highest percentage of the measured exchangeable ^{137}Cs (9.7 %) but in general, somewhat higher values of extractable radiocaesium. More than 20 % of ^{137}Cs was extracted altogether from the sediments which belongs to the fractions of exchangeable ions, organic matter (6.6 %), carbonates (2.4 %), amorphous silicates (1.1 %) and oxides and hydroxides of iron and manganese (1.1 %). Still, about 80 % of ^{137}Cs remains fixed in the residue and cannot be extracted by the performed 5-step procedure.

Position 6

The highest extraction degrees at position 6 were determined in the fraction of the exchangeable ions (4.5 %) and the organic matter (3.2 %), followed by lower percentage of extracted ^{137}Cs with the carbonates (1.8 %), oxides and hydroxides of iron and

manganese (0.7 %), and amorphous silicates (0.5 %). The total degree of extraction for ^{137}Cs is about 11 %.

Position 7

The portion of extracted ^{137}Cs in the first step is 0.9 %. With 2 % the largest extraction percentage is measured for the fraction of organic matter. Steps 2, 3 and 5 have very low values of extracted radiocaesium which are in the order of only 0.2 %. So, again about 97 % of the radionuclide is fixed to the phase which mainly consists of clay minerals, feldspars and quartz.
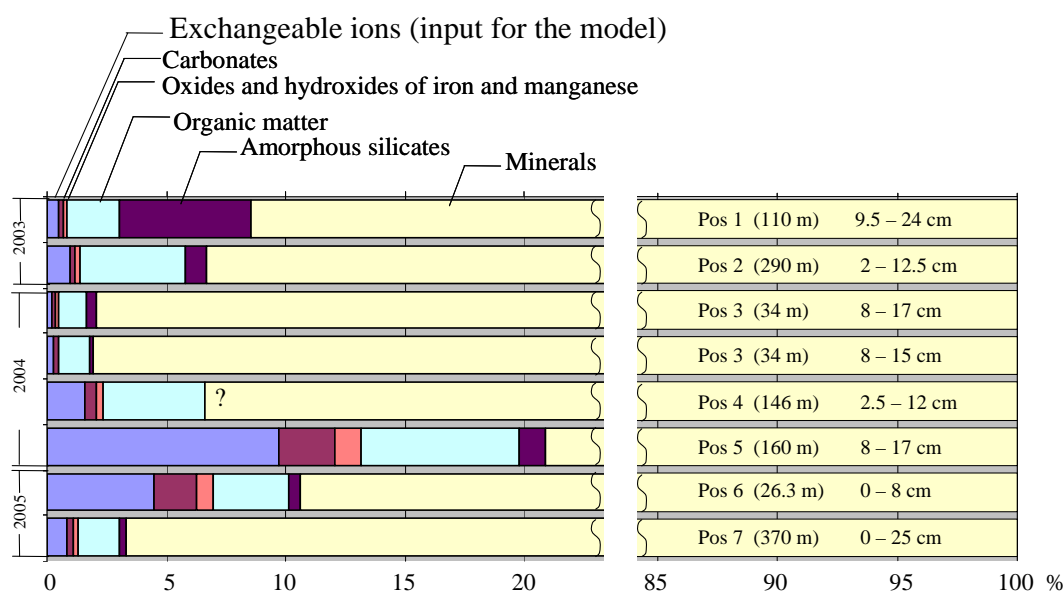
Fig. 4.18. Results of the 5-step sequential extraction experiments for different positions of Lago Maggiore. Given on the right side is: position, depth of the lake, and the sediment layer on which the extraction experiment was performed. On the left side the year of sediment sampling is marked as explained in the text.

General conclusions

The results of the 5-step sequential extraction procedure performed on sediments of Lago Maggiore show that ^{137}Cs is very tightly bound to the sediment. The percentage of

extractable ^{137}Cs during five steps is generally very low (1.9 – 8.5 %) except at the position 5 where it is rather high (20.9 %).

The lowest percentage of radiocaesium could be extracted in the third step with oxide and hydroxides of iron and manganese. The extraction degree of this phase is always below 1 % with an exception at position 5 where it amounts to 1.1 %. On the contrary, most of extracted ^{137}Cs was found in the organic fraction, followed by amorphous silicates and at some positions exchangeable ions of Cs.

As the portion of exchangeable ^{137}Cs in the sediment is very low and most of the Cs radionuclides are fixed to clay minerals, the importance of ^{137}Cs diffusion in the sediment and the danger of its redissolution into the water of Lago Maggiore is very low. Still, the exchangeable fraction of ^{137}Cs which is named α in the following chapters remains important for modeling the vertical distribution of radiocaesium in the sediment.

The measured portion α of exchangeable ^{137}Cs is taken as one of the input parameters of the model described in chapter 5. That ^{137}Cs which is associated to carbonates, oxides and hydroxides of iron and manganese, organic matter, amorphous silicates, and the rest is taken as the fixed fraction in the model.

4.3.3 Classification of positions

From the results of the granulometric composition of sediments, organic matter content, and ^{137}Cs association to the different geo-chemical fractions, it is possible to perform another classification of sediments of Lago Maggiore.

Here, the following factors will be discussed:

- organic content;
- measured portion of exchangeable [137]Cs.

Organic content

In Fig. 4.19 (A) the organic matter content for different positions of Lago Maggiore is shown. Each position is represented by the values measured in sediment profiles at a depth corresponding to the region of the Chernobyl peak.

According to the percentage of organic content, the positions of Lago Maggiore can be divided into three groups:

- organic matter larger than 3 % (position 5);
- content of organic matter varying between 2 % and 3 % (positions 1, 2, and 7, representing in that way the northern basin of the lake);
- fraction of organic matter not exceeding 2 % (positions 3, 4, and 6).
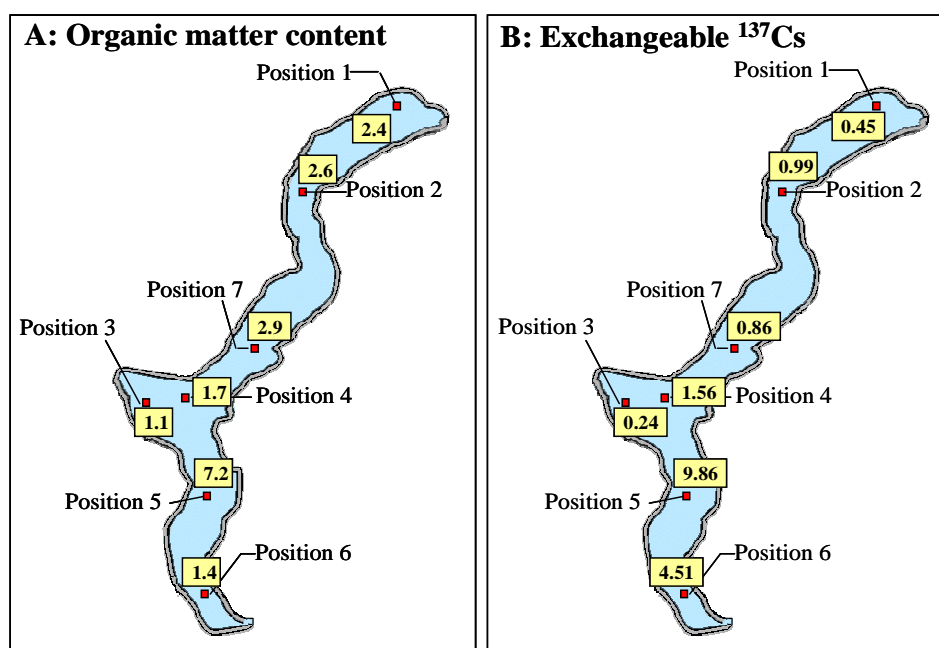
Fig. 4.19. Percentage of organic matter content in the sediments (A) and percentage of exchangeable ^{137}Cs measured at step 1 during the sequential extraction experiments (B) in the sediments from different positions of Lago Maggiore.

Measured portion of exchangeable [137]Cs

A similar classification of the positions can be done according to the percentage of the measured portion of exchangeable ^{137}Cs in the sediment profiles. Figure 4.19 (B) shows the portion of exchangeable ^{137}Cs ions measured in the sediments from different positions of Lago Maggiore.

Roughly, the lake can be divided into three parts:

- northern and central basins (positions 1, 2, 4 and 7) with a rather low percentage of exchangeable ^{137}Cs (0.45 – 1.56 %);

- southern basin (positions 5 and 6) which is characterized by much larger percentage of extracted exchangeable ^{137}Cs ions (4.5 – 9.9 %);

- position 3 which with the lowest portion of measured exchangeable ions of ^{137}Cs (0.24 %).

Generally, Lago Maggiore sediments are mainly characterized (except position 5) by low percentage of exchangeable and extractable during 5 step extraction procedure ^{137}Cs at the same positions.

4.4 Dating of sediment with ^{210}Pb

Dating of the sediments was carried out in the seven cores from different positions of Lago Maggiore. Based on the data on the content of unsupported ^{210}Pb in individual 1 cm layers of the depth profile, their age and the sedimentation rates were determined. To do these calculations, two different models were used: CRS and CIC (see chapter 3.6 and Appendix E). Additionally the independent linear depth-age relation based on ^{137}Cs is introduced.

4.4.1 Results and discussion on ^{210}Pb dating

Figures 4.22 to 4.28, part A, show the plot of ^{210}Pb activity versus the accumulated weight (calculated from the bulk density and thickness of the sediment sample) for 7 cores from different positions. In sediment cores from positions 1 to 5, and 7 the larger turbidites were taken out. Afterwards, a weighted least-square exponential fit to the data (pink line) was applied.

At positions 2 (Fig. 4.23), 4 (Fig. 4.25) and 6 (Fig. 4.27) the ^{210}Pb activity concentration can be described by exponential functions (CIC) rather well. However, the extrapolation down to infinity shows very low values as compared with the measured data. The reason for these higher unsupported ^{210}Pb activity concentrations might be the loss of ^{222}Rn from the sample of up to 30 % in the worst case. More probable is a deviation from the CIC model Also at other positions significant deviations from the best fit-line are observed. These deviations indicate that the accumulation rate varied: high activities indicate low accumulation rates and vice versa. Another reason of such large scatterings in ^{210}Pb activity concentration, e.g. at positions 1 (Fig. 4.22) and 7 (Fig. 4.28), might be the presence of many smaller turbidite layers which can be rather difficult to identify and are therefore not taken out from the ^{210}Pb fit.

The results of dating the seven cores are given in Fig. 4.22 to 4.28, part B. The age of individual sediment layers is shown as calculated according to CIC (thick green line, thin lines are the uncertainties) and CRS (the red points with the error bars calculated from the counting statistics of the ^{210}Pb measurement) models. The blue line (points) is an

independent time scale based on ^{137}Cs dating with maxima indicating Chernobyl fallout in 1986 and nuclear weapons testing in 1963, plotted versus corrected depth. On the secondary axis the sedimentation rate calculated from the CRS model is shown as a red dashed line.

Both, CIC and CRS dating results agree very well back to about 40 years for cores from positions 1 (Fig. 4.22), 3 (Fig. 4.24) and 7 (Fig. 4.28). Also the location of the ^{137}Cs maxima confirm these models, whereas at positions 4 (Fig. 4.25) and 6 (Fig. 4.27) is agrees only with the CIC model. Still, the ^{137}Cs model at position 3 gives an indication that the top layer of the sediment core might be missing. This fact is rather surprising because according to the photo of the profile a presence of the top was indicated by the layer of light brown colour. Probably, the explanation of such ^{137}Cs slope can be the presence of the turbidite which was found before the Chernobyl fallout and was not taken completely from the fit.

At position 5 (Fig. 4.26) rather good agreements can be seen between CRS and CIC models, but both do not agree with ^{137}Cs dating. There is a clear disagreement between three methods of age determination applied for the sediment core from position 2 (Fig. 4.23).
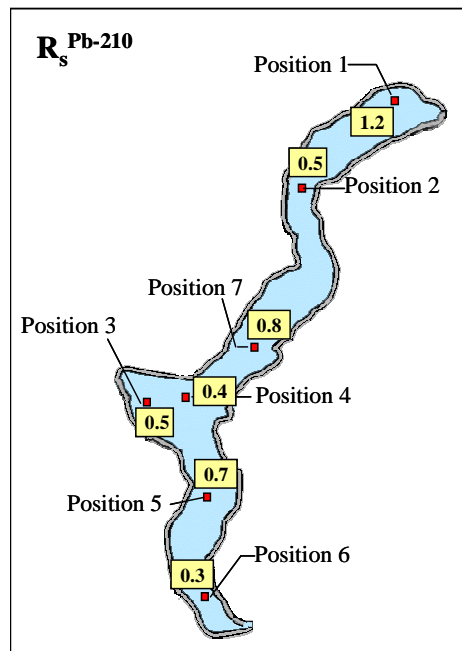
Fig. 4.21. Average sedimentation rates in g·(cm^2·a)$^{-1}$calculated using the CRS ^{210}Pb model.

From Fig. 4.21 it can be seen that the average sedimentation rate calculated using the ^{210}Pb data varies between 0.3 g·(cm^2·a)$^{-1}$ and 1.2 g·(cm^2·a)$^{-1}$.

However, the range of the sedimentation rate is from 0.7 to 2.2 g·(cm^2·a)$^{-1}$ (position 1), 0.01 to 1.1 g·(cm^2·a)$^{-1}$ (position 2), 0.2 to 1.5 g·(cm^2·a)$^{-1}$ (position 3), 0.02 to 0.9 g·(cm^2·a)$^{-1}$ (position 4), 0.2 to 1.6 g·(cm^2·a)$^{-1}$ (position 5), 0.04 to 0.6 g·(cm^2·a)$^{-1}$ (position 6) and 0.4 to 1.4 g·(cm^2·a)$^{-1}$ (position 7). These values can be compared later with the output of the modeling the ^{137}Cs vertical distribution in the sediment (chapters 5.6 and 5.7).

Position 1

A
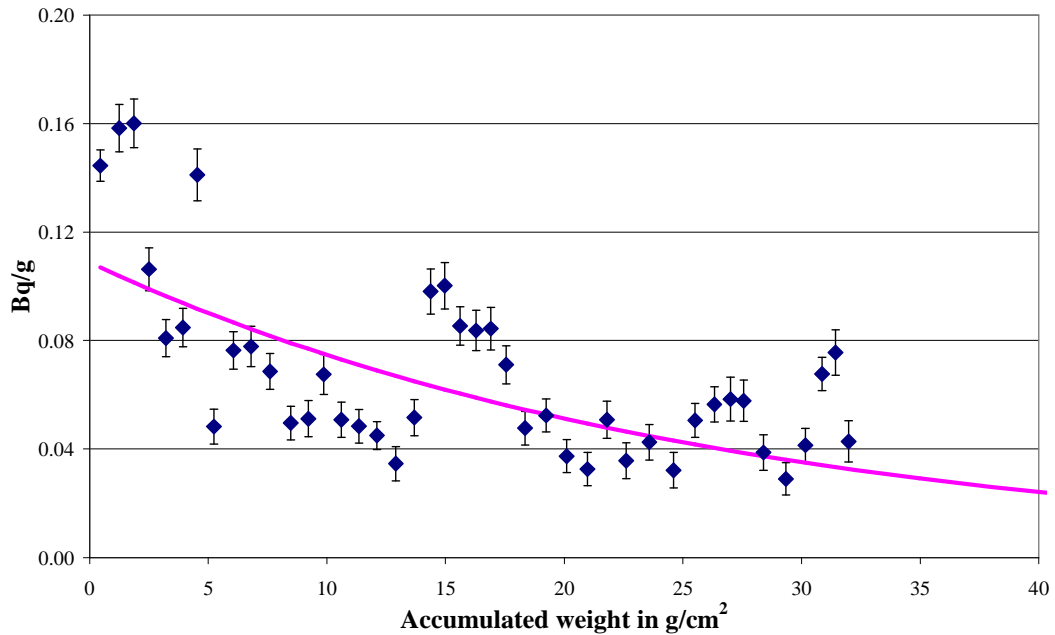
B
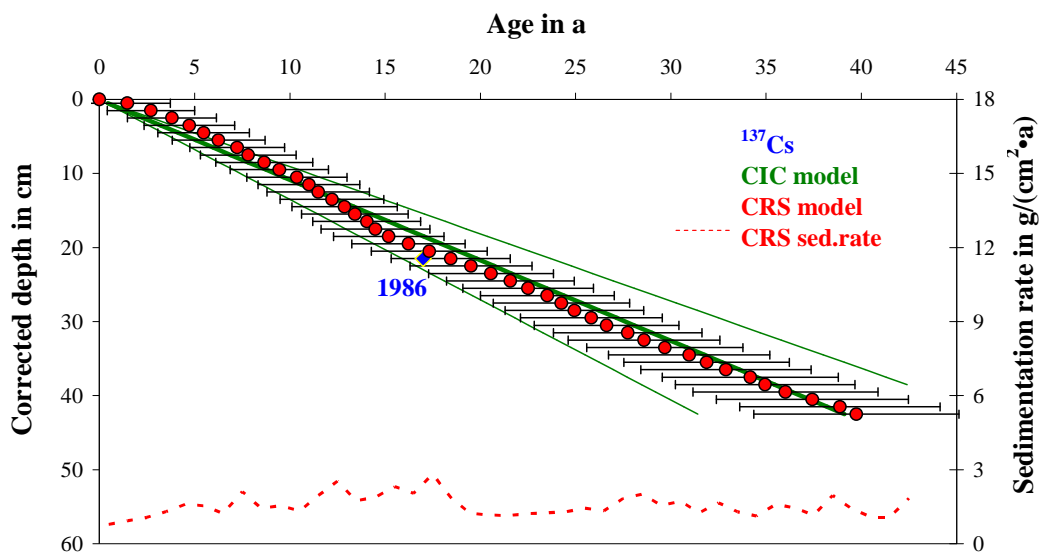
Fig. 4.22. Position 1. A: Measured unsupported ^{210}Pb activity concentration versus accumulated weight. The pink line is a weighted exponential fit to the data. **B**: Depth-age relation of the sediment as a result of dating. The dashed line shows the sedimentation rate calculated by the CRS model.

Position 2

A
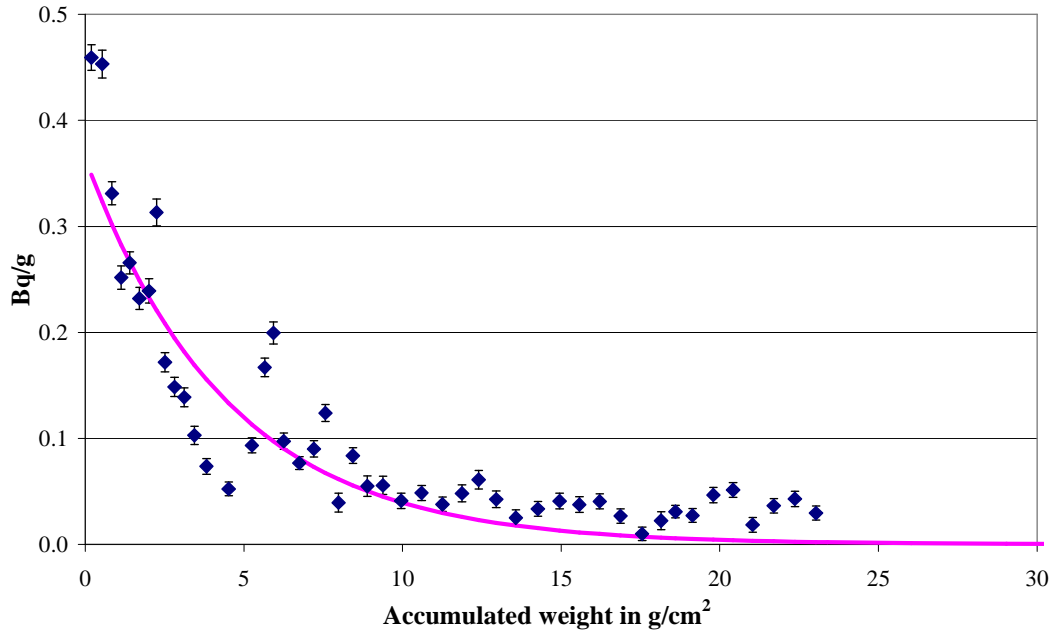
B
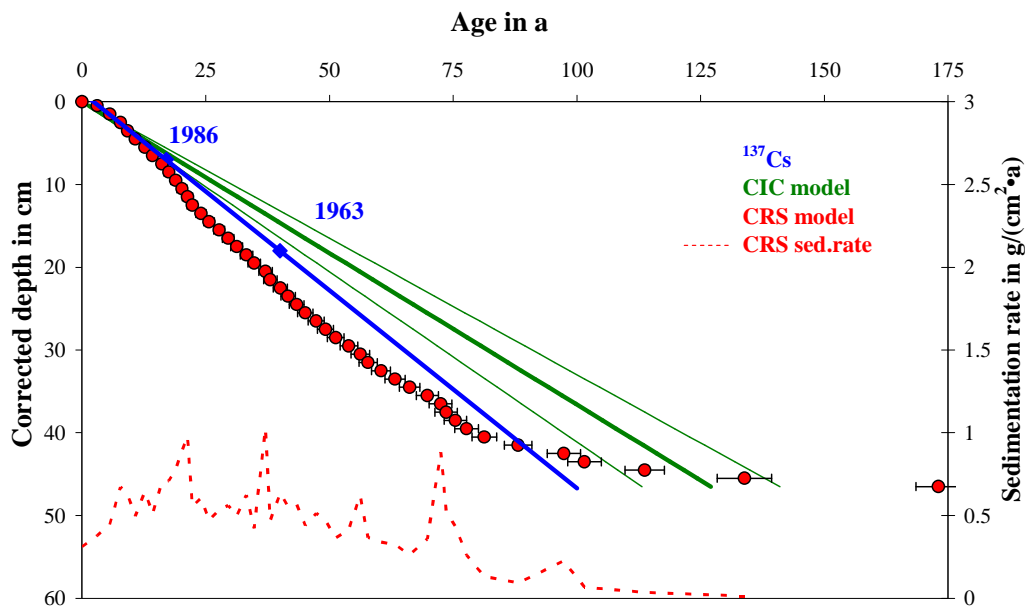
Fig. 4.23. Position 2. A: Measured unsupported ^{210}Pb activity concentration versus accumulated weight. The pink line is a weighted exponential fit to the data. **B**: Depth-age relation of the sediment as a result of dating. The dashed line shows the sedimentation rate calculated by the CRS model.

83

Position 3

A
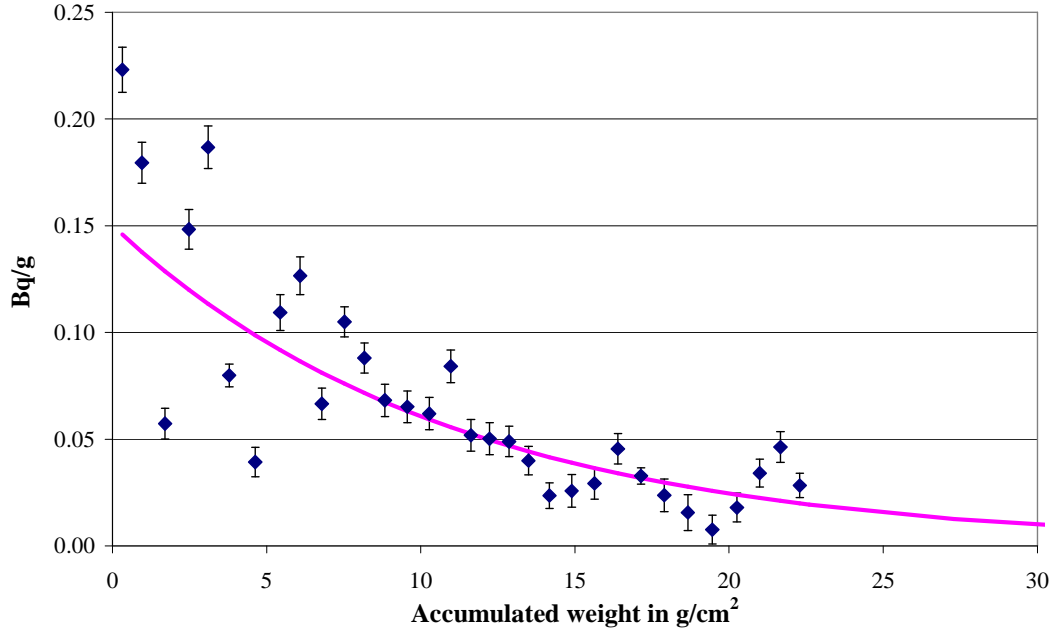
B
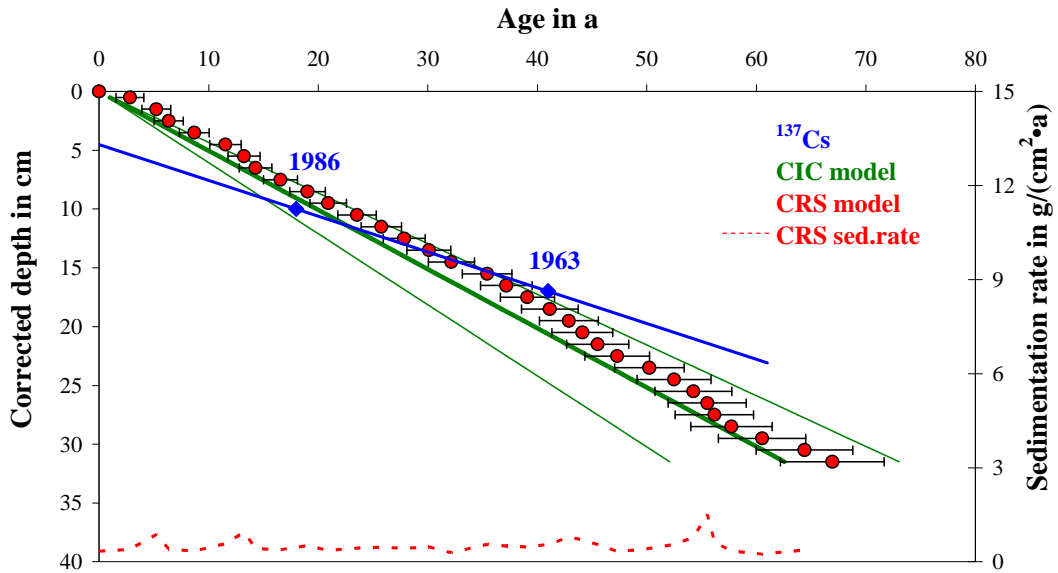
Fig. 4.24. Position 3. A: Measured unsupported ^{210}Pb activity concentration versus accumulated weight. The pink line is a weighted exponential fit to the data. **B**: Depth-age relation of the sediment as a result of dating. The dashed line shows the sedimentation rate calculated by the CRS model.

Position 4

A
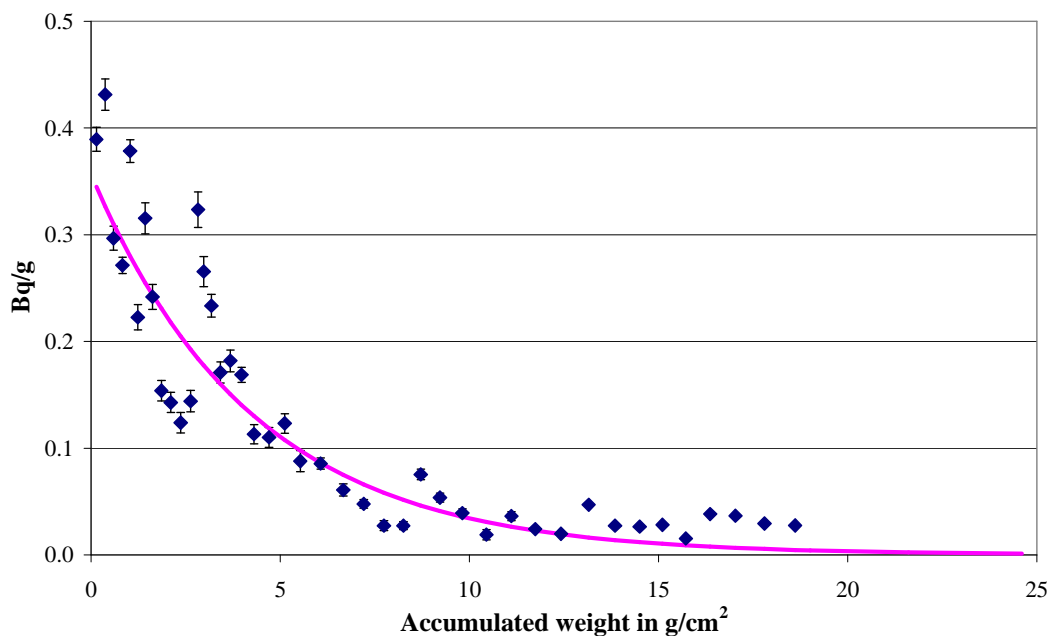
B
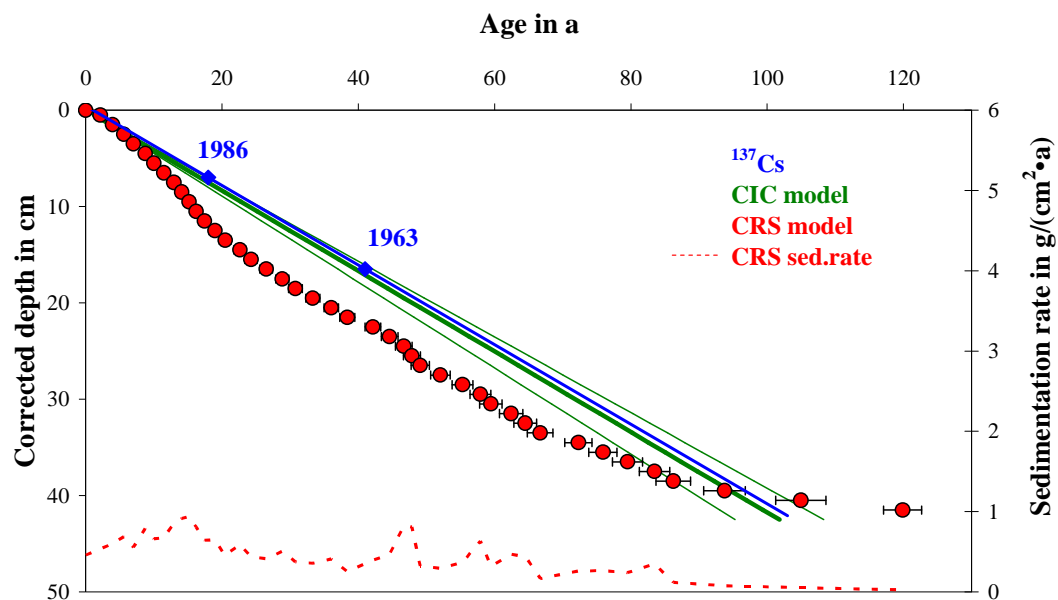
Fig. 4.25. Position 4. A: Measured unsupported ^{210}Pb activity concentration versus accumulated weight. The pink line is a weighted exponential fit to the data. **B**: Depth-age relation of the sediment as a result of dating. The dashed line shows the sedimentation rate calculated by the CRS model.

Position 5

A
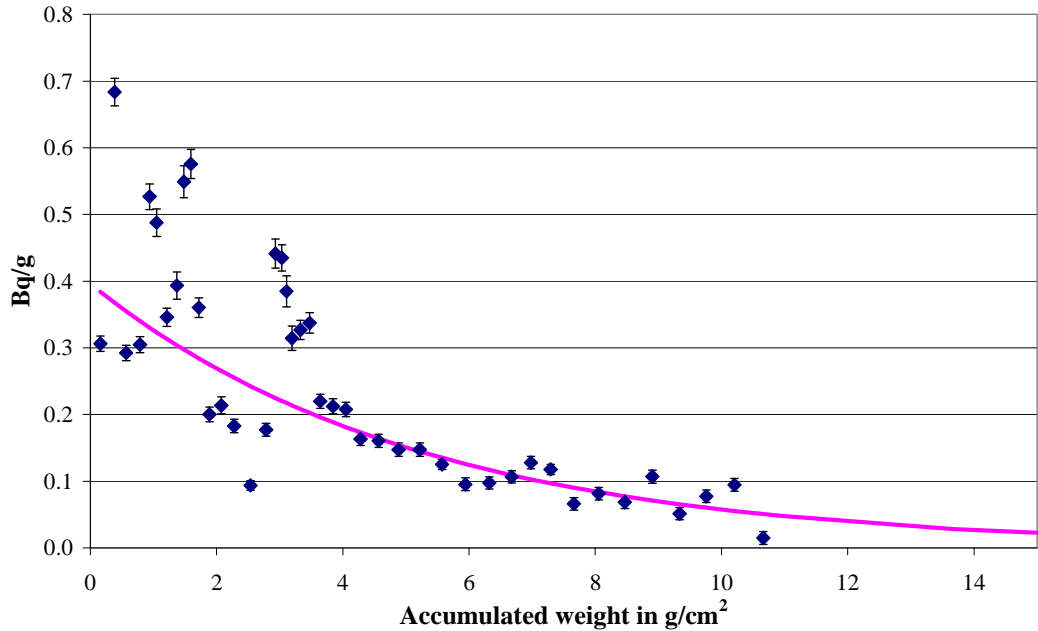
B
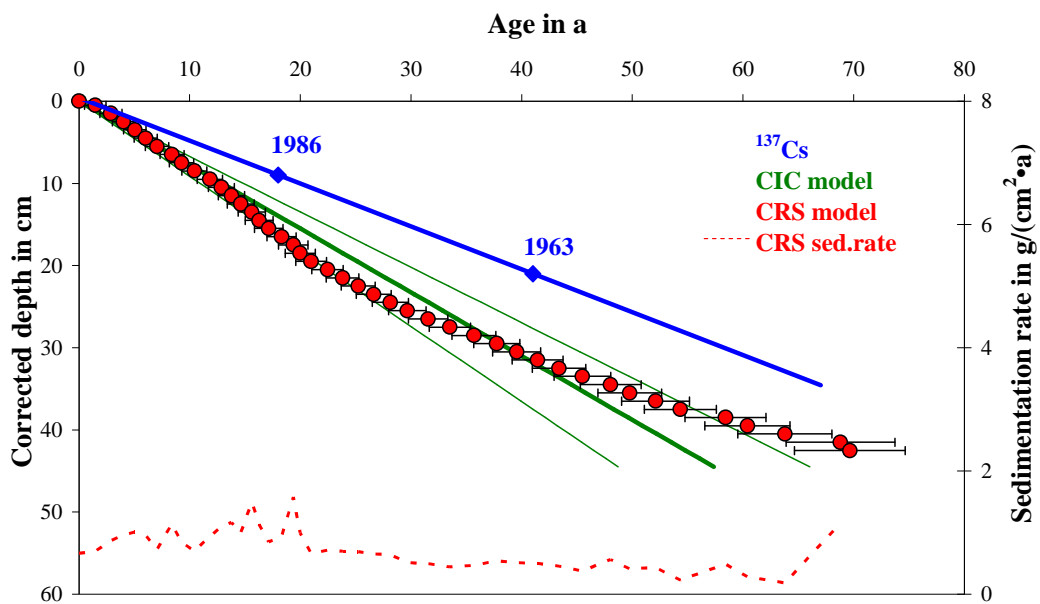
Fig. 4.26. Position 5. A: Measured unsupported ^{210}Pb activity concentration versus accumulated weight. The pink line is a weighted exponential fit to the data. **B**: Depth-age relation of the sediment as a result of dating. The dashed line shows the sedimentation rate calculated by the CRS model.

Position 6

A
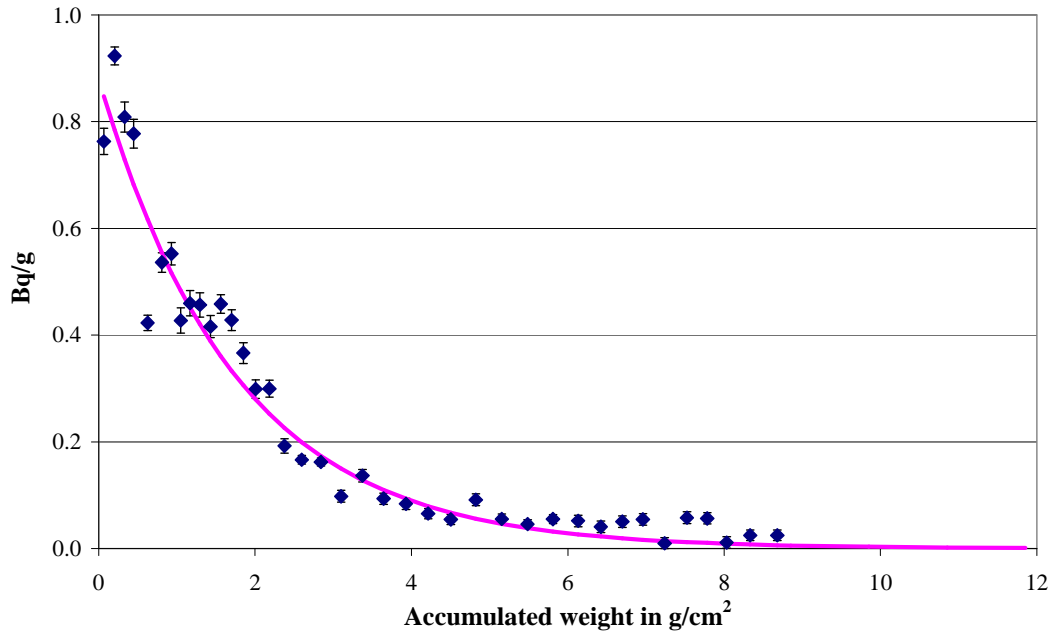
B
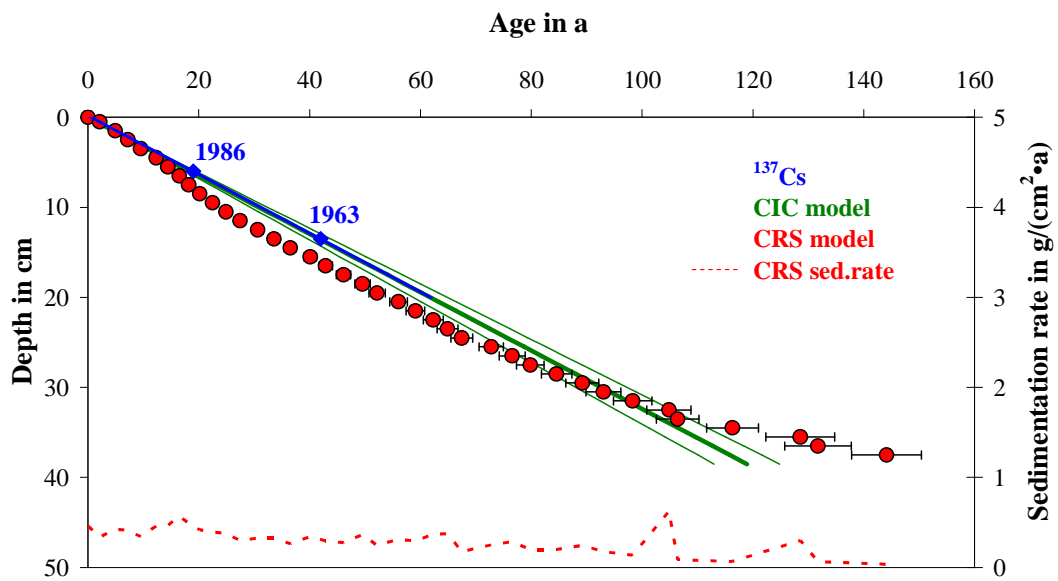
Fig. 4.27. Position 6. A: Measured unsupported ^{210}Pb activity concentration versus accumulated weight. The pink line is a weighted exponential fit to the data. **B**: Depth-age relation of the sediment as a result of dating. The dashed line shows the sedimentation rate calculated by the CRS model.

Position 7

A
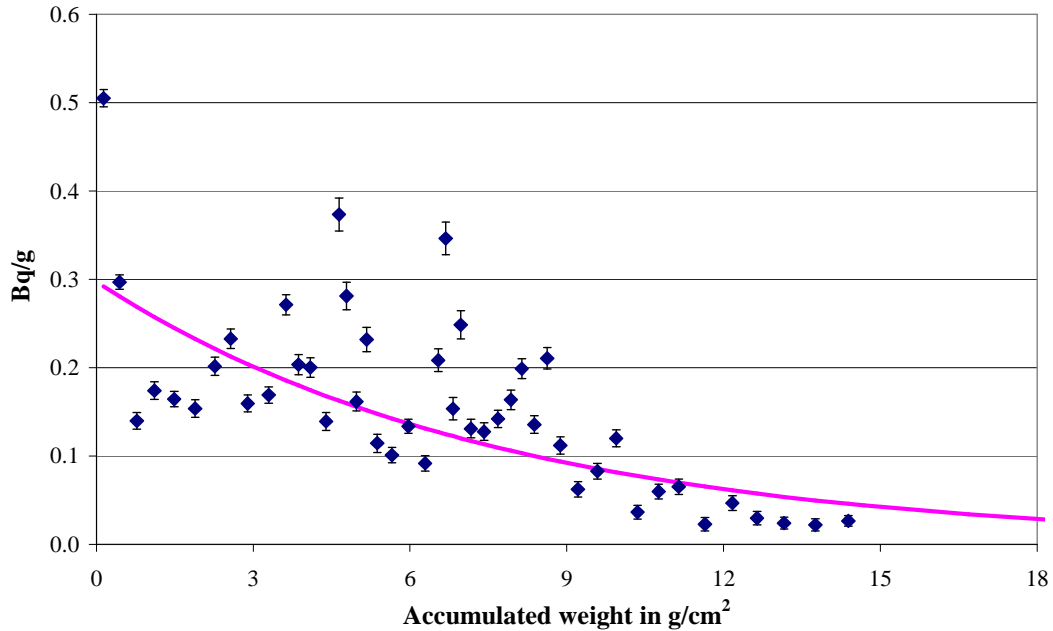
B
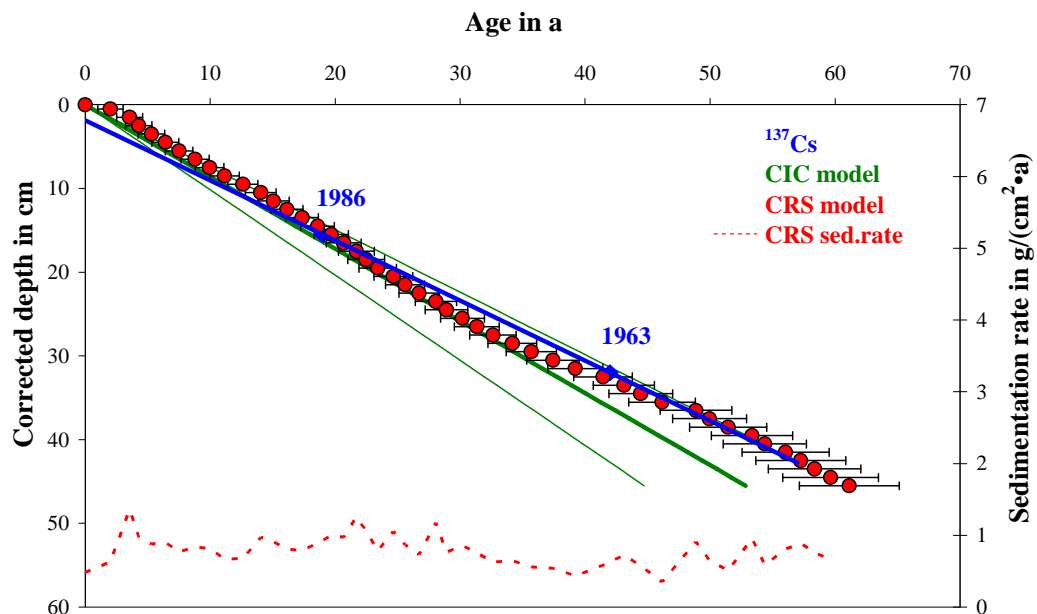
Fig. 4.28. Position 7. A: Measured unsupported ^{210}Pb activity concentration versus accumulated weight. The pink line is a weighted exponential fit to the data. **B**: Depth-age relation of the sediment as a result of dating. The dashed line shows the sedimentation rate calculated by the CRS model.

4.4.2 General conclusions on dating the sediments

For some of the sediment cores from Lago Maggiore both CIC and CRS models show rather good estimates of the sediments' age. It was supposed that due to varying sedimentation rates CRS version should be much better. However, as the age of sediment layers is determined via the ratio of integrals of the ^{210}Pb activity down to infinity, turbidites which add some more ^{210}Pb to the inventory tend to make the calculated age of sediment layers younger.

Of course, large turbidites can easily be identified on the photo of sediment cores. Nevertheless, smaller turbidites within the seasonal pattern in the photo of the core which have an influence on the age determination as well are more difficult to identify and to handle. Therefore, dating with radionuclides becomes rather difficult.

In general, together with ^{137}Cs, the ^{210}Pb methods CIC and CRS can provide reliable data for dating purposes and for sediment accumulation rate calculations.

5. MODELING OF RADIOCAESIUM IN WATER AND SEDIMENTS OF LAGO MAGGIORE

To predict the long-term behaviour and particularly the migration of radionuclides in the environment, different models were developed and used so far (Smith *et al.*, 2002; Kirchner, 1998; Klemt *et al.*, 2002; Monte *et al.*, 2003). Generally, two classes of migration models can be distinguished. The models of the first class – **simple compartment models** – use a number of compartments (which are defined as parts with constant concentrations) associated to soil/sediment layers, and calculate radionuclide fluxes between them, without making assumptions on the migration mechanisms (Bossew and Kirchner, 2004). Recently, however, it was pointed out (Kirchner, 1998) that this class of models which is using common differential equations implicitly assumes purely convective flow with dispersion characteristics defined by the number and size of compartments. The solution of such simple compartment models is presented as integration over time.

The models of the second class – **analytical models** – result in partial differential equations for the concentration $C\ (x,t)$, of a radionuclide in depth x below soil or sediment surface after migration time t. Basically, there are two types of analytical models. The *first type* makes assumptions on physico-chemical mechanisms which govern the migration of radionuclides in soil and their interaction with soil particles (Bossew, 2004). The *second type* tries to describe empirical profiles mathematically rather than explaining them, but due to their purely empirical basis, this type of models should not be used for predictions. Analytical models can be solved using both, finite differences (the solution is the averaged activity concentration within a certain layer) or finite element methods (the result is the continuous function instead of discretised constant values).

This work is devoted to a particular *analytical model of the first type* which assumes sedimentation and diffusion as two main processes controlling the vertical migration of ^{137}Cs in lake sediments. Another important mechanism which describes the interaction of

^{137}Cs between liquid and solid phase is sorption. The processes bio- and physical turbation as well as radioactive decay are taken into account in the model.

Within a joint project of the Radioecological Laboratory at the Hochschule Ravensburg-Weingarten (Germany) and the Spiez Laboratory (Switzerland) on the present radioecological situation of Lago Maggiore, the runoff of radiocaesium from the catchment area to the lake tributaries after a direct single-pulse deposition was modelled. It was sufficient to use a compartment model and to solve the common differential equations by the finite differences approach (Semizhon, 2005). In case of our model which describes migration processes in space and time and consists of a set of partial differential equations, a finite element program (FemLab) was used instead of finite differences (programs like ModelMaker, Powersim, etc.), although finite element programs are usually much more complicated. In this way we were able to describe the migration behavior of radionuclides by modeling their input into and the vertical distribution within the sediment as shown in this chapter.

5.1 Main processes in the "diffusion-convection" type model

In this chapter the main mechanisms controlling the migration processes of radiocaesium in the bottom sediments will be discussed in details.

5.1.1 Sorption

In deep lakes one of the processes by which radioactivity in the water column can be lost is sorption of radionuclides to particles which subsequently settle to the bottom sediment taking the radionuclide with them. Thus, a transfer of activity between the two phases (dissolved and particulate form) is taking place.

Exchangeable and fixed parts of radioactivity

In the solid phase of bottom sediments ^{137}Cs exists in two forms – exchangeable and fixed. The exchangeable form includes that ^{137}Cs which is most of its time adsorbed on the surface of particles and only part of its time dissolved in the pore water. The fixed

part of the radionuclide is bound to solids. The corresponding concentrations are given as C_E and C_F in Bq·m^{-2} per 1 cm layer of sediment. The interaction between the two parts can be described by first-order fixation and redissolution processes using the following differential equations (Konoplev *et al.*, 1996):

$$\frac{\partial C_E(x,t)}{\partial t} = -f \cdot C_E + r \cdot C_F \qquad (5.1)$$

$$\frac{\partial C_F(x,t)}{\partial t} = f \cdot C_E - r \cdot C_F \qquad (5.2)$$

where,

f and *r* are fixation and redissolution rates, respectively, in a^{-1}.

Schematically, one solution of these equations is shown in Fig. 5.1. Fixation and redissolution rates are *dynamic* parameters. As we do not intend to model seasonal variations (the time resolution is in terms of years), an equilibrium between fixation and redissolution can be assumed (Fig. 5.1). In this way the actual values of r and f become obsolete and only the ratio of r and f is important. The parameter f which is in the order of 2 a^{-1} (Spasova, 2003) is reasonable and we have equilibrium within one year.
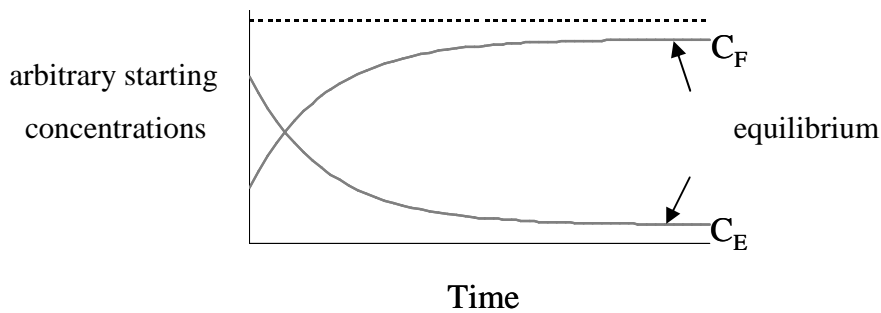
Fig. 5.1. A combination of fixation and redissolution processes describing the exchangeable and fixed parts of activity concentration.

The portion of exchangeable activity α is experimentally determined by the first step of extraction experiments (see chapter 4.3). Taking into account the statements described above we finally derive the following equilibrium equation:

$$\alpha \;=\; \frac{C_E}{C_E + C_F} \;=\; \frac{r}{r + f}\,. \tag{5.3}$$

Distribution coefficient

The distribution coefficient K_d is an *equilibrium* parameter which relates the activity concentration of the adsorbed ^{137}Cs to its activity concentration in the pore water (see chapter 3.2.4)

There are exchangeable (K_d^{ex}) and total (K_d^{tot}) distribution coefficients which can be calculated from the concentration of exchangeable ions sorbed on solids or from the total activity of the sediment, respectively. The ratio of these two coefficients gives the portion of exchangeable activity α within the sediment:

$$\alpha \;=\; \frac{K_d^{ex}}{K_d^{tot}}\,. \tag{5.4}$$

The value of the total distribution coefficient K_d^{tot}, is very much sensitive to radionuclide speciation in the solid phase (Konoplev and Bulgakov, 1995). In immediate term only the exchangeable portion of radionuclide contributes to solid-liquid interphase exchange. The advantage of K_d^{tot} is that its value is governed by ion exchange and can in principle be calculated on the basis of environment characteristics such as capacity of sorption sites and cation composition of solution.

Nevertheless, a rather constant K_d^{tot} for ^{137}Cs (over the period of 11 years after the Chernobyl fallout) was measured by Klemt *et al.* (2001) for the system "water – suspended matter" in Lake Lugano which is a neighbouring lake to Lago Maggiore. In our model with the first order fixation and redissolution processes we also use a constant distribution coefficient K_d^{tot}.

5.1.2 Sedimentation and compaction

Sedimentation is mathematically equivalent to convection with the only difference that convection is connected with dispersion while sedimentation processes take place without it. This process is described by the following differential equation:

$$\frac{\partial C}{\partial t} = v_s \cdot \frac{\partial C}{\partial x}, \qquad\qquad (5.5)$$

where v_s is a sedimentation speed in cm·a^{-1}.

Fig. 5.2 explains schematically the sedimentation process which describes the "movement" or transport of the activity with time through the profile. The black line indicates an arbitrary peak as initial condition at time t_0. If there are no other processes in the lake than sedimentation, with time the activity will be moved down to deeper layers of the sediment profile which correspond to the lighter lines in the figure.
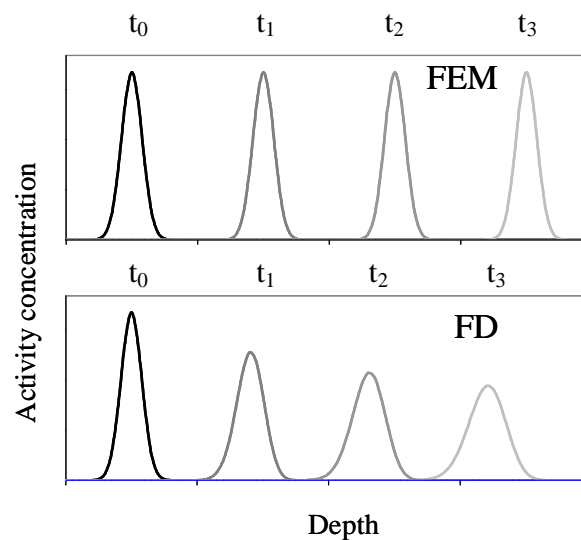
Fig. 5.2. Schematic description of the sedimentation processes in the lake sediments using finite differences (FD) and finite element methods (FEM) assuming a peak distribution in the sediment. Different colours indicate different time.

Here, it is also necessary to show one of the distinctions between the two approaches: finite differences and finite elements methods (see also chapter 5.5). The limited number of layers in the finite differences approach introduces a broadening of the peak (Fig. 5.2).

Experimentally it was found out that the bulk density of the sediment ρ_b (g·cm^{-3}) is not constant and increases with depth for most of the studied positions. Empirically it can be described as:

$$\rho_b(x) = \left(\rho_0 + \frac{d\rho}{dx} \cdot x\right),$$

(5.6)

where ρ_0 is the density of the top layer of the sediment, in g·cm^{-3}; x is depth in cm and

$\frac{d\rho}{dx}$, in g·cm^{-4}, defines the slope of the linear function of bulk density of a certain vertical

profile.

The compaction of sediments with depth is taken into account by weighing the sedimentation speed v_S (cm·a^{-1}) at depth x within the sediment by the measured bulk density ρ_b:

$$v_S(x) = v_0 \cdot \frac{\rho_0}{\rho_b(x)}.$$

(5.7)

The sedimentation rate R_S (g·cm^{-2} per year) which does not depend on the depth is used to describe the amount of sediment settling every year onto the bottom of the lake.

The ratio $\frac{R_S}{\rho_b}$ gives the sedimentation speed v_S which is introduced into the differential

equations describing the movement of the activity concentration due to the sedimentation process (see equation (5.5)):

$$\frac{\partial C_E}{\partial t} = \frac{\partial}{\partial x}\left(\frac{R_S}{\rho_b} \cdot C_E\right)$$

(5.8)

and

$$\frac{\partial C_F}{\partial t} = \frac{\partial}{\partial x}\left(\frac{R_S}{\rho_b} \cdot C_F\right).$$

(5.9)

In these differential equations the sedimentation speed has to be within the gradient as it is not constant.

5.1.3 Diffusion and turbation

In terms of fixed and exchangeable activities of ^{137}Cs, it is evident that the fixed portion C_F cannot diffuse in the sediment as it is bound to solid particles, whereas the exchangeable part C_E can be transported upwards and downwards due to diffusion processes in the pore water.

On the other hand, there are bio- and physical turbation processes which are important for the top sediment layer and describe the role of worms, wind, waves, etc. in the lake.

Diffusive transport in sediments

Thus, one of the main transport mechanisms which contribute to the mixing of radionuclides in lake sediment is molecular diffusion. Dissolved radionuclides tend to move from regions of high concentration to regions of low concentration according to Fick's first law of diffusion:

$$F = -D_E \cdot \frac{\partial C_E}{\partial x}, \tag{5.10}$$

where

F is the diffusion flux, in $Bq \cdot (cm^2 \cdot a)^{-1}$;

D_E is the effective diffusion coefficient, in $cm^2 \cdot a^{-1}$.

From the conservation of mass we know that

$$\frac{\partial C_E}{\partial t} = -\frac{\partial}{\partial x} F, \tag{5.11}$$

Combining this relation with the Fick's first law we get Fick's second law:

$$\frac{\partial C_E}{\partial t} = \frac{\partial}{\partial x} \left(D_E \cdot \frac{\partial}{\partial x} C_E \right) \tag{5.12}$$

and

$$\frac{\partial C_F}{\partial t} = \frac{\partial}{\partial x} \left(D_E \cdot \frac{\partial}{\partial x} C_F \right). \tag{5.13}$$

Only in case when D_E is independent on depth x it can be taken outside the gradient:

$$\frac{\partial C_E}{\partial t} = D_E \cdot \frac{\partial^2 C_E}{\partial x^2}. \qquad (5.14)$$

In Fig. 5.3 the effect of the diffusion process influencing a peak distribution of radioactivity in the sediment is shown schematically. The longer the diffusion takes place the broader the peak will be. Different curves show different time intervals.
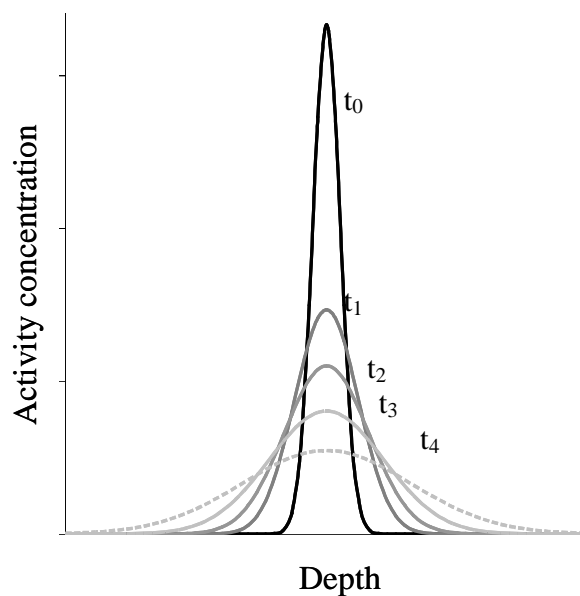
Fig. 5.3. Effect of diffusion on a peak distribution of activity within the sediment depending on time. Different colours indicate different times.

Retardation factor

The effective diffusion coefficient D_E is the diffusion coefficient in an adsorbing system. It is equal to the diffusion coefficient of ions under non-adsorbing conditions (D), divided by a retardation factor (R) of the adsorbing system:

$$D_E = \frac{D \cdot \tau}{R}. \qquad (5.15)$$

Here, τ ($\tau < 1$) is the dimensionless tortuosity factor which describes the decrease of D_E due to tortuous flow along the pores of the sediment. *D* is the diffusion coefficient of ions (in this study Cs^+) in water of a certain temperature in $cm^2 \cdot a^{-1}$.

The retardation factor is a dimensionless parameter characterizing the retarding effect of adsorption on solute transport. Mathematically, the retardation factor, R, is defined as:

$$R = 1 + \frac{\rho_b}{\theta} \cdot K_d^{ex}, \tag{5.16}$$

where

ρ_b is the measured bulk density of the sediment, in $g \cdot cm^{-3}$;

θ is a dimensionless parameter which describes the volumetric content of water.

Hence, it is evident that the larger the distribution coefficient is, the larger the retardation factor is. On the other hand, a lower pore water content can also lead to an increase of the retardation factor.

Tortuosity and porosity

In sediments, diffusive transport of ions and molecules is influenced by two sediment characteristics – tortuosity and porosity (Maerki *et al.*, 2004).

Tortuosity τ is a measure of the increase of the path length through the pores of sediment as compared to the direct path. It can be calculated as (Klute, 1986)

$$\tau = \theta^{\frac{7}{3}} \cdot \varepsilon^{-2}, \tag{5.17}$$

where ε is the dimensionless porosity of the sediment which is in the order of 80 – 90 % and θ is a volumetric content of water. The assumption that all pores in the sediment are filled with water leads to $\theta = \varepsilon$. Taking this fact into account, the equation for the tortuosity can be formulated as:

$$\tau = \varepsilon^{\frac{1}{3}}. \tag{5.18}$$

Having the values for particle density and bulk density of the sediment, it is possible to calculate the total porosity ε using the following equation:

$$\varepsilon = \left(1 - \frac{\rho_b}{\rho_p}\right). \tag{5.19}$$

Here, ρ_p is the mean particle density which according to Klute (1986), typically equals to 2.65 g·cm^{-3}. This value was also measured on some typical sediments by Spasova (2003). The total pore space increases as the bulk density decreases and vice-versa. The ratio $\dfrac{\rho_b}{\rho_p}$ gives the fraction of the total volume which is occupied by solids, thus, by subtracting this value from unity, one gets the fraction of the total volume occupied by pores.

Effective diffusion of ^{137}Cs in sediments

An important remark concerning the distribution coefficient in equation (5.16) should be mentioned here. As described above, our model introduces one distribution coefficient K_d which is responsible for the uptake of ^{137}Cs into the sediment. But we introduce another coefficient $K_{d\_dif}^{ex}$ which controls the diffusion within the sediment. The latter is decreased due to the enhanced concentration of competing ions (NH_4^+, K^+) in the pore water of the sediments as compared to the lake water. This $K_{d\_dif}^{ex}$ is used to calculate the retarded diffusion of ^{137}Cs within the pore water. Thus the final equation for the effective diffusion can be given by:

$$D_E = D \cdot \sqrt[3]{\varepsilon} \cdot \frac{1}{1 + \dfrac{\rho_b}{\varepsilon} \cdot K_{d\_dif}^{ex}}. \tag{5.20}$$

In this formula D is the constant of diffusion for metal ions in pure water as taken from Klute (1986) and recalculated to the average temperature of the lake water using the equation below:

$$D_{T°C} = \frac{M_{25°C}}{M_{T°C}} \cdot D_{25°C}, \tag{5.21}$$

where $M_{T°C}$ and $M_{25°C}$ are the viscosities of water, in cp, at the respective temperatures. In Lago Maggiore the temperature of the lake water below the epilimnion varies between 6°C and 8ºC for spring and autumn seasons. Thus, the diffusion constant D for Cs^+ at a temperature of 7 ºC (which is an average temperature of the deepest layers of the lake) equals to 405.35 $cm^2 \cdot a^{-1}$.

The exchangeable ^{137}Cs distribution coefficient $K_{d\_dif}^{ex}$ essentially reduces the effective diffusion of exchangeable ^{137}Cs in the sediment. The larger this coefficient is the lower the portion of time in which Cs^+ can diffuse in the pore water.

Competing ions

The major ions that compete with caesium for binding sites on illitic clays are NH_4^+ and K^+ (see chapter 1.2.1).

In a simple model we assume that the distribution coefficient $K_{d\_dif}^{ex}$ is inversely proportional to the concentration of competing ions in the pore water:

$$\frac{K_{d\_dif}^{ex}}{K_d^{ex}} = \frac{[K^+] + 5 \cdot [NH_4^+] \text{ in water}}{[K^+] + 5 \cdot [NH_4^+] \text{ in pore water}}. \tag{5.22}$$

Here, the constant "5" in front of ammonium concentration reflects the fact that the affinity of NH_4^+ cations to the selective sorption sites is about 5 times higher than the affinity of K^+.

In our model $K_{d\_dif}^{ex}$ is a free parameter which will only later be compared with the concentration of competing ions.

Bio- and physical turbation processes

In the top layers of sediment (several cm) two different processes may take place: *bioturbation* which is the mixing or alteration of sediment particles or pore water by

various organisms, or/and *physical turbation* which is caused by the action of waves, currents, winds, etc. Both processes influence the vertical migration of the exchangeable and non-exchangeable chemical form of radionuclides in the top layer of the bottom sediments leading to a mixing of this layer.

From a mathematical point of view these processes are similar to diffusion and can be described by the following equation:

$$F_{phys} = -D_{phys} \cdot \frac{\partial C}{\partial x}, \tag{5.23}$$

what allows simply to sum it up to the effective molecular diffusion:

$$\frac{\partial C_E}{\partial t} = \frac{\partial}{\partial x}\left(\left(D_E + D_{phys}\right) \cdot \frac{\partial}{\partial x} C_E\right) \tag{5.24}$$

and

$$\frac{\partial C_F}{\partial t} = \frac{\partial}{\partial x}\left(D_{phys} \cdot \frac{\partial}{\partial x} C_F\right) \tag{5.25}$$

Here, the term of D_{phys} implies that not only physical turbation but also bioturbation is included.

5.1.4 Radioactive decay

One of the processes leading to the decrease of activity concentration of radionuclides in the sediment is radioactive decay:

$$\frac{\partial C}{\partial t} = -\lambda \cdot C, \tag{5.26}$$

where λ is the decay constant in a^{-1}. It can be calculated from the half-life $T_{1/2}$ for a certain radionuclide:

$$\lambda = \frac{\ln 2}{T_{1/2}}. \tag{5.27}$$

Thus, for ^{137}Cs with the half-life $T_{1/2} = 30.07$ years λ equals to 0.023 a^{-1}.
Graphically this process is presented in Fig. 5.4.
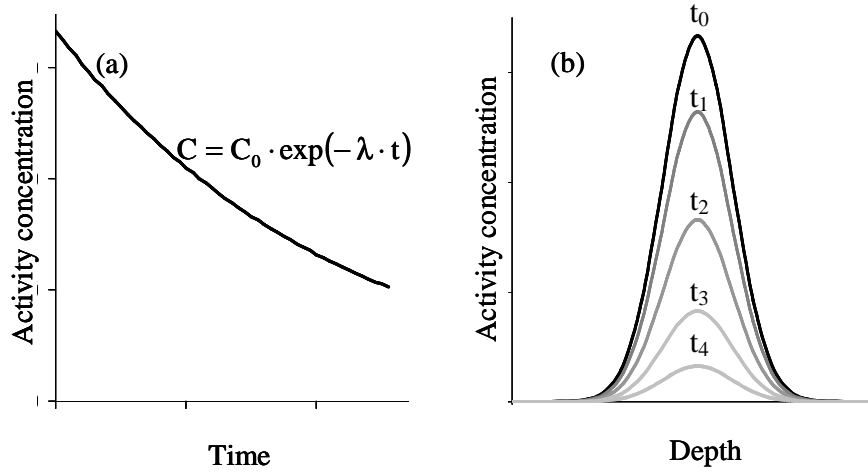
Fig. 5.4. The law of radioactive decay (a) and its influence on the decrease of activity concentration with time t on a vertical peak profile (b).

5.1.5 Complete system of coupled differential equations

Taking into account all the processes described above, the vertical distribution of activity within the sediment and the continuous input of ^{137}Cs into the lake can be comprised by the following system of two coupled partial differential equations:

$$\frac{\partial C_E(x,t)}{\partial t} = \frac{\partial}{\partial x}\left((D_E + D_{phys})\cdot \frac{\partial}{\partial x}C_E\right) + \frac{\partial}{\partial x}\left(\frac{R_S}{\rho_b}\cdot C_E\right) - f\cdot C_E + r\cdot C_F - \lambda\cdot C_E \quad (5.28)$$

$$\frac{\partial C_F(x,t)}{\partial t} = \frac{\partial}{\partial x}\left(D_{phys}\cdot \frac{\partial}{\partial x}C_F\right) + \frac{\partial}{\partial x}\left(\frac{R_S}{\rho_b}\cdot C_F\right) + f\cdot C_E - r\cdot C_F - \lambda\cdot C_F. \quad (5.29)$$

C_E and C_F are the exchangeable and fixed part of radioactivity, respectively, given in Bq·m^{-2} per 1 cm layer of sediment; λ (a^{-1}) denotes the ^{137}Cs radioactive decay constant, f (a^{-1}) and r (a^{-1}) are first order fixation and redissolution rates, R_S (g·cm^{-2}·a^{-1}) is the sedimentation rate, ρ_b (g·cm^{-3}) is the measured bulk density of the sediment, D_{phys} (cm^2·a^{-1}) the combined bio- and physical turbation acting only in the top layers of the sediment, and D_E (cm^2·a^{-1}) is the retarded constant of ^{137}Cs$^+$ diffusion.

103

5.2 Initial and boundary conditions

To solve the system of partial differential equations initial and boundary conditions are needed.

5.2.1 Initial conditions

The model presented in this study can describe not only the maximum in the vertical sediment profile related to the fallout in Chernobyl in 1986, but also those peaks which are related to the nuclear weapons testing fallouts with maxima in 1959 and 1963. In case that the total inventory in the vertical sediment profiles was not reached experimentally (e.g. position 1), modeling was possible only for the Chernobyl peak. Hence, as the time for the initial condition 01.01.59 (a rough time of the first nuclear weapons testing fallout maximum) or 01.05.86 (the time of the Chernobyl fallout) were chosen.

For both cases it was approximated that at initial time the activity concentration in the sediment was negligible:

$$C_E(t=0) \ = \ C_F(t=0) \ = \ 0 \, . \tag{5.30}$$

5.2.2 Boundary conditions

To solve the partial differential equations a Dirichlet boundary condition is used:

$$C \ (x=0) \ = \ K_d \cdot C_L \, . \tag{5.31}$$

This boundary condition describes the uptake of activity from water to the top layer of the sediment and - as an alternative interpretation - in combination with the sedimentation rate R_S it describes the uptake of settling suspended matter being in equilibrium with the dissolved activity in the surrounding water. In principle, activity diffusing within the sediment to its top layer could be taken out from the sediment and redissolved again in the water by this equation.

The radionuclide activity concentration in the lake water, C_L (Bq·m^{-3}), must be known from the time of deposition (Chernobyl or nuclear weapons testing fallouts) until the time to which the model should be calculated.

MOIRA and AQUASCOPE models as a tool to describe the activity concentration in the lake water

A variety of models predicting the behavior of radionuclides (most commonly ^{137}Cs and ^{90}Sr) in fresh water ecosystems has been developed and tested during recent decades (Monte *et al.*, 2003). Among them there are such models as MOIRA (Monte, 1991; Monte *et al.*, 2000) and AQUASCOPE (Smith *et al.*, 2005) which give average estimates for radionuclides in water bodies for all times after radioactive fallout. These are models which have been intensively calibrated and tested for Chernobyl-derived radionuclides in many European lakes. Thus, the output results are quite reliable.

The above mentioned models are, essentially, equivalent. They supply similar outputs for a suitable choice of their parameters and they are considered to be not very complicated in the sense that the information on input parameters is usually available and does not require complicated measurements.

MOIRA

For running MOIRA one has to know such general information on the lake and its watershed as mean and maximum depths, altitude, longitude and latitude, lake area, catchment area, average amount of precipitation as well as the deposition on the catchment area and lake itself. However, additional information about soil and bedrock type can be of great importance. MOIRA calculates the activity concentration of radionuclides taking into account their seasonal variations by introduction of seasonal moderator which (in case of Lago Maggiore) gives an increased transport of ^{137}Cs during the late spring – summer period with snow melting and maximum amount of precipitation.

AQUASCOPE

The AQUASCOPE model takes into account the following key processes of radionuclide transfer in a catchment-lake system: fallout to the catchment and lake surface, runoff of radionuclide from the catchment to the lake, removal of radionuclide from the lake water to sediments and removal of radionuclide via the lake outflow (Smith et al., 2005).

The ^{137}Cs activity concentration in the runoff water, C_R (Bq·m^{-3}), is given by the sum of three exponential functions:

$$C_R(t) = D_C \cdot (\alpha_{Cs} e^{-(\lambda + k_1)t} + \beta_{Cs} e^{-(\lambda + k_2)t} + \gamma_{Cs} e^{-(\lambda + k_3)t}), \qquad (5.32)$$

where D_C is the ^{137}Cs deposition to the catchment area (Bq·m^{-2}); λ (a^{-1}) is the ^{137}Cs radioactive decay constant; α_{Cs}, β_{Cs}, γ_{Cs} (m^{-1}) and k_1, k_2, k_3 (a^{-1}) are empirically determined constants. The three exponential terms in the equation (5.32) describe a very fast decrease of the ^{137}Cs activity due to a rapid washoff processes, a slow decline as a result of soil fixation and redistribution processes, and the very long term of "equilibrium" situation, respectively.

The initial mean ^{137}Cs activity concentration in the lake water, $C_L(0)$ (Bq·m^{-3}), can be estimated by:

$$C_L(0) = \frac{D_L}{d}, \qquad (5.33)$$

where D_L (Bq·m^{-2}) is the ^{137}Cs deposition to the lake surface and d (m) the mean depth of the lake, calculated by dividing the lake volume by the lake area.

Taking into account that the decline of radionuclide concentration in the lake water is determined by transfer of radionuclide to the bottom sediments, losses through the lake outflow and physical decay constant, the activity ^{137}Cs concentration in the lake can be calculated as:

$$\frac{\partial C_L}{\partial t} = \frac{C_R}{\tau_w} - \frac{C_L}{\tau_w} - \frac{C_L}{\tau_s} - C_L \lambda, \qquad (5.34)$$

where τ_w (a) is the water residence time of the lake and τ_s (a) is the time constant of ^{137}Cs transfer to the sediments. The inflow of ^{137}Cs into the lake is given by C_R (eq. 5.32).

The simplicity of the structure of the AQUASCOPE model (implemented in EXCEL) in comparison with the MOIRA model (based on the program Powersim) convinced us to use the AQUASCOPE model for predicting ^{137}Cs in Lago Maggiore and to implement it as a boundary condition for the set of two partial differential equations. Fig. 5.5. shows a comparison of the model outputs.
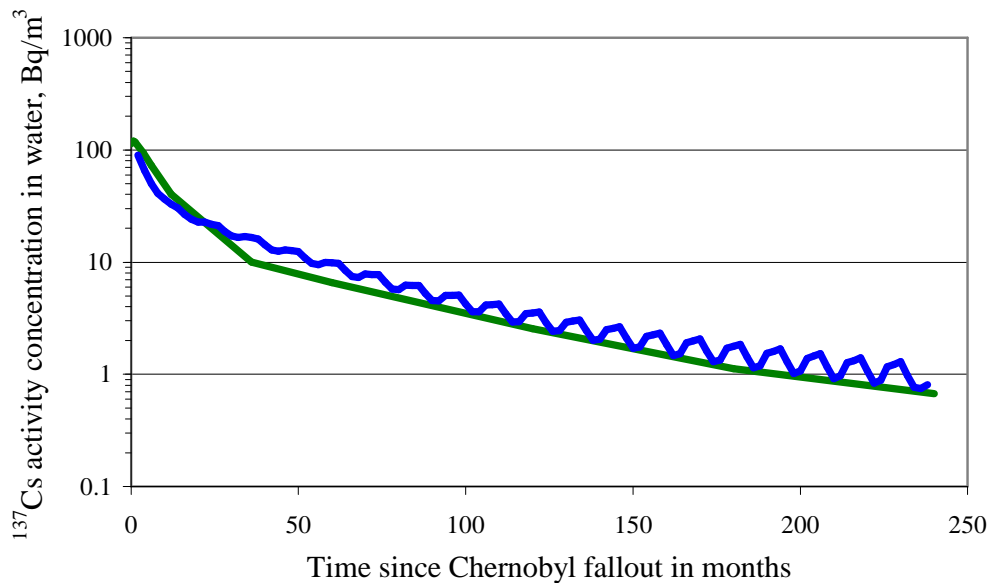
Fig. 5.5. Comparison of the results (concentration of ^{137}Cs in water of Lago Maggiore) of models MOIRA (blue curve with seasonal variations) and AQUASCOPE (green line).

After several runs of the lake models (MOIRA and AQUASCOPE) two parameters which have the main influence on the output result were singled out, these are – the mean precipitation and the deposition of ^{137}Cs on the catchment area. In Semizhon (2005), a sensitivity analysis of the run-off model for Lago Maggiore was performed which also showed that the most sensitive parameters are the initial deposition on the catchment area, the amount of precipitation, and the soil permeability factor (see chapter 4.1.5).

According to "Atlas of caesium deposition on Europe after the Chernobyl accident" (1998) the inventory of ^{137}Cs on the territory of the watershed of Lago Maggiore varies largely between 2 000 Bq·m^{-2} and 40 000 Bq·m^{-2}. The best fit to the measured data is shown in Fig. 5.6. As initial deposition on the catchment area of the lake in this case a value of 3 500 Bq·m^{-2} was taken. This value is in agreement with that of (5 000 ± 2 000) Bq·m^{-2} which was used in the catchment area model described in Semizhon (2005).

As the value for the average precipitation for Lago Maggiore and its watershed is known rather precise, it was not possible to vary it largely. Although the annual precipitations have rather strong variations (1226–3352 mm·a^{-1}), according to the maps of precipitation (Carollo, 1985) and data reported in the literature (de Bernardi *et al.*, 1984; Premazzi, 2003) the average rainfall in the watershed area of Lago Maggiore is 1833 mm·a^{-1}.

The other parameters used in AQUASCOPE model are the average deposition of ^{137}Cs to the lake (20 000 Bq·m^{-2}), the water residence time (3.8 a) and the areal fraction of organic boggy soils (0.05).

Nuclear weapon testing and Chernobyl fallout boundary conditions

The AQUASCOPE model was applied to Lago Maggiore and fitted to several measured surface water data points which were available from D'Alberti (2003), D'Alberti (2001–2002), Cazzaniga *et al.* (1996–1998), Cazzaniga *et al.* (1997), D'Alberti and Osmani (1995), Osmani *et al.* (1994), Dominici and Risposi (1990–1993), Dominici (1989 – 1980), from the "Radioactivity Environmental Monitoring (REM) database of the Institute for Environment and Sustainability, DG JRC, European Commission, and also to our measured data of the ^{137}Cs vertical distribution in the water column (Fig. 5.6). The output of the model gives the result as an average ^{137}Cs concentration over the water column.

The data points taken from the literature correspond to the surface water measurements, so it is reasonable to have very high values for the first months after Chernobyl accident when most of activity was deposited on the lake surface. Within the next months part of activity was transported with particles down to the bottom sediments and by this way was removed from the surface. This fact explains the lower values of the ^{137}Cs activity concentrations (blue points in Fig. 5.6). The measured points at different depths (every 30 – 50 m) of the lake water column are presented in red colour. The higher ^{137}Cs activity concentration was measured in the deeper layers while on the surface it was rather low.

To model the vertical distribution of ^{137}Cs over the whole sediment profile including the Chernobyl and nuclear weapons testing fallouts, the boundary conditions were derived in the following way: The activity concentration in the lake water after single pulse events

was calculated with the AQUASCOPE model (Fig. 5.6). This result was summed up three times with different amplitudes for the maxima of the weapon testing and Chernobyl fallouts in 1959, 63 and 86, respectively, as shown in Fig. 5.7.
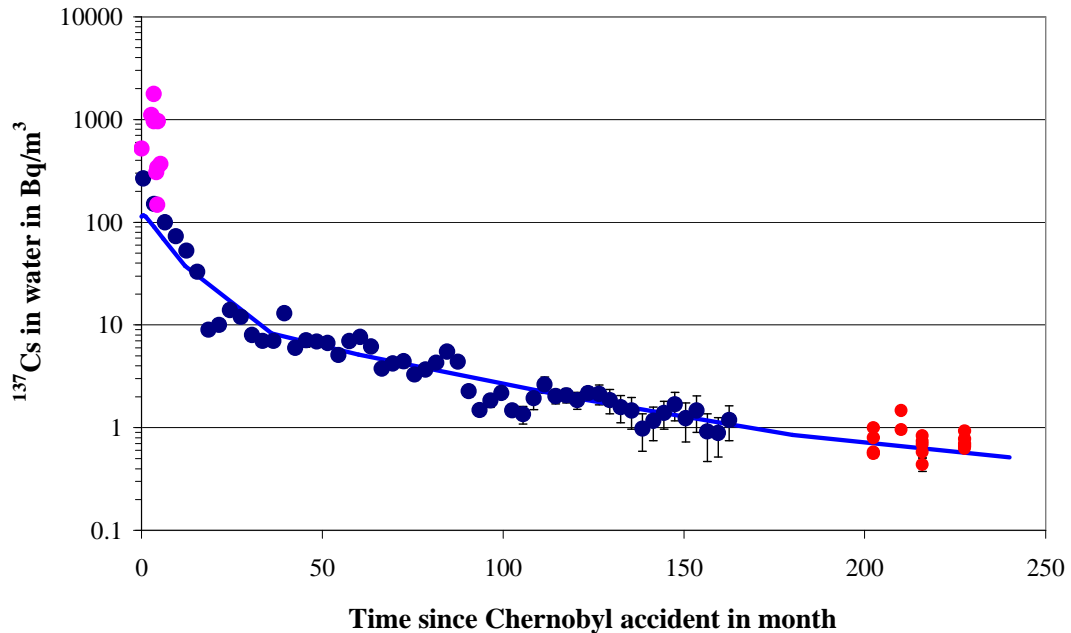
Fig. 5.6. Comparison between empirical data and AQUASCOPE model predictions of ^{137}Cs activity concentration in the water of Lago Maggiore. Blue points (D'Alberti, 2003; D'Alberti 2001–2002; Cazzaniga *et al.*, 1996–1998; Cazzaniga *et al.*, 1997; D'Alberti and Osmani, 1995; Osmani *et al.*, 1994; Dominici and Risposi, 1990–1993; Dominici, 1989 – 1980) and pink (REM database of JRC, Ispra, Italy) points are the values of ^{137}Cs activity concentration in the surface water, red are the measured values for different depths in the water column. The blue solid line is the output of the AQUASCOPE model which is an average ^{137}Cs concentration over the water column.
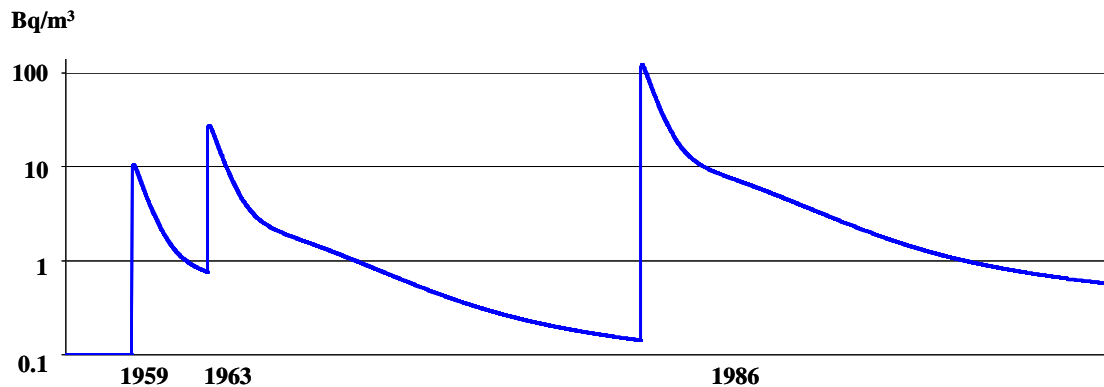
Fig. 5.7. Boundary condition: Activity concentration in the lake water.

The ratio of peaks in 1959 and 1963 is known to be about 2.6 (Bachhuber, 1982). The ratio of inventories of ^{137}Cs in the catchment area after the nuclear weapon testing fallout and after the Chernobyl fallout is one more free parameter of the model. It is sufficient to describe the nuclear weapon testing fallouts by two distinct incidents. The diffusion acting for more than 40 years smears these peaks to a broad feature in the vertical distribution which is observed nowadays.

5.4 Introduction of turbidites

As discussed in chapter 4.2.2 a distinctive feature of Lago Maggiore is the presence of turbidite layers in the sediment profiles. These turbidite layers were found nearly at all studied locations, so while modeling the vertical ^{137}Cs distribution in the sediments it appeared to be necessary to describe the real situation and to take turbidites into account as an instantaneous extra input of sediment.

To model such special events, the following parameters are needed:

- position of the turbidite;
- a very short fixed time interval for the deposition;
- a very large deposition speed;
- activity concentration inside the turbidite.

The position of the turbidite layers can be easily defined from photos of sediment core and the measured ^{137}Cs and bulk density vertical distributions. For the model the position of the turbidite should be given in terms of time and can be calculated knowing the depth where the turbidite layer is observed and the sedimentation speed of the sediment. Within the turbidite itself a deposition speed which is several orders of magnitude larger than the sedimentation speed of the sediment should be introduced in order to model the extra deposition of sediments during one single incident.

In most cases the activity concentration of ^{137}Cs inside the turbidite layer stays constant but it differs from that which is measured in the layers below and above. So, an additional coefficient for the ^{137}Cs activity concentration within the turbidite is included into the model.

All these parameters described above give no special insight into processes but they give the possibility to model the diffusion into or out of the turbidite.

5.5 Finite-element method for modeling the radionuclides in the sediment

To get a numerical solution of our model, which is a system of two coupled partial differential equations (5.28) – (5.29), a finite element method is used instead of a finite differences approach which was successfully applied so far for the calculation of the vertical ^{137}Cs distribution in sediments of three lakes with different limnological characters (Klemt *et al.*, 2002). In these applications of finite differences an artificial broadening of structures in the vertical distribution due to the sedimentation term could not be avoided. Also, the used program (ModelMaker) was not able to handle turbidites and the thousands of compartments which would have been needed to describe not only the Chernobyl but also the nuclear weapons testing fallouts.

The convection-diffusion type model in a 1-dimensional geometry was built using the MATLAB package FemLab. An example of the mathematical code of the model can be found in Appendix F.

5.6 Results of modeling radiocaesium in the sediments of Lago Maggiore from different positions

The model described above is applied to describe the vertical distributions of ^{137}Cs activity concentrations in sediments of Lago Maggiore. The model is adjusted to each particular case taking into account such measured parameters as exchangeable portion of radiocaesium α and the bulk sediment density ρ_b which may vary with depth. The height and the position of maxima is optimized by two parameters: the sedimentation rate R_s and the total distribution coefficient K_d^{tot}. Additionally, the distribution coefficient $K_{d\_dif}^{ex}$ responsible for the retarded diffusion within the sediment is optimized. All three free parameters are optimized together in a "non-weighted least squares fit". Such parameters as time of the turbidite, speed and the activity concentration within the turbidite, deposition onto the lake surface due to the nuclear weapon testing fallout are optimized by hand to reasonable values.

The results of modeling the vertical distribution of ^{137}Cs in the sediments of Lago Maggiore from different positions are shown in Fig. 5.8 to Fig. 5.16. For positions 1 (Fig. 5.8, 5.9) and 7 (Fig. 5.16) the peak related to the Chernobyl fallout is modeled. For other positions (2 to 6) the model describes the complete profile with two maxima related to both, the Chernobyl and the nuclear weapon testing fallouts.

In each figure the colored lines (part A) correspond to the inventories in single 1 cm sediment layers which are fitted to the measured data marked as red dots (the data corresponds to 2003 (17 years) for positions 1 and 2 (Fig. 5.8 to 5.11), to 2004 (45.3 years) for positions 3, 4, 5 (Fig. 5.12 to 5.14), and to 2005 (46.3 years) for positions 6 and 7, respectively (Fig. 5.15, 5.16)). The layer inventories are summed up to the total inventory of the sediment which is represented by the upper dark blue curve (Fig. 5.8 to 5.16, part A).

As a snapshot at the times of sampling the measured vertical ^{137}Cs distributions in the sediment are given (part B, columns) and compared to the modeled function (part B, line) and the layer average as calculated from the model (part B, points).

113

At present, a continuous decrease of radioactivity can be seen for each position. The maximum in total inventories of ^{137}Cs of most studied sediments profiles is observed 8 – 9 years after the Chernobyl accident and varies between 10 kBq·m^{-2} and 21 kBq·m^{-2}. An exception is position 6 where the total ^{137}Cs inventory is characterized by a maximum of about 6 kBq·m^{-2} reached already in 1988 (30 years in Fig. 5.15), 2 years after the Chernobyl fallout. The modeled total ^{137}Cs inventories are in a good agreement with our measurements (see chapter 4.2).

At those lake positions where two maxima are modeled it was necessary to introduce different sedimentation rates for the regions of Chernobyl and nuclear weapon testing maxima (Table 5.1). There is no common tendency of the sedimentation rate to increase or decrease with time but it is obvious that the conditions in the lake were changed during the studied period of time.

The turbidity flows (see chapter 4.2.2) are taken into account for the common fit and shown in figures as "turbidites". Hence, at *position 1* (Fig. 5.8, A) a turbidite can be observed as one instance in the year 1999 (13 years) and in Fig.5.8, B as the region between 4 cm and 7 cm. In another core from the same position a similar situation is expected. Indeed, from Fig. 5.9, A, it can be seen that a turbidite occurred in the same year 1999 (13 years) and corresponds to the layer between 3 cm and 7 cm in Fig.5.9, B.

In Fig. 5.10, A and 5.11, A, where the modeling of the ^{137}Cs vertical distributions in two different sediment cores at *position 2* are shown, a very large turbidite can be seen as one instance in the year 1976 (17.9 years). In Fig. 5.10, B and 5.11, B, it corresponds to the region between 13 and 32 cm.

At *position 3* (Fig. 5.12, A) two turbidites are observed in the years 1963 (4.6 years) and 1999 (41 years) which matches the layers 18.5–20.5 cm and 2–5 cm in Fig. 5.12, B.

The small turbidite layers between 0–3 cm and 1–4 cm at *positions 4* (Fig. 5.13) and *5* (Fig. 5.14), can be seen as one instance in the years 2004 (45 years) and 2001 (43 years) respectively. Finally, at *position 7* (Fig. 5.16) two turbidite layers between 10–12 cm and 15.5–18.5 cm are observed in the years 1999 (7.7 years) and 1995 (3 years), respectively.

The main parameters of the model are summarized in Table 5.1 and discussed in the following chapter 5.7.

Generally, the results of modeling show that maxima due to Chernobyl and nuclear weapon testing fallouts as well as intermediate turbidites are described quite well, except those positions where a lot of small turbidites are found which bring not only additional uncertainty to the model, but also makes the situation very complicated. For other positions good agreements are observed between measured ^{137}Cs activity concentrations and model predictions. This means that our model is able to describe quite realistically the distribution of ^{137}Cs in lake sediments and parameters describing the migration processes in the lake can be derived.

Table 5.1. Measured (bulk density of the top layer of the sediment ρ_0 and the slope of the bulk density $d\rho/dx$, portion of exchangeable radiocaesium α), free (sedimentation rate R_S, total distribution coefficient K_d^{tot} and coefficient $K_{d\_dif}^{ex}$ responsible for the diffusion within the sediment) and dependent (exchangeable distribution coefficient K_d^{ex}, effective diffusion of ^{137}Cs in the sediment D_E) parameters of the model.

	Measured parameters			Free fit parameters				Dependent parameters	
	Bulk density		α [1]	R_S [g·(cm^2·a)$^{-1}$]		K_d^{tot} [l·kg^{-1}]	$K_{d\_dif}^{ex}$ [l·kg^{-1}]	K_d^{ex} [l·kg^{-1}]	D_E [cm^2·a^{-1}]
	ρ_0 [g·cm^{-3}]	$d\rho/dx$ [g·cm^{-4}]		Chernobyl	NWT				
Pos 1 Core 1	0.73	0.0009	0.0045	0.94 ± 0.03	-	19 500 ± 8 000	29.3 ± 15	87.8 ± 38.7	12.0 ± 6.2
Pos 1 Core 4	0.76	0		0.61 ± 0.02	-	18 600 ± 7 100	25.2 ± 14.6	83.9 ± 38.0	13.3 ± 7.7
Pos 2 Core 1	0.29	0.009	0.0099	0.12 ± 0.01	0.24± 0.04	104 000 ± 27 000	335 ± 107	1030 ± 272	3.4 ± 1.1
Pos 2 Core 3	0.28	0.009		0.13 ± 0.01	0.25± 0.04	99 000 ± 9 000	194 ± 84	980 ± 102	6.1 ± 2.6
Pos 3 Core 3	0.70	0.0002	0.0021	0.42 ± 0.03	0.21 ± 0.04	18 600 ± 7 000	9.8 ± 6.7	39.0 ± 18.4	35.5 ± 24.2
Pos 4 Core 2	0.07	0.016	0.0156	0.054 ± 0.002	0.13 ± 0.03	110 500 ± 8 500	390 ± 83	1 724 ± 166	3.9 ± 0.9
Pos 5 Core 3	0.08	0.008	0.0968	0.052 ± 0.002	0.12 ± 0.02	210 000 ± 26 100	2 865 ± 1 888	13 170 ± 1370	0.8 ± 0.5
Pos 6 Core 3	0.11	0.006	0.0451	0.06 ± 0.01	0.30 ± 0.02	70 000 ± 1 200	480 ± 232	3 161 ± 230	5.1 ± 2.5
Pos 7 Core 1	0.22	0.004	0.0086	0.10 ± 0.01	-	44 500 ± 13 700	129 ± 77	387 ± 122	8.4 ± 5.0

Position 1 Core 1

A
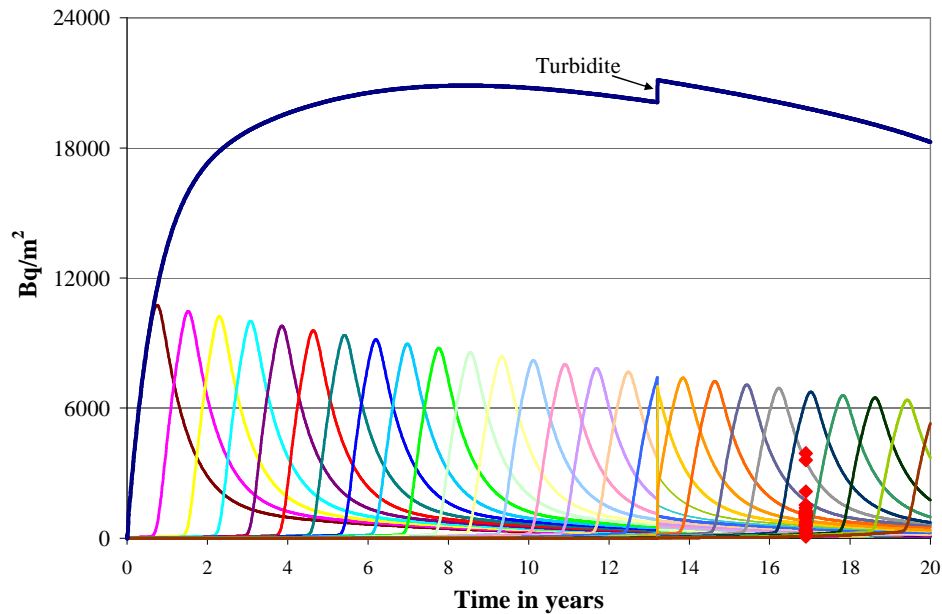
B
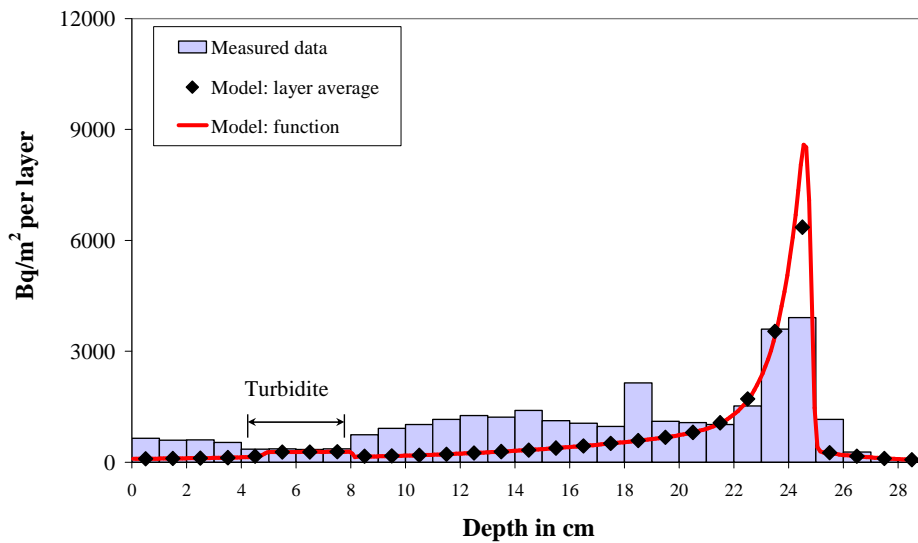
Fig. 5.8. Position 1 Core 1. A: Modeling of the time-dependency of the total inventory (upper dark blue curve) and the depth inventory of ^{137}Cs in the sediment (individual layers with thickness of 1 cm). Zero point of the abscissa is 1.5.1986. The red points represent the measured ^{137}Cs activity concentration in the vertical profile. **B**: The vertical ^{137}Cs distribution in the sediment: Measured data (columns), modeled function (line) and the layer average as calculated from the model (points).

Position 1 Core 4

A
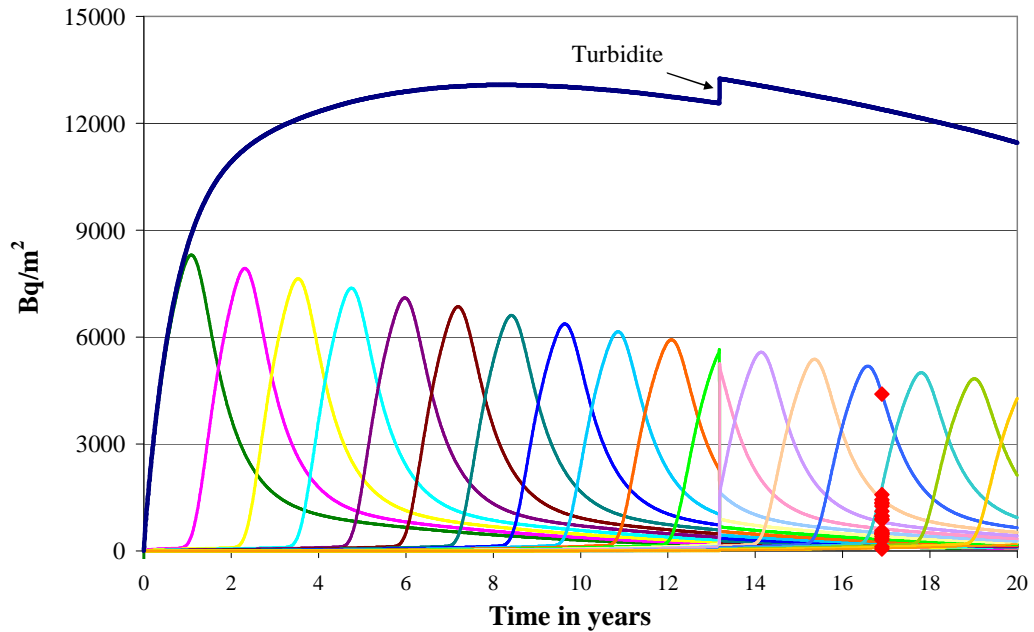
B
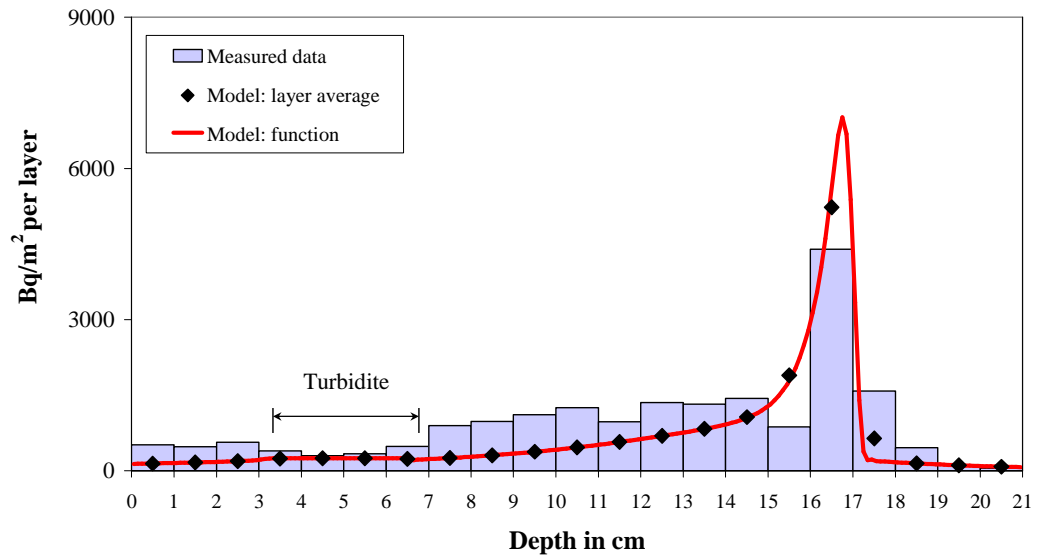
Fig. 5.9. Position 1 Core 4. A: Modeling of the time-dependency of the total inventory (upper dark blue curve) and the depth inventory of ^{137}Cs in the sediment (individual layers with thickness of 1 cm). Zero point of the abscissa is 1.5.1986. The red points represent the measured ^{137}Cs activity concentration in the vertical profile. **B**: The vertical ^{137}Cs distribution in the sediment: Measured data (columns), modeled function (line) and the layer average as calculated from the model (points).

118

Position 2 Core 1

A
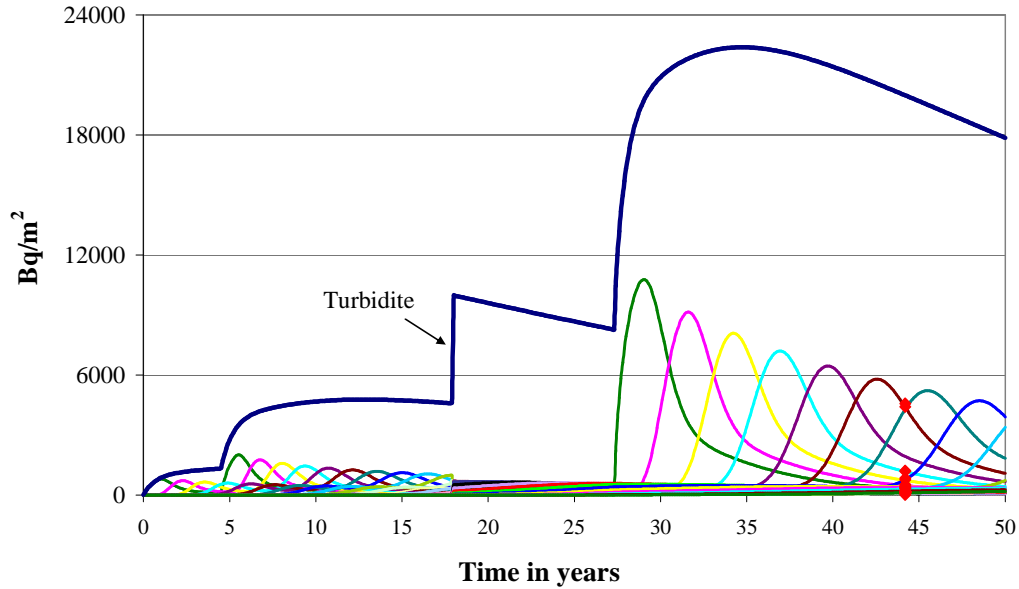
B
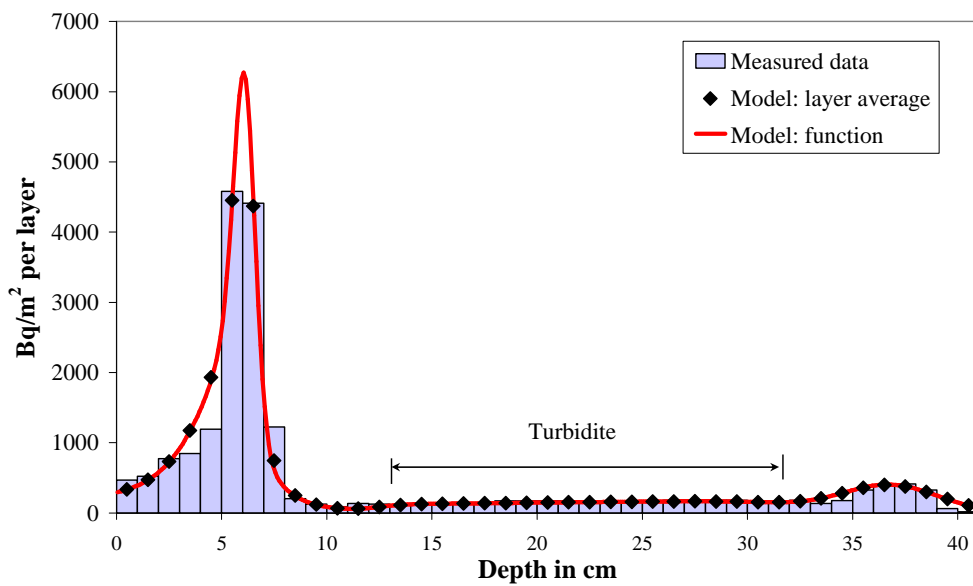
Fig. 5.10. Position 2 Core 1. A: Modeling of the time-dependency of the total inventory (upper dark blue curve) and the depth inventory of ^{137}Cs in the sediment (individual layers with thickness of 1 cm). Zero point of the abscissa is 1.5.1986. The red points represent the measured ^{137}Cs activity concentration in the vertical profile. **B**: The vertical ^{137}Cs distribution in the sediment: Measured data (columns), modeled function (line) and the layer average as calculated from the model (points).

Position 2 Core 3

A

B
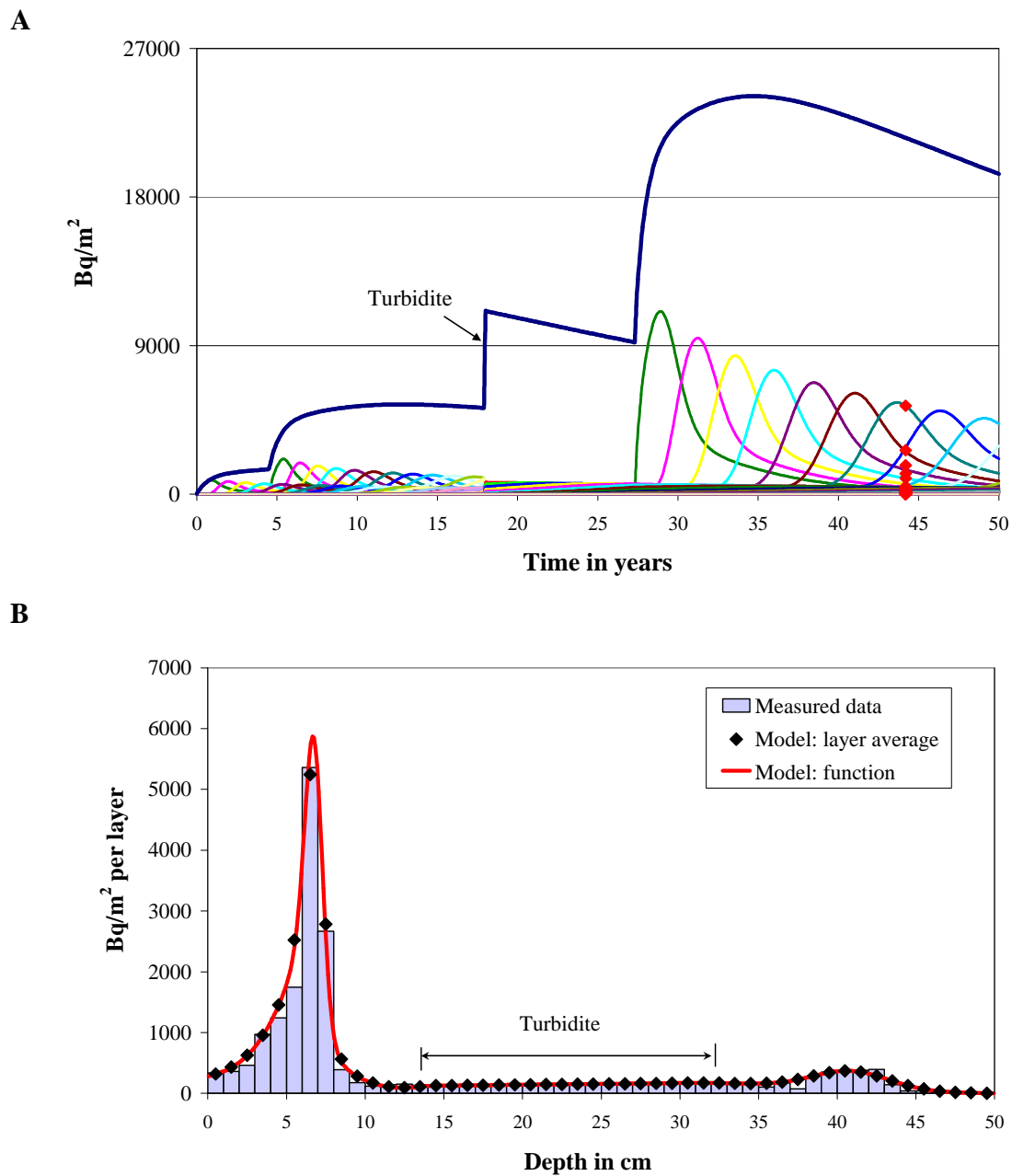
Fig. 5.11. Position 2 Core 3. A: Modeling of the time-dependency of the total inventory (upper dark blue curve) and the depth inventory of ^{137}Cs in the sediment (individual layers with thickness of 1 cm). Zero point of the abscissa is 1.5.1986. The red points represent the measured ^{137}Cs activity concentration in the vertical profile. **B**: The vertical ^{137}Cs distribution in the sediment: Measured data (columns), modeled function (line) and the layer average as calculated from the model (points).

Position 3 Core 3

A
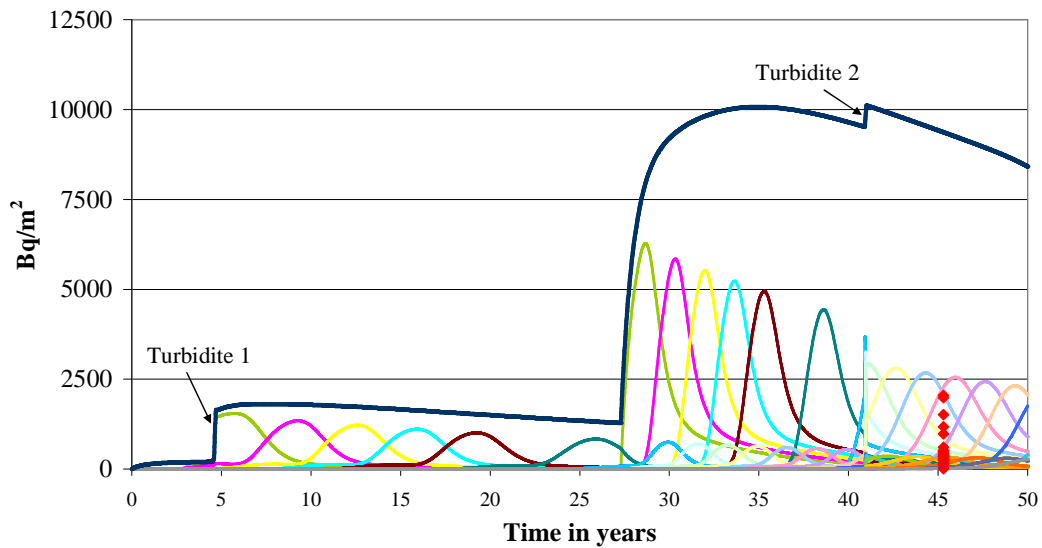
B
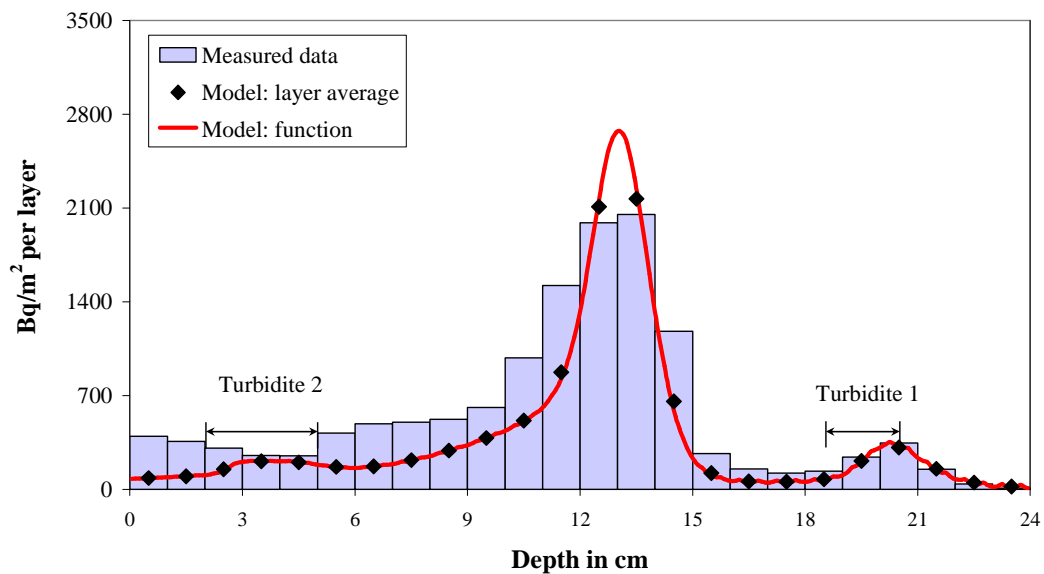
Fig. 5.12. Position 3 Core 3. A: Modeling of the time-dependency of the total inventory (upper dark blue curve) and the depth inventory of ^{137}Cs in the sediment (individual layers with thickness of 1 cm). Zero point of the abscissa is 1.1.1959. The red points represent the measured ^{137}Cs activity concentration in the vertical profile. **B**: The vertical ^{137}Cs distribution in the sediment: Measured data (columns), modeled function (line) and the layer average as calculated from the model (points).

121

Position 4 Core 2

A
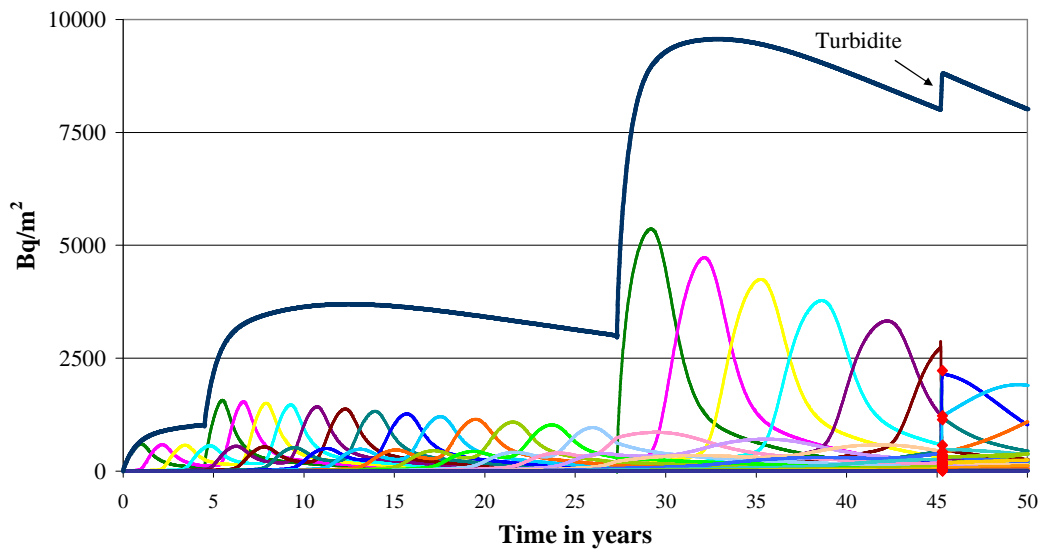
B
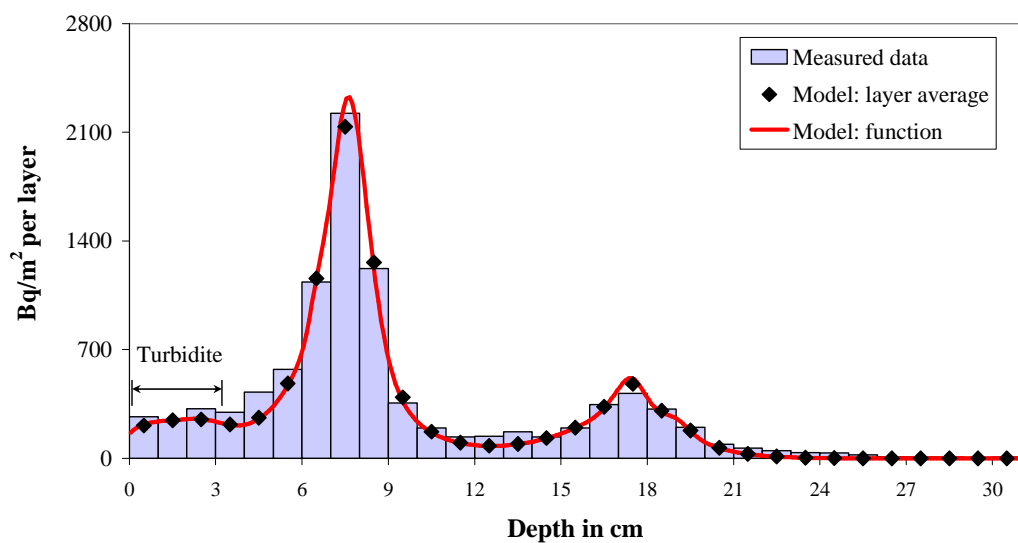
Fig. 5.13. Position 4 Core 2. A: Modeling of the time-dependency of the total inventory (upper dark blue curve) and the depth inventory of ^{137}Cs in the sediment (individual layers with thickness of 1 cm). Zero point of the abscissa is 1.1.1959. The red points represent the measured ^{137}Cs activity concentration in the vertical profile. **B**: The vertical ^{137}Cs distribution in the sediment: Measured data (columns), modeled function (line) and the layer average as calculated from the model (points).

Position 5 Core 3

A
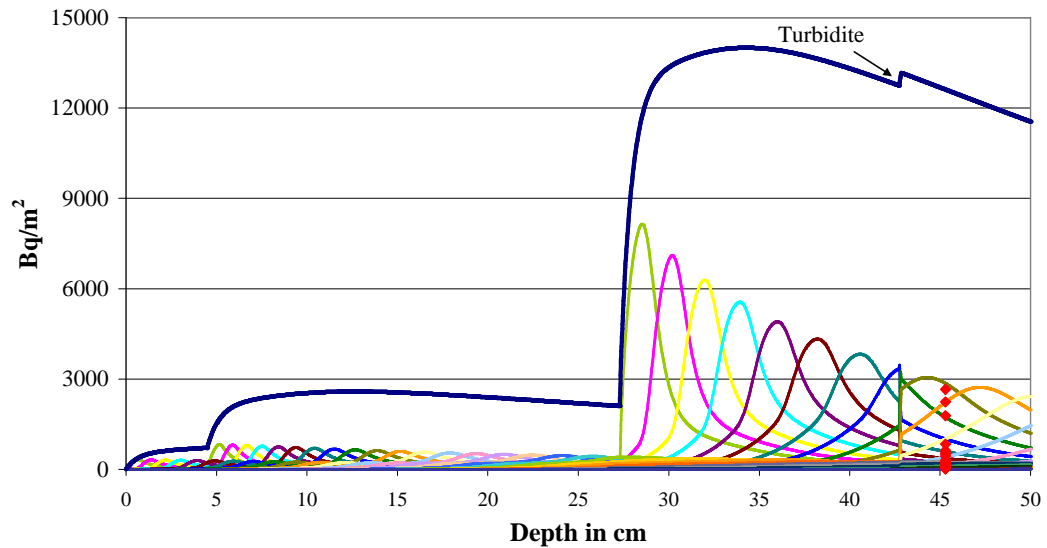
B
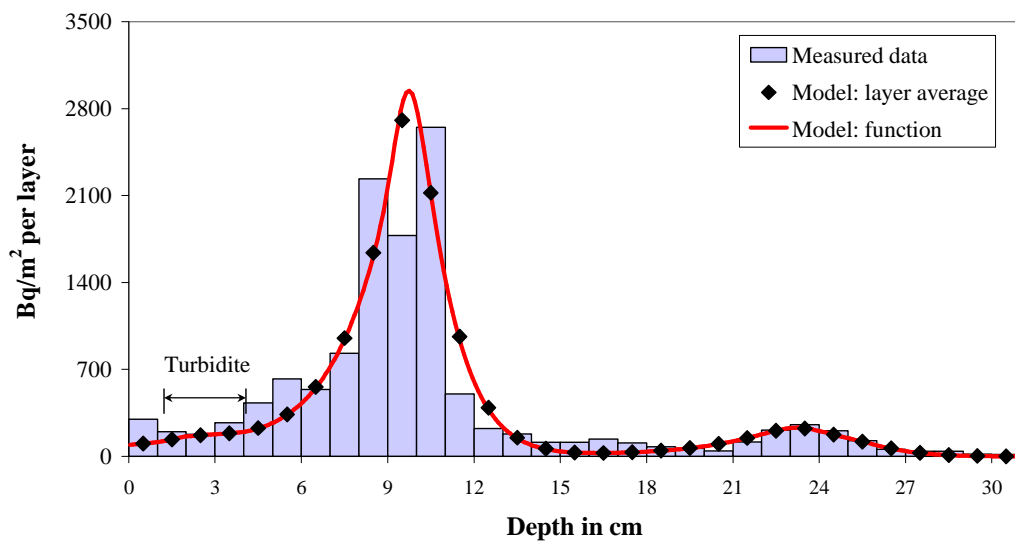
Fig. 5.14. Position 5 Core 3. A: Modeling of the time-dependency of the total inventory (upper dark blue curve) and the depth inventory of ^{137}Cs in the sediment (individual layers with thickness of 1 cm). Zero point of the abscissa is 1.5.1959. The red points represent the measured ^{137}Cs activity concentration in the vertical profile. **B**: The vertical ^{137}Cs distribution in the sediment: Measured data (columns), modeled function (line) and the layer average as calculated from the model (points).

Position 6 Core 3

A

B
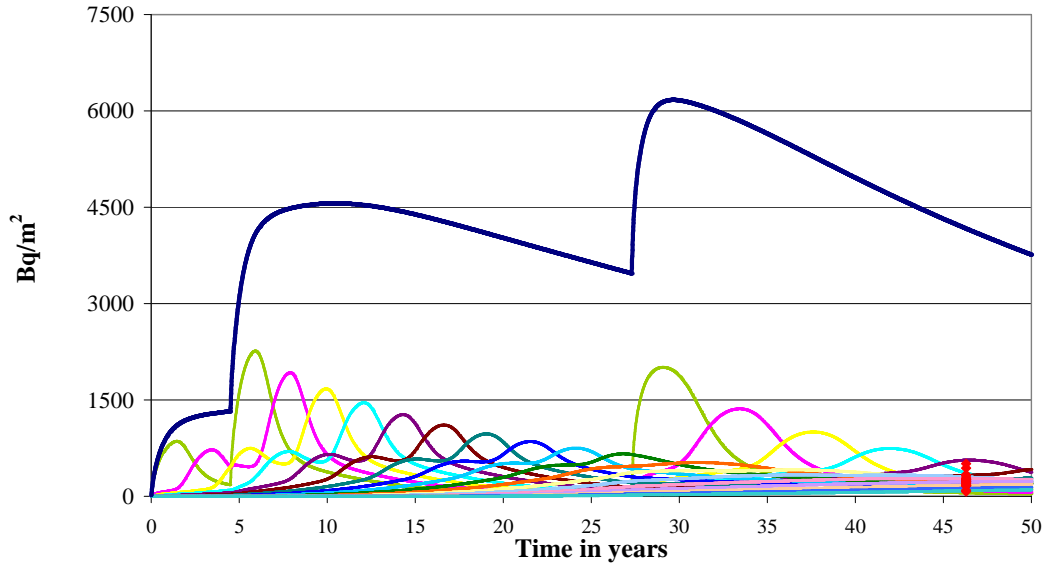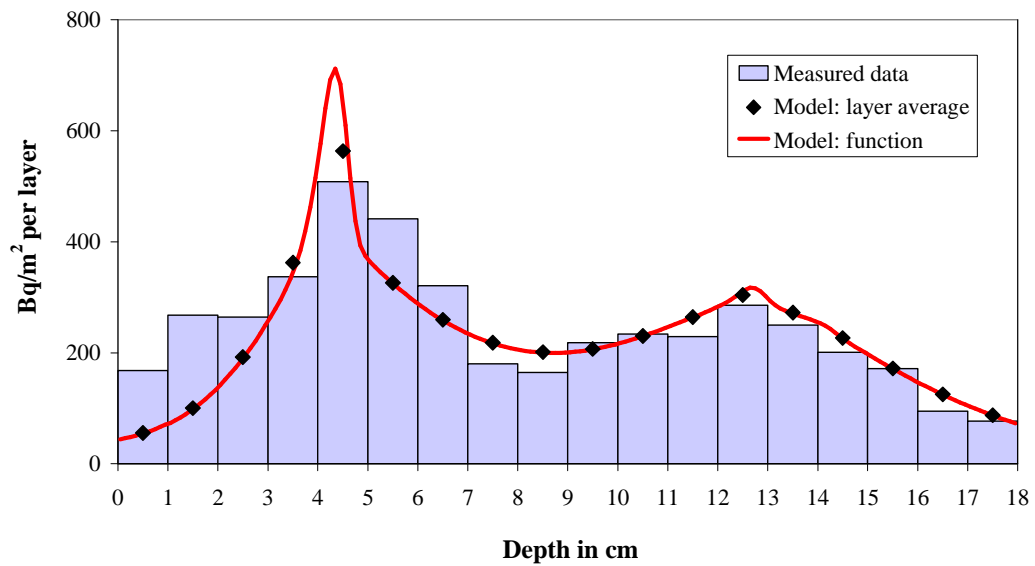
Depth in cm

Fig. 5.15. Position 6 Core 3. A: Modeling of the time-dependency of the total inventory (upper dark blue curve) and the depth inventory of ^{137}Cs in the sediment (individual layers with thickness of 1 cm). Zero point of the abscissa is 1.1.1959. The red points represent the measured ^{137}Cs activity concentration in the vertical profile. **B**: The vertical ^{137}Cs distribution in the sediment: Measured data (columns), modeled function (line) and the layer average as calculated from the model (points).

Position 7 Core 2

A
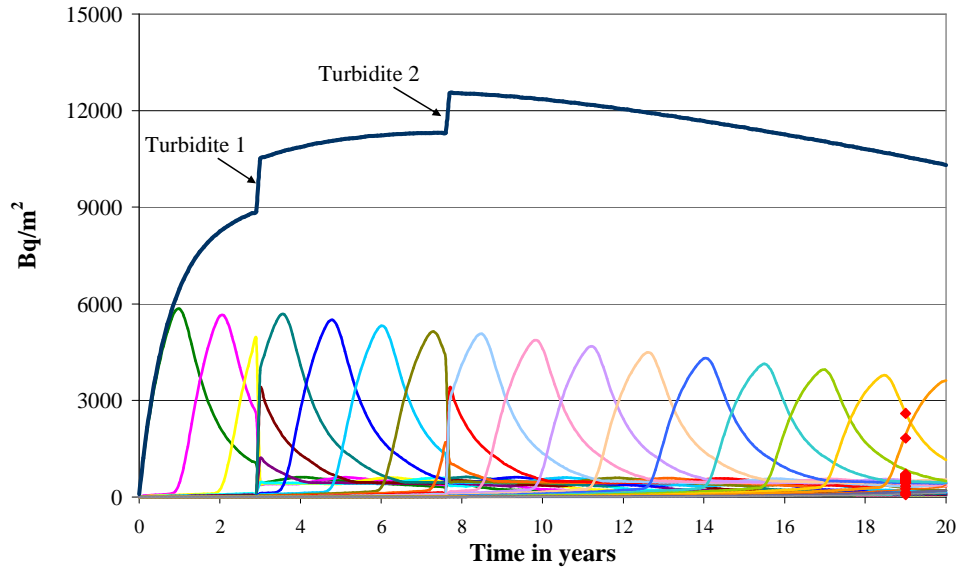
B
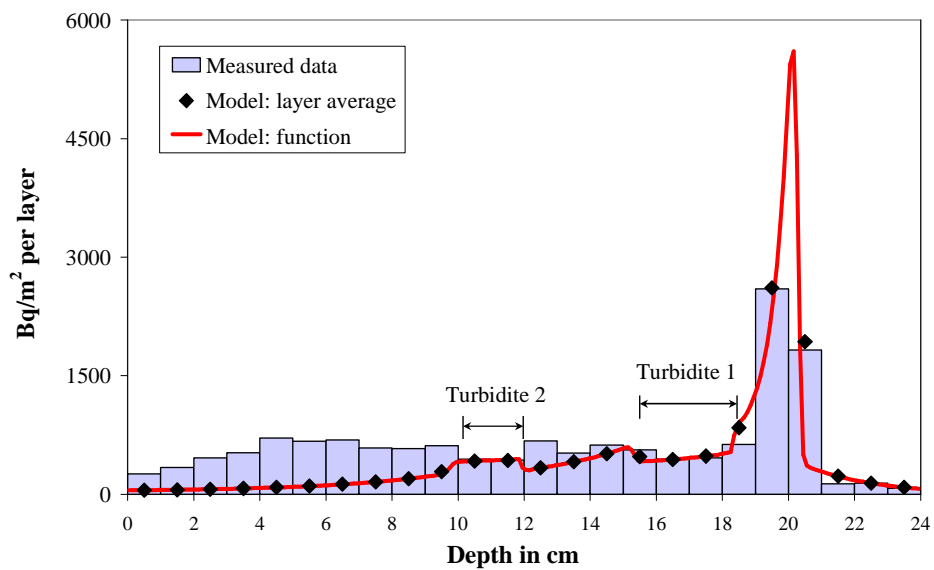
Fig. 5.16. Position 7 Core 1. A: Modeling of the time-dependency of the total inventory (upper dark blue curve) and the depth inventory of ^{137}Cs in the sediment (individual layers with thickness of 1 cm). Zero point of the abscissa is 1.5.1986. The red points represent the measured ^{137}Cs activity concentration in the vertical profile. **B**: The vertical ^{137}Cs distribution in the sediment: Measured data (columns), modeled function (line) and the layer average as calculated from the model (points).

5.7 Discussion on modeling: Free and dependent fit parameters

Table 5.1 summarizes the measured, optimized and calculated parameters of the model which was successfully applied to the vertical distributions of bottom sediments from 7 different positions of Lago Maggiore. Here, the main parameters will be discussed.

^{137}Cs distribution coefficient

In Fig. 5.17 the optimized total distribution coefficient is shown for different positions of Lago Maggiore.
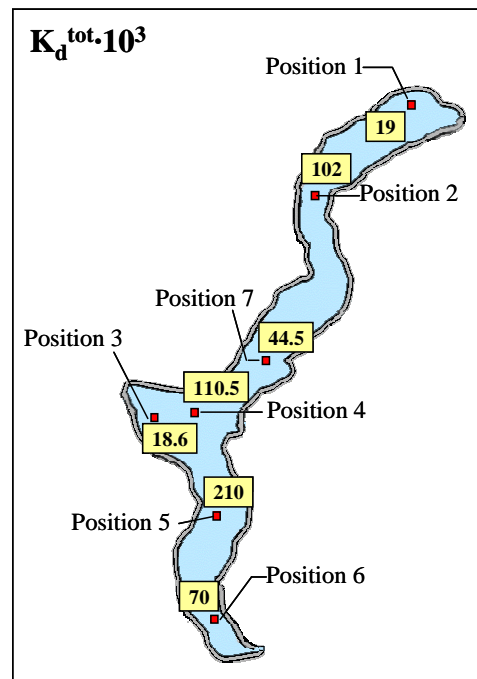
Fig. 5.17. Total ^{137}Cs distribution coefficient (K_d^{tot} in $10^3 \cdot l \cdot kg^{-1}$) for different basins of Lago Maggiore.

The highest values (more than 10^5 $l \cdot kg^{-1}$) are observed at positions 2, 4 and 5. In contrast, at positions 1, 3, 6 and 7 K_d^{tot}-values are 5 to 10 times lower. The low values at positions 1, 3 and 6 can be explained by their locations and lower depths as compared with other positions. For instance, at position 1 and 3 which are close to inflows to the lake, one of the reasons of low K_d^{tot} could be a non-equilibrium situation between the ^{137}Cs activity

126

concentration of the settling particles and ^{137}Cs activity dissolved in the lake water as it is also observed in the surface water of the lake. At position 6 water plants and reed at the bank of the lake indicate a more eutrophic state of this basin as compared to the rest of the lake.

In chapter 4.1.4 the values of distribution coefficients measured in the water column are given for the two deepest positions. The weighted averages over the water column (without upper 5 m surface layer) are (98000 ± 12000) l·kg^{-1} and (328000 ± 110000) l·kg^{-1} at positions 2 and 5, respectively. Within the uncertainties these values are in a good agreement with the total distribution coefficients which are the output parameter of the model (Table 5.2).

Table 5.2. Comparison between measured and modeled ^{137}Cs distribution coefficients (K_d^{tot}) in Lago Maggiore.

K_d (l·kg^{-1})		Position 2		Position 5	
	Measured values: water column	50 m	$63\,000 \pm 28\,000$	51 m	$278\,000 \pm 57\,000$
		100 m	$226\,000 \pm 64\,000$	110 m	$602\,000 \pm 84\,000$
		196 m	$117\,000 \pm 35\,000$	154 m	$315\,000 \pm 67\,000$
		200 m	$119\,000 \pm 26\,000$		
		275 m	$88\,000 \pm 17\,000$		
	Optimized values	$104\,000 \pm 27\,000$ $99\,000 \pm 9\,000$		$210\,000 \pm 11\,300$	

Another distribution coefficient $K_{d\_dif}^{ex}$ was introduced into the model to regulate the retarded diffusion within the sediments. In chapter 5.1.3 a simple model which assumes that the distribution coefficient $K_{d\_dif}^{ex}$ is inversely proportional to the concentration of competing ions (K^+ and NH_4^+) in the pore ware was described. According to this model the diffusion is increasing if the concentration of competing ions in the pore water is increased.

Using equation (5.22) and taking into account that the concentrations of K^+ and NH_4^+ were measured both in lake water and pore water at positions 2, 5 and 7 (see chapter 4.1.3) we result at ratios between $K_{d\_dif}^{ex}$ and K_d^{ex} of 0.03, 0.25 and 0.1, respectively. On

the other hand, for the same positions the ratios of the coefficient $K_{d\_dif}^{ex}$ and the correspondent distribution coefficient of exchangeable ^{137}Cs K_d^{ex} obtained from the model (see Table 5.1) are 0.3, 0.2 and 0.3, respectively. The tendency of a decreased distribution coefficient within the sediment comes out of the model correctly. The values are not always in perfect agreement mainly due to uncertainties introduced by varying sedimentation rates (mini-turbidites). Moreover, equation (5.22) might be a simplification of the real situation. Generally, our model shows that in sediments from Lago Maggiore $K_{d\_dif}^{ex}$ is 3 – 5 times lower than K_d^{ex}.

Sedimentation rates and effective diffusion

In Fig. 5.18, A sedimentation rates for the region above the Chernobyl maximum obtained from the model are shown for different positions of Lago Maggiore. In sediments of central and northern basin the sedimentation rates varies between 0.1 g·(cm^2·a)$^{-1}$ and 0.8 g·(cm^2·a)$^{-1}$. In the southern basin much lower rates (about 0.05 g·(cm^2·a)$^{-1}$) of sedimentation are obtained. The larger R_S of 0.4 g·(cm^2·a)$^{-1}$ at position 3 can be explained by the input of additional material with the inflow of the river Toce.

To be able to describe the two maxima of ^{137}Cs in the measured vertical profiles, it was necessary to introduce different sedimentation rates for the periods before the Chernobyl accident in 1.05.86 and after. Both optimized values for positions 3, 4, 5 and 6 are given in Table 5.3.

The values for R_S are in a good agreement with those which are calculated with the CRS ^{210}Pb model and discussed in chapter 4.4.1. Weighing the sedimentation rates for the region of Chernobyl maximum (obtained from our model, see Table 5.3) with the average bulk density we get the average sedimentation speeds at different positions. In Fig. 5.19 the comparison between these sedimentation speeds (A) and those measured in 1998 at different basins of Lago Maggiore by L. Langone (Marchetto and Musazzi, 2001) are shown.
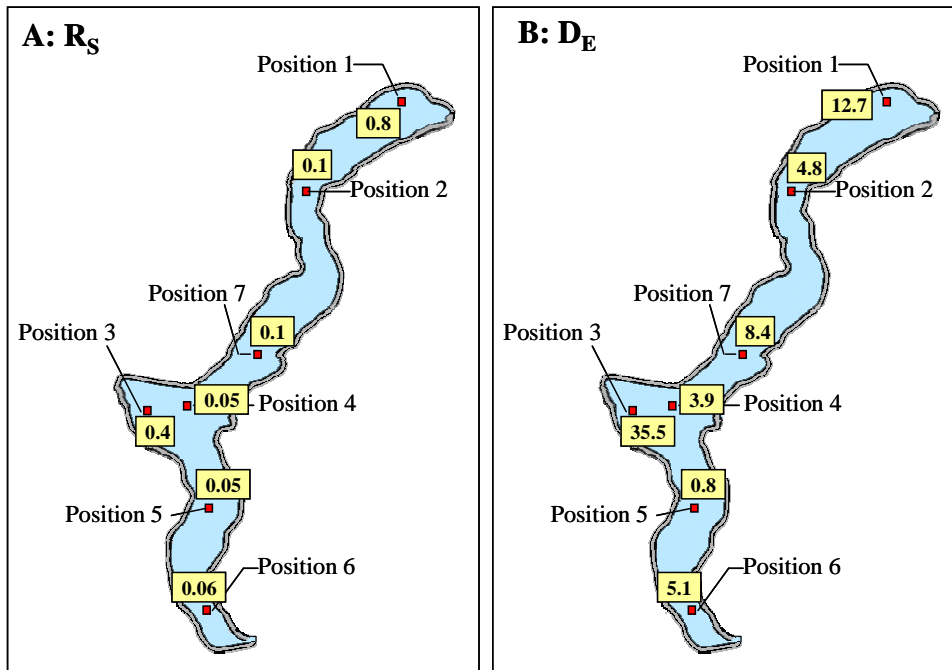
Fig. 5.18. A: Sedimentation rates (R_S in g·(cm²·a)$^{-1}$) for the region of Chernobyl maximum and **B:** Effective diffusion (D_E in cm²·a^{-1}) calculated by the model for different positions and basins of Lago Maggiore.
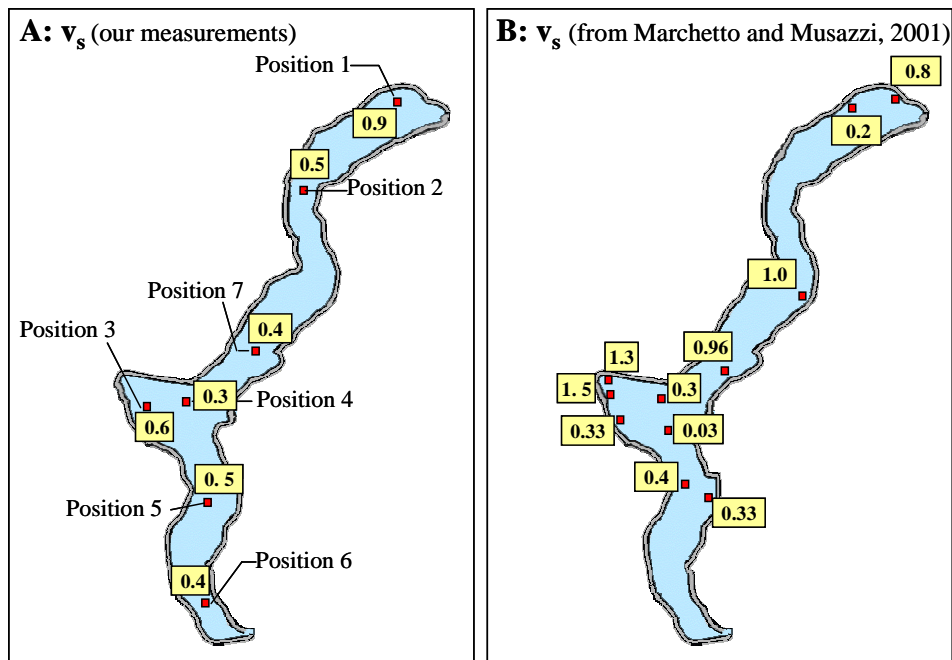
Fig. 5.19. Sedimentation speeds (v_S in cm·a^{-1}) (**A**) calculated from our model and (**B**) measured by L. Langone in 1998 (Marchetto and Musazzi, 2001) for different positions and basins of Lago Maggiore.

Both examples show variability of sedimentation speeds not only for different positions and basins but large variants within one position. In general, the values are in a rather good agreement. The differences at some positions can be explained by the compaction which is taken into account in case of our measurements (A). Those positions were the sediment bulk density is constant (e.g. position 1) show perfect agreement.

A parameter which is calculated from the $K_{d\_dif}^{ex}$ is the effective diffusion coefficient D_E. It varies between 0.8 $cm^2 \cdot a^{-1}$ and 8.4 $cm^2 \cdot a^{-1}$ for different positions of Lago Maggiore (Fig. 5.18, B). However, also larger values of 12.7 $cm^2 \cdot a^{-1}$ and 35.5 $cm^2 \cdot a^{-1}$ at positions 1 and 3 which are located close to the inflow of the rivers Ticino and Toce, respectively, are observed.

Other parameters

Because of low biological activity and a rather dense constitution of the sediments, the physical and bio-turbation is negligible. The fixation rate f was set for all cases as 2 a^{-1}. Together with the measured portion of exchangeable radioactivity it is used to calculate the redissolution rate r, which was rather low (0.009 – 0.1 a^{-1}).

Parameters which describe the position and the size of the turbidite are optimized by hand separately for each case.

If together with the Chernobyl maximum also the ^{137}Cs peak related to the nuclear weapon testing fallout is to be described by the model, the boundary conditions are introduced by the three identical sums of three exponential functions with different amplitudes for the different maxima (chapter 5.2.2). To fit the height of the peak related to the nuclear weapons testing fallout, the ratio of the ^{137}Cs inventories in the catchment area after the Chernobyl and nuclear weapons testing fallouts were adjusted additionally while modeling.

5.8 Comparison of ^{137}Cs behaviour in Lago Maggiore and other European lakes

The importance of the sorption properties of particulate matter of ^{137}Cs in Lago Maggiore can be demonstrated by a comparison of the concentrations of dissolved ^{137}Cs in three other prealpine lakes (Fig. 5.20) which experienced about the same amount of direct ^{137}Cs input from Chernobyl fallout. One of them is the neighbouring *Lake Lugano* (southern Switzerland, Italy) where roughly about 24 kBq·m^{-2} of ^{137}Cs was deposited onto the lake surface. *Lake Constance*, a large and rather deep mesotrophic hardwater lake at the borders of Germany, Austria and Switzerland, where the initial fallout of ^{137}Cs was about 17 kBq·m^{-2} (Mangini, 1990). Finally, on lake *Vorsee*, which is a small shallow (2.2 m maximum water depth) eutrophic lake in southern Germany supplied by a swampy watershed, the initial fallout of ^{137}Cs was about 30 kBq·m^{-2} (Kaminski *et al.*, 1998). Table 5.3 summarizes main characteristics of these lakes.
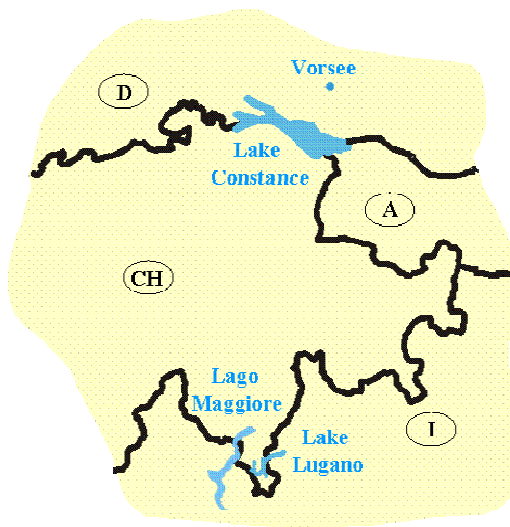
Fig. 5.20. Different European lakes.

Table 5.3. Main characteristics of different European lakes.

	Lake Constance	Lago Maggiore	Lake Lugano	Lake Vorsee
Lake surface (km[2])	572	212.5	48.9	0.09
Mean depth (m)	85	177.4	134	0.6
Maximum depth (m)	254	370	288	2.2
Residence time (a)	4.1	4	7	0.24
Catchment area (km[2])	11 487	6 599	615	1.27
[137]Cs deposition in 1986 (kBq·m^{-2})	17	20	24	28

131

5.8.1 ^{137}Cs in lake water

Characterized by similar initial depositions Lake Constance, Lago Maggiore, Lake Lugano and Vorsee have different ^{137}Cs activity concentrations in the water several years after the nuclear reactor accident in Chernobyl (Fig. 5.21). Such differences can be explained by differences in limnological character of these lakes.

The highest ^{137}Cs concentration is observed in lake Vorsee water over the whole time span as compared to the other three lakes. This high contamination levels are caused by a continuous input of ^{137}Cs from a swampy watershed (Kaminski *et al.*, 1994) into the lake which mainly has organic material in the sediment. Redissolution of ^{137}Cs from the sediment which occurs preferentially in winter and autumn when the ammonium concentration in the water increases due to the decomposition of organic matter. This leads to a seasonal cycling of the activity concentration.

Lowest ^{137}Cs concentrations were measured in Lake Constance (< 1 Bq·l^{-1} in 2005), a large and deep mesotrophic lake. The radiocaesium was rapidly removed from the water column and strongly bound to clay mineral particles in the sediment (Kaminski *et al.*, 1998).

In Lake Lugano with its permanently anoxic northern basin and monomictic (seasonally anoxic) southern basin, a slower removal of dissolved ^{137}Cs activity concentrations from the water compared to most other deep prealpine lakes of similar size was observed by Santschi *at al.* (1990). Here, a lower fixation of ^{137}Cs to suspended matter takes place due to ion exchange with NH_4^+. The strong increase of the ^{137}Cs concentration with depth is controlled by the increasing NH_4^+ concentration.

In contrast, in Lago Maggiore which is an oligotrophic lake, the dissolved oxygen concentration is rather large (6–11 mg·l^{-1}, see chapter 4.1.2) and stays nearly constant over the complete water column which results in a negligible NH_4^+ concentration (Table 5.4). The increase of the ^{137}Cs concentration with depth by a factor of two (see Fig. 5.21, where the single measurements in different depths are shown for Lago Maggiore water after month 200) is probably controlled by a slight decrease of pH.

Table 5.4. Comparison of main cation compositions of lake waters (The data for lake Vorsee, and Lake Constance: Konoplev *et al.*, 2002; Lake Lugano: Radioecological laboratory at the Hochschule Ravensburg-Weingarten (1999). The data for $[Ca^{2+}]$, $[Mg^{2+}]$, $[Na^+]$ in Lago Maggiore in 2005 are kindly given by Piero Guilizzoni).

	$[K^+]$ in mg·l^{-1}	$[NH_4^+]$ in mg·l^{-1}	$[Ca^{2+}]$ in mg·l^{-1}	$[Mg^{2+}]$ in mg·l^{-1}	$[Na^+]$ in mg·l^{-1}	pH
Vorsee	0.9–2.0	0.04–1.0	53–118	6.9–8.6	3.5–5.0	7.4–9.4
Lake Lugano (Southern basin)	1.6–2.1	0.007 – 0.028	29–39	7.8–9.1	5.0–6.3	7.7
Upper Lake Constance	1.1–1.3	< 0.01	48.7–54.1	6.7–9.7	4.4–4.7	7.5–8.1
Lago Maggiore	1.4–2.0	0.003–0.025	22.6–22.7	3.7	2.7–2.8	6.2–7.7

As can be seen from Table 5.4, all lake waters have rather similar ionic compositions. All four lakes are characterized by relatively high concentrations of calcium and relatively low concentrations of potassium. However, the substantial difference between the lakes is the different ammonium concentrations which have a great influence on the mobility of ^{137}Cs in the lake.

The ^{137}Cs concentration in the water column of four different lakes is shown in Fig. 5.21.
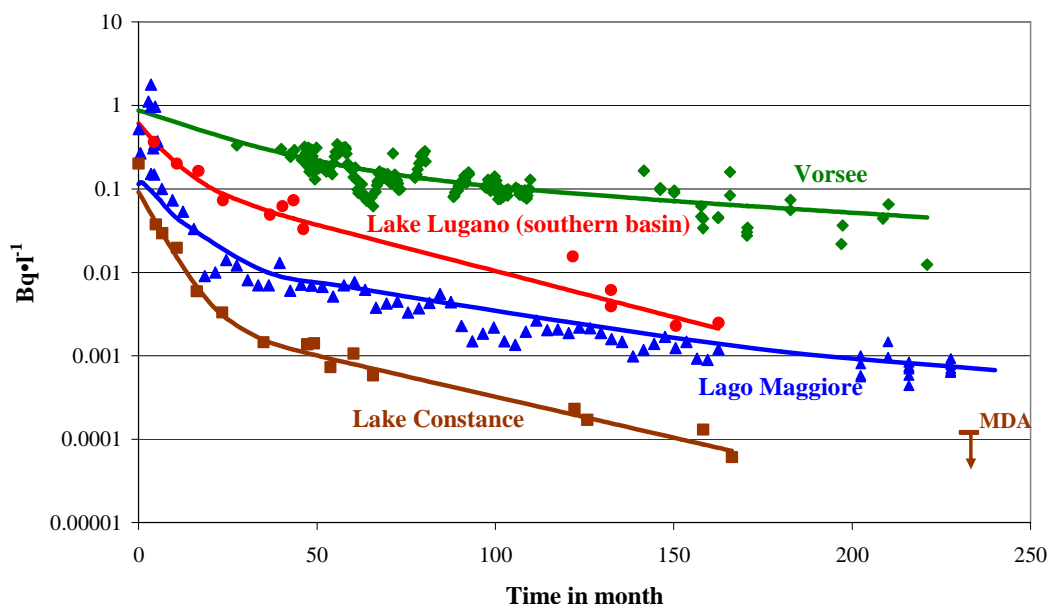
Fig. 5.21. Time-dependency of ^{137}Cs activity concentration in the water of Lake Constance (Santschi *et al.*, 1990; database of the Radioecological laboratory at the Hochschule Ravensburg-Weingarten), Lake Lugano (Dominik and Span, 1992; database of the Radioecological laboratory at the Hochschule Ravensburg-Weingarten), Vorsee (Zibold *et al.*, 2001), and Lago Maggiore (data from JRC in Ispra and our measurements). Zero point of the abscissa is 1.5.1986.

The time-dependency of the ^{137}Cs specific activities in lake water for Lake Constance, Lake Lugano and lake Vorsee is described by a sum of two exponential functions (non-weighted least squares fit). In Lago Maggiore the radiocaesium in the lake surface water is described by the AQUASCOPE model.

5.8.3 ^{137}Cs in sediments

The comparison of extractability of ^{137}Cs from the sediments measured by sequential extraction experiments shows some differences for the lakes with different limnological characteristics. Thus, for example, in Lake Constance with high self purification capacity, ^{137}Cs is strongly bound to illites and the percentages of total extracted (5 steps) radiocaesium is a factor of 2 to 8 lower than those of Lake Lugano (Kaminski *et al.*, 1998; Konoplev *et al.*, 1996).

In the glacially formed shallow eutrophic lake Vorsee caesium is mainly bound to organic material in the sediment and the percentages of total extracted caesium exceed those of Lake Lugano.

In Lago Maggiore ^{137}Cs is tightly bound to the clay minerals. The low portion of exchangeable ^{137}Cs of only about 1 % at some positions as compared to about 5 % in Lake Constance and Lake Lugano (Klemt *et al.*, 2000) is astonishing.

According to the model described above, in Lake Lugano and Lago Maggiore the maximum of total ^{137}Cs inventory was reached about 9 years after the Chernobyl accident as compared to 5 and 15 years in Lake Constance and in the shallow eutrophic lake Vorsee, respectively. Before the maximum is reached, the input into the sediments is the dominating process. Only afterwards the radioactive decay dominates the continuous input of activity into the lakes (Klemt *et al.*, 2000, 2005).

For comparison, in Table 5.5 measured and optimized model parameters of different European lakes are presented. The main differences were found for the distribution coefficients which are dependent on the amount of clay minerals in the system, for the sedimentation rates, and the bulk densities of the sediment.

Table 5.5. Comparison of bulk density of sediment (ρ_b), portion of exchangeable activity (α), sedimentation rate (R_S), total ^{137}Cs distribution coefficient (K_d^{tot}) and retarded diffusion of exchangeable ^{137}Cs activity (D_E) in Lago Maggiore and other European lakes.

	Measured parameters		Optimized parameters		
	ρ_b in g·cm^{-3}	α	R_S in g·(cm^2·a)$^{-1}$	K_d^{tot} in l·kg^{-1}	D_E in cm·a^{-1}
Lake Constance	0.27	0.04	0.12	165 000	0.18
Lake Lugano	0.17	0.05	0.06	49 100	0.82
Vorsee	0.02	0.04	0.10	17 600	23.80
Lago Maggiore (P2)	0.28	0.01	0.12	99 000	6.1
Lago Maggiore (P4)	0.21	0.02	0.05	110 000	3.9

A principal difference for the lake can be found in the bulk density of the sediments: in Lake Constance and Lago Maggiore the measured density of typical sediment is rather high, especially in comparison with lake Vorsee where it is more than one order of magnitude lower. For most positions of Lago Maggiore the sedimentation speed is not constant. The second parameter – portion of exchangeable ^{137}Cs – as discussed above is rather similar for all lakes except Lago Maggiore where at some positions very low percentage (< 1 %) of exchangeable Cs ions was measured.

Concerning optimized parameters, it can be seen that Lake Constance and Lago Maggiore are characterized by a total ^{137}Cs distribution coefficient of about 10^5 l·kg^{-1} which is twice or three times larger than that in Lake Lugano and about a factor 6–9 larger than that in the shallow lake Vorsee. The main reason for high values of K_d^{tot} are a high content of clay minerals in the lake sediments and very low concentration of competing ions (K^+ and NH_4^+).

The values of the distribution coefficient give the possibility to calculate the effective diffusion in the sediments which is negligible for Lake Lugano, Lago Maggiore and Lake Constance but it is important for lake Vorsee. However, in Lago Maggiore some positions exist (especially close to the tributaries) where diffusion cannot be neglected.

5.9 General conclusions on modeling

The suggested convection–diffusion model describes the continuous input of ^{137}Cs into the sediment and the vertical distribution of ^{137}Cs within the sediment of the deep prealpine Lago Maggiore reasonably well which also allows a prediction of its future conditions.

The model takes into account such basic processes as the exchange of ^{137}Cs between water and the top sediment layer via the distribution coefficient K_d, first-order ^{137}Cs fixation and redissolution, the retarded diffusion of ^{137}Cs within the sediment, and radioactive decay.

The main parameters determining the vertical distribution of ^{137}Cs in bottom sediments are the sedimentation rate R_S and two distribution coefficients K_d. The location of the maxima of the ^{137}Cs is mainly dependent on sedimentation rate, and the ^{137}Cs activity concentrations in sediments are determined by the value of one distribution coefficient. These parameters plus the distribution coefficient $K_{d\_dif}^{ex}$ which is responsible for the retarded diffusion within the sediment are the only free parameters of the model.

In the model a compaction of sediments with depth is also taken into account via the measured sediment density distribution.

Also modeling of turbidites as an instantaneous extra input of sediment is provided.

Taking the activity concentration of the water as the boundary condition for the differential equation a good agreement is achieved between experimental results and model predictions.

In case of Lago Maggiore, the development of the total ^{137}Cs inventories in the sediment with time shows that the maximum in total inventories is reached after 8–9 years after the Chernobyl accident.

There is a strong influence of the tributaries (input of Cs, organic matter, clay minerals) on the behavior of radiocaesium in the lake. Position 3 which is located in front of the mouth of the river Toce is one of the examples where this influence is observed.

Our model describes well the vertical ^{137}Cs distributions in the sediments, it also gives an idea about the importance of processes taking place at different positions and basins of the lake.

6. RADIOCAESIUM ACTIVITY CONCENTRATION IN FISH

Fish is one of the food resources for men. The contamination of an aquatic ecosystem, and particularly lakes, by radionuclides can therefore give rise to significant doses to man. After the Chernobyl accident, due to high radiocaesium bioaccumulation factors, fish remained contaminated despite relatively low radiocaesium levels in water. In that respect it is important to get an idea about the persistence and bioavailability of ^{137}Cs in the aquatic environment.

6.1 Dynamic model for ^{137}Cs uptake by fish and the concentration ratio

It is known that the bioaccumulation of radioactivity in fish is determined by numerous ecological and environmental factors such as fish species, the length of the food chain, water temperature and others (Smith and Beresford, 2005). Also the trophic level of the lake system is of great importance.

After the initial fry stage, many fish species occupy a typical food niche. They may either feed on plankton, benthos (non-predatory group, e.g. whitefish, roach and carp) or smaller fish (predatory group, e.g. pike and eel). However, several species change their habitat during their life, often in relation to body size (Brittain and Håkanson, 2002). Many investigations (Smith and Beresford, 2005) show that the ^{137}Cs accumulation in fish results in an increasing contamination with increasing fish size.

The uptake of radioactivity by aquatic biota is commonly described by the concentration ratio, CR, also known as concentration factor (CF). The concentration ratio CR (l kg^{-1}) of ^{137}Cs in fish is:

$$CR = \frac{^{137}Cs \text{ activity concentration per kg of fish (fresh weight)}}{^{137}Cs \text{ activity concentration per liter of water}} . \tag{6.1}$$

CR is an equilibrium parameter which means that the ^{137}Cs activity concentration in fish is assumed to be in equilibrium with that of water, for example during long times (years) after a fallout. In short-term releases when the equilibrium conditions are not yet reached, a dynamic approach is required.

A typical *dynamic model* for ^{137}Cs uptake by fish (Thomman, 1981; Smith and Beresford, 2005) can be described in the following way:

Change of ^{137}Cs concentration in fish	= + input from water – excretion – radioactive decay.

Assuming first order processes, this model in mathematical terms can be presented as:

$$\frac{dC_f}{dt} = + \ k_f C_L - k_b C_f - \lambda C_f, \qquad (6.2)$$

where

k_f – the rate constant describing the transfer of ^{137}Cs from water to fish, in ($l \cdot kg^{-1} \cdot a^{-1}$);

k_b – the backward rate constant describing the excretion of radioactivity from fish, in a^{-1};

λ – decay constant of ^{137}Cs, in a^{-1}.

C_f and C_L are activity concentrations of ^{137}Cs in fish ($Bq \ kg^{-1}$) and lake water ($Bq \ l^{-1}$), respectively.

By making the assumption that the rate constants k_f and k_b are much larger than the decay constant λ, the equation for the change of ^{137}Cs activity concentration can be simplified to:

$$\frac{dC_f}{dt} = k_f C_L - k_b C_f. \qquad (6.3)$$

In equilibrium conditions the activity concentration of fish does not change, $\frac{dC_f}{dt} = 0$, and therefore, the ratio of rates k_f and k_b gives the equilibrium concentration ratio CR ($l \cdot kg^{-1}$):

$$\frac{k_f}{k_b} = \frac{C_f}{C_L} (\ at\ equlibrium\ ) = CR. \qquad (6.4)$$

Typical values for k_f and k_b according to Smith *et al.* (2000) are given in Table 6.1. The equilibrium between ^{137}Cs activity concentration in fish and water will be reached after several time constants (the inverse of the rate constants) have passed. In this case it is appropriate to talk about a long-term time scale estimated in years.

Table 6.1. Typical values (according to Smith *et al.*, 2000) of rate constants describing the transfer of ^{137}Cs from water to fish (k_f) and excretion of radioactivity (k_b) from the non-predatory and predatory fish. These values are given for the concentration of potassium in the lake water of 1.56 mg·l^{-1}.

Fish	k_b in a[-1]	k_f in (l·kg^{-1}·a[-1])
Non-predatory	8.4	$11.5 \cdot 10^{-3}$
Predatory	0.5	$3.3 \cdot 10^{-3}$

In several studies it was found that the concentration ratio of ^{137}Cs in fish is inversely proportional to the potassium content in the lake (Smith and Beresford, 2005). As radiocaesium is chemically similar to potassium, an important nutrient, the increase of the ^{137}Cs concentration in fish takes place via the same accumulation mechanisms as for potassium. This fact leads to the higher concentration ratio of radiocaesium in the lakes with low content of potassium.

6.2 ^{137}Cs in fish from different lakes

The dynamics of radiocaesium in water and different kinds of fish (Table 6.2) from the eutrophic Lake Vorsee (Zibold *et al.*, 2001) and the mesotrophic Lake Constance (Kaminski *et al.*, 1998; Zibold *et al.*, 2002) is illustrated in Fig. 6.1 and Fig. 6.2, respectively.

The time-dependency of the ^{137}Cs specific activities in predatory and non-predatory fish and lake water in each case is described by a sum of two exponential functions (non-weighted least squares fit). To perform essentially a non-weighted least square fit for the ^{137}Cs specific activities in predatory fish in Lake Constance, the data for ^{137}Cs activity concentration measured before 1987 were not used, as during the first months after the Chernobyl fallout the accumulation in the food chain was not complete.

It can be seen that after the Chernobyl fallout, the ^{137}Cs uptake and excretion processes reached a steady state and the radiocaesium activity concentrations in fish changed at the same rate as in the water. So, an equilibrium between ^{137}Cs in water and fish can be assumed. Using this information, the fish–water concentration ratios CRs were calculated

as the ratio of the individual measurements of the ^{137}Cs activity concentration in fish and the ^{137}Cs specific activity in the lake water taken from the exponential fit.

In Fig. 6.3. and Fig. 6.4. it can be seen that the CR values stay more or less constant with time and are in agreement with earlier results for pike (Zibold *et al.*, 2001). The red and green lines on the diagrams show the calculated averages of concentration ratios CRs for predatory and non-predatory fish, respectively (Table 6.3).

Table 6.2. Non-predatory and predatory fish studied in different European lakes.

Non-predatory fish	
Bleak	*Alburnus alburnus*
Bream	*Albramis brama*
Carp	*Cyprinus carpio*
Perch	*Perca fluviatilis*
Roach	*Rutilus rutilus*
Rudd	*Scardinius erythropthalmus*
Siver bream	*Blicca bjoerkna*
Tench	*Tinca tinca*
Whitefish	*Coregonus* spp
Predatory fish	
Eel	*Anguilla anguilla*
Pike	*Esox lucius*
Wels Catfish	*Silurus glanis*

Table 6.3. Concentration factors of predatory and non-predatory fish in lakes.

Lake	Fish	CR in l·kg^{-1}
Vorsee	Predatory	4 630 ± 220
	Non-predatory	1 120 ± 30
Lake Constance	Predatory	12 880 ± 1 570
	Non-predatory	5 040 ± 240
Lago Maggiore	Non-predatory	4 360 ± 880

The concentration ratios of ^{137}Cs in predatory fish, both from Vorsee and Lake Constance, are a factor of 2 to 4 higher than those for non-predatory fish. A similar tendency, however, is observed for CR values between two lakes for one fish group. In lake Vorsee CRs of radiocaesium are lower than in Lake Constance which can be explained by the different trophic levels of the lakes.

6.3 ^{137}Cs in fish in Lago Maggiore

For Lago Maggiore some data on ^{137}Cs accumulation in fish for the period 1986 – 2002 were available from the Joint Research Center in Ispra. In 2005, we measured rather low levels of the ^{137}Cs specific activity in fish. The results of our measurements are given in Table 6.4.

Table 6.4. [137]Cs specific activities in fish of Lago Maggiore in 2005.

Fish	[137]Cs act.conc. in Bq·kg^{-1} (fresh weight)
Whitefish (*Coregonus lavaretus*)	1.05 ± 0.33
	2.12 ± 0.36
	1.15 ± 0.29
Zander (*Stizostedion Lucioperca*)	< 0.37

In Fig. 6.5. the time-dependencies of ^{137}Cs activity concentration in different species of fish (perch, whitefish, rudd and others) and in the lake surface water are shown. Here, radiocaesium in the water is described by the AQUASCOPE model, while essentially a non-weighted least squares fit is applied for the fish data. It can be seen that the decrease in the ^{137}Cs activity concentration in fish follows the decrease of radioactivity in the surface water. In Lake Constance as compared to lake Vorsee very low ^{137}Cs concentrations in fish of less than 1 Bq·kg^{-1} were measured in 2002. Similar levels as in Lake Constance are observed in Lago Maggiore in 2005.
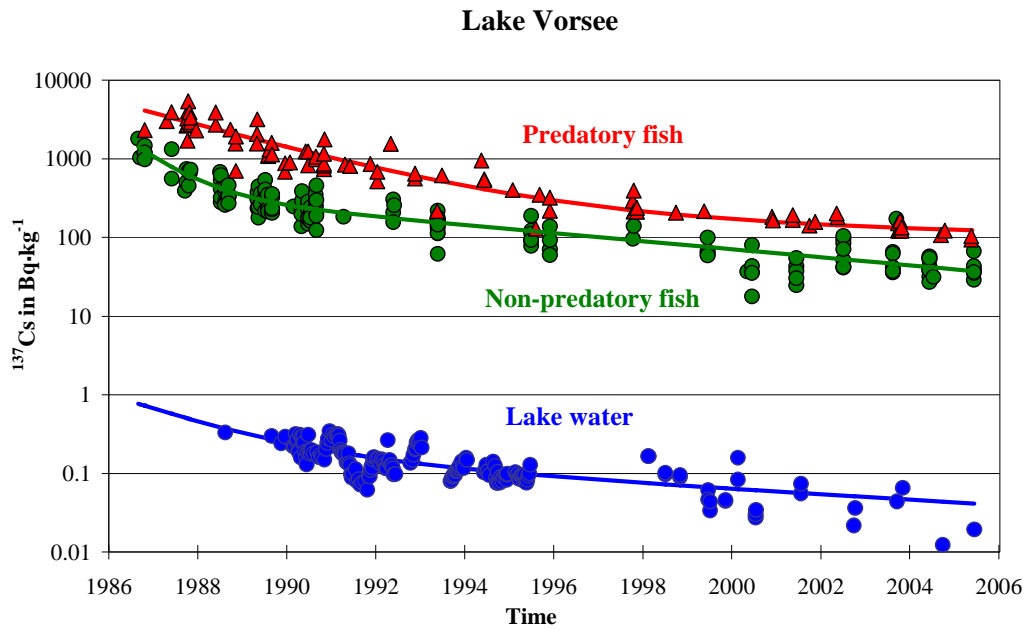
Lake Vorsee

Fig. 6.1. Time-dependency of the ^{137}Cs specific activities in water and fish (predatory and non-predatory) in lake Vorsee (Zibold *et al.*, 2001).
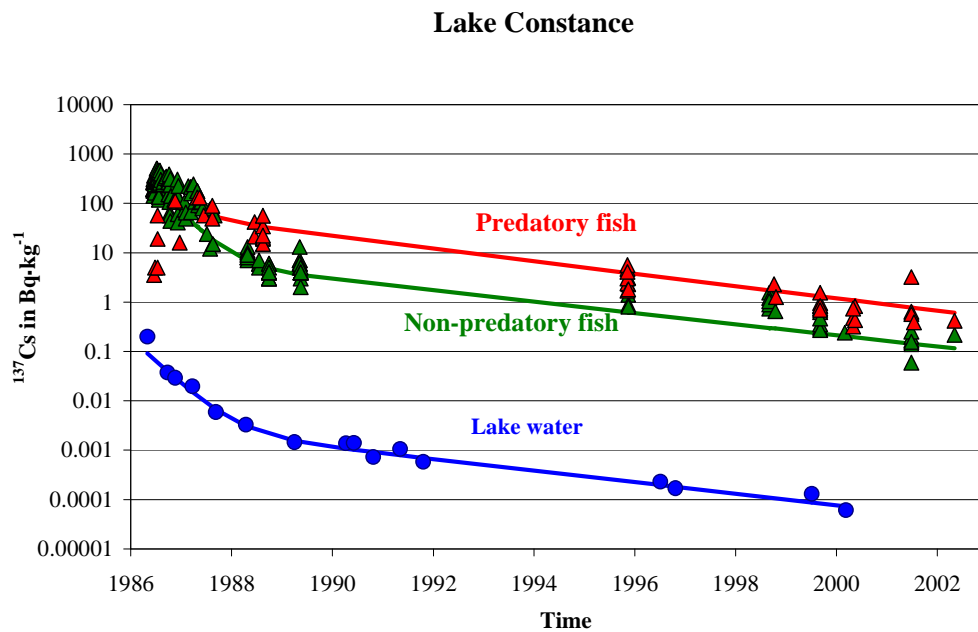
Lake Constance

Fig. 6.2. Time-dependency of the ^{137}Cs specific activities in water and fish (predatory and non-predatory) in Lake Constance (Zibold *et al.*, 2002).
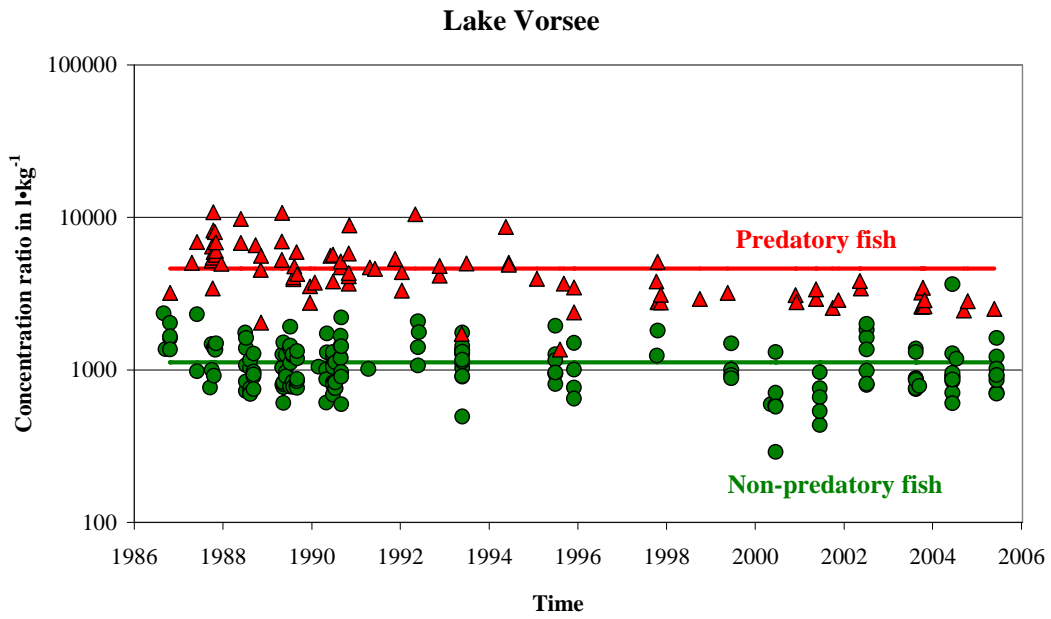
Lake Vorsee

Fig. 6.3. The concentration ratios (CRs) for ^{137}Cs in predatory (red triangles) and nonpredatory (green dots) fish from lake Vorsee. The lines are the calculated averages.
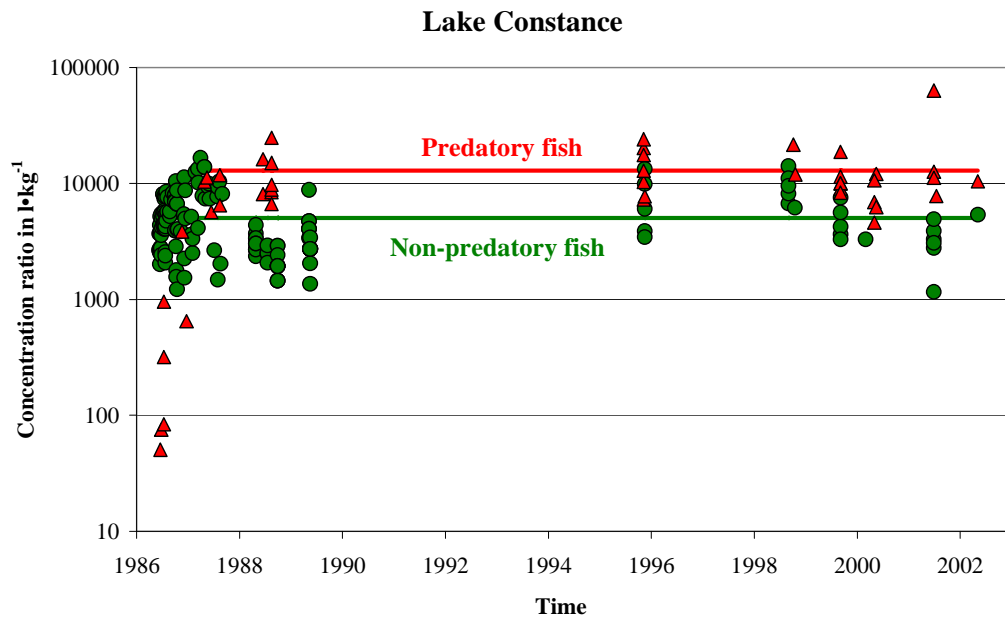
Lake Constance

Fig. 6.4. The concentration ratios (CRs) for ^{137}Cs in predatory (red triangles) and nonpredatory (green dots) fish from Lake Constance. The lines are the calculated averages.

145
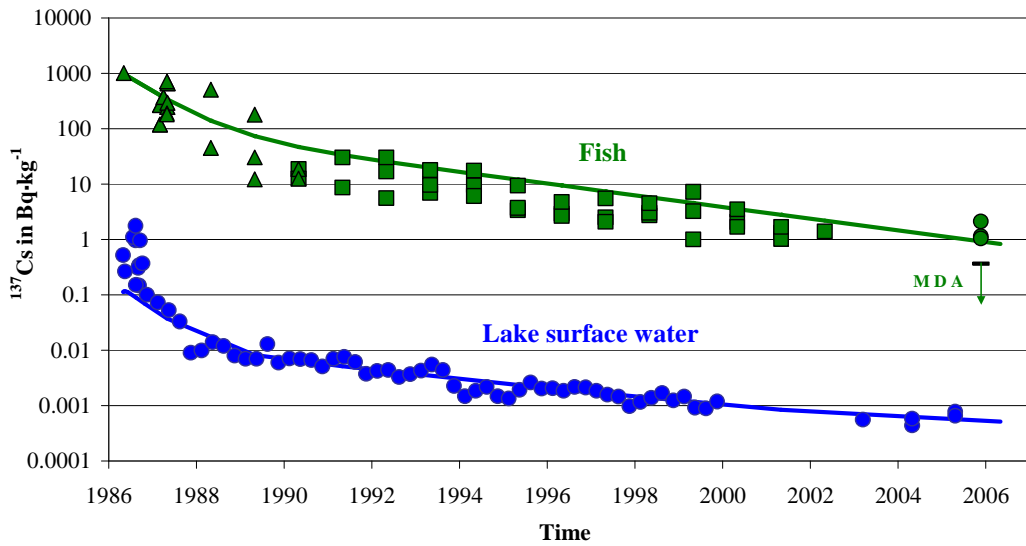
Lago Maggiore

Fig. 6.5. Time-dependency of the ^{137}Cs specific activities in fish and lake surface water in Lago Maggiore. The data for ^{137}Cs activity concentration in fish are taken from: *green triangles*– Radioactivity Environmental Monitoring (REM) database of the Institute for Environment and Sustainability, DG JRC, European Commission; *green squares* – D'Alberti (2001–2002), Cazzaniga et al. (1996–1998), Cazzaniga et al. (1997), D'Alberti and Osmani (1995), Osmani et al. (1994), Dominici and Risposi (1990–1993), Dominici (1989–1980); green points –our measurements in 2005.

Lago Maggiore
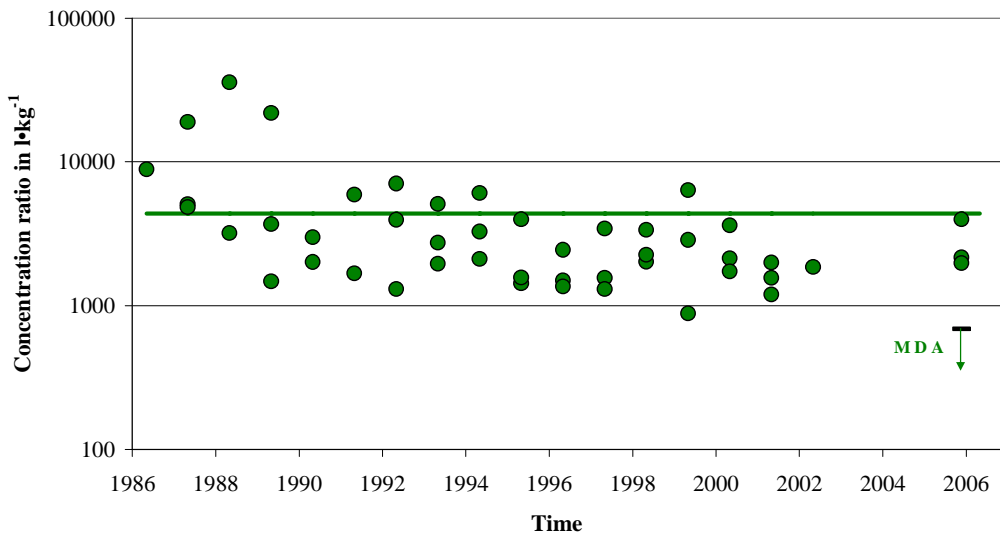
Fig. 6.6. Fish–water concentration ratios (CRs) for ^{137}Cs in non-predatory fish in Lago Maggiore.

The fish–water CRs of ^{137}Cs in Lago Maggiore are shown in Fig. 6.6. Here, the measured activity concentration of non-predatory fish is divided by the activity concentration in the lake water as calculated with the AQUASCOPE model. If the fish species was undefined the data was taken out from the common fit. The average CR value (4360 ± 880) l·kg^{-1} for Lago Maggiore agrees within the uncertainties with the average CR (5040 ± 240) l·kg^{-1} calculated for non-predatory fish in the mesotrophic Lake Constance (Table 6.3). This is a good indication that the CR can be transferred from one lake to another provided the trophic level of the lake is the same. The somewhat lower fish–water CR of ^{137}Cs in Lago Maggiore can be explained by the higher potassium concentration of 1.4–2 mg·l^{-1} (Guilizzoni, 2003–2005; our measurements – see chapter 4) as compared to that in Lake Constance with 1.1 – 1.3 mg·l^{-1} of potassium measured during the period 1976–1995 (Roßknecht, 1998).

As a conclusion the following statements can be formulated for the 3 lakes with different limnological properties. The concentration factor can be used several months after the fallout and it can be transferred from one lake to another considering the following dependencies:

- A factor 3 lower fish–water concentration ratio CR of ^{137}Cs is found in the eutrophic lake Vorsee as compared to those which are observed in mesotrophic and oligotrophic lakes, Lake Constance and Lago Maggiore, respectively.

- Within *one lake* the concentration factors for different fish groups vary largely. For example, in Lake Constance the CR for predatory fish is 2.6 times higher than CR for non-predatory fish. In lake Vorsee the CR value for predatory fish is a factor of 4 larger than for fish from the non-predatory group.

- The variability of CRs of ^{137}Cs within *one fish group* and *one lake* is rather high. The values of CR vary within one order of magnitude as observed in Lake Constance and Vorsee and even more in Lago Maggiore.

147

CONCLUSIONS

This work contains the present state of knowledge about the behaviour of the artificial caesium radionuclides introduced into the pre-alpine Lago Maggiore as a consequence of atmospheric nuclear weapons testing and the accident at the nuclear reactor in Chernobyl. Particularly, it provides a complete survey of the distribution of ^{137}Cs in the sediments of the lake and its participation in the sediment deposition processes. The most important results of field investigations, laboratory experiments and modeling are summarized as follows:

- During 2003 – 2005 the water sampling from the northern, southern and middle basins of the lake and its tributaries was done. In lake water as well as in tributaries the ^{137}Cs activity concentration is rather low with about 1 mBq·l^{-1}. The increase of the ^{137}Cs activity concentration with depth by a factor of two is probably controlled by a slight decrease of pH. The K^{+} concentration is constant in the water column; the oxygen concentration is also constant and rather large which results in a negligible NH$_4^{+}$ concentration.

- The ^{137}Cs activity concentration in the tributaries is compared to a run-off model (Håkanson, 2004) where one of the free parameters is the initial deposition on the catchment area. According to our measurements it must be in the order of 5 kBq/m^2.

- Sediment cores were taken at 7 different locations of Lago Maggiore in spring of 2003, 2004 and 2005. They were analyzed gamma spectrometrically for ^{137}Cs, unsupported ^{210}Pb, ^{134}Cs and ^{241}Am content. At most positions two maxima of ^{137}Cs were recognized which can be assigned to the fallouts after the Chernobyl accident and the atmospheric nuclear weapons testing fallouts in the 1960's.

- In bottom sediments of Lago Maggiore a considerable decrease of Chernobyl-derived ^{137}Cs inventories is observed between northern and southern positions, high values exceeding 30 kBq·m^{-2} in the northern and central basins and, low levels (7 kBq·m^{-2}) near the outflow. The maximum in total inventories is reached 8–9 years after the Chernobyl accident as compared to 5 and 15 years in Lake Constance and in the shallow eutrophic Lake Vorsee, respectively.

- The results of the 5-step sequential extraction procedure performed on sediments of Lago Maggiore show that ^{137}Cs is very tightly bound to the sediment. The percentage of exchangeable ^{137}Cs extracted during the first step is only about 1 % at some positions as compared to about 5 % in Lake Constance and Lake Lugano (Klemt *et al.*, 2000). Most of extracted ^{137}Cs was found in the organic fraction, followed by amorphous silicates.

- A model based on coupled sedimentation-diffusion equations was developed to describe migration processes of ^{137}Cs and it's distribution in the sediment of Lago Maggiore. This model can cover the time period from the nuclear weapon testing to the present and takes into account compaction of sediments, fixation and redissolution, influence of competing ions on the retarded diffusion within the sediments. The results of the model were compared with the water and sediment measurements from seven positions at different basins. Estimated ^{137}Cs activity concentrations are in good agreement with measured data.

- The free parameters of the model are the sedimentation rate (R_S) and two distribution coefficients: one (K_d) which is responsible for the uptake of ^{137}Cs into the sediment and another one ($K_{d\_dif}^{ex}$) which controls the diffusion within the sediment. Our model shows that generally in sediments from Lago Maggiore $K_{d\_dif}^{ex}$ is 3 – 5 times lower than the exchangeable distribution coefficient K_d^{ex}

- Estimated and measured values of a total ^{137}Cs distribution coefficient K_d^{tot} which characterizes the positions from the main basin of the lake are very large, about 10^5 l·kg^{-1}. Similar values are also observed in lake Constance which are twice larger than those in Lake Lugano and about a factor 5 larger than those in the shallow lake Vorsee. The main reason for high values of K_d^{tot} are a high content of clay minerals in the lake sediments and low concentration of competing ions K^+ and NH_4^+. However, the positions with lower depth which are located close to the tributaries have lower distribution coefficients of about 20 000 l·kg^{-1}. There is a strong influence of the tributaries on the behavior of radiocaesium in the lake.

- A lot of large and smaller turbidites which are the consequences of the underwater landslides of sediments due to the steep slopes of the lake basin or of the input of the allochthonous material with heavy rains or river floods are found in Lago Maggiore. An important improvement of the model is that it became possible to model turbidites as an instantaneous extra input of sediment. However, their presence makes it difficult to establish correctly the depth-age relation in the sediment profile and brings additional uncertainties into the model.

- A depth-age relation was established using a combination of the ^{137}Cs model with the ^{210}Pb CIC and CRS models. Together with a ^{7}Be check of the presence of the top layer it became sufficient to provide a reliable continuous time-scale and to verify the completeness of the sediment profile. The CRS model as well as the model which describes the ^{137}Cs vertical distribution showed the varying sedimentation rates over time. Higher sedimentation rates of $0.1 - 0.9$ g·(cm^{2}·a)$^{-1}$ are found in the southern and central basin while the northern basin is characterized mostly by lower rates of about 0.05 g·(cm^{2}·a)$^{-1}$.

- In 2005 very low ^{137}Cs concentrations of less than 1 Bq·kg^{-1} were measured in non-predatory fish from Lago Maggiore. Consequently, a ^{137}Cs fish–water concentration ratio (CR) of (4360 ± 880) l·kg^{-1} was calculated for Lago Maggiore. It agrees within the uncertainties with the average CR (5040 ± 240) l·kg^{-1} calculated for non-predatory fish in the mesotrophic Lake Constance. The decrease in the ^{137}Cs activity concentration in fish follows the decrease of radioactivity in the surface water.

ACKNOWLEDGEMENTS

REFERENCES

Albrecht, A., 1998. The Behavior of Nuclear Reactor Derived Metallic Radionuclides in the Aquatic System of Switzerland, Schriftenreihe der EAWAG, 13, 105 p.

Alexakhin, R.M. and Krouglov, S.V., 2001. Soil as the main compartment for radioactive substances in terrestrial ecosystems. In – Radioactive Pollutants: Impact on the environment (based on invited papers at the ECORAD 2001), F. Bréchignac and B. Howard Eds., EDP sciences, Les Ulis, pp. 149 – 174.

Ambrosetti, W., and Barbanti, L., 1999. Deep water warming in lakes: an indicator of climatic change. J. Limnol., 58 (1), pp. 1 – 9.

Ambrosetti, W., L. Barbanti and N. Sala, 2003. Residence time and physical processes in lakes. J. Limnol., 62 (1), pp. 1 – 15.

Appleby, P. G. and F. Oldfield, 1978. The Calculation of Lead-210 Dates Assuming a constant Rate of Supply of Unsupported Pb-210 to the Sediment. CATENA, Vol. 5, pp. 1 – 8.

Atlas of caesium deposition on Europe after the Chernobyl accident, 1998. Office for Official Publications of the Europe Communities, Luxemburg.

Bachhuber, H., Bunzl, K., Schimmack, W., Gans, J., 1982. The migration of Cs-137 and Sr-90 in multilayered soils: results from batch, column and fallout, Nuclear Technology, 59, pp. 291 – 301.

Bandong, Bryan B., Alan M. Volpe, Bradley K. Esser, Gregory M. Bianchini, 2001. Pre-concentration and measurement of low levels of gamma-ray emitting radioisotopes in coastal waters. Applied radiation and isotopes, 55, pp. 653 – 665.

Barbanti, L., 1975. Annuario 1974 dell'Osservatorio Meteorologico di Pallanza. Mem. Ist. Ital. Idrobiol., 32, pp. 393 – 471.

Barbieri, A.,Veronesi, M., Simona, M., Malusardi, S., and Straškrabová, V., 1999. Limnological survey in eight high mountain lakes located in Lago Maggiore watershed (Switzerland). J. Limnol., 58 (2), pp. 179 – 192.

Bertoni, R., Piscia, R., Callieri, C., 2004. Horizontal heterogeneity of seston, organic carbon and picoplancton in the photic zone of Lago Maggiore, Northern Italy. J. Limnol., 63(2), pp. 244 – 249.

Blanco, P., Tomé, F. V., Lozano, J. C., 2004. Sequential extraction for radionuclide fractionation in soil samples: a comparative study. Applied Radiation and Isotopes, 61, pp. 345 – 350.

Blott, Simon J. and Kenneth Pye, 2001. GRADISTAT: A grain size distribution and statistics package for the analysis of unconsolidated sediments. Earth Surf. Process. Landforms, 26, pp. 1237 – 1248.

Bonomi, G., Gerletti, M., Indri, E. and Tonolli, L., 1970. Report on Lake Maggiore. In: O.C.S.E., Symposium on large lakes and impoundments, Uppsala, May 1968, pp. 299 – 341.

Bossew, P., G. Kirchner, 2004. Modelling the vertical distribution of radionuclides in soil. Part 1: the convection-dispersion equation revised. J. Environ. Radioactivity, 73, pp. 127 – 150.

Calderoni, A., Mosello, R., 1996. L´eutrofizzazione del Lago Maggiore e il suo risanamento. Documenta Ist. ital. Idrobiol., 56, pp. 5 – 20.

Callieri, C., 1997. Sedimentation and aggregated dynamics in Lake Maggiore, a large, deep lake in Northern Italy. Mem. Ist. Ital. Idrobiol., 56, pp. 37 – 50.

Carollo, A., Contardi, F., Libera, V., Rolla, A., 1985. Basino idrografico del Lago Maggiore. Carta delle precipitazioni. Periodo osservazioni 1921-1980. Consiglio nazionale delle ricerche instituto Italiano di Idrobiologia. Cartografia Attilio e Fabrizio Bertocchi.

Cazzaniga, R., F. D'Alberti, C. Osmani, V. Vocino, 1996 – 1998. Misure di radioattività ambientale – Sito di Ispra 1996, 1997, 1998. Centro Comune di Ricerca-Ispra EUR-17741, 18732, 18989.it.

Cazzaniga, R., F. D'Alberti, C. Osmani, V. Vocino, 1997. Measurements of the environmental radioactivity – JRC Ispra 1997. Centro Comune di Ricerca-Ispra EUR-18700.en.

Celebi, O., Kilikli, A., Erten, H.N., 2009. Sorption of radioactive cesium and barium ions onto solid humic acid. Journal of hazardous materials, 168, pp. 695 – 703.

Comans, R. N. J., Haller, M. and De Preter, P., 1991. Sorption of cesium on illite: Non-equilibrium behaviour and reversibility. – Geochim. Cosmochim. Acta, 55, 433 – 440.

Commisione Internationale per la protezione delle Aque Italo-Svizzere, 2001. Ricerrche sull'evoluzione del Lago Maggiore, Campagna 2000. Instituto Italiano di Idrobiologia, Verbavia Pallanza.

Cremers, A., A. Elsen, P. De Preter and A. Maes, 1988. Quantitative analysis of radiocaesium retention in soils. Nature, 3352, pp. 247 – 249.

Czarnecki, J., Cartier, F., Honegger, P., Zurkinden, A.. 1986. Bodenverstrahlung in der Schweiz aufgrund des Reaktorunfalles in Chernobyl, in André, L., Born, E.J., Fischer, G. (Eds.), Radioaktivitaetsmessungen in der Schweiz nach Tschernobyl und Ihre Wissenschaftliche Interpretation, Tagungsberichte Compte-Rendu proceedins, Universität Bern, pp. 93–109.

de Bernardi, R., G. Giussani & E. Grimaldi, 1984. Lago Maggiore. In: F.B. Taub (ed.), Lakes and Reservoirs. Elsevier, Amsterdam, pp. 247 – 266.

D'Alberti, F., C. Osmani, 1995. Misuri di radioattività ambientale – Sito di Ispra 1995. Centro Comune di Ricerca-Ispra EUR-17706.it.

D'Alberti, F., 2001 – 2002. Misuri di radioattività ambientale e valutazione della dose alla popolazione – Sito di Ispra 1999–2001, 2002. Centro Comune di Ricerca-Ispra EUR-20534, 20852.it.

D'Alberti, F., 2003. Misuri di radioattività ambientale e valutazione della dose alla popolazione, CCR – Ispra 2003. Centro Comune di Ricerca-Ispra TN I.04.113.

Davidson, W., Hilton, J., Hamilton-Taylor, J., Kelly, M., Livens, F., Rigg, E., Carrick, T.R. And Singleton, D.L., 1993. The transport of Chernobyl-derived radiocaesium through two freshwater lakes in Cumbria, UK. J. Environ. Radioactivity, 19, 125–133.

Davis, J. J., 1963. Cesium and its relationships to potassium in ecology. in Schultz V., Klement A. W. Jr. (eds.). Radioecology, ReinholdPpubl, Comp., New York, 539–556.

De Preter, P., 1990. Radiocesium retention in the aquatic, terrestrial and urban environment: a quantitative and unifying analysis. PhD thesis, Katholieke Universiteit Leuven.

Dominici, G., 1980 – 1989. Misuri di radioattività ambientale – Ispra 1980, 1981, 1982, 1983, 1984, 1985, 1986, 1987, 1988, 1989. Centro Comune di Ricerca – Ispra EUR-7958, 8572, 9194, 9650, 10036, 10947, 11348, 11821, 12223, 12884.it.

Dominici, G., L. Risposi, 1990 – 1993. Misuri di radioattività ambientale – Ispra 1990, 1991, 1992, 1993. Centro Comune di Ricerca-Ispra EUR-14088, 14890, 15570, 16124.it.

Dominik, J. and Span, D., 1992. The fate of Chernobyl Cs-137 in Lake Lugano. Aquatic Sciences, 54, pp. 238 – 254.

Duursma, E.K., Carroll, J., 1996. Environmental compartments: equilibria and assessment of processes between air, water, sediments and biota. Springer-Verlag, Berlin Heidelberg, 275 p.

Facchinelli, A., Magnoni, M., Gallini, L., Bonifacio, E., 2002. [137]Cs contamination from Chernobyl of soils in Piemonte (North-West Italy): Spatial Distribution and deposition model. Water, Air, & Soil Pollution, V. 134, Issue 1 – 4, pp. 339 – 350.

Förster, U. 1985. Chemical forms and reactivities of metals in sediments. In: Laschber, R., Davis, K.D., L´Hermite, P. (eds.): Chemical methods for assessing bioavailable metals in sludges and soils. Elsevier Applied Science Publishers, London, pp. 1 – 30.

Guilizzoni Piero, CNR-Istituto Italiano di Idrobiologia Largo Tonolli, 5028922, Verbania Pallanza, Italy (p.guilizzoni@iii.to.cur.it). Personal communications, 2003 – 2005.

Håkanson, L., 2004. Modelling the transport of radionuclides from land to water. J. Environ. Radioactivity, 73, pp. 267 – 284.

Hessen, D.O. and Tranvik, L.J., (eds.), 1998. Aquatic humic substances: ecology and biogeochemistry. Ecological studies 133, Springer, Science, 346 p.

Hilton J., 2001. Dispersion and transfer in the aquatic environment. Radioecology: Radioactivity and Ecosystems. R. Kirchmann and E. van der Stricht (ed.). International union of radioecology. Fortemps, Liège, 603 p.

IAEA (International Atomic Energy Agency), 1991. The international Chernobyl project. An overview. Assessment fo radiological consequences and evaluation of protective measures. Report by an international advisory committee.

Ilus, E. and Saxén, R., 2005. Accumulation of Chernobyl-derived ^{137}Cs in bottom sediments of some Finish lakes. J. of Environ. Radioactivity, 82, pp. 199 – 221.

Kaminski, S., A. Konoplev, G. Lindner and H.G. Schröder, 1998. The fate of artificial caesium radionuclides in Lake Constance. Arch. Hydrobiol. Spec. Issues Advanc. Limnol., 53, pp. 369 – 409.

Kaminski, S., T. Richter, M. Walser, G. Linder, 1994. Redissolution of caesium radionuclides from sediments of freshwater lakes due to biological degradation of organic matter. Radiochimica Acta 66/67, pp. 433 – 436.

Kirchner, G., 1998. Modelling the migration of fallout radionuclides in soil using a transfer functions model. Health physics, 74 (1), pp. 78 – 85.

Klemt, E., Kaminski, S., Miller, R., Zibold, G., Astner, M., Burger, M., Schmid, E., 2000. Normierung von Extraktionsexperimenten zur Bestimmung der Bindung von Radiocaesium an Sedimente des Luganersees. In: Umweltradioaktivität und Strahlendosen in der Schweiz 1999, Bundesamt für Gesundheit B.4.4.1-5.

Klemt, E., A. Konoplev, G. Zibold, 2002. Modelling of the distribution of radiocaesium in sediments of lakes with different limnological character, In: F. Bréchignac (ed): The Radioecology – Ecotoxicology of Continental and Estuarine Environments ECORAD 2001. Radioprotection-colloques Vol.37, C1.

Klemt E., V. Putyrskaya, St. Röllin, G. Zibold, 2005. Migration of ^{137}Cs in Tributaries, Lake Water and Sediment of Lago Maggiore – Analysis and Comparison to other Lakes. Proceedings from the 2nd International Conference on Radioactivity in the Environment, pp. 266 – 269.

Klute, A., (ed.), 1992. Methods of Soil Analysis: Part I--Physical and minerological methods: Soil Science Society of America Book Series No. 5, Soil Science Society of America Inc., USA.

Konoplev, A.V., A. Förschner, S. Kaminski, T. Klenk, I. V. Konopleva, M. Walser, G. Zibold, 1996. Modelling of ^{137}Cs migration in sediments of two prealpine lakes, Proceedings of International symposium on ionising radiation Stockholm, pp. 693 – 698.

Konoplev A., S. Kaminski, E. Klemt, I. Konopleva, R. Miller, G.Zibold, 2002. Comparative study of ^{137}Cs partitioning between solid and liquid phases in Lake Constance, Lugano and Vorsee. J. Environ. Radioactivity, 58, pp. 1 – 11.

Krom, M.D., 1980. Spectrophotometric determination of ammonia: a study of a modified Berthelot reaction using salicylate and dichloroisocyanurate. Analyst, 105, 305–316.

Lehto, J., Haukka, S., Harjula, R., 1990. Mechanism of cesium ion exchange on potassium cobalt hexacyanoferrates (II). J. Chem. Soc. Dalton Trans. pp. 1007 –1011.

Maerki, M., B. Wehrli, C. Dinkel, and B. Müller, 2004. The influence of tortuosity on molecular diffusion in freshwater sediments of high porosity. Geochimica et Cosmochimica Acta, 68 (7), pp. 1519 – 1528.

Magnini, A., Christian, U., Barth, M., Schmitz, W., and Stabel, H.H., 1990. Pathways and residence times of radionuclides in Lake Constance. Large lakes: ecological structures and functions, in Tilzer, Max M. and Colette Serruya (Eds.), Springer-Verlag Berlin Heidelberg, pp. 245–264.

Maguire, S., Pulford, I.D., Cook, G.T., and Mackenzie, A.B., 1992. Caesium sorption-desorption in clay-humic acid systems. J. Soil Sci., 43, pp. 689 – 696.

Makhonko, K.P. (Ed.), 1990. Manual on organization of environmental monitoring around of nuclear power plants. Leningrad: Gidrometeoizdat, 264 p.

Marchetto, A. and S. Musazzi, 2001. Comparison between sedimentary and living diatoms in Lago Maggiore (N. Italy): implication of using transfer functions. J. Limnol., 60 (1), pp. 19 – 26.

Meischner, K.D. & Rumohr J. (1974). A light-weight, highmomentum gravity corer for subaqueous sediments. Senckenbergiana marit, v. 6, pp. 105 – 117.

Monte, L., 1991. A predictive model for the behavior of dissolved radioactive substances in stratified lakes. J. of Environ. Radioactivity, 13, pp. 297 – 308.

Monte, L., Van der Steen, J., Bergström, U., Gallego Díaz, E., Håkanson, L., J. Brittain, 2000. The project MOIRA: A Model-Based Computerised System for Management Support to Identify Optimal Remedial Strategies for Restoring Radionuclide Contaminated Aquatic Ecosystems and drainage Areas. Final Report. ENEA RT/AMB/2000/13, Italy.

Monte, L., Brittain, J.E., Håkanson, L., Heling, R., Smith, J.T., 2003. Zheleznyak M.: Review and assessment of models used to predict the fate of radionuclides in lakes. Journal of Environmental Radioactivity, 69, pp. 177 – 205.

Monte, L., Grimani, C., Desideri, D., Angeli, G., 2005. Modelling the long-term behaviour of radiocaesium and radiostrontium in two Italian lakes. J. Environ. Radioactivity, 80, 105–123.

Mosello, R., Barbieri, A., Brizzo M.C., Calderoni, A., Marchetto, A., Passera. S., Rogora, M., and Tartari, G., 2001. Nitrogen budget of Lago Maggiore: the relative importance of atmospheric deposition and catchment sources. J. Limnol., 60 (1), pp. 27 – 40.

Mudroch, A. & D. MacKnight, S. (ed.), 1991. Handbook of techniques for aquatic sediments sampling, CRC Press, Inc., United States, 210 p.

Mudrock, R.N., Johnson, M.S., Hemingway, J.D., and Jones, S.R., 1995. The distribution of radionuclides between the dissolved and particulate phases of a contaminated freshwater stream. Environ. Technology, 16, pp. 1 – 12.

Nembrini, G. P., Capobianco, J. A., Viel, M. and Williams, A.F., 1983. A Mössbauer and chemical study of the formation of vivianite in sediments of Lago Maggiore (Italy), Geochemical et Cosmochimica Acta, 47, pp. 1459 – 1464.

Niskin, Sh. I., 1962. A water sampler for microbiological studies. Deep-sea Research, 9, pp. 501 – 503.

Nordlinder, S., Bergstriim, U., & Brittain J.E., 1997. A generic dynamic model of Cs-137 turnover in Nordic lakes. J. Environ. Radioactivity, 37, pp. 175 – 191.

Oldfield, F., Appleby, P.G., 1984. Empirical testing of 210Pb-dating models for lake sediments. In: Hayworth EY and Lund JWG (Eds). Lake Sediments and Evironmental History. Leicester University Press, pp. 93 – 124.

Osimani, C., Vocino, V., D'Alberti, F., Cazzaniga, R., 1994. Misure di radioattivitata ambientale – Sito di Ispra 1994. Commissione delle Comunita Europee. Centro Commune di Ricerca – Ispra EUR-17309.it.

Ostapenya, A.P., Sokolik, G.A., Pavlyutin, 1999. Distribution of radionuclides between main components of lake ecosystems, "Весцi НАНБ", 2, pp. 134 – 139 (in Russian).

Owens, P.N., Walling, D.E., He, Q. (1996): The Behaviour of Bomb-Derived Caesium-137 Fallout in Catchment Soils. Journal of Environmental Radioactivity. 1996, Vol. 32, 3, pp. 169 – 191.

Piontelli, R. & V. Tonolli, 1964. Il tempo di residenza delle acque lacustri in relazione ai fenomeni di arricchimento in sostanze immesse, con particolare riguardo al Lago Maggiore. Mem. Ist. ital. Idrobiol., 17, pp. 247 – 266.

Premazzi, G., A. Dalmiglio, A. C. Cardoso and G. Chiaudani., 2003. Lake management in Italy: the implications of the Water Framework Directive. Lakes and Reservoirs: Research and Management, 8, pp. 41 – 59.

Prepas, E.E., Charette, T., 2003. Worldwide eutrophication of water bodies: causes, concerns, controls. Treatise on chemistry, Volume 9, pp. 311 – 331.

Putyrskaya, V., Klemt, E., Paliachenka, H., Zibold, G., 2004. Radiocaesium in water and sediments of Lago Maggiore: Measurements and Modeling. Advances in Nuclear and Radiochemistry. S.M. Qaim and H.H. Coenen (ed.). Schriften des Forschungszentrums Jülich, pp. 699 – 701.

Radioactivity Environmental Monitoring (REM) Database, 2005. European commission, Joint Research Center (JRC), Institute of environment and sustainability [Electronic resource]. – Mode of access: http://rem.jrc.cec.eu.int/ - Date of access: 13.03.2005.

Ranzi, R., 2001. Hydrological aspects in the Mesoscale Alpine Programme-SOP experiment: an overview. Ranzi, R. and B. Bacchi (eds.), Hydrological aspects in the Mesoscale Alpine Programme-SOP experiment, Univ. of Brescia, Dept. of Civil Engineering , Technical Report N. 10, 2000.

Ravera, O., Cenci, R., Beone, G.M., Dantas, M. and Lodigiani, P., 2003. Trace elements concentrations in freshwater mussels and macrophytes as related to those in their environment. J. Limnol., 62 (1), pp. 61 – 70.

Rezzoug, S., Michel, H., Fernex, F., Barci-Funel, G., Barci, V., 2006. Evaluation of ^{137}Cs fallout from the Chernobyl accident in a forest soil and its impact on Alpine Lake sediments, Mercantour Massif, S.E. France. J. Environ. Radioactivity, 85, 369–379.

Robbins, J. A., 1978. Geochemical and geophysical applications of radioactive lead. Biochemistry of lead, chapter 9. J. P. Nriagu (Ed.), Elsevier.

Robbins, J.A., Lindner, G., Pfeiffer, W., Kleiner, J., Stabel, H.H., Frenzel, P., 1992. Epilimnetic scavenging and fate of Chernobyl radionuclides in Lake Constance. – Geochim. Cosmochim. Acta, 56, 2339–2361.

Roßknecht Henno, 1998. Langjärige Entwicklung chemischer Parameter im Bodensee-Obersee. Internationale Gewässerschutzkommission für den Bodensee. Bericht Nr. 48, 143 p.

Santschi, P., S. Bollhalder, S. Zingg, A. Lück, K. Farrenkothen, 1990. The self-cleaning capacity of surface waters after radioactive fallout. Environmental Science and Technology, 24, pp. 519 – 527.

Schachtschabel, P., H.-P. Blume, G. Brümmer, K.-H. Hartge, U. Schwertmann, W. R. Fischer, M. Renger, O. Strebel, 1989. Lehrbuch der Bodenkunde, Enke, Germany.

Schertz, M., Michel, H., Barci-Funel, G., Barci, V., 2006. Transuranic and fission product contamination in lake sediments from an alpine wetland, Bore´ on (France). J. Environ. Radioactivity, 85, 380–388.

Semizhon, T., 2005. Measurements and modeling of ^{137}Cs activity concentration in tributaries of Lago Maggiore. Diploma thesis. Weingarten, Germany.

Smith, J.T., A.A. Bulgakov, R.N.J. Comans, M.A. Cross, A.V. Konoplev, A.V. Kudelsky, M.J. Madruga, I.N. Ryabov, O.V. Voitsekhovitch, G. Zibold, 2002. AQUASCOPE Technical Deliverable. Simplified models for predicting ^{89}Sr, ^{90}Sr, ^{134}Cs, ^{137}Cs, ^{131}I in water and fish of rivers, lakes and reservoirs. CEH Center for Ecology and Hydrology, Natural Environment Research Council.

Smith, J.T., A.A. Bulgakov, R.N.J. Comans, A.V. Konoplev, A.V. Kudelsky, M.J. Madruga, I.N. Ryabov, O.V. Voitsekhovitch, G. Zibold, 2005. The "AQUASCOPE" simplified model for predicting ^{89,90}Sr, ^{131}I and ^{134,137}Cs in surface water after a large-scale radioactive fallout. Health Physics, 89, pp. 628–644.

Smith, V.H., Tilman, G.D., Nekola, J.C., 1999. Eutrophication: impacts of excess nutrient inputs on freshwater, marine, and terrestrial ecosystems. Environ. Pollution, 100, pp. 179 – 196.

Smith, J.T. and N.A. Beresford, 2005. Chernobyl – Catastrophe and Consequences. Springer, Praxis Publishing Ltd, Chichester, UK, 310 p.

Spasova, Y., 2003. Artificial radionuclides in rivet-sediments: measurements and modelling of input, vertical distribution and binding to geochemical fractions in the case of the Yenisei River. PhDThesis, Technical University-Varna, Fachhochschule Ravensburg-Weingarten.

Spezzano, P., Hilton, J., Lishman, J.P., Carrick, T.R., 1993. The variability of Chernobyl Cs retention in the water column of lakes in the English Lake district, two years and four years after deposition. J. Environ. Radioactivity, 19, pp. 213–232.

Staunton, S. and Rouband, M., 1997. Adsorption of radiocaesium on montmorillonite and illite: effect of charge compensation cation, ionic strength, concentration of potassium, caesium and fulvic acid. Clays and Clay Minerals, 45, pp. 251 – 260.

Steinmann, P., Billen, T., Loizeau, J.-L., Dominik, J., 1999. Beryllium-7 as a tracer to study mechanims and rates of metal scavenging from lake surface waters. Geochimica et Cosmochimica Acta, 63 (11/12), pp. 1621 – 1633.

Stevenson, F.J., 1994. Humus chemistry: genesis, composition, reactions / F.J. Stevenson. – 2nd ed. New York: Wiley. 496 p.

Stumm, W. (ed.), 1985. Chemical processes in lakes. Environmental science and technology, Inc. by John Wiley & Sons, 435 p.

Stumm, W. and Morgan, J. (eds.), 1981. Aquatic chemistry: An introduction emphasizing chemical equilibria in natural waters, Inc. by John Wiley & Sons, New York, 780 p.

Tessier, A., Campell, P. G. C., Bisson, M., 1979. Sequential Extraction Procedure for the Speciation of Particulate Trace Metals, Analytical Chemistry, Vol. 51(7), pp. 844 – 851.

Tilzer, Max M. and Colette Serruya (ed.), 1990. Large lakes: ecological structures and functions. Springer-Verlag Berlin Heidelberg, 691 p.

Tipping, E., 2002. Cation binding by humic substances. Centre for ecology and hydrology, Windermere UK, Cambridge University Press, 456 p.

Tomman, R.V., 1981. Equilibrium model of fate of microcontaminants in diverse aquatic food chains. Can. J. Fish Aquatic Sci., 38, pp. 280 – 296.

Tonolli, V., 1961. The distribution of temperature and plankton along the axis of a Large lake (Lago Maggiore). Verh. Int. Ver. Limnol., 14, pp. 920 – 926.

UNSCEAR (United Nations Scientific Commitee on the Effects of Atomic Radiation), 2000. Sources and Effects of Ionizing Radiation. Report to the General Assembly of the United Nations, New York, United Nations.

Viel, M., Damiani,V., 1985. Sedimentological and geochemical study of recent deposits in Lago Maggiore (North Italy). Mem. Ist. Ital. Idrobiol. 43, 181-238.

Vintró, L. León, P.I. Mitchell and S.P. Nielsen, 2001. Hilton J., 2001. Marine environment. Radioecology: Radioactivity and Ecosystems. R. Kirchmann and E. van der Stricht (ed.). International union of radioecology. Fortemps, Liège, 603 p.

Voitsekhovich Oleg, Ukrainian Hydrometeorological Institute, 37 Nauka Ave., Kiev 252028, Ukraine (voitsekh@voi.vedos.kiev.ua). Personal communications, 2005.

Warner, F. and Harrison, R.M., (eds.), 1993. Radioecology after Chernobyl: Biogeochemical, Pathways of Artificial Radionuclides, 400 pp.

Wauters, J., M. J. Madruga, M. Vidal, and A. Cremers, 1996. Solid phase of radiocaesium in bottom sediments. Science of the Total Environment, 187, pp. 121 – 130.

Whitehead, N.E., Ditchburn, N.G., Mccabe, W.J., Mason, W.J., Irwin, J., Pickrill, R.A., Fish, G.R., 1998. New Zealand J. of Marine and Freshwater Research, 32, pp. 489 – 503.

Wu, J., Li, B., Liao, J., Feng, Y., Zhang, D., Zhao, J., Wen, W., Yang, Y., Liu, N., 2009. Behavior and analysis of cesium adsorption on montmorillonite mineral. J. Env. Radioactivity, V. 100, 10, pp. 914 – 920.

Zibold, G., A. Förschner, J. Drissner, E. Klemt, R. Miller and M. Walser, 2001. Time-dependency of the caesium-137 concentration factor in pike from lake Vorsee. Proc. UIR Topical Meeting. Mol, (Belgium), 1.-5. June 1998, E. Van der Stricht (Ed.), BVG, Balen, Belgium (2001), pp. 235 – 237.

Zibold, G., Kaminski S., Klemt E. & Smith J.T., 2002. Time-dependency of the ^{137}Cs activity concentration in freshwater lakes, measurement and prediction. Proceedings of the international congress on the radioecology of continental and estuarine environments. Radioprotection-Colloques, 37, C1-75-80.

www. bwg. admin.ch – Federal Office for Water and Geology (FOWG), Swiss National Hydrological Survey, CH – 3003 Berne – Ittigen.

LIST OF PUBLICATIONS RELEVANT TO THE THESIS

Peer-reviewed journals

Putyrskaya, V., Klemt, E., Röllin, St., 2009. Migration of ^{137}Cs in tributaries, lake water and sediment of Lago Maggiore – analysis and comparison to Lago di Lugano and other lakes. J. Environ. Radioactivity, 100, 35 – 48.

Putyrskaya, V., Klemt, E., 2007. Modeling ^{137}Cs migration processes in lake sediments. J. Environ. Radioactivity, 96, 54 – 62.

Other journals

Putyrskaya, V., Goncharova, N., Klemt, E., 2006. Biological availability of caesium-137 in European lakes. Natural Resources, 1, 89 – 97 (in Russian).

Putyrskaya, V., Klemt, E., Paliachenka, H., Zibold, G., 2005. Mathematical model for description of uptake and migration of Cs-137 in bottom sediments. Vestnik of State Polotsk University, 3, 61 – 66 (in Russian).

Conference proceedings

Putyrskaya, V., Klemt, E., Zibold, G., Goncharova, N., 2007. Comparative analysis of Cs-137 uptake dynamics in fish from different lakes. Proceedings of the 6th International Symposium on "Actual problems of dosimetry". Kundas, S., Melnov, S., Gurachevsky, V. (Eds.), Minsk, 85 – 91 (in Russian).

Putyrskaya, V., 2007. Radioactive contamination of lake ecosystems in Belarus and Europe: present state of knowledge. Proceedings of the 4th international Ecological Symposium "Regional ecological problems: ways of solutions", Novopolotsk, 1, 86 – 89.

Putyrskaya, V., Goncharova, N., Klemt, E., 2006. Dating of sediments using Lead-210 method // Proceedings of the 6th International conference "Sakharov Readings 2006: Environmental problems of 21th century". Kundas, S., Melnov, S., Poznyak, S. (Eds.), Minsk, 250 – 252 (in Russian).

Klemt, E., Putyrskaya, V., Röllin, St., Zibold, G., 2005. Migration of ^{137}Cs in Tributaries, Lake Water and Sediment of Lago Maggiore – Analysis and Comparison to other

Lakes // Proceedings from the 2nd International Conference on Radioactivity in the Environment, Nice, 266–269.

Putyrskaya, V., Klemt, E., Zibold, G., 2005. Modeling of Migration Processes of ^{137}Cs in Lake Sediments // Proceedings from the 2nd International Conference on Radioactivity in the Environment, Nice, 467–470.

Putyrskaya, V., Klemt, E., 2005. Peculiarities of modeling the behavior of Cs-137 in lake ecosystems // Proceedings of the 5th International conference "Sakharov Readings 2005: Environmental problems of 21th century", Minsk, 21–22 May 2005, 123–124 (in Russian).

Putyrskaya, V., Klemt, E., Zibold, G., Paliachenka, H., 2004. Radiocaesium in water and sediments of Lago Maggiore: Measurements and Modeling // Advances in Nuclear and Radiochemistry / eds. S.M. Qaim, H.H. Coenen. – Schriften des Forschungszentrums Jülich, 699–701.

Putyrskaya, V., Klemt, E., Zibold, G., Paliachenka, H., 2004. Measurements and modeling of Cs-137 distribution in Lago Maggiore // Proceedings of the 4th International conference "Sakharov Readings 2004: Environmental problems of 21th century", Minsk, 21–22 May 2004, 175–177.

Others

Klemt, E., Putyrskaya, V., Röllin, S., 2009. ^{137}Cs in Wasser und Sedimenten des Lago Maggiore (Kapitel 4.5). Umweltradioaktivität und Strahlendosen in der Schweiz 2008, 73–77.

Semizhon, T., Klemt, E., Putyrskaya, V., Goncharova, N., 2008. Comparison of artificial radionuclides distribution in sediments of lakes and rivers with forest and agricultural soils // Book of abstracts of XXXVIII ESNA Meeting: New methods in agricultural environment and hazard assessment. August 27–31, 2008, Krakow, Poland. P. 137.

Putyrskaya, V., Goncharova, N., 2007. Comparative analysis of radiocaesium behaviour in lake ecosystems of Belarus and Europe. Book of abstracts of the 7th International conference "Sakharov Readings 2007: Environmental problems of 21th century". Kundas, S., Melnov, S., Poznyak, S. (Eds.), Minsk, 175–176 (in Russian).

Klemt E., Putyrskaya, V., Semizhon, T., 2006. Migration of Cs-137 in lake sediments and binding to different geochemical fractions // Book of abstracts of 10th International symposium on Environmental radiochemical analyses 13–15 September, 2006, Oxford, England. – Oxford. – P. 9.

Putyrskaya, V., Goncharova, N., Klemt, E., 2006. Radionuclide migration in bottom lake sediments: Influence of turbidity flows on sediment age determination. Book of abstracts of the Scientific conference "State and ways of development of rational nature management and preservation of the environment of Belarus and Russia", Polotsk, 136–137 (in Russian).

Goncharova, N., Putyrskaya, V., Semizhon, T., Klemt, E., Zibold G. Studies of input and migration of Cs-137 in bottom sediments // Book of abstracts of International conference: «Chernobyl 20 year after. Strategy of reconstructing and sustainable development of contaminated regions». – Gomel, 2006. – P. 174 (in Russian).

Putyrskaya, V., Klemt, E., Zibold, G., 2005. Progress in modeling the input and the vertical distribution of Cs-137 in lake sediments // Verhandlungen der 69th Jahrestagung der Deutschen Physikalischen Gesellschaft (DPG): Simposien, Berlin, 4–9 März 2005 / Humboldt-Universität zu Berlin, Technische Universität Berlin, 79–80.

Putyrskaya, V., Klemt, E., Zibold, G., 2005. New results on Cs-137 in water, sediments, and tributaries of Lago Maggiore // Verhandlungen der 69th Jahrestagung der Deutschen Physikalischen Gesellschaft (DPG), Simposien, Berlin, 4–9 März 2005 / Humboldt-Universität zu Berlin, Technische Universität Berlin, P. 80.

Putyrskaya, V., Klemt, E., Zibold, G., 2004. Cs-137 in sediments of Lago Maggiore: Measurements and Modeling // Verhandlungen der 68th Deutschen Physikalischen Gesellschaft (DPG), Simposien, München, 22–26 März 2004.– Vol. 39. – P. 180.

Klemt, E., Putyrskaya V., Paliachenka, H., Zibold, G., Astner, M., Röllin, St., 2004. Radiocäsium im Lago Maggiore. Umweltradioaktivität und Strahlendosen in der Schweiz 2003. Bundesamt für Gesundheit, B.441–B.445.

APPENDIX A:

Activity concentration of radionuclides in the sediments of Lago Maggiore

Activity concentrations (decay-corrected to the date of sampling) of different radionuclides in sediment samples from different positions of Lago Maggiore evaluated with the software Genie 2000 and LabSOCS, statistical uncertainties of the spectrometric measurement and MDA (minimum detectable activity) levels are given in the following tables.

Sampling dates:
Positions 1 and 2 – 12.03.2003
Positions 3, 4 and 5 – 26.04.2004
Positions 6 and 7 – 18.04.2005

Table A.1. Activity concentrations (in Bq·kg⁻¹) of radionuclides in sediments from **Position 1 Core 1** (lake depth 110 m)

	Cs-134			*Cs-137*			*Pb-210*		
	Act.	Unc.	MDA	Act.	Unc.	MDA	Act.	Unc.	MDA
0-1	1.09	0.24	1.85	71.48	1.34	2.17	185.65	5.72	18.50
1-2	--	--	3.02	88.52	2.14	3.83	200.63	8.58	28.70
2-3	--	--	3.54	106.35	2.44	3.72	197.11	8.81	29.10
3-4	--	--	2.92	77.71	1.98	3.70	157.24	7.76	27.83
4-5	--	--	2.92	38.48	1.41	3.35	79.42	6.36	25.90
5-6	--	--	2.22	42.05	1.36	2.95	80.52	5.84	23.10
6-7	--	--	2.34	37.50	1.24	2.81	88.16	5.64	23.50
7-8	--	--	2.61	44.27	1.40	2.77	79.77	5.85	22.90
8-9	--	--	2.77	102.99	2.18	3.39	116.51	6.77	26.20
9-10	--	--	2.16	131.35	2.48	3.23	118.52	6.95	26.80
10-11	--	--	2.91	196.35	3.46	4.25	184.22	9.35	33.90
11-12	--	--	2.51	135.03	2.38	3.10	97.61	6.22	25.30
12-13	--	--	2.60	161.86	2.72	3.17	120.28	6.71	25.10
13-14	--	--	2.77	173.64	2.88	3.21	127.54	7.18	27.50
14-15	--	--	2.54	154.56	2.53	2.91	120.70	6.45	24.80
15-16	--	--	2.12	133.51	2.32	3.06	101.33	6.01	24.00
16-17	--	--	2.16	122.14	2.24	3.40	109.83	6.46	25.90
17-18	--	--	2.98	144.28	2.69	3.65	113.99	7.19	29.50
18-19	--	--	2.63	265.14	3.54	3.13	94.12	6.27	25.20
19-20	1.39	0.35	3.04	161.83	2.76	3.39	77.24	6.04	25.40
20-21	--	--	2.18	130.57	2.06	2.61	79.84	5.05	21.00
21-22	--	--	2.83	133.04	2.48	3.43	74.84	6.11	226.30
22-23	--	--	2.61	194.89	3.01	3.24	93.41	6.36	24.00
23-24	2.08	0.43	3.66	607.17	6.56	3.97	133.68	8.13	30.80
24-25	--	--	3.60	654.86	6.88	5.40	137.28	8.30	33.40
25-26	--	--	3.12	166.92	2.90	3.43	111.24	6.88	26.90
26-27	--	--	3.11	42.99	1.52	3.42	116.47	7.23	25.40
27-28	--	--	3.11	20.88	1.13	3.82	132.15	7.63	28.50
28-29	--	--	3.07	10.05	0.87	3.38	107.54	6.82	25.30
29-30	--	--	2.56	8.75	0.70	2.81	99.13	6.03	21.40
30-31	--	--	2.12	6.88	0.66	2.82	91.68	5.94	23.60

31-32	--	--	2.39	8.26	0.70	2.99	86.65	5.97	24.80
32-33	--	--	2.52	7.71	0.67	2.69	84.29	5.86	24.20
33-34	--	--	2.74	8.75	0.74	3.05	93.04	6.60	27.10
34-35	--	--	2.41	8.13	0.64	2.46	93.56	5.88	23.60
35-36	--	--	2.83	6.09	0.57	3.31	78.67	6.33	26.60
36-37	--	--	2.17	4.40	0.68	3.47	72.38	6.35	28.10
37-38	--	--	2.58	9.12	0.74	3.01	86.36	6.05	25.80
38-39	--	--	2.59	12.52	0.83	3.06	98.42	6.31	24.80
39-40	--	--	3.42	12.53	0.98	3.97	104.80	7.83	30.70
40-41	--	--	3.18	8.36	8.32	3.56	113.48	7.33	29.70
41-42	--	--	2.81	2.72	0.60	3.78	78.49	6.31	26.80
42-43	--	--	2.66	4.73	0.57	2.73	74.90	5.72	21.80
43-44	--	--	2.65	5.49	0.65	3.15	86.91	6.01	24.90
44-45	--	--	2.54	7.95	0.72	3.01	116.44	5.93	23.10
45-46	--	--	3.43	15.34	1.04	3.89	134.00	8.09	31.20
46-47	--	--	3.45	9.34	0.97	3.84	89.72	7.33	30.40
47-48	--	--	3.52	12.49	0.94	3.46	75.33	7.06	31.30
48-49	--	--	3.54	15.27	1.08	4.13	92.82	7.66	30.60
49-50	--	--	2.46	17.97	0.94	2.89	118.52	6.37	23.20
50-51	--	--	2.57	19.39	1.05	3.22	129.50	6.90	25.90
51-53	--	--	3.05	22.71	1.17	3.46	124.74	7.59	29.80

	Pb-214			*Bi-214*			*Am-241*		
	Act.	**Unc.**	**MDA**	**Act.**	**Unc.**	**MDA**	**Act.**	**Unc.**	**MDA**
0-1	41.08	1.20	4.58	29.37	1.44	5.27	--	--	2.03
1-2	42.33	1.84	7.45	36.09	2.27	8.53	--	--	2.89
2-3	37.03	1.94	8.17	26.53	2.34	9.43	--	--	3.05
3-4	50.90	1.87	7.18	38.32	2.25	8.09	--	--	2.79
4-5	39.20	1.76	7.03	31.35	2.21	8.54	--	--	2.96
5-6	41.72	1.57	5.98	33.90	1.92	7.13	--	--	2.50
6-7	40.06	1.48	5.75	34.49	1.83	6.81	--	--	2.53
7-8	31.43	1.53	6.58	26.95	1.83	7.04	--	--	2.55
8-9	35.66	1.64	6.58	29.12	2.04	8.07	--	--	2.85
9-10	33.70	1.67	7.11	2.97	0.56	7.84	--	--	2.63
10-11	43.13	2.11	9.08	33.07	2.55	10.00	--	--	3.58
11-12	49.28	1.64	6.49	41.74	0.53	7.03	--	--	2.74

12-13	43.91	1.68	6.51	35.66	2.05	7.56	--	--	2.56
13-14	49.75	1.80	6.93	44.62	2.25	7.76	--	--	2.90
14-15	52.10	1.65	6.02	45.76	2.03	7.13	--	--	2.50
15-16	51.71	1.63	6.19	40.23	1.95	6.90	--	--	2.46
16-17	58.61	1.76	6.58	46.93	2.16	7.56	--	--	2.40
17-18	46.43	1.84	7.12	31.27	2.18	8.18	--	--	3.13
18-19	43.33	1.66	6.58	36.10	2.00	7.26	--	--	2.52
19-20	28.80	1.62	6.96	18.75	1.93	7.98	--	--	2.78
20-21	34.76	1.34	5.45	30.32	1.63	6.17	--	--	2.10
21-22	40.24	1.67	6.74	30.94	1.91	7.90	--	--	2.76
22-23	41.90	1.67	6.57	33.27	2.02	7.20	--	--	2.78
23-24	35.60	1.95	8.43	27.81	2.34	9.47	--	--	3.03
24-25	38.44	1.98	8.56	26.64	2.26	9.42	--	--	3.34
25-26	25.81	1.65	7.24	18.35	2.00	8.34	--	--	2.77
26-27	32.77	1.79	7.51	27.13	2.21	8.41	--	--	2.77
27-28	47.76	1.97	7.55	35.33	2.40	9.04	--	--	3.14
28-29	36.36	1.73	6.72	27.66	2.10	8.08	--	--	2.82
29-30	51.42	1.64	5.91	41.21	1.98	6.94	--	--	2.60
30-31	39.31	1.56	5.88	31.30	1.90	7.14	--	--	2.53
31-32	49.18	1.63	5.97	39.49	1.98	6.91	--	--	2.72
32-33	51.69	1.63	5.89	43.30	2.00	6.98	--	--	2.54
33-34	42.17	1.72	6.52	34.50	2.11	7.63	--	--	2.98
34-35	57.78	1.68	6.06	48.37	2.02	6.85	--	--	2.41
35-36	36.15	1.71	6.84	30.60	1.86	8.16	--	--	2.85
36-37	40.22	1.74	7.00	41.16	0.61	8.04	--	--	3.00
37-38	35.76	1.58	6.46	34.15	2.01	7.35	--	--	2.71
38-39	41.90	1.62	6.25	37.63	1.13	7.50	--	--	2.46
39-40	46.36	2.10	8.56	36.18	2.60	9.82	--	--	3.10
40-41	55.68	2.07	7.89	46.77	2.52	9.35	--	--	2.99
41-42	39.85	1.71	6.77	32.73	2.09	7.83	--	--	2.76
42-43	45.91	1.64	6.18	31.93	1.96	7.24	--	--	2.59
43-44	45.57	1.68	6.45	34.32	2.03	7.44	--	--	2.51
44-45	48.76	1.58	6.03	38.39	1.93	7.15	--	--	2.23
45-46	58.29	2.18	8.20	43.20	2.65	9.92	--	--	3.44
46-47	46.94	2.08	8.42	39.64	2.55	9.51	--	--	3.39
47-48	39.68	2.00	8.28	33.09	2.51	9.65	--	--	3.30

48-49	48.83	2.12	8.42	35.05	2.60	10.00	--	--	3.15
49-50	60.58	1.70	6.02	50.76	2.06	6.76	--	--	2.76
50-51	68.31	1.86	6.31	54.38	6.05	7.29	--	--	2.67
51-53	71.98	2.15	7.59	63.07	2.60	8.72	--	--	3.16

Table A.2. Activity concentrations (in Bq·kg⁻¹) of radionuclides in sediments from **Position 1 Core 4** (lake depth 96 m)

	Cs-134			*Cs-137*		
	Act.	**Unc.**	**MDA**	**Act.**	**Unc.**	**MDA**
0-1	--	--	2.92	72.41	2.59	3.20
1-2	--	--	3.52	80.12	2.95	3.83
2-3	--	--	3.88	98.68	3.02	3.79
3-4	--	--	2.46	43.90	1.66	3.02
4-5	--	--	2.47	33.12	1.41	2.81
5-6	--	--	2.21	37.07	1.47	2.63
6-7	--	--	2.60	60.51	2.20	3.08
7-8	--	--	3.27	128.73	3.87	3.59
8-9	--	--	3.77	167.08	4.94	4.15
9-10	--	--	2.63	129.94	3.77	3.04
10-11	--	--	2.95	166.12	4.73	3.25
11-12	--	--	2.33	94.50	2.94	2.39
12-13	--	--	2.79	145.18	3.90	2.70
13-14	--	--	2.94	166.07	4.98	2.87
14-15	--	--	2.67	163.11	4.55	2.64
15-16	--	--	2.42	116.85	3.48	2.47
16-17	--	--	4.35	713.10	18.06	3.88
17-18	--	--	3.13	220.86	5.79	3.62
18-19	--	--	3.61	77.57	2.87	4.06
19-20	--	--	2.33	16.65	0.89	3.60
20-21	--	--	2.49	6.14	0.71	2.75
21-22	--	--	2.14	4.50	0.52	2.48
22-23	--	--	2.41	5.65	0.60	2.62
23-24	--	--	3.87	10.59	0.86	3.09
24-25	--	--	2.62	7.10	0.69	2.73
25-26	--	--	2.62	5.98	0.64	2.75
26-27	--	--	3.07	6.97	0.73	4.21
27-28	--	--	2.82	4.96	0.59	2.60
28-29	--	--	2.04	5.00	0.50	2.29
29-30	--	--	2.62	6.68	0.68	2.86
30-31	--	--	2.99	10.07	0.83	3.02

31-32	--	--	3.53	11.63	1.01	4.14
32-33	--	--	3.06	6.31	0.72	3.32
33-34	--	--	2.39	2.49	0.49	2.68
34-35	--	--	2.44	2.63	0.50	2.63
35-36	--	--	2.65	5.04	0.65	3.12
36-37	--	--	3.30	13.50	0.99	3.39
37-38	--	--	3.14	10.83	0.89	3.45
38-39	--	--	3.03	10.30	0.88	3.36
39-40	--	--	3.09	13.59	1.02	3.42
40-41	--	--	3.27	14.58	1.03	3.59
41-44	--	--	1.60	20.18	1.08	1.86
44-47	--	--	1.68	20.49	1.28	1.83
47-50	--	--	1.71	20.83	1.29	1.81
50-53	--	--	1.74	21.65	1.35	2.01

Table A.3. Activity concentrations (in Bq·kg⁻¹) of radionuclides in sediments from **Position 2 Core 1** (lake depth 285 m)

	Cs-134			*Cs-137*			*Pb-210*		
	Act.	Unc.	MDA	Act.	Unc.	MDA	Act.	Unc.	MDA
0-1	--	--	2.82	121.98	2.38	3.31	528.22	11.90	27.30
1-2	--	--	3.38	178.16	3.17	3.76	518.86	13.00	3.18
2-3	--	--	2.91	240.14	3.41	3.27	411.40	10.74	29.10
3-4	--	--	3.81	317.60	4.56	6.34	311.70	10.65	4.43
4-5	2.34	0.48	3.94	458.01	5.23	4.09	328.82	1027	3.15
5-6	--	--	3.65	1297.27	10.90	4.04	290.45	10.15	34.40
6-7	--	---	4.91	1748.91	14.44	4.85	283.34	11.27	39.90
7-8	--	--	4.38	535.06	6.54	4.82	354.23	12.45	38.30
8-9	--	--	3.37	71.90	1.92	4.50	239.30	8.82	40.60
9-10	--	--	3.18	39.46	1.45	3.46	229.68	8.88	28.70
10-11	--	--	3.37	30.33	1.35	4.53	201.15	8.76	28.00
11-12	--	--	2.96	39.49	1.43	3.47	183.88	8.30	27.60
12-13	--	--	2.68	29.85	1.17	3.20	164.57	7.20	25.10
13-14	--	--	2.51	16.27	0.81	3.18	103.24	5.51	21.40
14-18	--	--	3.81	21.91	1.15	3.95	126.61	7.19	28.80
18-22	--	--	4.32	28.31	1.41	4.38	148.74	8.81	34.00
22-26	--	--	3.63	29.35	1.27	3.80	130.35	7.43	29.30
26-30	--	--	4.03	29.14	1.53	4.61	111.71	8.30	34.60
30-31	--	--	2.71	24.10	1.01	2.88	105.42	5.78	22.30
31-32	--	--	3.00	17.75	0.96	3.26	93.31	6.29	25.50
32-33	--	--	3.28	38.26	1.29	3.23	147.88	7.00	26.50
33-34	--	--	3.31	42.63	1.51	3.47	213.02	8.60	2.81
34-35	--	--	3.95	79.54	2.23	4.51	256.88	10.21	32.00
35-36	--	--	3.06	77.87	1.95	3.21	152.56	7.54	26.50
36-37	--	--	2.66	68.63	1.47	2.80	139.59	5.97	23.20
37-38	--	--	3.25	113.87	2.32	3.42	162.26	7.56	24.90
38-39	--	--	3.20	90.50	2.11	3.48	176.67	7.98	26.20
39-40	--	--	4.48	13.93	1.15	4.94	116.97	8.68	34.40
40-41	--	--	2.96	4.19	0.58	2.95	159.99	7.13	24.40
41-42	--	--	4.56	--	--	4.32	157.67	9.30	35.30
42-43	--	--	4.16	--	--	3.60	115.04	8.31	34.20

43-44	--	--	3.36	--	--	3.23	99.75	6.96	25.60
44-45	--	--	3.51	--	--	3.23	99.80	6.91	27.10
45-46	--	--	3.45	--	--	2.89	81.58	6.61	27.50
46-47	--	--	3.83	--	--	3.53	107.62	7.83	31.30
47-48	--	--	4.44	--	--	3.79	124.92	8.42	32.30
48-49	--	--	3.87	--	--	4.44	112.39	7.13	40.90
49-50	--	--	3.76	--	--	3.04	98.81	7.27	29.30
50-51	--	--	3.19	--	--	3.02	108.10	6.62	25.30
51-52	--	--	3.77	--	--	3.72	101.48	7.23	28.70
52-53	--	--	3.62	--	--	3.28	105.50	7.11	26.50
53-54	--	--	3.48	--	--	3.19	101.30	6.89	26.80
54-55	--	--	3.46	--	--	3.06	94.30	6.47	28.50
55-56	--	--	3.40	--	--	3.10	79.92	6.00	25.20
56-57	--	--	4.57	--	--	4.05	77.69	8.08	35.00
57-58	--	--	3.34	--	--	2.84	68.01	5.62	24.70
58-59	--	--	3.56	--	--	2.96	80.77	6.25	25.40
59-60	--	--	3.17	--	--	3.14	95.81	6.92	28.10
60-61	--	--	3.15	--	--	3.04	101.55	6.76	26.30
61-62	--	--	3.62	--	--	3.31	80.12	6.75	25.70
62-63	--	--	3.48	--	--	2.95	94.67	6.75	25.90
63-64	--	--	3.80	--	--	3.15	92.84	7.05	27.90
64-65	--	--	3.40	--	---	2.98	92.33	6.54	24.50

	Pb-214			*Bi-214*			*Am-241*		
	Act.	**Unc.**	**MDA**	**Act.**	**Unc.**	**MDA**	**Act.**	**Unc.**	**MDA**
0-1	68.89	1.95	7.06	66.39	2.57	7.77	--	--	2.78
1-2	65.61	2.17	8.23	48.35	2.76	9.38	--	--	3.37
2-3	80.24	2.07	7.26	73.02	2.69	8.12	--	--	2.74
3-4	54.34	2.22	11.80	37.55	2.62	10.00	--	--	3.15
4-5	63.24	2.11	8.33	51.30	2.67	9.46	--	--	3.02
5-6	58.37	2.05	8.64	51.86	2.70	8.61	--	--	3.56
6-7	44.16	2.35	1.13	34.51	2.82	10.80	--	--	3.95
7-8	40.94	2.36	10.50	33.60	2.97	11.20	--	--	3.99
8-9	65.11	2.04	9.52	55.20	2.86	8.88	--	--	2.91
9-10	81.18	2.17	7.39	62.82	2.74	8.52	--	--	3.09
10-11	62.33	2.08	7.81	51.19	2.65	8.76	--	--	2.93

11-12	80.91	2.14	7.17	61.11	2.66	8.26	--	--	2.67
12-13	90.99	1.99	6.16	69.30	1.18	7.26	--	--	2.74
13-14	52.18	1.51	5.78	44.92	1.98	6.73	--	--	2.21
14-18	73.61	2.18	7.88	64.29	2.84	9.32	--	--	2.91
18-22	67.45	2.39	10.70	54.78	2.98	10.70	--	--	3.37
22-26	78.38	2.19	7.91	70.79	1.42	9.64	--	--	3.19
26-30	51.59	2.29	9.14	50.26	3.08	10.50	--	--	3.29
30-31	48.97	1.59	6.01	42.84	2.08	6.97	--	--	2.39
31-32	39.89	2.16	6.71	39.89	2.15	7.72	--	--	2.58
32-33	54.51	1.82	7.11	39.21	2.31	8.39	--	--	2.55
33-34	46.12	1.87	7.19	44.79	2.35	8.40	--	--	2.90
34-35	57.32	2.30	8.91	51.24	3.04	10.70	--	--	3.14
35-36	55.21	1.84	6.74	46.99	0.55	7.60	--	--	2.70
36-37	62.82	1.64	6.02	55.93	0.70	6.93	--	--	2.38
37-38	72.24	2.00	7.04	66.58	1.77	7.98	--	--	2.52
38-39	52.84	1.86	6.99	49.70	2.46	7.89	3.54	0.54	2.86
39-40	77.57	2.51	8.99	76.11	3.18	10.90	--	--	3.76
40-41	76.25	1.82	5.60	68.68	2.21	7.05	--	--	2.59
41-42	102.84	2.72	9.01	130.36	3.72	10.30	--	--	4.02
42-43	59.28	2.20	8.01	60.07	2.74	9.98	--	--	3.25
43-44	58.46	1.93	7.12	52.34	6.71	8.31	--	--	2.70
44-45	51.28	1.87	6.99	46.69	2.25	8.52	--	--	2.73
45-46	43.86	1.73	6.62	45.85	2.15	7.95	--	--	2.93
46-47	59.54	2.16	7.93	56.03	2.60	9.46	--	--	3.19
47-48	63.90	2.25	8.51	57.29	2.71	9.93	--	--	3.19
48-49	72.50	2.15	9.69	56.39	2.54	15.40	--	--	3.19
49-50	73.72	2.05	6.81	64.84	2.50	8.61	--	--	2.98
50-51	74.61	1.92	6.25	65.99	2.32	7.55	--	--	3.02
51-52	60.65	2.03	7.15	--	--	13.70	--	--	2.84
52-53	67.89	2.04	7.06	--	--	13.80	--	--	2.70
53-54	60.73	1.93	6.87	--	--	13.20	--	--	2.55
54-55	67.56	1.97	6.92	--	--	13.30	--	--	2.72
55-56	70.03	1.97	6.95	--	--	13.70	--	--	2.63
56-57	55.40	2.23	8.87	48.61	1.08	10.70	--	--	3.27
57-58	37.15	1.66	6.84	--	--	11.60	--	--	2.62
58-59	53.40	1.84	6.69	--	--	12.60	--	--	2.80

59-60	49.19	1.94	7.42	43.19	2.49	8.50	--	--	3.04
60-61	50.24	1.91	7.45	38.07	2.40	8.61	--	--	3.11
61-62	61.63	1.97	6.77	--	--	13.10	--	--	2.74
62-63	58.31	1.83	6.58	--	--	11.90	--	--	2.74
63-64	49.77	1.89	7.39	--	--	12.40	--	--	2.80
64-65	62.69	1.89	6.36	--	--	12.20	--	--	2.71

Table A.4. Activity concentrations (in Bq·kg⁻¹) of radionuclides in sediments from **Position 2 Core 3** (lake depth 290 m)

	Cs-134			*Cs-137*		
	Act.	Unc.	MDA	Act.	Unc.	MDA
0-1	--	--	5.87	105.80	4.38	7.37
1-2	--	--	8.57	161.37	6.98	9.50
2-3	--	--	6.02	204.60	7.08	7.25
3-4	--	--	5.95	266.27	8.40	6.37
4-5	--	--	5.77	352.33	10.71	6.63
5-6	--	--	8.78	749.56	23.69	9.64
6-7	--	--	5.85	1454.02	43.49	6.68
7-8	--	--	10.70	1460.80	49.68	12.50
8-9	--	--	4.68	130.57	4.65	5.66
9-10	--	--	5.77	54.49	2.83	6.68
10-11	--	--	6.84	35.81	2.28	6.71
11-12	--	--	5.14	38.59	2.22	5.74
12-13	--	--	6.18	32.84	1.86	5.07
13-16	--	--	1.56	23.51	1.12	1.78
16-19	--	--	1.41	21.82	1.15	1.74
19-22	--	--	2.21	25.94	1.45	2.00
22-25	--	--	1.58	27.43	1.52	1.93
25-28	--	--	1.27	29.62	1.55	1.49
28-31	--	--	1.65	33.01	1.65	2.03
31-32	--	--	3.33	30.23	1.58	5.65
32-33	--	--	3.22	26.70	1.41	3.82
33-34	--	--	2.06	13.88	0.79	2.49
34-35	--	--	3.50	30.16	1.61	4.17
35-36	--	--	2.67	23.12	1.28	4.34
36-37	--	--	6.60	55.08	2.89	10.10
37-38	--	--	13.60	54.90	4.40	20.20
38-39	--	--	6.15	85.88	3.69	7.43
39-40	--	--	4.31	75.22	2.99	5.24
40-41	--	--	3.86	68.84	2.61	4.47
41-42	--	--	5.18	94.48	3.70	5.56
42-43	--	--	5.81	114.88	4.29	6.97

43-44	--	--	5.43	37.49	2.20	5.66
44-45	--	--	4.00	8.12	1.01	4.82
45-46	--	--	3.10	7.94	0.82	4.83
46-47	--	--	4.70	3.46	0.94	5.31
47-48	--	--	4.24	--	--	4.93
48-49	--	--	4.14	--	--	4.51
49-50	--	--	4.16	--	--	4.11
50-51	--	--	3.32	--	--	3.15
51-52	--	--	3.29	--	--	3.68
52-53	--	--	4.00	--	--	4.29
60-61	--	--	3.43	--	--	3.25
68-69	--	--	2.32	--	--	2.05

Table A.5. Activity concentrations (in Bq·kg^{-1}) of radionuclides in sediments from **Position 3 Core 3** (lake depth 160 m)

	Cs-134			*Cs-137*			*Pb-210*		
	Act.	**Unc.**	**MDA**	**Act.**	**Unc.**	**MDA**	**Act.**	**Unc.**	**MDA**
0-1	--	--	3.73	61.37	1.99	4.35	263.46	10.41	33.33
1-2	--	--	3.86	56.81	1.90	5.55	214.02	9.39	31.20
2-3	--	--	2.90	32.28	1.12	3.06	95.85	5.93	23.70
3-4	--	--	3.27	26.45	1.26	3.63	65.54	6.13	28.90
4-5	--	--	3.15	25.71	1.31	5.08	72.47	6.28	39.70
5-6	--	--	3.54	48.21	1.70	3.89	88.46	6.96	29.20
6-7	--	--	3.45	74.01	2.08	4.02	194.29	9.13	32.40
7-8	--	--	3.68	84.20	2.24	4.32	237.83	9.84	33.30
8-9	--	--	2.17	68.21	1.31	2.49	129.86	5.11	19.30
9-10	--	--	3.58	66.01	1.96	4.96	77.54	6.61	30.10
10-11	--	--	3.41	142.35	2.80	4.17	152.02	8.17	30.80
11-12	--	--	3.83	254.31	4.12	4.42	167.95	8.63	45.20
12-13	--	--	3.54	246.44	3.90	4.48	102.43	7.20	44.30
13-14	--	--	3.38	306.69	4.38	4.02	104.96	7.09	42.40
14-15	--	--	3.06	188.40	3.02	3.73	129.82	6.84	27.30
15-16	--	--	3.56	37.98	1.55	5.30	106.30	7.30	30.80
16-17	--	--	3.56	20.43	1.19	3.84	102.31	7.17	43.30
17-18	--	--	3.53	17.96	1.16	4.28	107.70	7.28	30.30
18-19	--	--	3.46	18.96	1.16	4.01	124.58	7.41	28.70
19-20	--	--	2.52	57.32	1.35	2.83	177.17	6.36	22.40
20-21	--	--	3.71	71.55	2.09	5.43	135.32	7.97	5.43
21-22	--	--	3.62	25.72	1.34	4.24	101.88	7.16	4.34
22-23	--	--	3.66	6.36	0.83	4.12	101.91	7.24	44.40
23-24	--	--	3.41	1.27	0.61	4.08	99.10	6.85	41.20
24-25	--	--	3.24	--	--	3.33	87.08	6.46	41.20
25-26	--	--	2.98	--	--	2.89	83.57	5.81	2.48
26-27	--	--	3.41	--	--	3.47	99.40	7.34	28.80
27-28	--	--	3.63	--	--	3.68	83.52	7.02	31.60
28-29	--	--	3.56	--	--	3.55	92.66	6.86	42.20
29-30	--	--	1.76	--	--	1.65	78.99	3.70	14.60
30-31	--	--	3.53	--	--	3.64	86.00	7.36	30.00

32-33	--	--	3.53	--	--	3.58	66.15	6.45	43.50
33-34	--	--	2.97	--	--	3.46	75.57	6.47	41.70
34-35	--	--	3.45	--	--	3.30	85.34	6.31	39.80
35-36	--	--	3.54	--	--	3.81	99.84	6.84	28.60
36-37	--	--	2.81	--	--	2.70	88.82	5.46	23.90

	Bi-214			*Pb-214*			*Am-241*		
	Act.	**Unc.**	**MDA**	**Act.**	**Unc.**	**MDA**	**Act.**	**Unc.**	**MDA**
0-1	28.82	2.39	9.63	40.28	1.95	8.50	--	--	3.26
1-2	24.90	2.30	9.55	34.47	1.88	8.43	--	--	4.04
2-3	29.14	1.82	7.37	44.28	1.52	6.24	--	--	2.63
3-4	33.16	2.29	8.81	37.66	1.80	7.82	--	--	2.81
4-5	13.69	2.08	9.37	24.35	1.72	8.13	--	--	2.64
5-6	24.64	2.22	8.85	31.14	1.77	8.00	--	--	2.54
6-7	39.55	2.44	9.14	45.96	1.95	8.14	--	--	3.16
7-8	43.05	2.52	9.63	51.01	2.01	8.28	--	--	3.48
8-9	36.30	1.58	5.85	49.99	1.29	5.13	--	--	2.17
9-10	35.66	1.19	9.43	38.25	1.85	7.95	--	--	2.99
10-11	34.82	2.28	8.61	42.64	1.86	8.06	--	--	2.93
11-12	32.81	2.46	9.88	41.35	2.02	8.86	--	--	3.62
12-13	20.41	2.22	9.50	35.82	1.87	8.50	--	--	3.29
13-14	33.47	2.24	9.17	33.47	1.85	7.93	--	--	3.22
14-15	30.90	2.08	8.11	41.83	1.71	6.99	--	--	2.90
15-16	34.86	2.44	9.41	38.08	2.44	8.12	--	--	3.24
16-17	30.63	2.32	9.22	37.13	1.85	8.08	--	--	2.99
17-18	28.93	2.37	9.50	45.51	1.97	7.85	--	--	3.10
18-19	28.00	2.34	9.50	40.37	1.89	7.76	--	--	3.04
19-20	44.95	1.85	6.82	52.61	1.49	5.72	--	--	2.53
20-21	39.17	2.50	9.45	52.60	2.05	8.41	--	--	3.29
21-22	38.32	2.51	9.80	50.06	2.01	8.25	--	--	3.07
22-23	42.50	1.27	9.52	51.70	2.01	8.07	--	--	3.57
23-24	37.42	2.39	9.10	50.17	1.95	7.64	--	--	3.39
24-25	39.18	2.29	8.81	47.12	1.83	7.54	--	--	4.65
25-26	52.97	2.13	7.28	60.03	1.70	6.75	--	--	2.50
26-27	66.67	2.77	9.24	73.63	2.21	8.07	--	--	3.08
27-28	43.57	2.62	9.42	54.29	2.09	7.99	--	--	3.29

28-29	37.52	24.17	9.25	47.16	1.94	7.80	--	--	3.17
29-30	36.49	1.30	4.76	46.22	1.04	4.06	--	--	1.45
30-31	55.42	2.72	9.56	62.31	2.14	7.99	--	--	3.13
32-33	50.61	2.66	9.60	58.54	2.08	7.81	--	--	3.05
33-34	58.63	2.69	9.07	57.63	2.06	7.78	--	--	2.89
34-35	41.24	2.33	8.95	51.23	1.90	7.53	--	--	3.12
35-36	46.58	2.56	9.28	53.52	2.02	8.10	--	--	3.02
36-37	48.65	2.05	7.60	60.52	1.65	6.19	--	--	2.52

Table A.6. Activity concentrations (in Bq·kg⁻¹) of radionuclides in sediments from **Position 4**
Core 2 (lake depth 150 m)

	Cs-134			*Cs-137*			*Pb-210*		
	Act.	**Unc.**	**MDA**	**Act.**	**Unc.**	**MDA**	**Act.**	**Unc.**	**MDA**
0-1	--	--	3.85	91.70	2.37	4.47	405.29	12.11	33.90
1-2	--	--	3.29	91.62	2.06	3.79	454.70	11.09	29.00
2-3	--	--	3.71	87.76	2.31	4.42	315.59	10.80	34.10
3-4	--	--	4.83	150.04	3.32	4.89	493.30	14.51	38.50
4-5	--	--	3.48	174.79	3.22	4.10	335.41	11.15	31.90
5-6	1.34	0.31	2.28	256.83	2.90	2.81	334.41	1.81	21.80
6-7	1.10	0.38	3.31	605.95	5.88	3.68	430.84	10.50	30.70
7-8	2.34	0.57	4.48	1030.25	10.09	5.45	263.44	11.64	41.90
8-9	2.40	0.68	5.47	705.85	8.45	6.07	365.35	14.41	44.70
9-10	--	--	4.38	168.58	3.40	4.68	309.14	11.42	34.50
10-11	--	--	3.74	76.74	2.15	4.03	226.58	9.35	31.20
11-12	--	--	3.99	55.99	1.86	4.15	202.67	9.21	31.80
12-13	--	--	3.82	53.06	1.85	4.11	192.36	9.37	32.90
13-14	--	--	3.73	66.50	2.01	4.29	221.61	9.75	32.70
14-15	--	--	6.29	100.60	3.35	6.93	365.81	16.24	52.60
15-16	--	--	5.63	122.99	3.36	6.25	308.79	13.81	45.60
16-17	--	--	4.00	142.04	2.99	4.51	271.45	10.44	32.90
17-18	--	--	4.20	173.81	3.31	4.67	229.04	9.74	32.10
18-19	--	--	4.05	110.97	2.59	4.46	246.19	9.99	33.30
19-20	--	--	2.67	66.04	1.45	2.80	222.38	6.86	22.60
20-21	--	--	3.67	26.22	1.36	4.31	180.56	8.80	31.40
21-22	--	--	3.88	14.97	1.09	4.31	181.98	9.02	32.20
22-23	--	--	3.61	12.83	1.00	3.96	177.87	8.93	32.90
23-24	--	--	4.97	8.68	1.08	5.20	150.30	9.43	37.60
24-25	--	--	2.23	5.32	0.48	2.39	132.88	5.14	18.50
25-26	--	--	2.79	4.28	0.55	2.80	115.40	5.65	20.70
26-27	--	--	1.92	1.83	0.32	1.87	101.30	3.96	16.30
27-28	--	--	2.15	1.75	0.37	1.99	94.13	4.37	17.70
28-29	--	--	1.69	1.53	0.28	1.64	96.54	3.57	14.20
29-30	--	--	2.25	1.03	0.35	2.03	132.13	4.80	18.10
30-31	--	--	4.98	1.26	0.33	4.08	103.59	3.97	1.62

31-32	--	--	1.95	--	--	1.71	99.70	3.87	15.50
32-33	--	--	2.46	--	--	2.11	83.86	4.54	19.30
33-34	--	--	2.16	--	--	1.98	88.05	4.11	16.90
34-35	--	--	1.89	--	--	1.65	79.94	3.53	14.00
35-36	--	--	2.63	--	--	2.30	88.52	4.94	20.40
36-37	--	--	2.37	--	--	1.99	88.11	4.31	17.80
37-38	--	--	2.49	--	--	2.28	71.55	4.16	18.80
38-39	--	--	2.70	--	--	2.26	83.41	4.94	21.10
39-40	--	--	2.54	--	--	2.11	85.21	4.60	18.60
40-41	--	--	2.61	--	--	2.24	85.11	4.76	19.50
41-42	--	--	2.12	--	--	1.87	103.54	4.33	15.90
42-43	--	--	2.39	--	--	2.02	90.85	4.59	18.30
43-44	--	--	2.34	--	--	2.02	78.76	4.47	18.20
44-45	--	--	2.61	--	--	2.26	81.56	4.92	19.00

	Bi-214			*Pb-214*			*Am-241*		
	Act.	**Unc.**	**MDA**	**Act.**	**Unc.**	**MDA**	**Act.**	**Unc.**	**MDA**
0-1	49.30	2.60	9.49	60.43	2.15	8.34	--	--	3.23
1-2	50.31	2.32	8.37	64.94	1.88	6.82	--	--	2.76
2-3	55.02	2.71	9.58	60.27	2.14	8.40	--	--	3.26
3-4	46.49	3.07	12.00	61.84	2.49	9.97	--	--	3.55
4-5	25.17	2.29	9.55	38.64	1.90	8.05	--	--	3.02
5-6	49.52	1.81	6.57	63.00	1.50	5.83	--	--	2.12
6-7	39.49	1.91	8.93	52.30	1.87	8.32	--	--	3.27
7-8	40.81	2.83	11.00	40.71	2.25	10.80	--	--	4.20
8-9	34.93	3.21	13.50	49.93	2.63	12.10	--	--	5.13
9-10	50.68	2.88	11.10	67.25	2.41	9.47	--	--	3.60
10-11	64.27	2.80	9.34	72.68	2.25	8.16	--	--	3.09
11-12	54.44	2.64	9.02	59.92	2.10	8.25	--	--	3.13
12-13	55.21	2.72	9.43	68.47	2.29	8.40	--	--	3.18
13-14	69.98	2.87	9.56	77.52	2.28	8.09	--	--	3.23
14-15	39.53	3.98	16.00	42.25	3.07	14.20	--	--	7.10
15-16	44.89	3.60	14.30	43.28	2.79	12.80	--	--	4.52
16-17	24.65	2.34	10.00	37.94	1.94	8.61	--	--	3.49
17-18	51.10	2.72	10.00	58.01	2.14	8.52	6.80	0.70	3.56
18-19	58.51	2.73	9.79	64.33	2.18	8.33	2.77	0.62	3.73

19-20	45.00	1.84	6.78	53.62	1.48	5.54	2.65	0.43	2.46
20-21	52.88	2.67	9.85	67.44	2.16	8.26	--	--	4.10
21-22	63.46	2.80	9.60	71.78	2.23	7.97	--	--	3.33
22-23	45.61	2.53	9.21	54.67	2.05	8.14	--	--	3.15
23-24	49.79	3.15	11.50	62.44	2.54	10.20	--	--	4.09
24-25	44.78	0.86	5.87	47.24	1.26	4.86	--	--	1.99
25-26	43.02	1.89	7.01	54.52	1.53	5.71	--	--	2.02
26-27	41.41	1.17	4.86	53.51	1.10	4.12	--	--	2.15
27-28	53.35	1.58	5.47	66.75	1.30	4.57	--	--	2.22
28-29	61.85	1.35	4.50	69.09	1.07	3.70	--	--	1.31
29-30	45.34	1.55	5.48	56.74	1.25	4.63	--	--	1.72
30-31	39.38	1.35	4.98	49.89	1.08	4.08	--	--	1.62
31-32	49.96	1.37	4.85	60.61	1.10	3.98	--	--	1.62
32-33	54.94	1.69	5.92	65.01	1.36	4.87	--	--	2.09
33-34	42.43	0.72	5.28	51.72	1.16	4.51	--	--	1.65
34-35	46.40	1.30	4.64	55.84	1.03	3.91	--	--	1.59
35-36	61.65	1.87	6.39	68.77	1.52	5.41	--	--	2.10
36-37	31.07	1.43	5.65	41.16	1.15	4.64	--	--	1.70
37-38	36.93	1.54	6.09	44.12	1.25	4.95	--	--	2.04
38-39	52.27	1.73	6.23	57.08	1.41	5.18	--	--	1.97
39-40	51.36	1.69	5.91	56.99	1.33	4.97	--	--	1.99
40-41	65.05	1.77	5.91	69.71	1.40	4.99	--	--	1.91
41-42	52.17	1.48	5.15	65.26	1.21	4.21	--	--	1.61
42-43	40.94	1.54	5.58	54.09	1.27	4.72	--	--	1.77
43-44	40.05	1.51	5.57	49.46	1.22	4.61	--	--	1.91
44-45	53.35	1.70	6.19	54.03	1.38	5.05	--	--	1.96

Table A.7. Activity concentrations (in Bq·kg⁻¹) of radionuclides in sediments from **Position 5 Core 3** (lake depth 40 m)

	Cs-134			*Cs-137*			*Pb-210*		
	Act.	Unc.	MDA	Act.	Unc.	MDA	Act.	Unc.	MDA
0-1	--	--	3.51	93.71	2.37	4.21	364.73	11.60	33.40
1-2	--	--	4.59	114.41	3.01	5.59	508.41	15.39	41.60
2-3	--	--	6.07	153.75	4.02	7.09	649.29	20.30	56.70
3-4	--	--	5.03	207.06	4.49	7.15	731.17	20.28	53.00
4-5	--	--	3.67	182.24	3.31	4.22	337.11	11.18	31.00
5-6	--	--	3.88	315.52	4.52	4.56	361.56	11.79	36.51
6-7	--	--	6.11	507.57	7.25	7.41	550.18	18.83	57.41
7-8	--	--	6.74	710.33	9.63	8.14	534.67	20.11	58.92
8-9	--	--	4.07	1069.76	10.30	4.94	399.90	13.40	42.70
9-10	--	--	8.02	1569.57	16.33	8.85	439.05	20.30	69.30
10-11	--	--	3.51	93.71	2.37	4.21	364.74	11.60	33.45
11-12	--	--	6.57	430.57	7.38	7.77	580.70	21.06	61.53
12-13	--	--	4.62	166.80	3.57	5.93	411.97	14.44	46.30
13-14	--	--	3.67	89.50	2.38	4.53	270.44	10.76	35.07
14-15	--	--	4.57	65.67	2.43	5.56	256.89	12.62	42.00
15-16	--	--	3.84	49.61	1.80	4.17	218.83	9.81	33.43
16-17	--	--	2.41	47.08	1.37	3.04	171.36	6.95	23.66
17-18	--	--	3.28	55.31	1.73	3.73	238.01	9.36	30.33
18-19	--	--	7.05	76.51	3.40	8.70	492.91	21.26	69.01
19-20	--	--	7.29	69.56	3.01	8.04	446.42	19.56	66.15
20-21	--	--	9.30	75.75	3.71	14.60	383.40	22.22	126.17
21-22	--	--	7.01	104.07	3.73	8.40	330.11	18.00	61.64
22-23	--	--	5.04	135.43	3.58	6.09	337.53	14.40	45.20
23-24	--	--	5.55	191.03	4.26	6.55	361.52	15.24	50.40
24-25	--	--	3.69	103.09	2.50	6.57	263.04	10.34	34.40
25-26	--	--	3.81	62.55	2.10	4.65	262.50	11.04	34.32
26-27	--	--	3.96	27.54	1.49	4.65	240.27	10.79	36.61
27-28	--	--	3.22	16.00	1.09	4.12	215.43	9.45	32.73
28-29	--	--	3.53	13.50	1.01	3.81	240.49	9.82	32.94
29-30	--	--	3.43	5.91	0.84	4.11	230.64	9.83	32.03
30-31	--	--	3.09	4.36	0.78	4.11	237.21	9.94	33.92

31-32	--	--	2.50	2.87	0.56	3.14	217.47	7.50	25.60
32-33	--	--	3.54	2.44	0.71	4.16	189.93	9.17	33.50
33-34	--	--	3.39	--	--	3.54	187.30	8.70	32.21
34-35	--	--	3.18	--	--	3.60	193.94	8.84	31.40
35-36	--	--	3.57	--	--	3.83	183.20	9.24	33.20
36-37	--	--	2.77	--	--	3.01	198.20	7.45	26.40
37-38	--	--	3.54	--	--	3.63	175.36	8.97	32.45
38-39	--	--	3.61	--	--	3.70	181.29	8.94	33.10
39-40	--	--	3.65	--	--	3.57	186.46	9.20	34.13
40-41	--	--	3.77	--	--	3.75	202.39	9.48	34.81
41-42	--	--	3.68	--	--	3.75	143.45	8.80	33.90
42-43	--	--	3.68	--	--	3.72	188.42	9.01	32.50
43-44	--	--	3.50	--	--	3.84	192.19	9.30	34.54
44-45	--	--	3.77	--	--	3.77	161.34	9.12	34.70

	Pb-214			*Bi-214*			*Am-241*		
	Act.	**Unc.**	**MDA**	**Act.**	**Unc.**	**MDA**	**Act.**	**Unc.**	**MDA**
0-1	58.59	2.09	7.82	47.90	3.06	11.00	--	--	3.41
1-2	22.17	2.17	10.70	12.52	2.85	12.72	--	--	4.28
2-3	46.52	3.24	15.00	20.13	3.92	17.81	--	--	6.18
3-4	47.54	3.02	14.20	35.73	3.87	16.20	--	--	5.15
4-5	44.78	1.98	8.47	31.56	2.36	9.73	--	--	3.33
5-6	56.69	2.25	9.43	49.61	2.79	10.51	--	--	3.81
6-7	23.40	3.03	20.10	6.12	3.84	17.73	--	--	5.30
7-8	46.99	3.51	21.80	11.72	4.14	19.90	--	--	6.87
8-9	54.06	2.41	10.80	31.83	2.72	11.60	--	--	4.02
9-10	45.65	3.77	25.50	28.51	3.33	20.90	--	--	7.65
10-11	58.59	2.09	7.82	47.90	3.06	11.00	--	--	3.41
11-12	4.92	5.20	22.20	--	--	19.80	--	--	5.79
12-13	51.63	2.69	15.50	29.11	3.26	13.92	--	--	4.90
13-14	70.20	2.35	9.22	50.00	1.54	10.90	--	--	3.60
14-15	43.25	2.55	11.20	31.92	3.15	12.67	--	--	4.61
15-16	35.88	1.94	8.20	22.61	2.37	10.04	--	--	3.57
16-17	77.78	1.78	5.99	65.02	2.19	7.04	--	--	2.82
17-18	60.89	2.10	8.08	47.56	2.57	9.56	--	--	3.17
18-19	51.57	3.97	17.90	37.36	4.98	21.60	--	--	6.91

19-20	11.64	3.46	17.40			21.19	--	--	5.84
20-21	12.13	3.34	28.80	13.52	1.92	28.79	--	--	4.21
21-22	15.68	3.20	17.10	3.10	0.43	20.12	--	--	6.41
22-23	10.73	2.35	12.50			14.21	--	--	4.75
23-24	24.28	2.72	13.90	20.23	2.24	15.01	9.60	1.04	7.82
24-25	43.03	2.06	8.79	27.51	2.50	10.33	4.24	0.68	5.64
25-26	50.07	2.28	9.21	34.90	2.72	10.63	3.40	0.69	4.02
26-27	32.72	2.09	9.53	20.41	2.52	10.80	--	--	3.77
27-28	52.04	1.99	10.00	44.53	2.53	9.39	--	--	3.99
28-29	79.45	2.28	7.99	65.88	2.81	9.71	--	--	3.13
29-30	83.45	2.34	8.29	61.57	2.82	9.67	--	--	3.26
30-31	89.80	2.40	8.26	70.35	1.45	9.90	--	--	3.57
31-32	92.35	1.90	6.40	72.45	2.30	7.41	--	--	2.80
32-33	103.62	2.52	8.62	81.28	3.05	9.98	--	--	3.90
33-34	89.86	2.29	7.84	74.36	2.79	9.07	--	--	3.39
34-35	87.33	2.28	7.82	62.44	2.70	9.46	--	--	3.22
35-36	55.40	2.12	7.87	45.00	2.64	9.97	--	--	3.40
36-37	80.59	1.86	6.45	61.90	2.25	7.71	--	--	2.61
37-38	109.33	2.52	8.29	85.52	3.04	9.82	--	--	3.31
38-39	99.92	2.44	8.21	73.57	2.87	9.41	--	--	3.61
39-40	111.79	2.55	8.12	81.58	3.02	9.89	--	--	3.58
40-41	95.49	2.45	8.27	77.64	2.97	9.74	--	--	3.31
41-42	92.23	2.41	8.11	76.46	2.96	9.69	--	--	3.40
42-43	111.10	2.54	8.23	85.24	1.87	9.72	--	--	3.47
43-44	97.73	2.45	8.23	74.76	2.94	9.60	--	--	3.53
44-45	146.54	2.86	8.65	109.37	3.34	10.23	--	--	3.48

Table A.8. Activity concentrations (in Bq·kg⁻¹) of radionuclides in sediments from **Position 6 Core 3** (lake depth 29 m)

	Cs-134			*Cs-137*			*Pb-210*		
	Act.	**Unc.**	**MDA**	**Act.**	**Unc.**	**MDA**	**Act.**	**Unc.**	**MDA**
0-1	--	--	6.93	124.90	3.65	12.10	798.52	24.41	83.10
1-2	--	--	4.05	193.91	2.87	5.70	970.55	16.86	49.40
2-3	--	--	8.09	226.20	5.31	14.70	812.87	27.13	98.80
3-4	--	--	8.02	288.62	5.93	10.70	791.75	26.71	99.40
4-5	--	--	4.30	214.33	3.74	5.26	440.37	14.45	49.00
5-6	--	--	5.90	337.30	4.91	7.61	568.13	18.11	66.40
6-7	--	--	6.64	274.58	4.94	8.83	564.96	20.78	84.00
7-8	--	--	8.27	154.29	4.51	11.20	439.83	23.56	98.50
8-9	--	--	8.33	136.76	4.26	14.90	478.85	2.33	97.80
9-10	--	--	7.37	166.71	4.43	10.10	468.52	22.25	87.30
10-11	--	--	7.12	165.02	4.22	9.08	440.33	20.62	83.30
11-12	--	--	5.61	185.10	3.51	7.39	480.28	17.03	62.90
12-13	--	--	6.38	187.63	4.21	8.55	445.62	19.10	72.60
13-14	--	--	6.66	168.21	4.14	8.72	388.81	19.27	81.40
14-15	--	--	6.19	120.79	3.34	7.72	322.06	17.22	72.70
15-16	--	--	5.81	93.08	2.74	7.09	329.68	15.43	63.00
16-17	--	--	5.13	47.07	1.91	6.08	226.52	13.09	56.70
17-18	--	--	2.70	--	--	4.91	252.84	8.22	32.80
18-19	--	--	2.52	18.12	0.87	3.44	211.67	7.32	29.90
19-20	--	--	4.60	1.33	1.21	5.69	151.51	11.05	45.50
20-21	--	--	4.70	8.49	1.09	5.54	182.19	11.46	47.90
21-22	--	--	4.66	6.54	1.09	5.85	141.12	10.35	46.40
22-23	--	--	4.66	5.61	1.03	5.49	127.41	10.09	47.70
23-24	--	--	4.64	1.88	0.90	5.21	104.10	9.35	43.20
24-25	--	--	4.63	2.49	0.93	5.30	82.84	9.19	45.90
25-26	--	--	4.48	2.04	0.89	5.19	140.15	10.76	49.10
26-27	--	--	4.48	0.27	0.86	4.77	99.05	9.17	43.00
27-28	--	--	3.81	2.08	0.77	4.04	86.21	8.01	39.50
28-29	--	--	3.69	1.80	0.72	4.27	8.84	8.28	36.80
29-30	--	--	4.86	--	--	4.96	8.51	10.63	46.90
30-31	--	--	4.68	--	--	4.83	83.71	10.59	49.70

	Act.	Unc.	MDA	Act.	Unc.	MDA	Act.	Unc.	MDA
31-32	--	--	4.82	--	--	5.14	88.99	10.61	49.30
32-33	--	--	4.66	--	--	5.32	92.57	10.31	47.40
33-34	--	--	4.65	--	--	4.93	57.42	10.03	47.20
34-35	--	--	4.90	--	--	5.19	9.60	10.75	51.00
35-36	--	--	4.61	--	--	5.07	90.31	10.29	5.03
36-37	--	--	4.63	--	--	7.17	61.16	10.42	50.30
37-38	--	--	4.81	--	--	5.57	87.36	9.77	68.90
38-39	--	--	4.81	--	--	5.57	87.36	9.77	68.90

	Bi-214			*Pb-214*			*Am-241*		
	Act.	**Unc.**	**MDA**	**Act.**	**Unc.**	**MDA**	**Act.**	**Unc.**	**MDA**
0-1	119.09	4.50	16.20	35.42	3.68	19.60	--	--	7.45
1-2	57.25	3.11	13.00	47.15	2.49	11.70	--	--	3.90
2-3	--	--	23.80	3.86	7.07	22.80	--	--	7.57
3-4	4.41	5.38	24.70	14.15	4.06	28.20	--	--	9.09
4-5	13.52	2.96	12.70	17.35	2.21	11.60	--	--	4.78
5-6	28.30	4.19	17.60	31.94	3.18	16.40	--	--	5.25
6-7	23.11	4.34	20.70	12.24	3.46	18.50	--	--	6.28
7-8	12.17	5.00	24.50	--	--	22.60	--	--	7.94
8-9	15.33	5.51	23.70	19.07	4.12	23.40	--	--	7.76
9-10	11.34	4.98	21.90	11.78	4.49	20.10	5.84	1.35	8.18
10-11	101.46	4.41	16.90	24.28	3.55	18.60	6.72	1.38	7.28
11-12	115.58	3.48	12.70	21.69	2.99	15.60	3.44	1.07	6.47
12-13	88.32	2.14	20.90	17.45	3.32	17.10	--	--	6.56
13-14	87.46	4.05	16.10	22.29	3.43	18.00	5.47	1.28	10.40
14-15	70.81	3.11	19.90	23.19	3.11	16.80	5.25	1.16	6.94
15-16	84.22	1.54	13.00	30.04	2.80	15.10	--	--	5.99
16-17	74.11	1.23	16.70	34.22	2.58	12.90	--	--	4.84
17-18	52.71	1.17	9.26	86.45	1.53	5.94	--	--	3.14
18-19	49.69	1.91	7.73	49.56	1.58	7.03	--	--	2.34
19-20	45.82	3.13	12.00	53.57	2.44	14.40	--	--	4.42
20-21	36.42	2.99	12.30	45.66	2.37	11.50	--	--	4.99
21-22	43.06	3.06	12.00	47.66	2.43	11.50	--	--	4.56
22-23	36.74	3.02	12.30	43.61	2.38	14.60	--	--	4.63
23-24	26.83	2.85	12.10	38.63	2.27	14.10	--	--	4.43
24-25	22.90	2.81	12.10	28.46	2.25	11.70	--	--	4.63

25-26	49.78	3.11	11.90	48.94	2.45	10.90	--	--	4.42
26-27	34.48	2.85	11.90	43.54	2.27	10.80	--	--	4.77
27-28	35.70	2.54	10.10	40.41	2.01	9.34	--	--	3.55
28-29	23.23	2.30	9.87	33.23	1.83	11.60	--	--	3.41
29-30	31.40	2.99	12.30	33.37	2.37	15.20	--	--	4.65
30-31	34.51	3.07	12.70	43.00	2.42	11.50	--	--	4.52
31-32	30.01	2.98	12.40	38.56	2.39	11.50	--	--	4.54
32-33	32.64	3.01	11.90	38.01	2.39	11.60	--	--	5.48
33-34	38.70	3.05	12.20	47.52	2.40	11.60	--	--	4.90
34-35	31.32	3.01	12.50	38.25	2.41	15.20	--	--	4.64
35-36	34.51	2.98	12.50	33.75	2.27	11.60	--	--	4.30
36-37	46.08	1.53	12.50	50.12	2.46	11.70	--	--	4.46
37-38	54.33	3.51	12.30	62.45	2.59	14.10	--	--	4.76
38-39	54.33	3.51	12.30	62.45	2.59	14.10	--	--	4.76

Table A.9. Activity concentrations (in Bq·kg⁻¹) of radionuclides in sediments from **Position 7**
     Core 2 (lake depth 370 m)

	Cs-134			*Cs-137*			*Pb-210*		
	Act.	**Unc.**	**MDA**	**Act.**	**Unc.**	**MDA**	**Act.**	**Unc.**	**MDA**
0-1	--	--	2.00	94.93	1.54	2.50	578.96	9.60	21.20
1-2	--	--	1.94	100.96	1.70	2.52	352.93	7.95	20.00
2-3	--	--	3.28	141.70	2.75	3.90	188.72	9.24	31.80
3-4	--	--	3.27	148.59	2.94	3.96	205.44	9.70	32.60
4-5	--	--	2.91	178.43	2.83	3.55	210.07	8.55	27.80
5-6	--	--	3.48	166.47	4.23	3.48	199.60	9.80	32.90
6-7	--	--	3.49	198.06	3.45	4.21	239.77	10.18	31.40
7-8	--	--	3.30	220.90	3.67	4.29	289.62	10.99	33.40
8-9	--	--	3.70	151.31	2.91	4.30	205.48	9.34	30.90
9-10	--	--	3.57	93.12	2.31	4.24	106.69	7.23	42.50
10-11	--	--	3.27	47.54	1.60	3.88	63.09	5.96	39.20
11-12	--	--	3.17	102.77	2.35	5.51	212.56	8.98	44.30
12-13	--	--	3.48	272.65	4.04	4.47	336.64	11.26	31.80
13-14	--	--	3.70	233.98	3.94	4.48	246.41	11.13	36.60
14-15	--	--	3.57	267.70	4.20	4.46	248.60	10.81	33.90
15-16	--	--	2.64	131.35	2.22	3.38	101.87	6.29	24.00
16-17	--	--	3.47	108.13	2.51	4.31	140.00	8.01	31.00
17-18	--	--	3.45	119.00	2.63	4.17	125.51	7.86	31.50
18-19	--	--	3.45	115.51	2.40	4.09	116.01	7.30	27.90
19-20	1.27	0.44	3.66	713.42	7.48	4.38	199.56	9.81	32.80
20-21	1.67	0.68	6.30	1358.90	14.04	7.23	394.14	18.43	60.00
21-22	--	--	5.46	87.45	2.90	6.10	337.84	15.23	44.90
22-23	--	--	3.61	60.76	1.96	4.51	230.64	10.46	34.20
23-24	--	--	4.99	47.11	2.15	6.04	290.23	13.42	44.40
24-25	--	--	3.20	54.28	1.81	4.40	206.18	10.01	34.20
25-26	--	--	3.22	46.78	1.59	3.79	162.65	8.42	27.40
26-27	--	--	2.73	60.14	1.60	3.41	193.34	7.89	24.70
27-28	--	--	3.11	49.00	1.68	3.76	139.86	8.32	30.00
28-29	--	--	4.95	52.28	2.27	7.57	259.04	12.63	41.80
29-30	--	--	6.61	70.73	2.97	7.67	376.24	18.14	57.10
30-31	--	--	5.13	40.15	2.03	5.93	171.88	12.27	44.30
31-32	--	--	5.78	89.81	3.22	7.10	291.81	15.76	53.00

	Bi-214			Pb-214			Am-241		
	Act.	Unc.	MDA	Act.	Unc.	MDA	Act.	Unc.	MDA
32-33	--	--	3.84	111.02	2.66	4.33	203.69	10.21	33.50
33-34	--	--	3.37	127.89	2.80	4.30	184.96	9.67	32.90
34-35	--	--	3.44	159.41	3.06	3.97	210.56	9.76	31.70
35-36	--	--	3.83	119.78	2.89	4.48	211.98	10.79	35.50
36-37	--	--	3.90	82.88	2.27	4.35	258.85	10.99	35.00
37-38	--	--	3.36	20.94	1.26	4.38	202.47	9.69	30.40
38-39	--	--	4.27	10.93	1.09	4.85	272.24	11.97	37.40
39-40	--	--	3.55	7.05	0.86	4.08	175.81	9.63	33.30
40-41	--	--	3.64	2.12	0.70	4.27	122.57	8.50	32.30
41-42	--	--	3.50	1.64	0.64	3.80	136.13	8.61	31.80
42-43	--	--	3.28	1.17	0.63	3.64	177.12	9.30	30.90
43-44	--	--	3.22	--	--	3.60	82.35	7.44	29.40
44-45	--	--	3.50	--	--	3.49	129.00	7.88	30.30
45-46	--	--	3.73	--	--	3.71	120.83	8.45	32.30
46-47	--	--	3.21	--	--	3.49	57.61	7.31	32.20
47-48	--	--	3.38	--	--	3.76	96.45	8.07	32.80
48-49	--	--	3.50	--	--	3.38	79.64	7.37	30.20
49-50	--	--	3.01	--	--	3.02	67.90	6.46	27.10
50-51	--	--	3.19	--	--	3.07	62.31	6.59	28.70
51-52	--	--	2.75	--	--	2.43	68.07	5.69	23.20
52-53	--	--	2.96	--	--	3.17	48.44	5.46	25.50
53-54	--	--	3.33	--	--	3.31	34.60	6.21	27.10
54-55	--	--	2.71	--	--	2.70	67.40	5.66	23.30
55-56	--	--	2.83	--	--	2.72	70.07	5.28	23.10
56-57	--	--	2.86	--	--	3.06	84.95	6.50	26.00
57-59	--	--	2.94	--	--	2.99	63.97	6.08	26.00
59-61	--	--	3.16	--	--	3.07	68.26	6.82	28.30
61-63	--	--	2.75	--	--	2.84	41.12	4.98	24.20
63-65	--	--	2.32	--	--	2.28	50.64	4.87	20.90

	Bi-214			Pb-214			Am-241		
	Act.	Unc.	MDA	Act.	Unc.	MDA	Act.	Unc.	MDA
0-1	58.95	1.71	5.76	73.78	1.44	4.90	--	--	1.96
1-2	48.01	1.63	5.70	56.01	1.36	4.75	--	--	2.06
2-3	35.59	2.30	9.06	48.92	1.91	9.91	--	--	2.92
3-4	23.43	2.22	9.23	31.29	1.81	10.30	--	--	3.77

4-5	31.61	2.04	8.22	45.61	1.70	9.29	--	--	3.30
5-6	47.14	2.58	9.00	45.74	2.00	8.43	--	--	3.56
6-7	31.50	2.37	9.33	38.07	1.89	8.00	--	--	3.12
7-8	51.80	2.63	9.49	56.79	2.11	8.71	--	--	3.28
8-9	31.99	2.29	9.26	45.89	1.91	10.30	--	--	3.02
9-10	18.05	2.14	9.55	28.50	1.77	10.60	--	--	3.02
10-11	20.16	2.05	8.71	30.62	1.68	9.42	--	--	2.67
11-12	32.60	2.22	8.66	43.50	1.87	8.09	--	--	3.03
12-13	47.70	2.51	9.53	64.73	2.12	8.17	--	--	3.11
13-14	31.72	2.53	10.40	42.87	2.11	12.00	--	--	3.81
14-15	35.21	2.53	10.00	48.31	2.14	9.05	--	--	3.60
15-16	40.21	1.94	7.43	51.89	1.63	6.34	--	--	2.41
16-17	53.00	2.67	9.71	70.30	2.25	0.12	--	--	0.06
17-18	40.58	2.48	9.40	52.96	2.03	7.77	--	--	3.48
18-19	31.74	2.33	9.01	39.23	1.90	10.00	--	--	2.06
19-20	44.92	2.54	9.67	60.31	2.25	9.06	--	--	3.24
20-21	7.42	3.09	17.20	20.63	3.06	16.60	--	--	5.58
21-22	38.68	3.64	15.00	56.70	2.97	15.80	--	--	5.21
22-23	54.88	2.76	9.88	68.88	2.30	8.48	--	--	3.30
23-24	44.34	3.00	14.10	58.35	2.92	16.10	--	--	4.31
24-25	74.74	2.89	9.23	91.65	2.42	8.33	--	--	3.62
25-26	54.77	2.49	8.62	61.69	2.03	7.54	--	--	2.95
26-27	46.42	2.14	7.62	59.61	1.78	8.72	--	--	3.12
27-28	31.11	2.28	9.08	48.14	1.92	9.85	--	--	3.27
28-29	44.05	3.45	13.50	50.43	2.79	11.30	--	--	4.21
29-30	13.51	4.42	18.90	29.86	3.24	20.10	--	--	5.96
30-31	5.52	3.02	13.90	18.29	2.45	12.10	--	--	4.29
31-32	38.02	3.86	15.70	43.27	3.06	13.90	--	--	5.29
32-33	52.42	2.79	10.40	72.67	2.33	8.49	--	--	3.69
33-34	43.91	2.54	9.28	57.28	2.14	8.33	--	--	4.59
34-35	45.20	2.55	9.54	68.46	2.20	8.12	4.76	0.65	3.48
35-36	41.45	2.80	10.70	48.26	2.23	9.25	6.14	0.88	4.13
36-37	41.78	2.74	10.60	59.96	2.26	8.71	5.39	0.67	3.36
37-38	54.02	2.73	9.69	66.87	2.27	7.83	--	--	3.38
38-39	46.07	2.95	11.10	61.46	2.41	12.20	--	--	4.03
39-40	51.30	2.76	9.99	63.76	2.23	10.60	--	--	3.61

40-41	51.42	2.69	9.95	60.25	2.22	8.29	--	--	3.12
41-42	37.19	2.43	9.16	53.18	2.02	7.84	--	--	3.37
42-43	41.66	2.55	9.59	57.00	2.12	10.30	--	--	4.51
43-44	36.03	2.41	9.28	45.84	1.95	7.72	--	--	3.20
44-45	52.28	2.67	9.59	69.14	2.24	7.72	--	--	3.37
45-46	48.27	2.66	9.57	55.47	2.13	8.14	--	--	3.47
46-47	27.98	2.38	9.15	34.86	1.81	7.97	--	--	3.07
47-48	38.64	2.46	9.32	49.55	2.02	8.16	--	--	2.94
48-49	34.15	2.50	9.39	50.00	2.01	8.26	--	--	3.00
49-50	32.04	2.13	8.29	44.00	1.77	7.17	--	--	3.91
50-51	29.12	2.12	8.58	40.20	1.75	7.19	--	--	2.92
51-52	31.51	1.87	7.28	41.41	1.53	6.02	--	--	3.42
52-53	19.69	1.98	8.39	26.86	1.64	6.94	--	--	2.56
53-54	16.02	2.04	9.10	22.95	1.64	7.56	--	--	2.77
54-55	29.30	1.84	7.52	38.37	1.49	6.04	--	--	2.86
55-56	40.26	1.99	7.43	50.14	1.64	8.28	--	--	2.35
56-57	40.74	2.17	8.05	44.82	1.70	6.89	--	--	2.45
57-59	28.00	1.97	7.83	37.55	1.61	6.86	--	--	2.53
59-61	23.50	2.06	8.43	30.19	1.64	7.18	--	--	2.70
61-63	17.24	1.84	7.84	23.52	1.45	6.77	--	--	2.38
63-65	14.52	1.48	6.53	25.40	1.22	6.80	--	--	2.46

APPENDIX B:

Bulk density of the sediments of Lago Maggiore

Table B.1. Measured bulk density of dry sediments of Lago Maggiore, in g·cm^{-3}.

Sed. layer, cm	Pos 1 Core 1	Pos 1 Core 4	Pos 2 Core 1	Pos 2 Core 3	Pos 3 Core 3	Pos 4 Core 2	Pos 5 Core 3	Pos 6 Core 3	Pos 7 Core 1
0-1	0.91	0.71	0.38	0.32	0.64	0.29	0.32	0.13	0.27
1-2	0.68	0.60	0.29	0.22	0.63	0.27	0.17	0.14	0.34
2-3	0.57	0.57	0.32	0.23	0.95	0.36	0.12	0.12	0.33
3-4	0.69	0.90	0.27	0.36	0.96	0.20	0.13	0.12	0.35
4-5	0.94	0.91	0.26	0.35	0.98	0.24	0.24	0.24	0.40
5-6	0.88	0.92	0.35	0.23	0.87	0.22	0.20	0.13	0.40
6-7	0.93	0.80	0.25	0.37	0.66	0.19	0.11	0.12	0.35
7-8	0.83	0.70	0.23	0.18	0.59	0.22	0.12	0.12	0.27
8-9	0.73	0.59	0.29	0.30	0.77	0.17	0.21	0.12	0.38
9-10	0.70	0.86	0.32	0.33	0.93	0.21	0.11	0.13	0.66
10-11	0.52	0.76	0.30	0.32	0.69	0.25	0.11	0.14	0.93
11-12	0.87	1.03	0.34	0.37	0.60	0.25	0.12	0.12	0.42
12-13	0.78	0.93	0.42	0.46	0.81	0.27	0.13	0.15	0.25
13-14	0.71	0.80	0.69	0.57	0.67	0.26	0.20	0.15	0.22
14-15	0.91	0.88	0.61	0.57	0.63	0.14	0.17	0.17	0.23
15-16	0.84	0.74	0.61	0.57	0.70	0.16	0.23	0.18	0.43
16-17	0.62	0.62	0.61	0.61	0.75	0.24	0.29	0.20	0.41
17-18	0.68	0.69	0.61	0.61	0.67	0.24	0.20	0.24	0.39
18-19	0.81	0.59	0.61	0.61	0.72	0.29	0.10	0.24	0.55
19-20	0.69	0.73	0.61	0.58	0.42	0.30	0.09	0.28	0.36
20-21	0.83	0.85	0.61	0.58	0.48	0.35	0.06	0.27	0.13
21-22	0.77	0.89	0.61	0.58	0.58	0.45	0.11	0.28	0.15
22-23	0.78	0.78	0.56	0.55	0.63	0.39	0.16	0.29	0.23
23-24	0.59	0.74	0.56	0.55	0.64	0.44	0.13	0.28	0.16
24-25	0.60	0.83	0.56	0.55	0.63	0.65	0.20	0.30	0.24
25-26	0.69	0.85	0.56	0.58	0.73	0.54	0.20	0.33	0.32
26-27	0.65	0.71	0.63	0.58	0.72	0.54	0.21	0.34	0.31
27-28	0.61	0.80	0.63	0.58	0.76	0.52	0.26	0.32	0.33
28-29	0.69	0.89	0.63	0.54	0.75	0.51	0.31	0.34	0.17
29-30	0.90	0.83	0.63	0.54	0.75	0.42	0.33	0.30	0.12

30-31	0.87	0.74	0.70	0.54	0.75	0.59	0.34	0.28	0.16
31-32	0.87	0.61	0.98	0.58	--	0.59	0.36	0.27	0.15
32-33	0.89	0.70	0.48	0.60	0.81	0.68	0.39	0.26	0.24
33-34	0.73	0.97	0.33	1.08	0.79	0.64	0.38	0.30	0.27
34-35	0.92	0.87	0.23	0.57	0.70	0.62	0.33	0.27	0.27
35-36	1.03	0.78	0.42	0.45	0.64	0.75	0.28	0.24	0.22
36-37	1.01	0.66	0.56	0.30	0.62	0.71	0.34	0.25	0.20
37-38	0.80	0.64	0.36	0.14	--	0.68	0.39	0.35	0.28
38-39	0.81	0.68	0.36	0.33	--	0.63	0.40	0.35	0.21
39-40	0.54	0.66	0.46	0.47	--	0.58	0.42	--	0.28
40-41	0.59	0.64	0.44	0.55	--	0.66	0.45	--	0.39
41-42	1.07	0.61	0.47	0.40	--	0.62	0.41	--	0.35
42-43	0.83	0.61	0.51	0.34	--	0.72	0.43	--	0.36
43-44	0.79	0.61	0.64	0.38	--	0.81	0.46	--	0.45
44-45	0.61	0.60	0.65	0.50	--	0.81	0.46	--	0.36
45-46	0.54	0.60	0.68	0.50	--	--	--	--	0.40
46-47	0.55	0.60	0.54	0.42	--	--	--	--	0.60
47-48	0.55	0.60	0.51	0.48	--	--	--	--	0.45
48-49	0.53	0.60	0.60	0.45	--	--	--	--	0.50
49-50	0.44	0.60	0.64	0.55	--	--	--	--	0.54
50-51	0.40	0.55	0.75	0.64	--	--	--	--	0.65
51-52	0.41	--	0.61	0.61	--	--	--	--	0.61
52-53	--	--	0.64	0.66	--	--	--	--	0.90
53-54	--	--	0.65	0.61	--	--	--	--	0.85
54-55	--	--	0.66	0.55	--	--	--	--	0.80
55-56	--	--	0.70	0.52	--	--	--	--	0.75
56-57	--	--	0.50	0.52	--	--	--	--	0.63
57-58	--	--	0.40	0.61	--	--	--	--	1.21
58-59	--	--	0.68	0.83	--	--	--	--	1.21
59-60	--	--	0.64	0.68	--	--	--	--	1.48
60-61	--	--	0.61	0.64	--	--	--	--	1.48
61-62	--	--	0.62	0.65	--	--	--	--	2.03
62- 63	--	--	0.72	0.75	--	--	--	--	2.03
63- 64	--	--	0.61	0.73	--	--	--	--	1.85
64- 65	--	--	0.72	0.68	--	--	--	--	1.85
65- 66	--	--	--	0.68	--	--	--	--	0.85

66- 67	--	--	--	0.61	--	--	--	--	0.67
67- 68	--	--	--	0.57	--	--	--	--	0.54
68- 69	--	--	--	0.82	--	--	--	--	0.58
69- 70	--	--	--	0.83	--	--	--	--	0.67

APPENDIX C:

Results of grain-size distribution analyses

Table C.1. Percentage of grain-size distribution and organic matter content of sediment profiles at different positions of Maggiore.

Position (sediment layer)	Sediment fraction in %			
	Sand	Silt	Clay	Organic matter
Pos 1 (0 - 9.5 cm)	14.6	66.1	16.9	2.4
Pos 1 (9.5 - 24 cm)	23.4	59.2	12.2	5.2
Pos 2 (0 - 2 cm)	65.3	18.8	13.0	2.9
Pos 2 (2 - 12.5 cm)	65.9	21.0	10.9	2.2
Pos 2 (12.5 - 14.5 cm)	43.4	33.5	22.1	1.0
Pos 2 (39 - 47 cm)	31.2	40.1	27.0	1.7
Pos 3 (5 - 18 cm)	22.3	64.9	11.7	1.1
Pos 4 (0 - 15 cm)	1.1	67.1	30.1	1.8
Pos 4 (15 - 30 cm)	1.7	52.0	44.6	1.7
Pos 4 (30 - 45 cm)	9.6	58.3	28.3	3.8
Pos 4 (45 - 60 cm)	8.8	70.4	16.8	4.0
Pos 5 (0 - 20 cm)	2.4	78.9	11.5	7.2
Pos 6 (8 - 28 cm)	10.9	41.1	46.6	1.4
Pos 7 (0 - 25 cm)	26.8	45.2	25.1	2.9
Pos 7 (25 - 50 cm)	4.8	48.9	44.1	2.2

APPENDIX D:

Results of 5-step sequential extraction procedure

Table D.1. Percentage of extracted ^{137}Cs during 5-step sequential procedure.

Position (sediment layer, cm)	Step 1, %	Step 2, %	Step 3, %	Step 4, %	Step 5, %	Rest (residue), %
Pos 1 (9.5–24)	0.45 ± 0.11	0.23 ± 0.08	0.15 ± 0.06	2.20 ± 0.16	5.51 ± 0.33	91.46 ± 0.40
Pos 2 (2–12.5)	0.99 ± 0.05	0.20 ± 0.03	0.21 ± 0.02	4.40 ± 0.21	0.90 ± 0.05	93.30 ± 0.22
Pos 3 (8–17)	0.21 ± 0.06	0.16 ± 0.16	0.08 ±0.03	1.17 ± 0.10	0.43 ± 0.06	97.95 ± 0.15
Pos 3 (8–15)	0.29 ± 0.06	0.16 ± 0.06	0.05 ± 0.06	1.26 ± 0.09	0.14 ± 0.03	98.10 ± 0.14
Pos 4 (2.5–12)	1.56 ± 0.09	0.52 ± 0.04	0.23 ± 0.02	4.27 ± 0.20	--	93.42 ± 0.22
Pos 5 (8–17)	9.68 ± 0.56	2.38 ± 0.20	1.11 ± 0.16	6.58 ± 0.40	1.12 ± 0.16	79.13 ± 0.75
Pos 6 (0–8)	4.51 ± 0.32	1.76 ± 0.22	0.68 ± 0.11	3.18 ± 0.21	0.50 ± 0.10	89.37 ± 0.47
Pos 7 (0–25)	0.86 ± 0.07	0.24 ± 0.06	0.18 ± 0.05	1.78 ± 0.12	0.25 ± 0.04	96.69 ± 0.17

Step 1 – Exchangeable ions of ^{137}Cs;

Step 2 – Carbonates;

Step 3 – Oxides and hydroxides of ion and manganese;

Step 4 – Organic matter;

Step 5 – Amorphous silicates.

Rest (residue) – Clay minerals, quartz, feldspars.

APPENDIX E:

Constant rate of supply model for sediment dating

The Constant Rate of Supply (CRS) model is based on the assumption that the supply of unsupported ^{210}Pb to the accreting material is constant for each time interval. This approach does not require the rate of sediment accumulation to be constant over time. In that case the initial concentration $A_0(t)$ (Bq·g^{-1}) of unsupported ^{210}Pb in the sediment satisfies:

$$A_0(t) \cdot R_S(t) = \text{const}, \qquad (E.1)$$

where $R_S(t)$ is the dry mass sedimentation rate in g·(cm^2·a)$^{-1}$ and t is time in a.

The present concentration of unsupported ^{210}Po at a present depth x can be calculated from (Appleby & Oldfield, 1978):

$$A(x) = A_0(t) \cdot e^{-\lambda t}, \qquad (E.2)$$

where A_0 and $A(x)$ are the initial and present activity concentration of unsupported ^{210}Pb in the layer at depth x, respectively, and λ is radioactive decay constant for ^{210}Pb (0.031 a^{-1}).

A sediment deposited during a small period of time Δt occupies a layer of thickness Δx:

$$\Delta x = \frac{R_S(t)}{\rho_b(x)} \cdot \Delta t, \qquad (E.3)$$

where $\rho_b(x)$ in g·cm^{-3} is the bulk density of the sediment at depth x and $R_S(t)$ is the dry mass sedimentation rate in g·(cm^2·a)$^{-1}$. The rate of change of depth is:

$$\dot{x} = \frac{R_S(t)}{\rho_b(x)}. \qquad (E.4)$$

Substituting (E.4) and (E.2) into (E.1), leads to:

$$A_0(t) \cdot r(t) = A_0(0) \cdot r(0)$$

$$A(x) \cdot r(t) = A_0(0) \cdot r(0) \cdot e^{-\lambda t}$$

$$A(x) \cdot \rho_b(x) \cdot \dot{x} = A(0) \cdot \rho_b(0) \cdot \dot{x}(0) \cdot e^{-\lambda t}. \tag{E.5}$$

The total residual (cumulated) unsupported ^{210}Pb $A_r(x)$ (Bq·cm^{-2}) in the sediment below the depth x is:

$$A_r(x) = \int_x^\infty \rho_b(x) \cdot A(x) \cdot dx \tag{E.6}$$

and, accordingly,

$$A_r(0) = \int_0^\infty \rho_b(x) \cdot A(x) \cdot dx. \tag{E.7}$$

From equations (E.5) and (E.6) it follows that:

$$\dot{A}_r = -\rho_b(x) \cdot A(x) \cdot \dot{x} = -\rho_b(0) \cdot A(0) \cdot \dot{x}(0) \cdot e^{-\lambda t}. \tag{E.8}$$

Integrating this equation with regard to time we obtain:

$$A_r(x) = \rho_b(0) \cdot A(0) \cdot \dot{x}(0) \cdot \int_t^\infty e^{-\lambda t} \cdot dt$$

$$A_r(x) = \frac{1}{\lambda} \cdot \rho_b(0) \cdot A(0) \cdot \dot{x}(0) \cdot e^{-\lambda t} \tag{E. 9}$$

$$A_r(x) = A_r(0) \cdot e^{-\lambda t}. \tag{E.10}$$

This calculation is based on the fact that cumulated unsupported ^{210}Pb below any given depth in a core can be compared to the total unsupported ^{210}Pb in the core and the age calculated for that particular depth. A series of these age calculations can be used to develop a graph of age versus depth of the core.

The age of the layer of depth x can be calculated as:

$$t = \frac{1}{\lambda} \cdot \ln \frac{A_r(0)}{A_r(x)}. \tag{E.12}$$

$A_r(x)$ is calculated by numerical integration of the graph of $\rho_b \cdot A / x$.

Whereas, for the constant input concentration (CIC) model the age of the layer of depth x is:

$$t = \frac{1}{\lambda} \cdot \ln \frac{A(0)}{A(x)} \tag{E.13}$$

Hence, from equations (E.4), (E.8) and (E.9) the rate of sedimentation $R_s(x)$ in $g \cdot (cm^2 \cdot a)^{-1}$ is given by:

$$R_s(t) = \rho_b(x) \cdot \dot{x}$$

$$R_s(t) = -\frac{\dot{A}_r}{A(x)}$$

$$R_s(x) = \frac{\lambda \cdot A_r(x)}{A(x)}. \tag{E.14}$$

Depending on the core, age determination older than 60-100 years should be treated with caution because statistical uncertainties and small variations in the background ^{210}Pb can cause large changes in the age estimation.

APPENDIX F:

Example of modeling: Mathematical code for Matlab

```
% FEMLAB Model M-file
% Generated by FEMLAB 3.0 (FEMLAB 3.0.0.181, $Date: 2004/01/29 19:04:14 $)

clear;
clc;

flclear fem

% Femlab version
clear vrsn
vrsn.name = 'FEMLAB 3.0';
vrsn.ext = '';
vrsn.major = 0;
vrsn.build = 181;
vrsn.rcs = '$Name:  $';
vrsn.date = '$Date: 2004/01/29 19:04:14 $';
fem.version = vrsn;

% Geometry
g1=solid1([0,90]);
clear s
s.objs={g1};
s.name={'depth'};
s.tags={'g1'};

fem.draw=struct('s',s);
fem.geom=geomcsg(fem);

% Constants
% Rs86 - sedimentation rate after the Chernobyl accident, g/(cm²·a)
% Rs63 - sedimentation rate after the nuclear weapons testing fallout, g/(cm²·a)
% fix - fixation rate, 1/a
% lambda - radioactive decay constant, 1/a
% alphabar - portion of exchangeable radioactivity (dimensionless)
% D - Diffusion constant of Cs⁺ ions in the pure water at certain temperature, cm²/a
% Kdtot - total distribution coefficient, ltr/kg
% Kddiffusion - distribution coefficient which is responsible for the retarded diffusion within the sediment
% ro0 - bulk density for the top layer of the sediment, g/cm³
% R - radius of the sediment corer, m
% rop - mean particle density, g/cm³
% LA - lake area, m²
% CA - catchment area, m2
% Pr - precipitation (net annual rainfall), mm/a
% DL86 - Average deposition on the lake in 1986, Bq/m²
% DL63 - Average deposition on the lake in 1963, Bq/m²
% DC - Average deposition to the catchment, Bq/m²
% MD - Lake mean depth, m
% B1 to B6 – constants of the AQUASCOPE model
t1 – time of the nuclear weapons testing fallout, a
t2 – time of the Chernobyl accident, a
```

t3 and t4 – time of the turbidite, a
par1 – constant describing the sedimentation speed within in the turbidite
par2 – constant describing the amplitude of the turbidite


```
fem.const={'Rs86','0.128', ...
      'Rs63','0.25',...
      'fix','2', ...
      'lambda','log(2)/30.07', ...
      'alphabar','0.0099', ...
      'D','417.63', ...
      'Kdtot','99000', ...
      'Kddiffusion','193.8',...
      'ro0','0.2781', ...
      'R','0.02865', ...
      'rop','2.65', ...
      'LA','213000000', ...
      'CA','6390000000', ...
      'Pr','1.752', ...
      'DL86','20000', ...
      'DC86','5000', ...
      'DL63','2330', ...
      'MD','176.5', ...
      'B1','0.3', ...
      'B2','18', ...
      'B3','0.41', ...
      'B4','0.02', ...
      'B5','0.00535', ...
      'B6','0.00029', ...
      't1','4.5', ...
      't2','27.3', ...
      't3','17.9', ...
      't4','18', ...
      'par1','440', ...
      'par2','2.1', ...
      'scale','0.001'};


% Initialize mesh
fem.mesh=meshinit(fem, ...
            'hmax',[], ...
            'hmaxfact',1, ...
            'hgrad',1.3, ...
            'xscale',1.0);

% Refine mesh
fem.mesh=meshrefine(fem);
fem.mesh=meshrefine(fem);
fem.mesh=meshrefine(fem);
fem.mesh=meshrefine(fem);
fem.mesh=meshrefine(fem);
fem.mesh=meshrefine(fem);
fem.mesh=meshrefine(fem);
```

```
% Application mode 1
clear appl
appl.mode.class = 'FlPDEC';
appl.mode.type = 'cartesian';
appl.dim = {'u1','u2','u1_t','u2_t'};
appl.sdim = {'x','y','z'};
appl.name = 'c';
appl.shape = {'shlag(2,"u1")','shlag(2,"u2")'};
appl.sshape = 2;
appl.border = 'off';
appl.assignsuffix = '_c';
clear prop
prop.elemdefault='Lag2';
prop.wave='off';
prop.weakconstr=struct('value',{'off'},'dim',{{'lm1','lm2','lm3','lm4'}});
appl.prop = prop;
clear bnd
bnd.weak = 0;
bnd.dweak = 0;
bnd.constr = '0';
bnd.q = 0;
bnd.h = 1;
bnd.g = 0;
bnd.r = {0,{'Ce';'Cf'}};
bnd.type = {'neu','dir'};
bnd.ind = [2,1];
appl.bnd = bnd;
clear equ
equ.shape = [1;2];
equ.gporder = 4;
equ.cporder = 2;
equ.init = 0;
equ.usage = 1;
equ.weak = 0;
equ.dweak = 0;
equ.constr = '0';
equ.c = {{'c11';'c22'}};
equ.a = {{'a11','-a12';'-a21','a22'}};
equ.f = 0;
equ.da = 1;
equ.al = '-vs';
equ.be = 0;
equ.ga = 0;
equ.ind = [1];
appl.equ = equ;
fem.appl{1} = appl;
fem.sdim = {'x'};


% Simplify expressions
fem.simplify = 'on';

% Global expressions
% RT - Water residence time of the lake, a
% LV - lake volume
% Kappa - Caesium removal rate, 1/a
```

% DC86 - Average deposition to the catchment in 1986, Bq/m^2
% DC63 - Average deposition to the catchment in 1963, Bq/m^2
% RT - Water residence time of the lake, a
% MD - Lake mean depth, m
% Kappa - Caesium removal rate, 1/a
% cw – concentration in the lake water, mBq/l
% Ce – exchangeable part of radioactivity, Bq/m^2 per 1 cm layer
% Cf – fixed part of radioactivity, Bq/m^2 per 1 cm layer
% Kdturbidite – distribution coefficient which is dependent on time and includes the terms describing the turbidite
% reisol – redissolution rate, 1/a
% Dphys – combined bio- and physical turbation, cm^2/a
% De – retarded diffusion, cm^2/a
% epsilon – porosity, dimensionless
% rob – bulk density of the sediment, g/cm^3
% vs – sedimentation speed, cm/a


```
fem.expr = {'LV','LA*MD', ...
        'RT','LV/(Pr*CA)', ...
        'Kappa','(1/RT)+(8/MD)+1', ...
        'cw86','(T186+((DC86.*exp(-(t-t2).*lambda))/RT).*(T286+T386+T486)).*(t>t2)', ...
        'T186','DL86/MD*exp(-(t-t2)*(Kappa+lambda))', ...
        'T286','(B1*(exp(-(t-t2)*B2)-exp(-(t-t2)*Kappa)))/(Kappa-B2)', ...
        'T386','(B5*(exp(-(t-t2)*B3)-exp(-(t-t2)/RT)))/(1/RT-B3)', ...
        'T486','(B6*(exp(-(t-t2)*B4)-exp(-(t-t2)/RT)))/(1/RT-B4)', ...
        'cw63','(T163+((DC63.*exp(-(t-t1).*lambda))/RT).*(T263+T363+T463)).*((t>=t1)&(t<=t2))', ...
        'T163','DL63/MD*exp(-(t-t1)*(Kappa+lambda))', ...
        'T263','(B1*(exp(-(t-t1)*B2)-exp(-(t-t1)*Kappa)))/(Kappa-B2)', ...
        'T363','(B5*(exp(-(t-t1)*B3)-exp(-(t-t1)/RT)))/(1/RT-B3)', ...
        'T463','(B6*(exp(-(t-t1)*B4)-exp(-(t-t1)/RT)))/(1/RT-B4)', ...
        'cw59','(T159+((DC59.*exp(-t.*lambda))/RT).*(T259+T359+T459)).*(t<t1)', ...
        'T159','DL59/MD*exp(-t*(Kappa+lambda))', ...
        'T259','(B1*(exp(-t*B2)-exp(-t*Kappa)))/(Kappa-B2)', ...
        'T359','(B5*(exp(-t*B3)-exp(-t/RT)))/(1/RT-B3)', ...
        'T459','(B6*(exp(-t*B4)-exp(-t/RT)))/(1/RT-B4)', ...
        'T2','(B1*(exp(-t*B2)-exp(-t*Kappa)))/(Kappa-B2)', ...
        'T3','(B5*(exp(-t*B3)-exp(-t/RT)))/(1/RT-B3)', ...
        'T4','(B6*(exp(-t*B4)-exp(-t/RT)))/(1/RT-B4)', ...
        'DC63','DL63/4', ...
        'DL59','DL63/2.6', ...
        'DC59','DL63/2.6/4', ...
        'cw','cw59+cw63+cw86', ...
        'Ce','cw.*Kdturbidite.*(alphabar*ro0*0.01)', ...
        'Cf','cw.*Kdturbidite.*((1-alphabar)*ro0*0.01)', ...
        'a11','lambda+fix', ...
        'a22','lambda+redisol', ...
        'a12','redisol', ...
        'a21','fix', ...
        'c22','Dphys', ...
        'c11','De+Dphys', ...
        'Dphys','0.01*(x<=1)', ...
        'De','(D*(epsilon)^(1/3))*(1/(1+(rob/epsilon*Kddiffusion)))', ...
        'Kdex','alphabar*Kdturbidite',...
        'Kdturbidite','Kdtot.*(1+(flsmhs((t-t3),scale)-flsmhs((t-t4),scale))*par2)',...
        'redisol','alphabar*fix/(1-alphabar)', ...
```

```
            'epsilon','1-rob/rop', ...
            'rob','ro0+0.0088.*x', ...
            'vs','((Rs086+Rs063)/rob).*(1+(flsmhs((t-t3),scale)-flsmhs((t-t4),scale))*par1)', ...
            'Rs086','(Rs86)*(t>=27.3)',...
            'Rs063','(Rs63)*(t<27.3)',...
            'c','u1+u2'};


% Functions
fem.functions = {};

% Multiphysics
fem=multiphysics(fem);

% Extend mesh
fem.xmesh=meshextend(fem,'geoms',[1],'eqvars','on','cplbndeq','on','cplbndsh','off');


% Solve problem
fem.sol=femtime(fem, ...
            'nullfun','flnullorth', ...
            'blocksize',5000, ...
            'complexfun','off', ...
            'conjugate','on', ...
            'symmetric','off', ...
            'solcomp',{'u2','u1'}, ...
            'outcomp',{'u2','u1'}, ...
            'rowscale','on', ...
            'tlist',[0:0.1:44.2], ...
            'atol',{'0.000000010'}, ...
            'rtol',0.1, ...
            'maxorder',1, ...
            'masssingular','maybe', ...
            'consistent','2', ...
            'estrat',0, ...
            'tout','tlist', ...
            'tsteps','strict', ...
            'complex','off', ...
            'linsolver','umfpack', ...
            'thresh',0.1, ...
            'umfalloc',0.7, ...
            'uscale','auto');

% Save current fem structure for restart purposes
fem0=fem;
```

Erklärung

Die vorliegende Arbeit entstand im Institut für Angewandte Forschung der Hochschule Ravensburg-Weingarten unter der wissenschaftlichen Betreuung von Herrn Prof. Dr. Eckehard Klemt.

Es haben keine weiteren Promotionsverfahren stattgefunden.

Ich erkenne die Promotionsordnung der Fakultät für Mathematik und Naturwissenschaften der Technischen Universität Dresden vom 20.03.2000 in der Fassung vom 16.04.2003 sowie gemäß der Änderungssatzung vom 17.07.2008 an.

Versicherung

Hiermit versichere ich, dass ich die vorliegende Arbeit ohne unzulässige Hilfe Dritter und ohne Benutzung anderer als der angegebenen Hilfsmittel angefertigt habe; die aus fremden Quellen direkt oder indirekt übernommenen Gedanken sind als solche kenntlich gemacht. Die Arbeit wurde bisher weder im Inland noch im Ausland in gleicher oder ähnlicher Form einer anderen Prüfungsbehörde vorgelegt.

Dresden, den 23.04.2010

Viktoryia Putyrskaya